Universität Stuttgart

Institut für Wasser- und Umweltsystemmodellierung

Mitteilungen

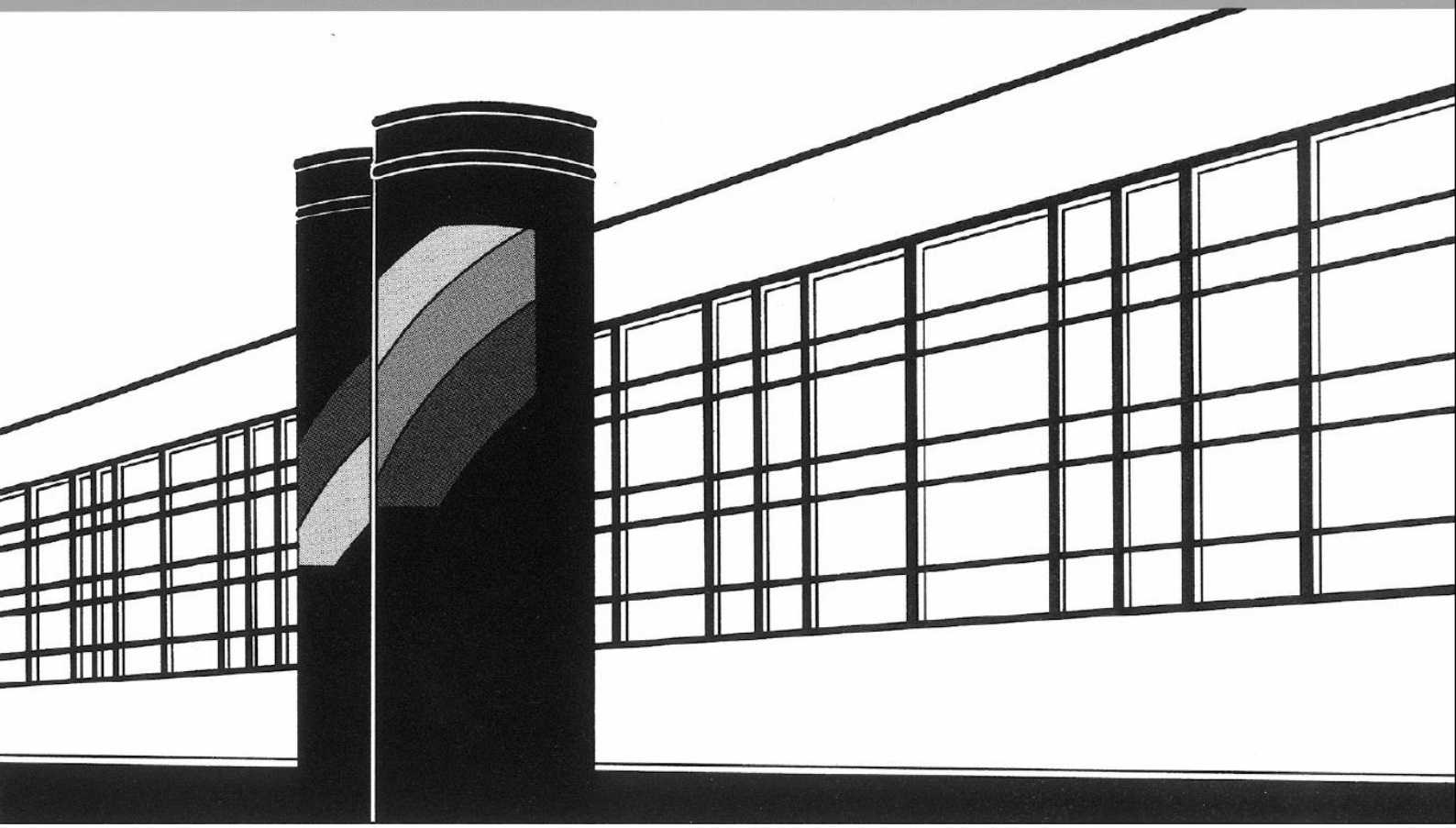

Heft 232

Takayuki Sugimoto

Copula based Stochastic Analysis of Discharge Time Series

Copula based Stochastic Analysis of Discharge Time Series

Von der Fakultät Bau- und Umweltingenieurwissenschaften
der Universität Stuttgart zur Erlangung der Würde eines
Doktor-Ingenieurs (Dr.-Ing.) genehmigte Abhandlung

vorgelegt von

Takayuki Sugimoto
aus Kyoto, Japan

Hauptberichter: Prof. Dr. rer.nat. Dr.-Ing. András Bárdossy
Mitberichter: Prof. Geoffrey GS Pegram PhD

Tag der mündlichen Prüfung: 8.05.2014

Institut für Wasser- und Umweltsystemmodellierung
der Universität Stuttgart
2014

Heft 232

Copula based Stochastic Analysis of Discharge Time Series

von
Dr.-Ing.
Takayuki Sugimoto

Eigenverlag des Instituts für Wasser- und Umweltsystemmodellierung der Universität Stuttgart

D93 **Copula based Stochastic Analysis of Discharge Time Series**

Bibliografische Information der Deutschen Nationalbibliothek
Die Deutsche Nationalbibliothek verzeichnet diese Publikation in der Deutschen Nationalbibliografie; detaillierte bibliografische Daten sind im Internet über http://www.d-nb.de abrufbar

Sugimoto, Takayuki:
Copula based Stochastic Analysis of Discharge Time Series, Universität Stuttgart. - Stuttgart: Institut für Wasser- und Umweltsystemmodellierung, 2014

(Mitteilungen Institut für Wasser- und Umweltsystemmodellierung, Universität Stuttgart: H. 232)
Zugl.: Stuttgart, Univ., Diss., 2014
ISBN 978-3-942036-36-8

NE: Institut für Wasser- und Umweltsystemmodellierung <Stuttgart>: Mitteilungen

Herausgegeben 2014 vom Eigenverlag des Instituts für Wasser- und Umweltsystem-modellierung

Druck: Document Center S. Kästl, Ostfildern

Acknowledgment

I would like to show my best respect and appreciation to my doctor father, Prof. Dr. rer.nat. Dr.-Ing. András Bárdossy, for offering the best opportunity to work in this institute with nice people for interesting topic. It is his wide range of knowledge, experiences, insights and ideas, which lead me to this accomplishment from the beginning to the end. Also I have nothing but admiring his personality as a scientist and human being which facilitate fine and excellent engineering works involving attractive people all over the world. I wish all the best for his further success and hope to be a part of it.

Also I want to acknowledge Prof. Pegram for nicely accepting the role of my second supervisor, spending precious time in seriously discussing with me and giving valuable comments on my work, beside his daily works and tight schedules. This kept encouraging me towards the success of this study and makes my work rich and robust. I deeply appreciate and respect his generosity and discipline.

I want give special thanks to my colleagues in my office. Dirk is the person with whom I met first and he offered the numerous help from the first day to the last moment. Thomas, he warmly offered guidance when I arrived at the institute for the first time and gave me navigation when I had the troubles with the computer. Magdalena und Theresia, I appreciate again their patience and understanding of my working style.

Many thanks to the secretaries, Frau Uhrmann and Frau Lemp; they are the people who are really driving the scientific work and many sorry for bothering them due to my carelessness.

Also I would like to show my gratitude to other colleagues in the institute like Jochen Seidel, Felix Herma, Tobias Mosthaf, Thomas Müller und Sebastian Hörning, who are together in coffee break, lunch time, playing soccer and off-university activities.

The international colleagues in our institute like Yulizar, Yingchun Huang and some of them had already left the institute like Min Liu, Shailesh Singh, Jing Li, Jhan Rodriguez, but they offered enormous friendship and cheerful atmosphere. I appreciate also all the members of ENWAT and Dr.-Ing. Hartmann for helping this international multicultural unification.

All the students with whom I worked together like Kitti Kamkaew, I want to express my gratitude to them.

I cannot forget the involvement of my father and mother. My existence, personality and achievements are all owing to their understanding and support.

I will express my gratefulness to all the people, professors, colleagues, students, friends, family who helped me to come here and in the completion of this work.

Since I know I have very little capacity to please the people, I did my best effort to make some scientific progress and entertain the people with it, although it is quite a little in comparison to the works done by all the ancestors in the field of natural sciences, mathematics and hydrological engineering.

Hereby, I declare I will devote this work to all the people who wish to share the achievement, I will never forget any contribution of all the people who supported me and at the end I would like to say thank you from bottom of my heart to all the people.

Best Regards
Takayuki Sugimoto

Contents

List of Figures

List of Table

Notation

The following table shows the significant symbols used in this work. Local notations are explained in the text.

Symbol	Unit	Definition
Chapter 2:		
$C(\mathbf{u})$		copula
$F(\mathbf{x})$		cumulative distribution function
$F_{X_i}(x_i)$		marginal distribution of *i*-th random variable X_i
$C_n(\mathbf{u})$		empirical copula (cumulative)
$c_n(\mathbf{u})$		empirical copula (density)
k	[*day*]	lag
$A_1(k)$		asymmetry1 corresponding to lag *k*
$A_2(k)$		asymmetry2 corresponding to lag *k*
$Q(t)$	[m^3/day]	discharge at time *t*
$B(\alpha,\beta)$		beta function with parameter α and β
Chapter 3:		
$\mu_{t\|365}$		annual cycle of mean
$\sigma_{t\|365}$		annual cycle of standard deviation
$A_{2,\min}$		minimum of asymmetry2
$L_{\min}$		lag at minimum
Chapter 5:		
$P(t)$	[*mm/day*]	precipitation at time *t*
$API(t)$	[*mm/day*]	antecedent precipitation index at time *t*
α		parameter of API

Chapter 6:

$MELT$	**[**mm**]**	snowmelt rate as water equivalent
DD	[$mm\ °C^{-1}\ day^{-1}$]	degree-day factor
T	[$°C$]	mean daily air temperature
TT	[$°C$]	threshold temperature for snowmelt initiation
PE_a	[$mm \cdot \text{day}^{-1}$]	adjusted potential evapotranspiration
C		model parameter accounting for snow melting
T	[$°C$]	mean daily air temperature
T_m	[$°C$]	long-term mean monthly air temperature
PE_m	[$mm \cdot \text{day}^{-1}$]	long-term mean monthly potential evapotranspiration
E_a	[$mm \cdot \text{day}^{-1}$]	actual evapotranspiration
PWP	[mm]	soil moisture limit where evapotranspiration decreases
SM	[mm]	actual soil-moisture (water) content
P_{eff}	[mm]	effective precipitation
FC	[mm]	field capacity, maximum soil-moisture storage capacity
β		a model parameter, shape coefficient
P	[mm]	daily sum precipitation
Q_0	[$mm \cdot day^{-1}$]	near-surface flow
Q_1	[$mm \cdot day^{-1}$]	interflow
Q_{perc}	[$mm \cdot day^{-1}$]	percolation
Q_2	[$mm \cdot day^{-1}$]	baseflow
K_0	[day^{-1}]	near-surface flow storage coefficient
K_1	[day^{-1}]	interflow storage coefficient
K_{perc}	[day^{-1}]	percolation coefficient
K_2	[day^{-1}]	baseflow storage coefficient
S_i	[mm]	upper zone reservoir water storage level
S_b	[mm]	lower zone reservoir water storage level
L	[mm]	threshold water level for near-surface flow
A_{sc}	[km^2]	catchment or subcatchment area

Chapter 7:

D	copula distance
$D_1(t)$	copula distance type1 at time t
$D_2(t)$	copula distance type2 at time t
$D_3(t)$	copula distance type3 at time t
$c^*_{loacl}(\mathbf{u})$	local copula
$c^*_{global}(\mathbf{u})$	global copula
$Var_{cop}(c)$	copula variance
$Cov_{cop}(c)$	copula covariance
$Cor_{cop}(c)$	copula correlation

List of Abbreviations

GRDC	Global Runoff Data Centre, an international archive of discharge data
BW	Baden-Württemberg, a state located in South West Germany
ANDE	Andernach, a name of discharge gauging station
KAUB	Kaub, a name of gauging station for discharge
WORM	Worms, a name of gauging station for discharge
MAXA	Maxau, a name of gauging station for discharge
COCH	Cochem, a name of gauging station for discharge
PLOC	Plochingen, a name of gauging station for discharge
KALK	Kalkofen, a name of gauging station for discharge

Kurzfassung

Hintergrund und Motivation

Der globale Klimawandel hat möglicherweise Auswirkungen auf den Wasserhaushalt von Flussgebieten Weltweit. Um ein sicheres Hintergrundwissen als Grundlage für die Bewertung künftiger Entwicklungen zu erlangen und vorzuhalten ist eine wissenschaftliche Untersuchung von bisher gemessenen Daten notwendig.

Das Global Runoff Data Center der BfG vereinigt seit 1988 die weltweit größte Sammlung von Abflussdaten aller Kontinente und bietet die Gelegenheit, durch statistische Auswertung des ständig wachsenden Datensatzes neue Erkenntnisse zu gewinnen.

Diese Studie beschäftigt sich mit Bewertungen und Analysen der deutschen hydrologischen Gegebenheiten und bedient sich moderner Methoden der nichtparametrischen Statistik.

Die Vergleiche zwischen den verschiedenen Einzugsgebieten erlauben eine fundierter Bewertung der kausalen Zusammenhänge von Bewirtschaftungsmaßnahmen struktureller Art, Landnutzungs-änderungen, veränderten Antriebskräften und des hydrologischen Regimes und damit letztendlich der Wasserbilanz.

Zeitreihenanalyse mit Copula

Copula ist ein statistisches Konzept, das die Beziehung zwischen mehreren Zufallsvariablen beschreibt ähnlich wie Kovarianz und Korrelation. Ein Vorteil einer Anwendung von Copulas besteht darin, dass die Abhängigkeitsstruktur unabhängig von deren Randverteilung konstruktiert werden kann. Das heißt, man kann zwei Datensätze mit verschiedenen Maßstäben oder Einheiten in einer uniformierten Definitionsmenge vergleichen.

Außerdem besteht die Möglichkeit der flexibleren Modellierung, und dadurch ist Copula-basierte stochastische Analyse für Bewertung der Abflussdaten ermöglicht. Ein /Das Ziel dieser Arbeit ist es, ein neues Zeitreihenmodell mit Copula zu entwickeln,

Ein Vorteil einer Anwendung von Copulas besteht darin, dass man zwei Datensätze mit verschiedenen Maßstäben oder Einheiten in einer uniformierten Definitionsmenge vergleichen kann. Außerdem besteht die Möglichkeit der flexibleren Modellierung, und dadurch ist Copula-basierte stochastische Analyse für Bewertung der Abflussdaten ermöglicht. Ein /Das Ziel dieser Arbeit ist es, ein neues Zeitreihenmodell mit Copula zu entwickeln.

Asymmetrie in Abflüssen und Niederschlägen

Asymmetrie ist eine Funktion, die in Copulas definiert ist. Im Zusammenhang mit *Niederschlag-Abfluss-Ereignissen* kann angenommen werden, dass Asymmetrie mit Eigenschaften des Einzugsgebiets zusammenhängt. Zuerst wird die Asymmetrie für die Daten des Rheingebiets berechnet, aber auch für andere Einzugsgebiete in Deutschland, um die Beziehung zwischen Einzugsgebiet und Asymmetrie zu valideren. Zweitens werden die zeitlichen Änderungen der Asymmetrie berechnet. Dabei wird die Asymmetrie als Zeichen der *anthropogenen* Beeinflussung interpretiert.

Im ersten Schritt wird eine Eigenschaft der Copula, die Asymmetrie, definiert und für die gegebenen Abflussdaten aus dem Rheingebiet analysiert, um die Gültigkeit der Asymmetrie als Maß zur Quantifizierung von charakteristischen Zusammenhängen zu testen. Außerdem wird die zeitliche Änderung der Asymmetrie als Zeichen möglicher anthropogener Auswirkungen untersucht. Auch wurde eine detaillierte Analyse durch die Trennung der Daten nach den verschiedenen Jahreszeiten durchgeführt.

Asymmetrie hat interessante Eigenschaften und kann ein Werkzeug sein, um unbekannte Informationen zu beleuchten. Jedoch ist es schwierig zu unterscheiden, ob die Änderung der Asymmetrie durch anthropogene Einwirkungen oder durch zufällige zeitliche Variationen in den Niederschlägen verursacht wurde. Daher werden die Niederschlagsdaten aus 525 Messstationen in der Oberrheinebene mit Hilfe von API (Vorläufer-Niederschlagsindex) ausgewählt und in ähnlicher Weise wie der Abfluss untersucht. Das Ergebnis zeigt: API verhält sich in ähnlicher Weise wie der Abfluss, was darauf hinweist, dass die zeitliche Änderung der Asymmetrie aus der zeitlichen Änderung des Niederschlags entstanden sind.

Hydrologisches Modell und Copula-Distanz

In diesem Stadium der Forschung ist es noch nicht sicher, ob eine Beziehung besteht zwischen den charakteristischen Eigenschaften des Einzugsgebiets und der Asymmetrie. Der in diesem Abschnitt vorgestellte Ansatz ist, dass der anthropogene Einfluss mit Hilfe eines hydrologischen Modells mit festen Parametern für den gesamten Simulationszeitraum beseitigt werden kann. Dabei werden beobachtete Niederschläge als Eingangsdaten verwendet. Die beobachteten und die vom HBV-Modell simulierten Abflüsse werden im Hinblick auf Asymmetrie und Copula-Distanz verglichen. Die Copula-Distanz ist eine Maßnahme, um die Ähnlichkeit von zwei Copulas zu vergleichen. Dieses Kriterium basiert auf der Eigenschaft der Copula, dass die mehrdimensionale Verteilung der multivariaten Zufallsvariablen uniformiert wird. Das Ergebnis zeigt, dass es bestimmte stochastische Unterschiede zwischen simulierten und beobachteten Abflussdaten gibt. Auch die Copulavarianz, definiert als die Variabilität der Copula, ist deutlich kleiner für die beobachteten Daten. Diese deutet auf Unterschiede zwischen Computer-basierter Simulation und Naturprozess hin

Copula-basierte statistische Simulation

Ähnlich wie bei ARIMA können Zeitreihenmodelle auf der Grundlage der zeitlichen Beziehung zwischen den Zufallsvariablen mit Hilfe von Copulas definiert werden. In diesem Abschnitt wird die Leistung der statistischen Simulation mit Copulas getestet. Die Copula wird durch Kerndichte-schätzung mit Beta- Kernel geschätzt. Interessant ist, dass auch 2- oder 3-dimensionale Copulas die

Ganglinien während der Niederschlag-Abfluss-Ereignisse gut reproduzieren können, während das ARIMA-Modell nicht solche Eigenschaften zeigt. Dies kann daran liegen, dass die Copula von Kerndichteinformationen geschätzte deutlich mehr Informationen enthält als die Autokorrelations-matrix.

Abstract

Background and Motivation

Global climate change can have impacts on characteristics of rainfall-runoff events and also on the water regime in the catchment. It is of importance to investigate the existing data for detecting the impact of structural modification of the river, change of land use and hydrological regime beside the computer simulations with complex physically based models.

The objective of this thesis is to develop a statistical methodology for the identification of hydrological characteristics in the catchment, which is transferable to different catchments, using multinational and global long-term runoff data offered from GRDC.

For this aim, statistical dependency should be analysed for a large number of hydrological time series data sets not only with parametric statistics but also with non-parametric statistics. Until now the widely used time series models such as ARIMA are based on linear combinations of autocovariances. However, such statistical measure cannot describe all the details of the dependence structure, and subsequently could lose crucial information. Instead, statistical concepts such as copulas have the advantage of being able to measure the details of dependence structure and possibly to reveal significant information about the dependency from a variety of data sets.

Time series analysis with Copula

Copula is a statistical concept, which describes the relationship between two random variables similar to covariance and correlation. The advantage to use this measure is that the random variables can be compared independent from the marginal distribution. This means, it is possible to compare two time series observed in two different gauging stations in the uniformed way even if the scales or unit of the two datasets is different.

While the classical time series model ARIMA (Auto regressive integrated moving average) or the ARCH (autoregressive heteroskedasticity models) model are based on the covariance or correlation matrix, this study challenges also to develop a new methodology of time series analysis and modelling using copulas in the context of hydrological modelling.

Asymmetry in Precipitation and Discharge

In the first step, a property of copula, asymmetry, is defined and analysed for the given discharge data sets from the Rhine basin in order to quantify the validity of asymmetry as a measure related to the catchment characteristic. Secondary, the temporal change of the asymmetry is examined as a sign of possible anthropogenic impact. Also detailed analysis was performed by separating the data into different seasons.

Asymmetry has interesting characteristics and can be a tool to illuminate unknown information. However, it is hard to confirm whether the change of asymmetry is originated from anthropogenic impact or temporal random behaviour of rainfall. Therefore, the precipitation data from 525 measuring stations in the upper Rhine region are chosen and investigated in the similar way to of discharge by using API (antecedent precipitation index). The result shows API behaves in a similar way to discharge, which indicates that the temporal change of asymmetry is originated from the temporal configuration of precipitations.

Hydrological model and Copula Distance

At this stage of this research, it is still not sure that there exists a relation between the catchment characteristics and asymmetry. The approach introduced in this section is that the anthropogenic impact can be eliminated by using the hydrological model HBV with fixed parameters for the entire simulation period and observed precipitation as input data. The observed and simulated discharges are compared by asymmetry and additionally with copula distance. Copula distance is a measure to compare the similarity of two copulas. This criterion is derived based on the property of copula. The result indicates that there is certain stochastic difference between simulated and observed discharge time series. Also copula variance, defined as the variability of copula, is clearly smaller for the observed data, which can indicates the difference of complexity between hydrological models based simulation and nature process.

Copula based statistical simulation

Similar to ARIMA, time series model based on the relation between the random variables in time domain can be defined with the help of copula. In this section, the performance of the statistical simulation using copula is tested, where copula is estimated by kernel density estimation with beta kernel. The interesting point is that even 2 or 3 dimensional copula can reproduce well the hydrograph during rainfall-runoff events, while the ARIMA model does not show such characteristics. This can be explained based on the fact that a copula estimated by kernel density information has clearly more information than the autocorrelation matrix.

1 Introduction

1.1 Background and Motivation

Global climate change can have impact on characteristics of rainfall-runoff event and also on the water regime in the catchment. It is of importance to investigate the existing data to detect the impact of structural modification of the river, change of land use and hydrological regime besides the computer simulations with complex physically based models. The objective of this thesis is to develop a statistical methodology for the identification of hydrological characteristics in the catchment, which is transferable to different catchments, with multinational and global long-term runoff data offered from Global Runoff Data Center (GRDC) in the Federal Institute of Hydrology in Germany.

For this aim, statistical dependency should be analysed for a large number of hydrological time series datasets. Until now the widely used time series models are based on linear combinations of autocovariances. However, such statistical measure cannot describe all the details of the dependence structure, and subsequently has the risk of losing crucial information. Instead, statistical concepts, copulas, have the advantageous ability to measure more detailed dependence structure and possibly to reveal significant information about the dependency from a variety of datasets.

Asymmetry is one of the measures defined on the copula (Bárdossy 2006). This characteristic can be related to the natural properties of the catchment, which should be taken into account for statistical analysis in practical sense. For example, in the hydrograph, usually the discharge sharply increases to the peak after an intensive rainfall event, but the recession of water is relatively slower. Such a property in discharge data can be associated with asymmetry in copulas.

1.2 The Literature Review

1.2.1 Hydrology

Water is the most common and essential resource as well as a critical substance for all the living creatures on the earth. Its sound circulation is not only important for biological systems but also for human society. The management of water is fundamentally important, attempting to prevent damage due to destructive force of water flow or the stress due to its scarcity in certain region. Since the ancient period, there have been numerous human endeavours to grasp the behaviour of water in nature, but the entire spectrum of the system is not yet revealed. Stochastic analysis of the Rhine River with copulas is related to this paradigm.

Hydrology is the study to understand the water cycle with the focus on the water quantity. The early work of the hydrology is first pronounced in the early 20th century in textbook of hydrology (e.g. Mead 1919) where ground water and geology are mainly articulated. Thereafter, huge advances in hydrological science were achieved concerning statistical method to practically tackle with

problems as well as physically based models where the dominant process is extracted and solved with the aid of computer based technology and techniques.

However, as part of a general circulation model, circulation of water on the earth is not yet fully foreseeable. One of the major problems is the scale diversity of physical mechanisms dominating its behaviour. Downscaling is the one of the major issues how to overcome the scale difference (von Storch, Zorita, and Cubasch 1993).

But perfect model seems not feasible and it can be even impossible in terms of data acquisition and verification of its accountability. Therefore certain amount of simplification such as conceptual hydrological model is still needed, which can substitute the nature complexity with proper amount of parameterization and its calibration.

Acquisition and management of data as well as analysing technique also keep improving. The modelling with data supported system appears to be more in use. However, just vast amount of raw data cannot easily be utilized and careful processing of data based on the importance of information is needed. Shannon defined information entropy (Shannon 1948) and several studies are done in the hydrologic sciences (Singh 1997) , but there are still necessities of improvement. This study also treats large amount of data, aiming at contributing to this end by illuminating the relation between data itself and possible relation between data and model.

1.2.2 Time Series Analysis and Time Series Model

Time series analysis is a method to elucidate the underlying system of given time series with certain assumptions. In this way, a time series model can be set up based on the understanding of the system to predict the future.

One of the traditional approaches is Fourier Analysis which decomposes given time series into trigonometric components with the help of Fourier Transformation (FT). Due to the mathematical constraints, stationarity of the system is required, therefore its applicability is limited to the case that existence of cyclic behaviour is assured (Fleming et al. 2002). In general, this assumption is not fulfilled if the human interaction should be considered.

One of the classical time series model, autoregressive integrated moving average (ARIMA), is a stationary stochastic process to describe the time series by the values observed in the past and randomness added at each time step (Box and Jenkins 1976). Stationarity of the system should be guaranteed, but not assured in reality, which is similar to Fourier analysis.

Autoregressive Conditional Heteroskedasticity (ARCH) models loose the assumption of stationarity to a certain extent so that variance is not constant and models the variance in the similar way to ARIMA. Variance of discharge seems to change depending on the calendar day for example, but modeling the variance is not only the purpose for investigation, thus not focused in this study.

Empirical mode decomposition (Huang et al. 1998) is the method to overcome the drawbacks of FT based analysis by allowing the frequency to vary within a component and separate the signal adaptively by its scale. There are efforts to identify the period of hydrologic cycles with this method (Sang, Wang, and Liu 2012), but the interpretation of decomposition is still difficult due to the existence of noise and complexity of periodic behaviour in hydrology.

There are also non-stationary approaches as often referred as data assimilation in climatic researches. Parameter of hydrological model or physical constant of governing equation can be treated as state variable, then the techniques of data assimilation are applicable (Moradkhani et al. 2005).

1.2.3 Copula

Copula (Sklar 1959) is a multivariate probability distribution to flexibly model dependence structure in uniformed domain. It is widely applied in financial sector to evaluate the risk in joint behaviour of several random variables. The use of copula in hydrology can be found for the assessment of extreme events by considering flooding as joint behaviour of peak and volume (De Michele and Salvadori 2003) or drought as joint behaviour of duration magnitude and intensity (Kim, Valdés, and Yoo 2003). Copulas are applied to describe stochastic system of spatial temporal uncertainty of precipitation (Bárdossy and Pegram 2009), or inhomogeneity of the properties in soil (Bárdossy and Li 2008). Asymmetry in the time series can be tested in the framework of finite state Markov chain with a transition probability matrix (Sharifdoost, Mahmoodi, and Pasha 2009). The autocopula defined in this study also describes the relation between random variables at current time step and next time step similar to a transition probability matrix in Markov chain. The existence of asymmetry can be statistically tested, but the existence of asymmetry in discharge time series seems clear.

1.3 Outline of Thesis

For the first part of this research, therefore, a variety of analyses was done for a wide range of discharge data throughout the Rhine and partially for the Danube and the Weser Rivers in order to test the plausibility of the asymmetry concept for explaining catchment characteristic.

For the second part, it was necessary to eliminate the influence of precipitation in the discharge data. An alternative approach was implemented by using a hydrological model for eliminating the stochastic property of anthropogenic impacts in discharge data. At this stage, the investigation using copula distance was introduced, which could bring new insight to the stochastic property of time series and model uncertainty.

Additionally, non-Gaussian statistic simulation was tested using the copula estimated by kernel-density estimation. Similar to the correlation matrix in the autoregressive process of order *n*, a *n*-dimensional empirical copula is constructed and the new values are simulated based on the conditional distribution of the corresponding copula model. In this way, the simulated time series data is not only accounting for the correlation matrix of given time series, but also for more detailed characteristics of the original data such as asymmetry.

2 Methodology

The objective of statistical analysis is the inference of the property of the population and possibly to find any relations between random variables, which are caused by certain mechanisms of nature. However those mechanisms cannot be easily recognized by human perspective or is too difficult to mathematically describe. The observed data set has the raw information, which is considered to reflect the mechanisms of nature. The statistical methods in this study aim at illuminating the underlying physical processes and extracts practical information by carefully treating the data.

For example, we have the scatter plot of two random variables, namely two time series data sets from different gauging stations. This raw information with numerous points has the information about the observed dependency between two random variables. But, the classical statistical measure such as correlation or covariance, which regress the statistical information to a single value, will fail to capture all the information about dependency between two datasets.

In this context, a statistical concept, copulas, is tested in order to capture more precise dependence structure of various random hydrological variables and detect significant key information. The point is that, in copulas, multivariate distribution is separated into marginal distributions and dependence structure on the transformed uniformed domain, which has certain advantages compared to classical statistics without copulas.

In this section basic definitions and ideas of how to apply copulas to investigate the temporal variability as well as the measures to distinguish Gaussian and non-Gaussian dependence, which are introduced by Bárdossy and Li (2008).

2.1 Basic methodology

Copulas are defined as a distribution function on the n dimensional unit cube. All marginal distributions are uniform on [0, 1]. Formally

$$C:[0,1]^n \to [0,1] \tag{2.1}$$

$$C\left(\mathbf{u}^{(i)}\right) = u_i \quad \text{if} \quad u^{(i)} = (1,\ldots,u_i,1,\ldots,1) \tag{2.2}$$

For every n dimensional hypercube in the unit hypercube the corresponding probability has to be non-negative:

$$\sum_{i=0}^{2^n-1} (-1)^{n-\sum_{i=1}^{n} j_i}\, C\left(u_1 + j_1\Delta_1,\ldots,u_n + j_n\Delta_n\right) \geq 0 \tag{2.3}$$

$$\text{if} \quad 0 \leq u_i \leq u_i + \Delta_i \leq 1 \quad \text{and} \quad i = \sum_{k=0}^{n-1} j_k\, 2^k \tag{2.4}$$

If the condition (2.4) is fulfilled, then copulas and multivariate distributions are linked to each other by Sklar's Theorem (Sklar 1959). Sklar proved that each multivariate distribution $F(x_1,\ldots x_n)$ can be represented with the help of a copula:

$$F(\mathbf{x}) = C\left(F_{X_1}(x_1),\ldots,F_{X_n}(x_n)\right) \tag{2.5}$$

Where $F_{X_1}(x_1)$ represents the i-th one dimensional marginal distribution of the multivariate distribution. If the distribution is continuous then the copula C in Eq. (2.2) is unique. Copulas can be constructed from distribution functions, as described by (Nelsen 1999):

$$C(\mathbf{u}) = F\left(F_{X_1}^{-1}(u_1),\ldots,F_{Xn}^{-1}(u_n)\right) \tag{2.6}$$

The advantage of using a copula is that it is invariant to strictly increasing monotonic transformations of the variables. Thus the frequent dilemma whether to transform data or not (for example taking the natural logarithms) does not occur in this case. An interesting and important property of a copula is whether the corresponding dependence is the same for high or low values. A bivariate copula expresses a symmetrical dependence, if:

$$C(u,v) = C(1-u,1-v) - 1 + u + v \tag{2.7}$$

This means that the copula density is symmetrical with respect to the secondary diagonal $u = 1 - v$ of the unit square and the copula density c fulfills:

$$c(u,v) = c(1-u,1-v) \tag{2.8}$$

More details can be found in Joe (1997), Nelsen (1999), Salvadori and Michele (2007).

2.2 Empirical Copulas

Besides theoretical copulas such as the normal copula or the t-copula, empirical copulas are introduced to represent empirical distribution of rank transformed data. Empirical copulas are defined as frequencies of observations similar to empirical cumulative distribution functions. For 2 dimensional case, let $\{(R_i, S_i)\}$ be the ranks associated with the random sample $\{(X_i, Y_i)\}$ for $i = 1,2,\ldots,n$. Then, the corresponding empirical copula C_n is:

$$C_n(u,v) = \frac{1}{n}\sum_{i=1}^{n} \mathbf{1}\left(\frac{R_i}{n+1} \le u, \frac{S_i}{n+1} \le v\right) \tag{2.9}$$

Where $u, v \in \mathbf{I}$ and $\mathbf{1}$ is an indicator function, n is the size of data. So, the transformation of the observed data $\{(X_i, Y_i)\}$ is given by taking the rank of each set of observed variables.

Nelsen (1999) defined *empirical copula frequency* by:

$$c_n\left(\frac{i}{n}, \frac{j}{n}\right) = \begin{cases} 1/n, & \text{if } (R_i, S_j) \text{ is an element of the sample} \\ 0, & \text{otherweise} \end{cases} \tag{2.10}$$

Empirical copula frequency represents the plots in scattergram. If one of data associated with rank $\{(R_i, S_i)\}$ exists on the $n \times n$ girds, the value of c^* at the coordinate is 1, otherwise the value is 0.

The estimation of the empirical bivariate copulas can be defined by counting the number of plots in each grid (Bárdossy 2006) smilar to relative frequency and this can be empirical version of copula density:

$$\begin{aligned} & c^*\left(\frac{2i-1}{2g}, \frac{2j-1}{2g}\right) \\ & = \frac{g^2}{n} \cdot \left| \left\{ (u_1, u_2) \in \left\{ \left(F_Z(z(t)), F_Z(z(t+k))\right) \right\}; \frac{i-1}{g} < u_1 < \frac{i}{g} \text{ and } \frac{j-1}{g} < u_2 < \frac{j}{g} \right\} \right| \end{aligned} \tag{2.11}$$

g is the number of grid, i and j are the indices of grids for u_1 and u_2 coordinates respectively. The equation indicates counting the number of data in the grids with the size $1/g \times 1/g$ for each and dividing by the total number of the data. Please note that empirical copula in this study refers to this definition of empirical copula.

The empirical copulas calculated from single time series data with certain time lag are called autocopulas. In the previous definition, 2 dimensional empirical copulas are calculated from 2 samples X_t and Y_t. But, for autocopula, its empirical copula is calculated from single sample X_t but with certain lag k. This means sample are expressed as $\{(X_t, X_{t+k})\}$ and its empirical autocopula is described as $c(u_t, u_{t+k})$. Also multidimensional empirical autocopulas with arbitrary dimension and time lags can be constructed in the similar way.

2.3 Basic Hypothesis of Temporal Copulas

For the application of copulas for time series analysis, a stochastic system is assumed, where the random variable at time *t* is described as *Z(t)* and there exists a dependency among the elements between *Z(t)*. As only one single realization is observed for a number of random variables, some assumptions have to be made:

1. Stationarity: for each set of times $\{t_1,\ldots t_n\}\subset N$ and time lag *k* such that $\{t_1+k,\ldots t_n+k\}\subset N$ and for each set of possible values $z_1,\ldots z_n$:

$$P\left(Z\left(t_1\right)<z_1,\ldots,Z\left(t_n\right)<z_n\right)=P\left(Z\left(t_1+k\right)<z_1,\ldots,Z\left(t_n+k\right)<z_n\right) \tag{2.12}$$

   This implies that for any two selected points at time t and $t+k$ in the investigated time interval, the bivariate temporal copula $\mathbf{C}_t$ corresponds to the random variable *Z(t)* and *Z(t+k)* is assumed to be function of time lag k and independent of the time *t*:

$$\mathbf{C}_t\left(k,u_1,u_2\right)=P\left[F_z\left(Z\left(t\right)\right)<u_1,F_z\left(Z\left(t+k\right)\right)<u_2\right]=C\left(F_z\left(Z\left(t\right)\right),F_z\left(Z\left(t+k\right)\right)\right) \tag{2.13}$$

2. The parameterization of the copula should enable the multivariate copula corresponding to any selected *n* times to reflect their temporal configuration.

3. The parameterization should allow arbitrarily strong dependence. This means that for a set of very close times, there should be a parameterization of copulas which is close to full dependence (Fréchet upper bound).

This stationarity is basic hypothesis to understand the time series, but it is not always valid and the system changes with time as it will be shown in the following chapters.

2.4 Measure of Asymmetry

In multivariate statistics, statistical information such as covariance or correlation can be obtained, which means, however, the loss of certain information. The advantage of applying copulas is that multivariate distributions can be described in the standardized form while still keeping the dependence structure.

Measuring the asymmetry of copulas could reveal another aspect of time series data. Asymmetry can be defined for the bivariate copula with time lag *k* (Li 2010):

$$\begin{aligned} A_1(k) &= E\left[(U_t - 0.5)(U_{t+k} - 0.5)\left((U_t - 0.5) + (U_{t+k} - 0.5)\right)\right] \\ A_2(k) &= E\left[-(U_t - 0.5)(U_{t+k} - 0.5)\left((U_t - 0.5) - (U_{t+k} - 0.5)\right)\right] \\ U_t &= F_{Z_t}(z_t), U_{t+k} = F_{Z_{t+k}}(z_{t+k}) \end{aligned} \tag{2.14}$$

Where $A_1(k)$ is *asymmetry1*, $A_2(k)$ is *asymmetry2*. If we set $X = U_t - 0.5$ and $Y = U_{t+k} - 0.5$, this can be more simply described:

$$\begin{aligned} A_1(k) &= E\left[XY(X+Y)\right] \\ A_2(k) &= E\left[-XY(X-Y)\right] \end{aligned} \tag{2.15}$$

This means, if more realizations of X and Y are both positive, *asymmetry1* would be positive. If more realization of X and Y are both negative, then *asymmetry1* could be negative. The functions of contribution of each realization to the asymmetries are visualized in Figure 2-1 and Figure 2-2.

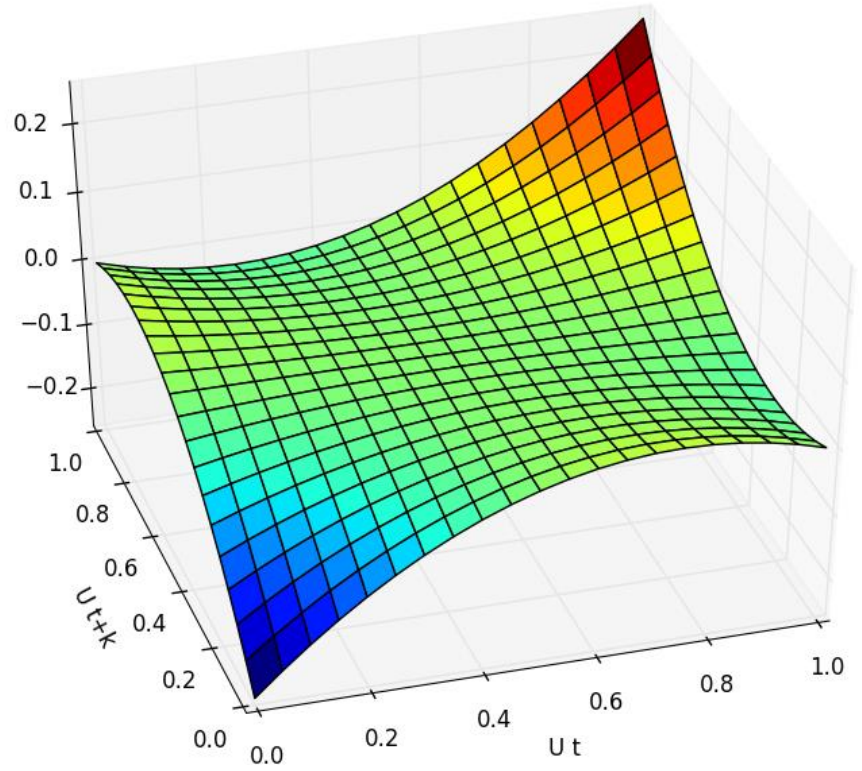

Figure 2-1 visualization of asymmetry function (*asymmetry1*)

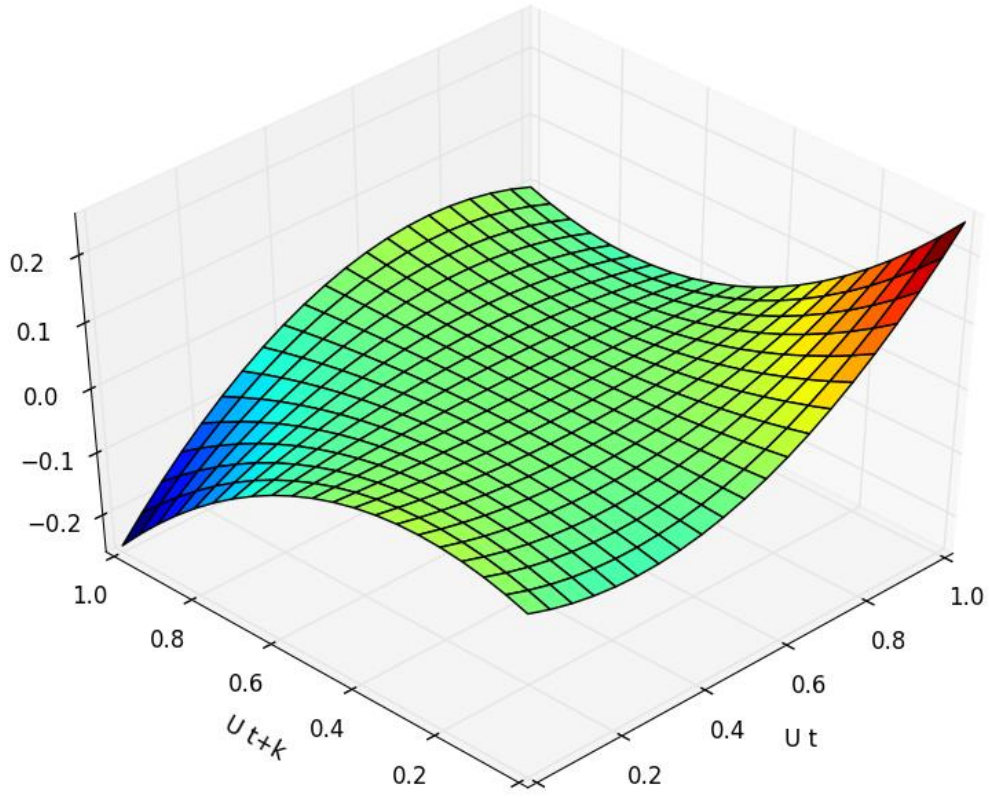

Figure 2-2 visualization of asymmetry function (*asymmetry2*)

2.5 Asymmetry of Discharge Data

The hydrograph of sample discharge data from the measuring station "Andernach" and its scatter plot of empirical copula $c_n\left(u_t, u_{t+5}\right)$ is shown in the Figure 2-3.

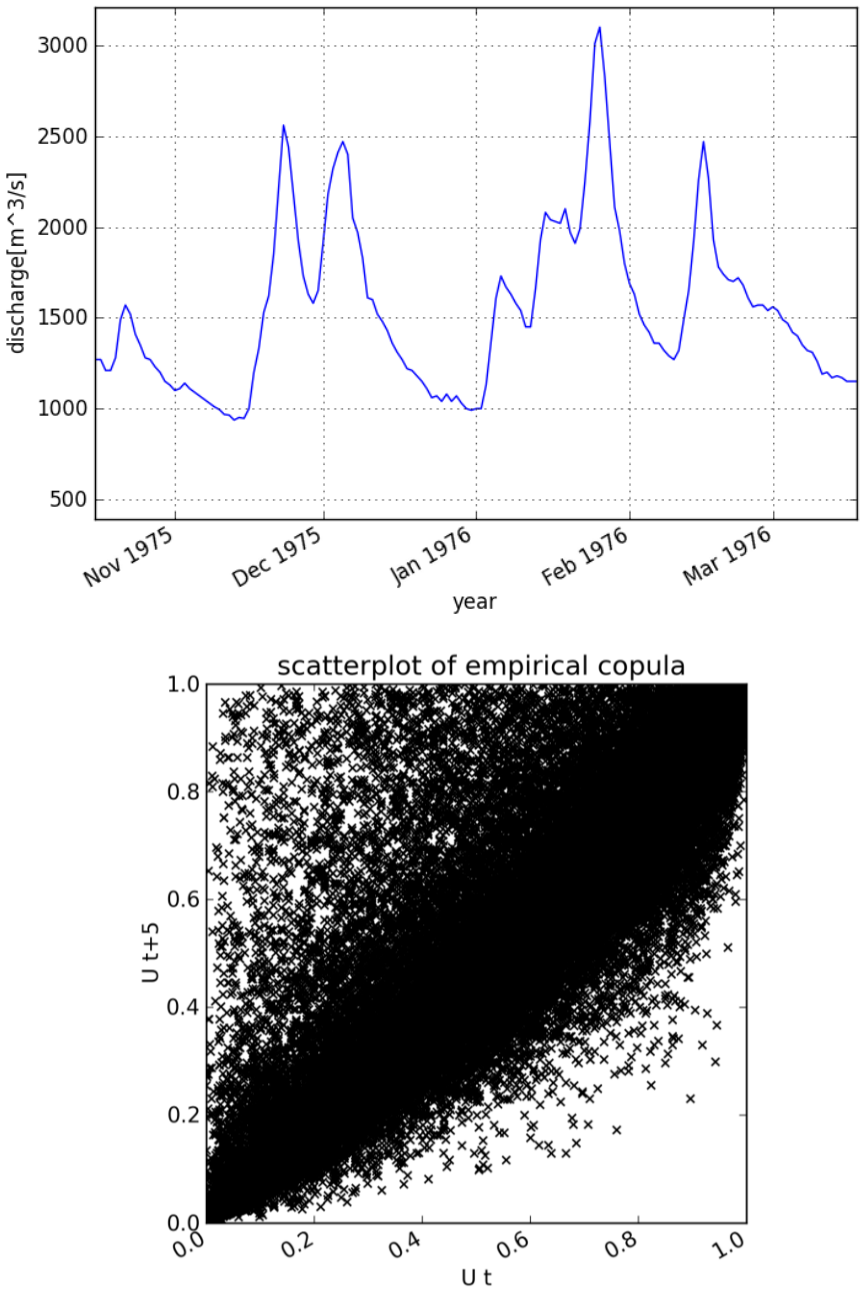

Figure 2-3 example of the discharge data (top) and its empirical copula corresponding to time lag *k = 5* [*days*] (bottom)

By looking at the hydrograph and scatter plot two asymmetric characteristics can be recognized (Figure 2-4).

1. The first point is that the duration of high flow period and low flow period is not symmetric. Rainfall events, which cause large peak discharge, are less likely to continue for long time and most of the time it has a small amount of discharge. This leads to the *asymmetry1*.

2. The second point is the recession curve. Right after the rainfall, the catchment responds instantaneously and the discharge amount rises sharply. Once rain stops and peak discharge is observed, then the water level start to decrease usually slower than the increase. This characteristic can be called *asymmetry2*.

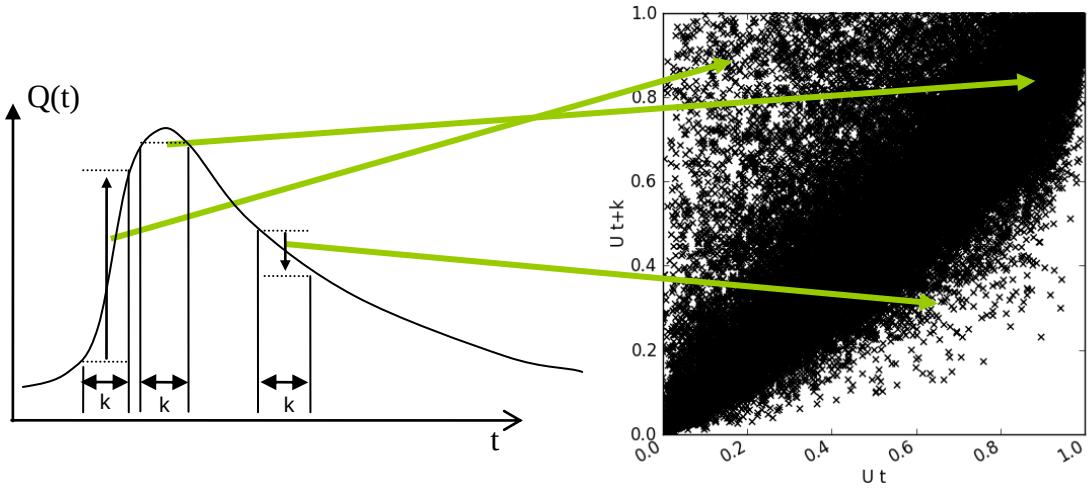

Figure 2-4 the source of the asymmetry in the discharge data

These characteristics can be seen in Figure 2-5 as asymmetric property on *2*-dimensional copula domain in the direction of each diagonal.

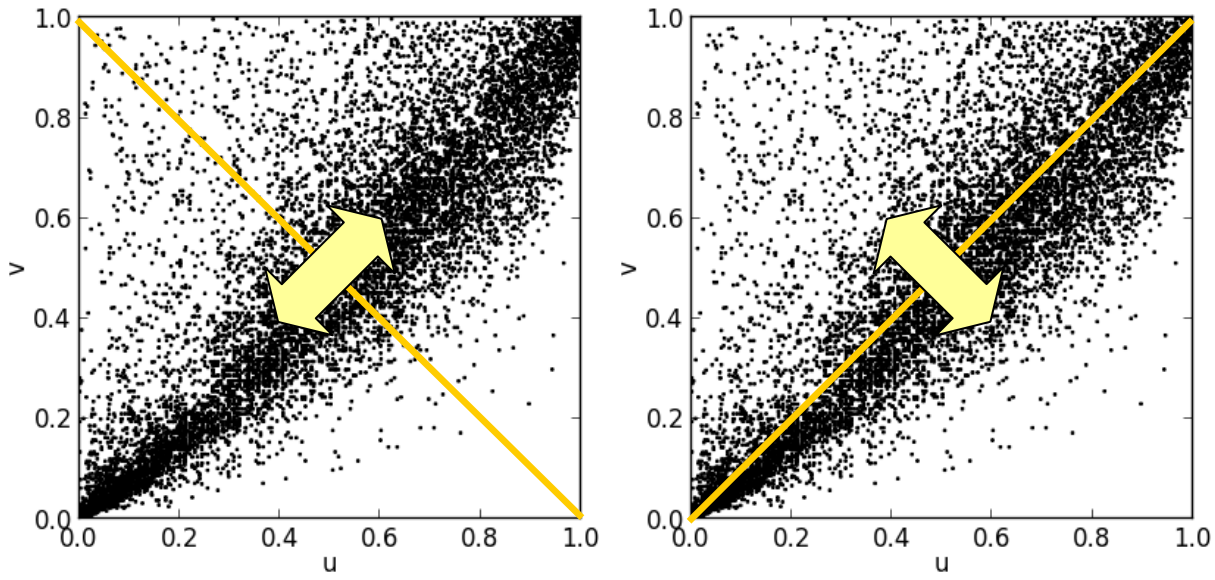

Figure 2-5 conceptual sketch of asymmetry1 (left) and asymmetry2 (right)

For the case of *asymmetry1* (Figure 2-5 left), there are more points around (u,v) = (0,0) than (u,v) = (1,1), which is due to the characteristic that low flow period is longer than high flow, eventually *asymmetry1* is apt to be negative for the discharge data. For the case of *asymmetry2* (Figure 2-5

right), the upper-left part of empirical copula is denser than bottom-right corner, which accounts for the property that increases of discharge are faster than the decreases.

Through the above discussion, it is suggested that asymmetry can be a new criterion relevant to the catchment characteristics. Now, these characteristics are empirically analysed for different catchments for different time periods.

2.6 Kernel Density Estimation of Copula with Beta Kernel

Kernel density estimation is the non-parametric way to estimate probability distribution functions. Although the choice of the kernel has impacts on the tail, standard normal density function is typically used. The well-known problem of kernel density estimation for copulas, "Curse of Dimension", is that the bias of the copula estimator at the corner and border expands as dimension increases. This bias is caused by symmetric and unbounded kernel. For example, if a standard Gaussian kernel is chosen for copula kernel density estimation, assuming there is an observation such that $u = 0$. Because standard Gaussian kernel is symmetry, the half part of its kernel exceeds the boundary, which doesn't contribute to the density at $[0,1]^d$

One of the methods to avoid the boundary bias of copula estimation is to introduce bounded and adaptive kernel such as beta kernel (Chen 2000) as defined below:

$$K\left(x, X_i\right) = \frac{x^{\frac{X_i}{h}}\left(1-x\right)^{\frac{1-X_i}{h}}}{B\left(\frac{X_i}{h}+1, \frac{1-X_i}{h}+1\right)} = \frac{x^{\alpha-1}\left(1-x\right)^{\beta-1}}{B\left(\alpha,\beta\right)} \tag{2.16}$$
$$\alpha = \frac{X_i}{h}+1, \qquad \beta = \frac{1-X_i}{h}+1$$

Similar to the beta distribution, distribution of beta kernel is bounded in [0,1] and the form of the kernel changes with the position of kernel in the domain. Figure 2-6 displays the sample of beta distribution for *1*-dimensional case.

Autocopulas estimated with beta kernel are the smoothed version of empirical copula. It needs more calculation power, but it could reduce the impacts of uncertainty for small amount data, which are used for the analysis of copula distance in chapter 7 and the non-Gaussian statistical simulation in chapter 8.

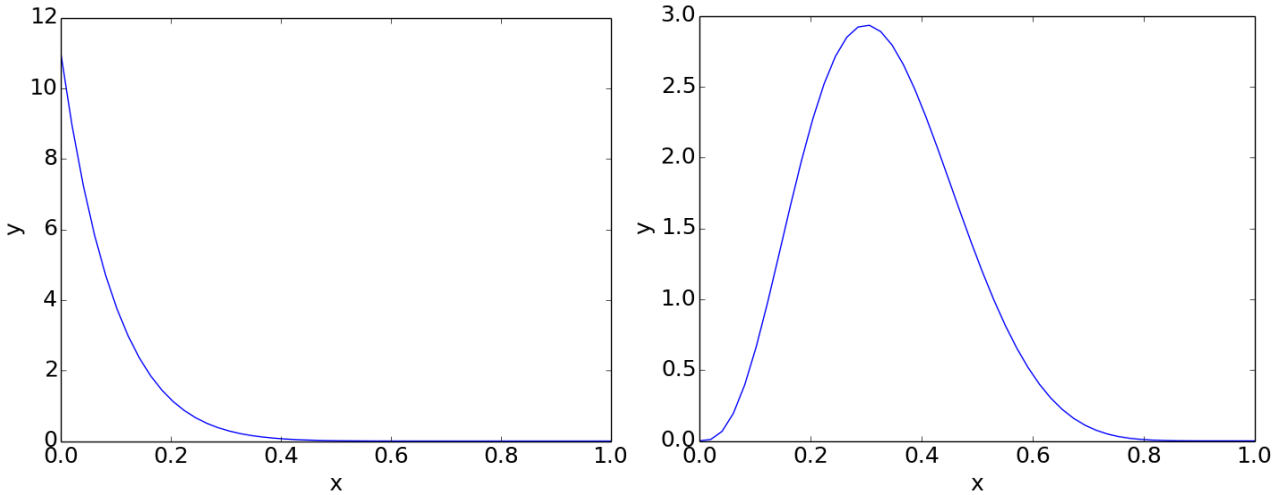

Figure 2-6 sample of the beta distribution with parameter $h=0.1$, $x = 0$ (left) and $x = 0.3$, $h = 0.1$ (right)

3 Analysis of Empirical Copula with Asymmetry

3.1 Simple Application of Empirical Copula

For the purpose of investigating the applicability of copula based analysis in certain spatial and temporal extent, the time series data from 7 gauging stations along the Rhine River are chosen. For these gauging stations, daily discharge data exists from the years 1900 to 2000. The gauging stations Andernach, Kaub, Worms and Maxau are located in the main stream of the Rhine while Kalkofen, Cochem and Plochingen are located in tributaries as shown in Figure 3-1.

Figure 3-1 measuring stations of 7 discharge data located in the Rhine and its tributaries (Ullrich 2005)

3.1.1 Cross Copulas

As a first step for the spatial analysis of discharge data, cross copulas are introduced as a matrix of bivariate empirical copulas which are calculated from all the bivariate combinations of time series data of 7 gauging stations as shown in Figure 3-2.

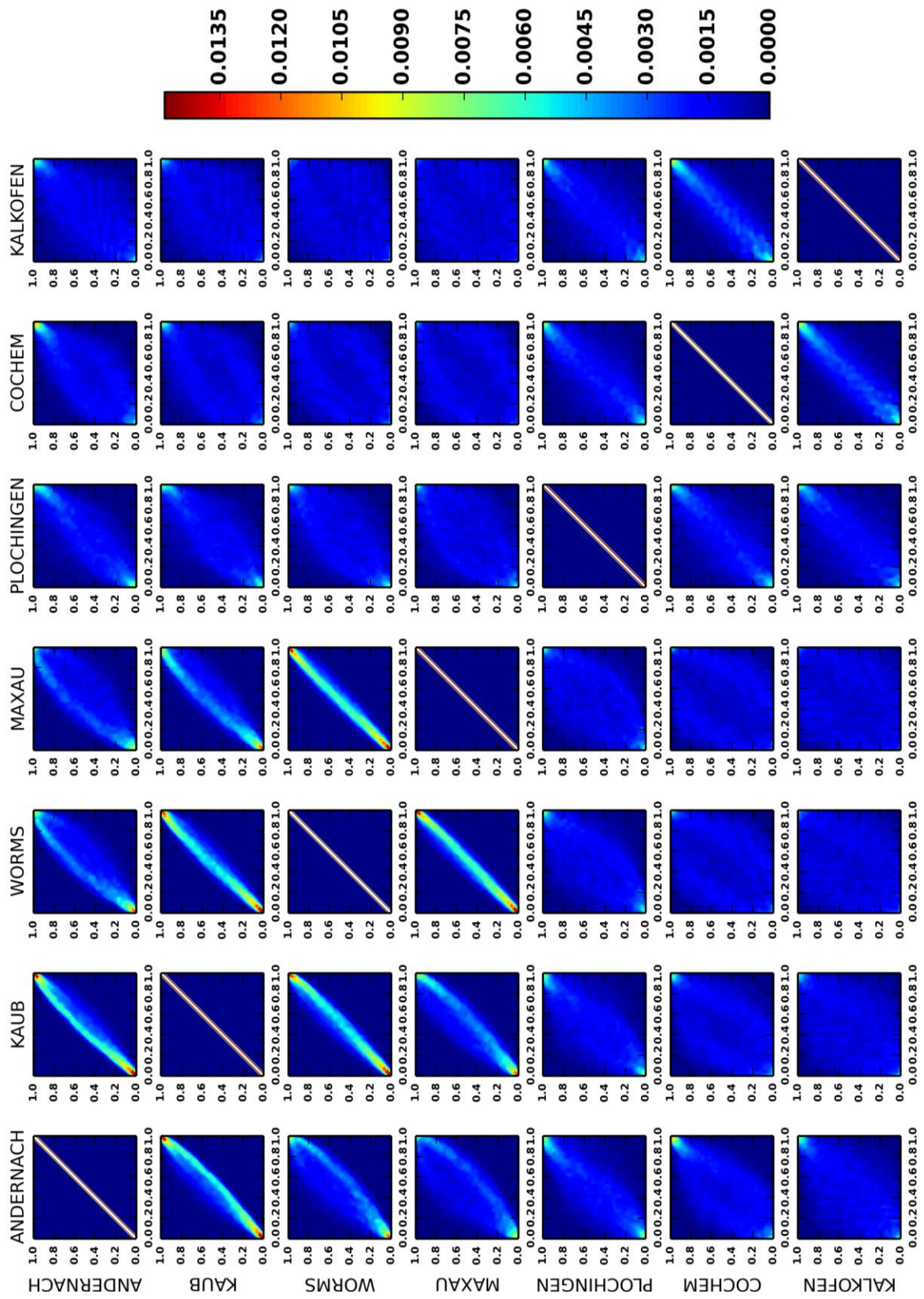

Figure 3-2 cross copulas of discharge data from 7 gauging stations

Similar to covariance matrix, copulas in upper right triangle of cross copulas are same to the copula in lower left triangle of cross copulas. The copulas on the diagonal line of cross copulas are copulas of two identical discharge data, thus this shows linear relationship between two variables.

The variations of dependence structures between different discharge data combinations are simply the consequence of spatial configuration of gauging stations as summarized below:

1. Quasi Linear Dependency (example: Andernach ⇔ Kaub)

   As shown in Figure 3-3 (left), the empirical copulas show strong dependency due to the spatial proximity of gauging station being located in the same river reach.

2. Weaker Dependency (example: Kaub ⇔ Plochingen)

   One of the gauging station is located in the tributary and the other located in the main stream of the river Rhine. As a consequence, the impact of the discharge on the other station is mitigated by confluence and dependency become weaker as shown in Figure 3-3 (center).

3. Almost no dependency (example: Worms ⇔ Kalkofen)

   The measuring stations are remotely located. Also, one (or both) of the measuring stations has small discharge. Therefore, the dependency between 2 stations is very weak.

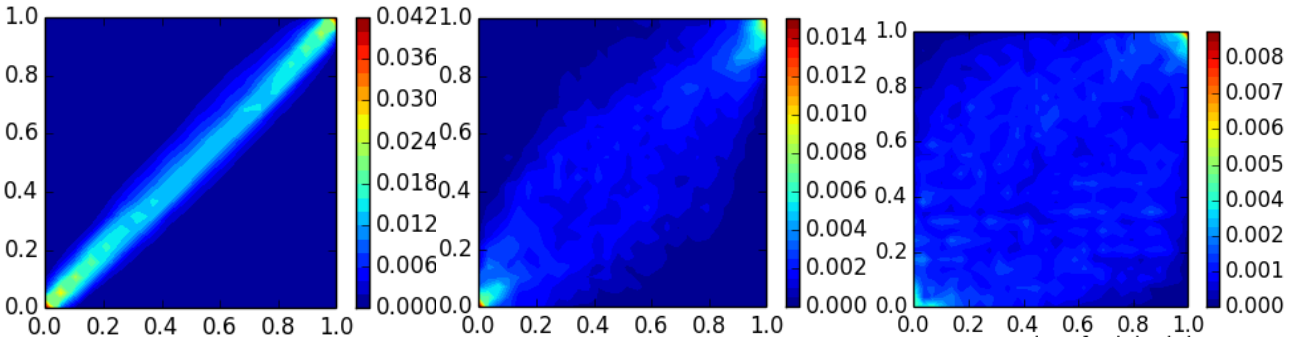

Figure 3-3 Bivariate empirical copula of two discharge time series from Worms and Maxau (left) Kaub and Plochingen(center) and Worms and Kalkofen(right)

(Colour legends in these figures are different from the legend of empirical copulas in Figure 3-2)

3.1.2 Autocopulas

Secondary, bivariate empirical autocopulas are calculated from single discharge time series after subtraction of annual cycle of mean for each gauging station with different time lag *k*. Figure 3-4 shows empirical autocopulas of 7 gauging stations corresponding to time lag *k* = *1,3,7,15,30,180,365*[days].

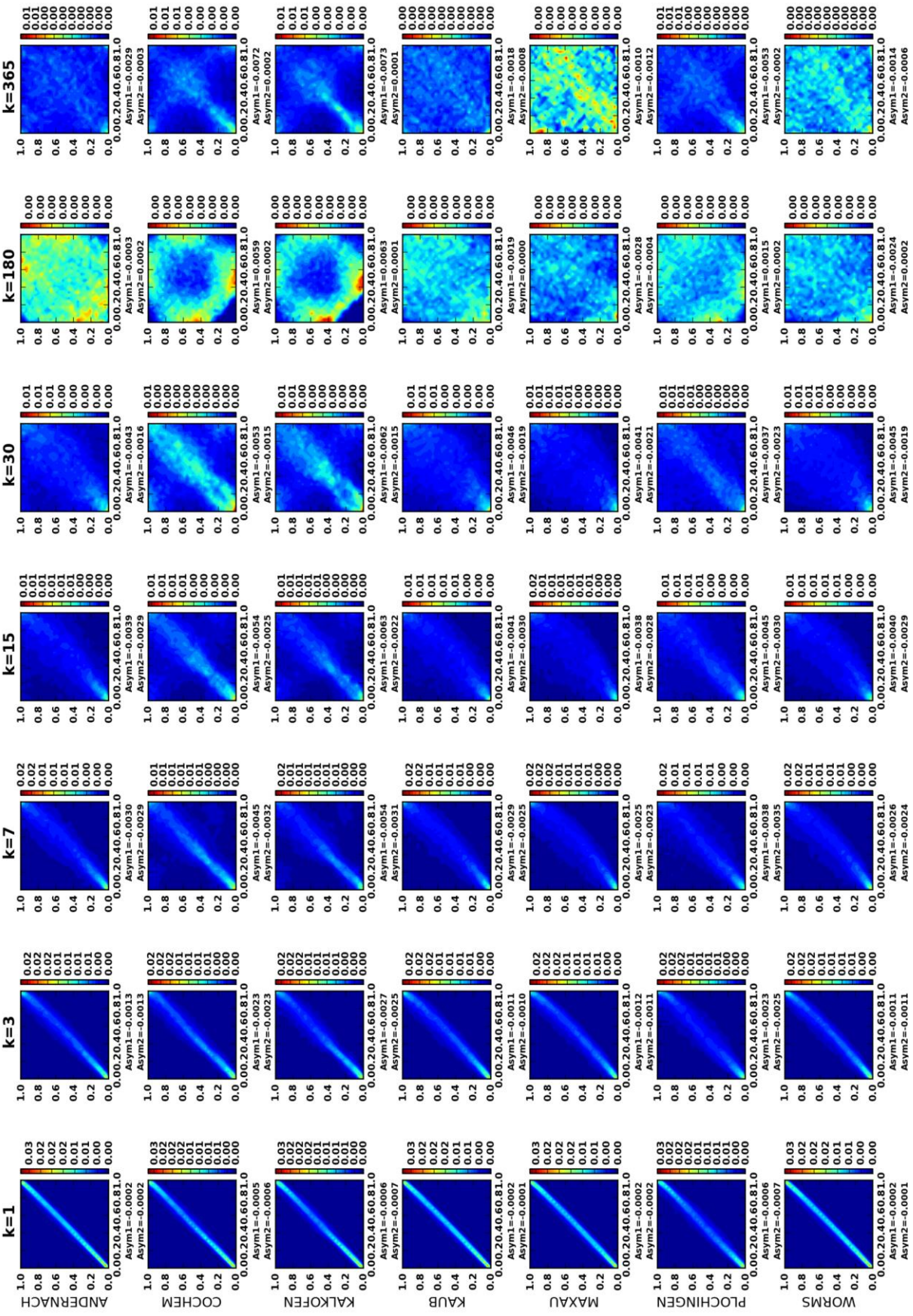

Figure 3-4 Autocopulas of discharge data corresponding to different time lags k after subtraction of annual cycle of mean (standardization1)

For time lag $k = 0$, the autocopulas show for sure linear relationship. On the other hand, for the autocopulas with lag $k > 0$, the asymmetric characteristic of the time series evolves as time lag k increases and shows different structures.

The property of autocopulas corresponding to different lags is summarized below:

1. There exists strong dependency for smaller lags (for lag $k = 1\sim3$)

   The relation is close to linear as shown in Figure 3-5 (left).This dependency is caused by the simple fact, that if the water level of river is high today, tomorrow also likely to be high. If the water level today is low, tomorrow also likely to be low. Furthermore, the duration that water level high is shorter than the duration that the water level is low in general. This causes the more points at lower left corner of bivariate empirical copula. Therefore, dependency in smaller values is stronger than bigger one, which causes negative value in *asymmetry1* according to the definition in Eq. (2.14).

2. Dependency becomes asymmetric as lag time increases (for lag $k = 7\sim30$)

   As shown in Figure 3-5 (center), the autocopula with this time lag is less symmetric for both directions of diagonals. Usually, water level reaches to the peak soon after the rainfall event, but the period of recession to normal water level takes longer. The *asymmetry2* with time lags (k = 5~30) is caused by unequal increment and decrement of discharge in a flood event. In this way, the copulas with smaller lag time ($k = 7\sim30$) tend to capture the property of flood events.

3. Capture the seasonal property of rainfall (for lag $k > 50$)

   As shown in Figure 3-5 (right), the distribution of copulas gets scattered all over the copula domain as the lag time k increases. It does not show linear relationship like autocopula with $k = 1\sim30$ shows, therefore its rank correlation of autocopulas gets smaller. Due to the big time lag, there will be no more direct relation between two time points. Instead, it starts to capture the seasonal characteristic as shown in Figure 3-5(right), even though the annual average is subtracted from the original data. The reason of this result will be discussed in section 3.4. In the case for lag $k = 365$, which means comparing the two values with one year separation, the autocopulas are supposed to show the relation between the values in the same season.

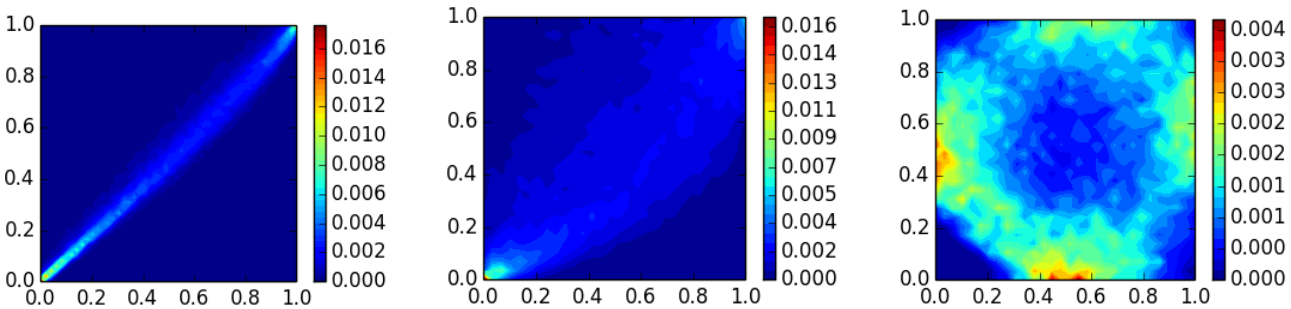

Figure 3-5 Bivariate empirical autocopulas of discharge time series of Andernach with lag $k = 3$ [days](left), Maxau with lag $k = 15$[days](centre) and Cochem with lag $k = 180$[days](right)

3.2 Asymmetry Changes corresponding to Time Lag k

Now, the study is focusing more on the asymmetry changes corresponding to time lag *k*, partially because it might represents more the catchment characteristics, which can be transferable for the different catchments, and potentially could introduce new insights into time series analysis.

In the previous sections, it is acknowledged that for the different lag times *k* the dependence structure develops in a different way. In addition, it is desirable to know how much impact time lag *k* has on the asymmetries.

In this section, the changes of asymmetries are plotted along the time lag *k* similar to correlograms (Box and Jenkins 1976) in time series analysis, which plots the autocorrelation over the time lag *k*.

3.2.1 Asymmetry1

Asymmetry1 was defined in the section 2.4 as shown in Figure 2-5. It reflects the temporal configuration of high and low flow periods.

$$A_1(k) = E\left[\left(F_{Z_t}(z_t) - 0.5\right)\left(F_{Z_{t+k}}(z_{t+k}) - 0.5\right)\left(\left(F_{Z_t}(z_t) - 0.5\right) + \left(F_{Z_{t+k}}(z_{t+k}) - 0.5\right)\right)\right] \qquad (3.1)$$

In the Figure 3-6 the variation of *asymmetry1* is plotted for lag *k = 1* up to lag *k = 365* for discharge data sets from 7 different gauging stations. The most remarkable behaviour for all the data sets is that the *asymmetry1* drops down (as far as -0.008) for time lag *k = 0~30* and rises slowly back to 0. For smaller *k*, *asymmetry1* simply reflects the characteristic that the low flow conditions last longer than periods of flood events. As time lag *k* increases (*k > 30*), it is supposed seasonal characteristics of the catchment get more dominant. For the gauging stations, Worms, Maxau and Kaub, *asymmetry1* is positive for time lags k around 140 – 220 days. One possible reason of that unusual behaviour of *asymmetry1* is the influence of snow melt: the rainy season in summer and snow melt in spring coincide at time lag *k = 140~220*. Except for these three gauging stations, after lag k > 100, *asymmetry1* does not show any notable behaviour and rather seems dominated by noise.

Figure 3-7 shows the variation of *asymmery1* for larger time lag *k* (*0 < k < 1200*). This figure demonstrates, variation of *asymmery1* behaves periodic way with the cycle of 1 year (k = 365), reflecting the nature characteristic that season has 1 year cycle.

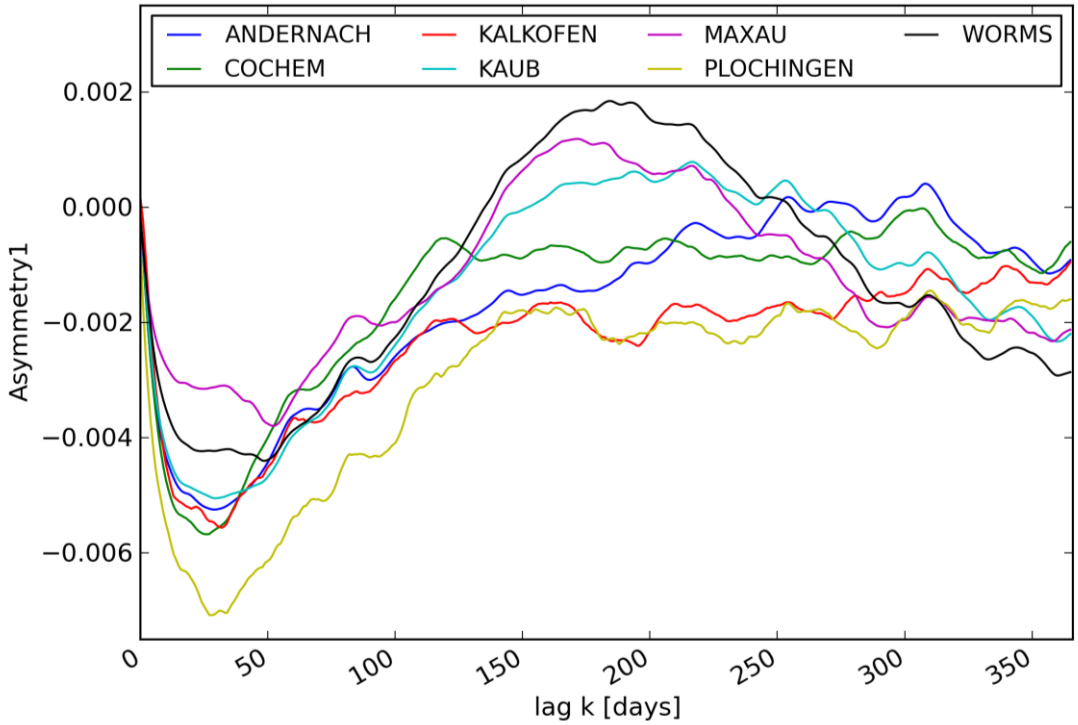

Figure 3-6 variation of *asymmetry1* corresponding to lag time k [days]

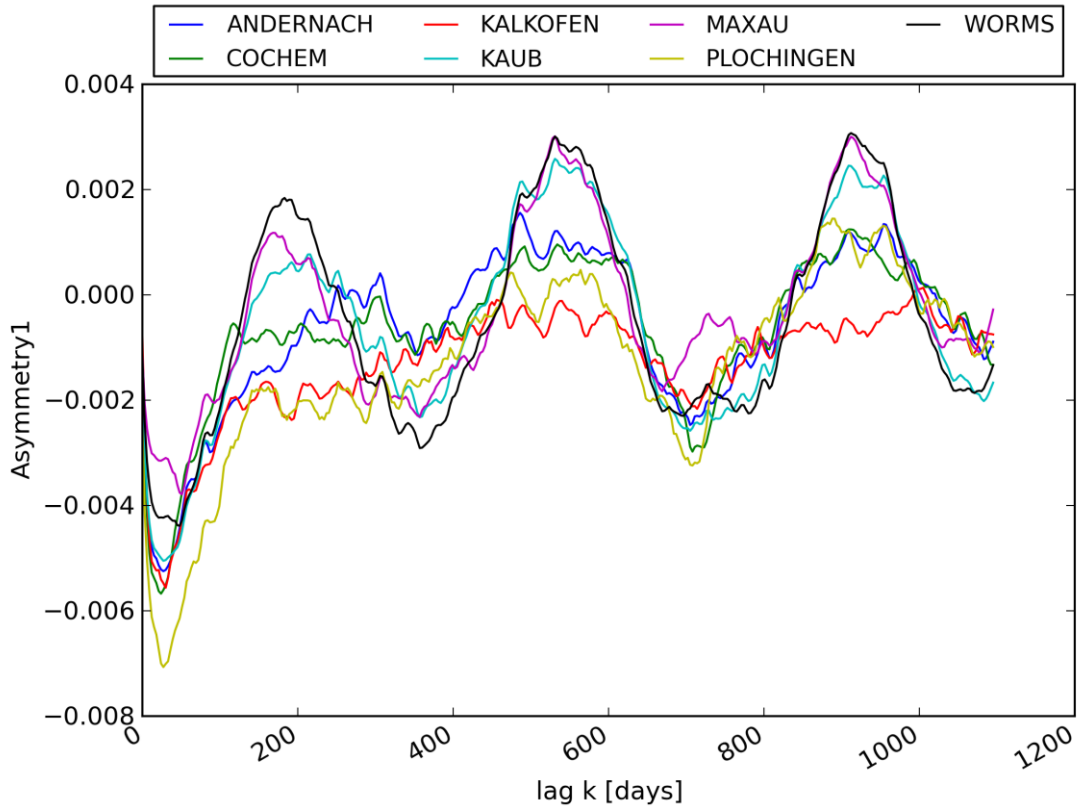

Figure 3-7 variation of *asymmetry1* corresponding to lag time k [days] for $0 < k < 1200$

3.2.2 Asymmetry2

Asymmetry2 was defined in section 2 as shown in Figure 2-5. It reflects the difference of increment and decrement of discharge; especially, it is related to the time that water level increases to the peak flow and recedes to the base flow. Figure 3-8 and Figure 3-9 shows the variation of *asymmetry2* corresponding to the time lag *k*.

$$A_2(k) = E\left[-\left(F_{Z_t}(z_t) - 0.5\right)\left(F_{Z_{t+k}}(z_{t+k}) - 0.5\right)\left(\left(F_{Z_t}(z_t) - 0.5\right) - \left(F_{Z_{t+k}}(z_{t+k}) - 0.5\right)\right)\right] \quad (3.2)$$

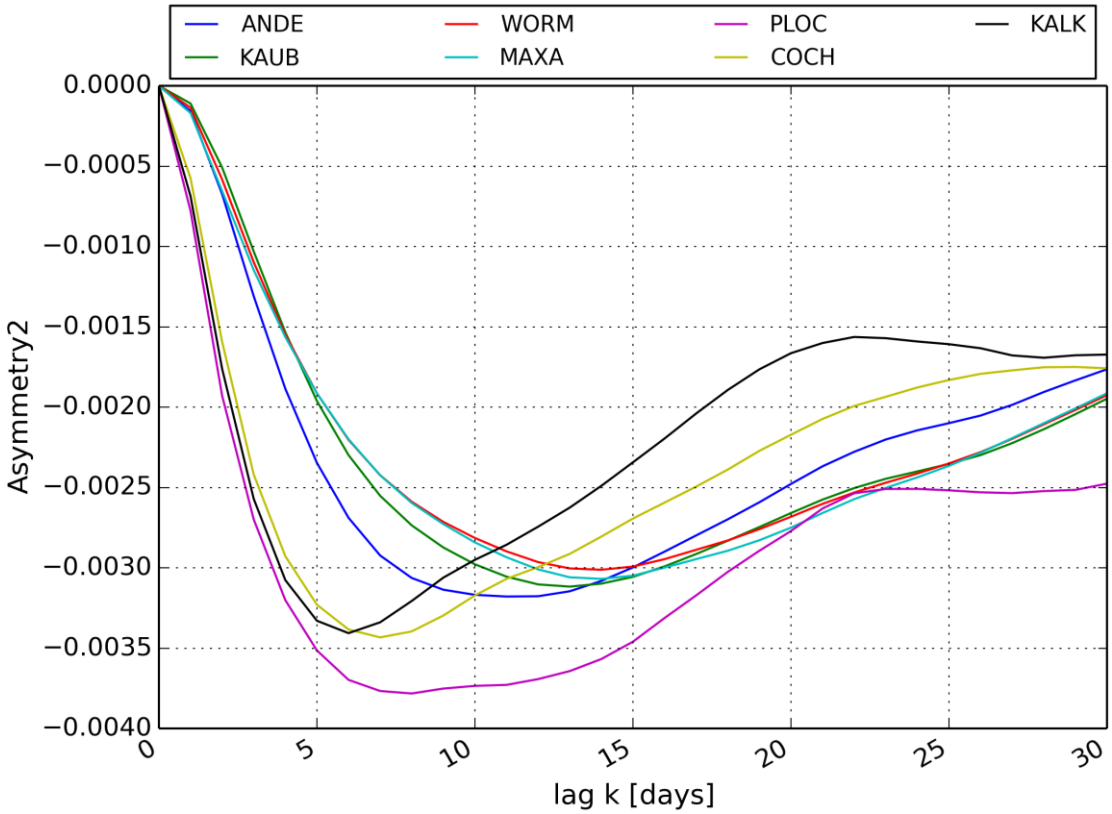

Figure 3-8 variation of *asymmetry2* corresponding to lag *k* [days] (for *0 < k 30*)

For time lags *0 < k < 30*, we can see a small drop of *asymmetry2* down to values around *-0.002 ~ -0.004*. This is caused by the difference between the duration that water level increases to the peak discharge and recedes to the normal state after rainfall event. The number of flood events affects the intensity of drop down of *asymmetry2*, because it gives more points in the lower right side in bivariate empirical copula with time lag *k*.

For time lags *30 < k < 180*, a different behaviour of *asymmetry2* can be seen for each river. The reason could be the difference of seasonality as it can be seen in annual cycle of mean (Figure 3-11). The figure shows annual cycles of mean are different for different rivers, which are supposed to be causing asymmetric behaviour for the bigger lag time *k* (*k > 30*). For example, the annual cycle of mean is big in the spring due to the snow melting. As a result, the annual cycle of Maxau and Worms looks more symmetric than the annual cycle of other stations. Therefore, the value of *asymmetry2* is relatively stable for Maxau and Worms in Figure 3-8, while the amplitude of oscillation of *asymmetry2* is big for the results of other stations.

For the lag *k = 183* [days], *asymmetry2* converge to 0 for Andernach, Worms, Cochem and Kalkofen. For Kaub, Maxau and Plochingen get close to 0 for k = *183* [days]. The cycle of seasonality, namely cycle of annual cycle is 365 days (or 366 days for leap year), therefore calculate copulas with time lag *k =183* means, we put the same amount of seasonality in empirical copulas in terms of *asymmetry2*. For example, if a plot of empirical copulas can be obtained from a pair of data (*X(t), X(t+183)*), the one data can be a combination of the data from winter and summer. Then another pair of data (*X(t+183), X(t+183×2)*) means the data from summer and winter, which cancels out *assymmetry2* in copulas. Thus, empirical copulas with time lag k = 183 tends to be symmetric and result in *assymmetry2 = 0.*

For the lag *k > 183*, say *assymmetry2* increases and decreases somehow symmetric for the case of lag *k < 183*. *Asymmetry2* decreased to 0 at time lag *k = 365* due to the same reason that *asymmetry2* will be 0 for the lag *k = 183* days. In fact, the seasonal cycle of *asymmetry2* can be seen as in Figure 3-9.

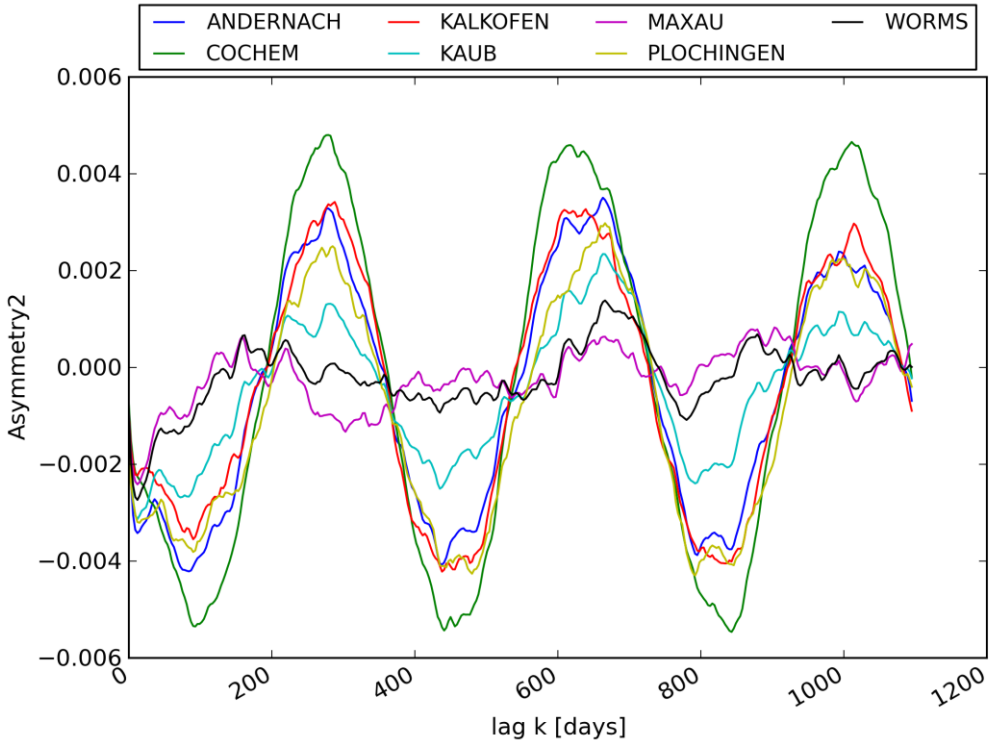

Figure 3-9 variation of *asymmetry2* corresponding to lag *k* [days] (for *0 < k <1200*)

3.3 Smoothed Annual Cycle

In the previous analysis, the possibility was pointed out that seasonality affects the asymmetry changes for larger time lag *k*. One way to reduce the seasonal effects is to subtract the annual cycle from original data. Another way is to divide the original time series by the annual cycle of standard deviation. It is possible to estimate the annual cycle by fitting Fourier series. But, in this study, the annual cycles are calculated by smoothing values around each calendar day with weighting function.

In general, annual cycle could indicate the expectation (mean) of discharge on each calendar day, but it also can be annual cycle of standard deviation or any seasonal behavior of time series (Wu et al. 2008). In this study, annual cycle of mean is calculated by averaging values on each calendar day as follows:

$$\mu_{t|365} = E\left[X_{t|365} \right] \tag{3.3}$$

where t is the time step, $t|365$ means $t \bmod 365$, therefore $t|365$ indicates the calendar day at time step t [*day*] (leap year is taken into account in the calculation). This result is shown in Figure 3-10.

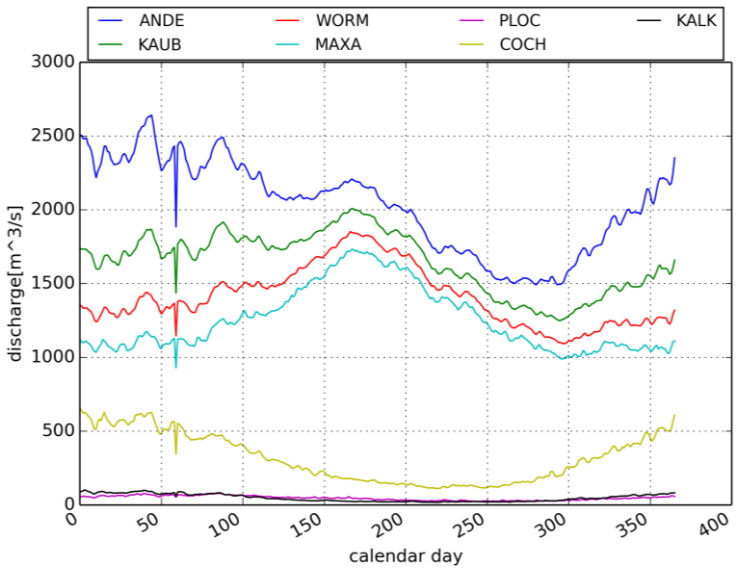

Figure 3-10 annual cycle of mean for discharge time series without smoothing

After this calculation, the annual cycles are smoothed by taking the weighting average for 90 days:

$$\mu^{*}_{t|365} = \frac{1}{2N}\sum_{i=0}^{N/2}\left(\frac{1}{2} - \frac{i}{N}\right)\left(\mu_{t+i|365} + \mu_{t-i|365}\right) \tag{3.4}$$

Where N is the length of the smoothing window. The smoothed annual cycles for $N = 90$[days] are shown in Figure 3-11 and the seasonality is clearly seen in this figure. For example, the high values are seen around calendar day 170 for the rivers in which snow melt is dominant. For the rivers, in which there is less impact of snow melt, the peaks of annual cycle of mean are in calendar day 0~50, which correspond to January or February.

The reason that N = 90[days] was chosen in this study is that it looks more spiky and less smooth for *N = 30* or *60* as shown in Figure 3-12

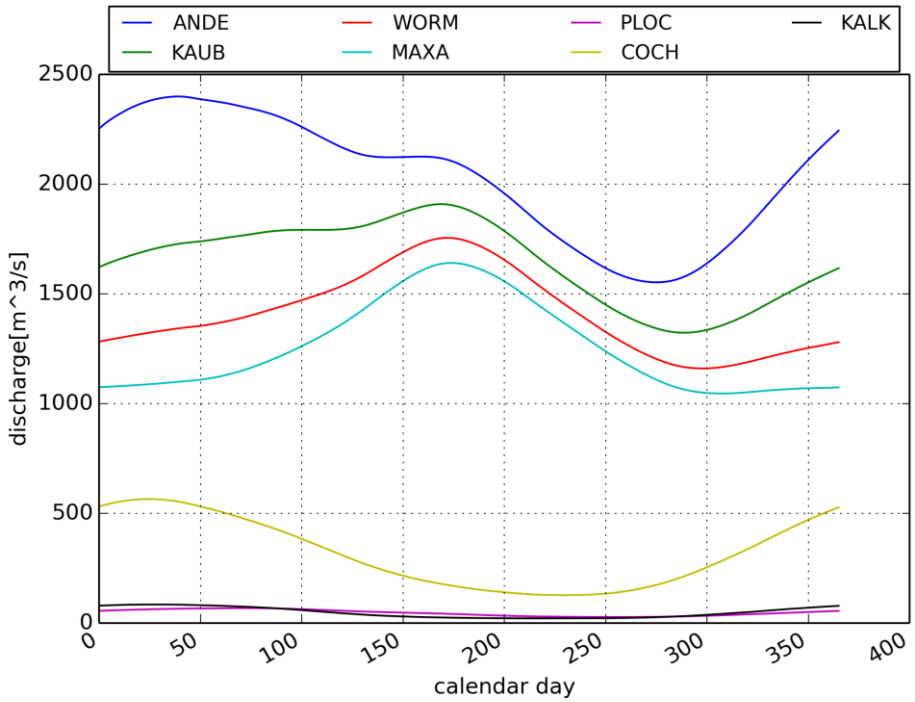

Figure 3-11 annual cycle of mean for discharge time seires *N = 90*[days]

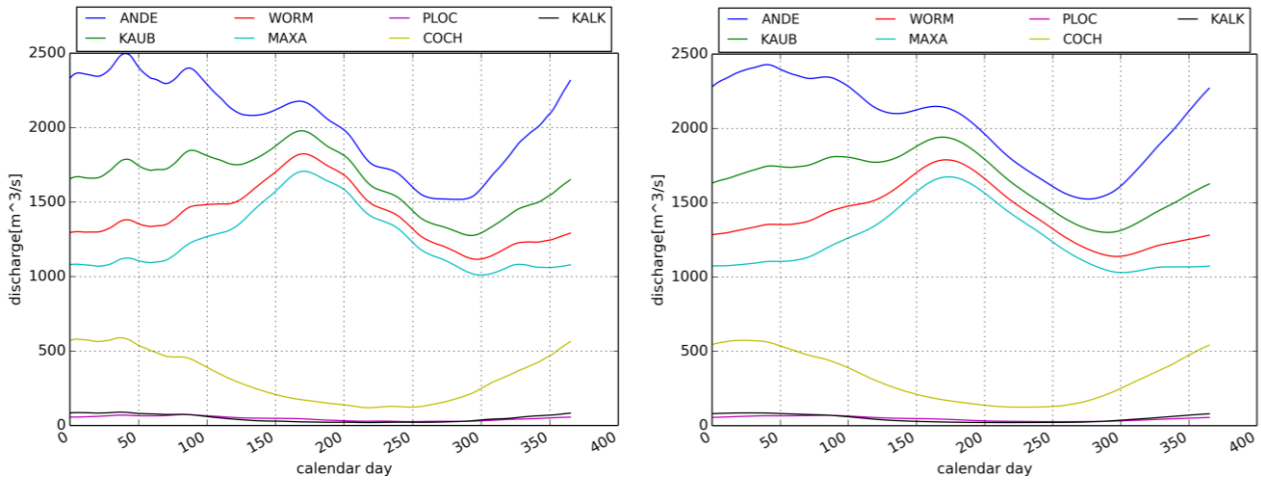

Figure 3-12 annual cycle of mean for discharge time seires *N = 30*[days] (left) and *N = 60*[days](right)

3.3.1 Standardization1: Subtraction of Annual Cycle of Mean

Now, for the elimination of this seasonality, annual cycle of mean is subtracted from the original time series. This type of standardization is called Standardization1 in this study and used in the further analyze. Figure 3-13 shows part of this discharge time series.

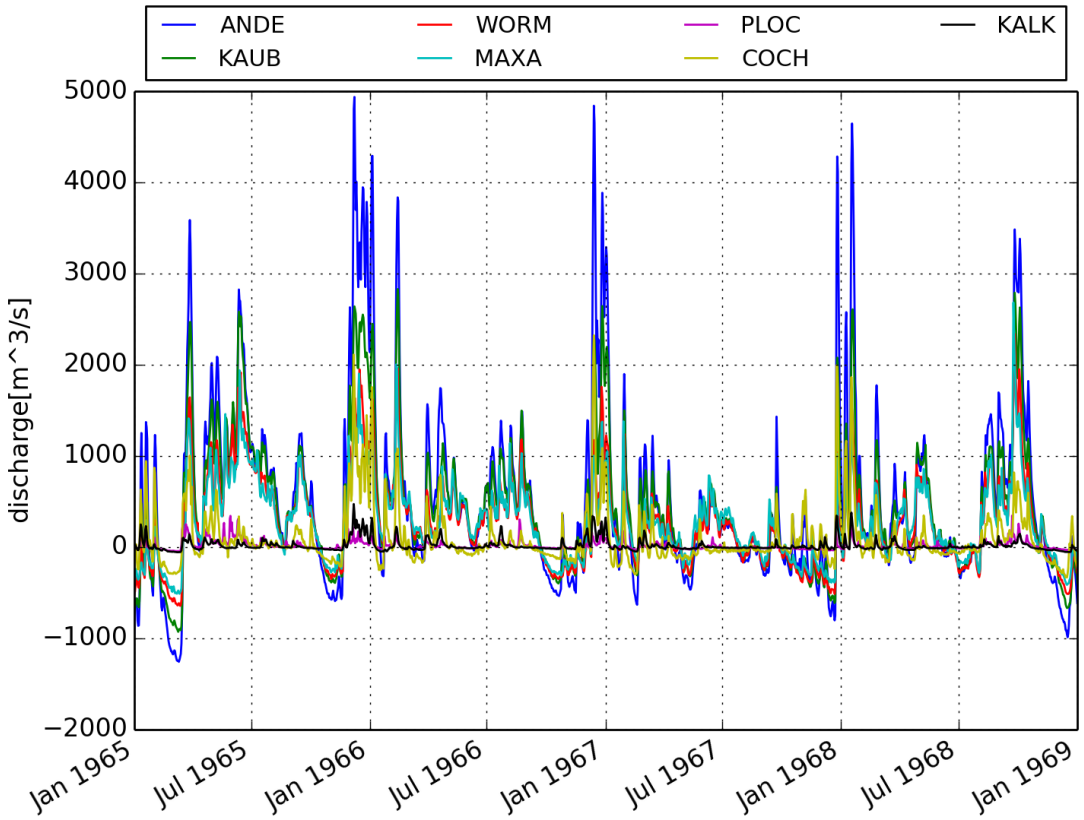

Figure 3-13 sample of discharge time series after subtraction of annual cycle (standardization1)

What interesting in Figure 3-13 is that, although the annual cycle of mean is subtracted from the original time series, the seasonal behavior can be still identified. That is, it can be seen that clear and strong oscillations exist for the river Andernach and Kaub in winter period due to the seasonal rainfall. Also for some gauging stations, peaks are observed in the beginning of spring due to snow melt. This characteristic can be said to seasonal variance, which is calculated as annual cycle of standard deviation as follow:

$$\sigma_{t|365} = E\left[\sqrt{\left(X_{t|365} - \mu_{t|365}\right)^2}\right] \tag{3.5}$$

Where $\sigma_{t|365}$ is the standard deviation of calendar day.

Similar to the case of annual cycle of mean, annual cycle of deviation is smoothed for $N = 90$[days] and shown in Figure 3-14. This figure shows annual cycle of standard deviation is high in winter, while annual cycle of standard deviation is low in summer, although the annual cycle of mean is high in summer. This could indicates, the impacts of rainfall events in summer on discharge is less intensive. It is also possible that the increase of discharge due to the snow melt causes smaller standard deviation in this season.

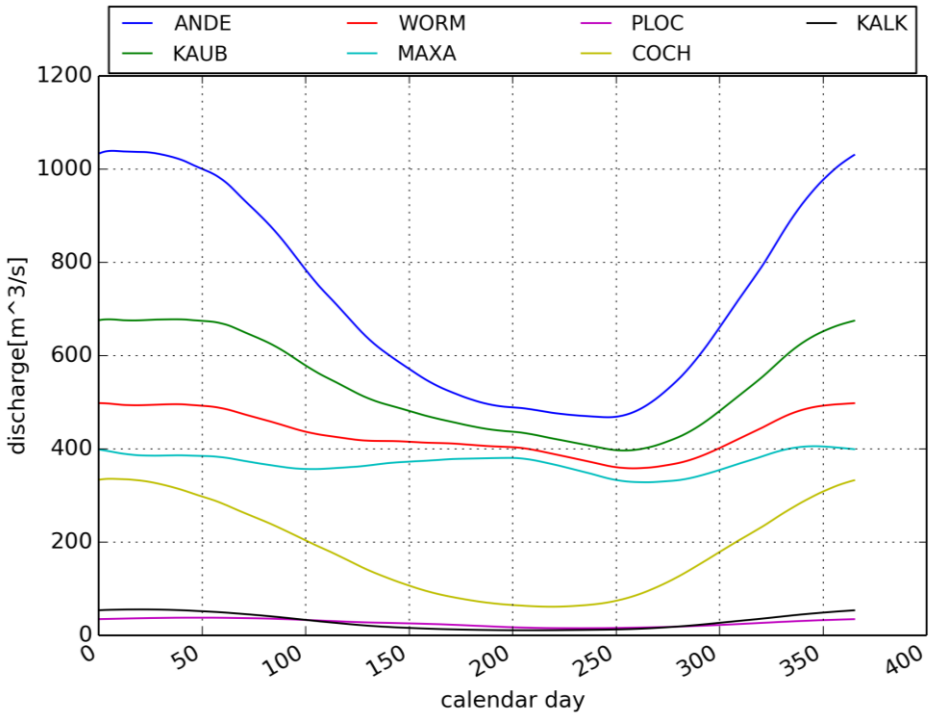

Figure 3-14 annual cycle of standard deviation of discharge time series

It is also true in Figure 3-14 that standard deviation is in general big for the gauging station in which the average discharge is big.

In Figure 3-15, it was checked how much deviation exists per annual cycle of mean, dividing the annual cycle of standard deviation by annual cycle of mean for each calendar day. This means the value on January 1st is calculated by dividing the annual cycle of standard deviation on January 1st by the value of annual cycle of mean on January 1st. Figure 3-15 shows there are clear difference between the river with smaller discharges (Kalkofen, Cochem, Plochingen) and the rivers with the bigger discharges (Andernach, Kaub, Worms, Maxau).

This can be understood in a way that bigger discharge means the catchment of the river is big , as a consequence, the impacts of rainfall events from smaller catchments is damped, therefore standard deviation per annual cycle of mean gets smaller.

Figure 3-16 shows the annual cycle of mean after subtraction of annual cycle of mean from the original time series. In comparison with Figure 3-11, the range of annual cycle of mean is much reduced between -40 and 40 [m3/s], while the annual cycle of mean before the subtraction is approximately between 0 and 2400 [m3/s]. It should be noted, although the scale is changed, there is seasonal difference in annual cycle of mean.

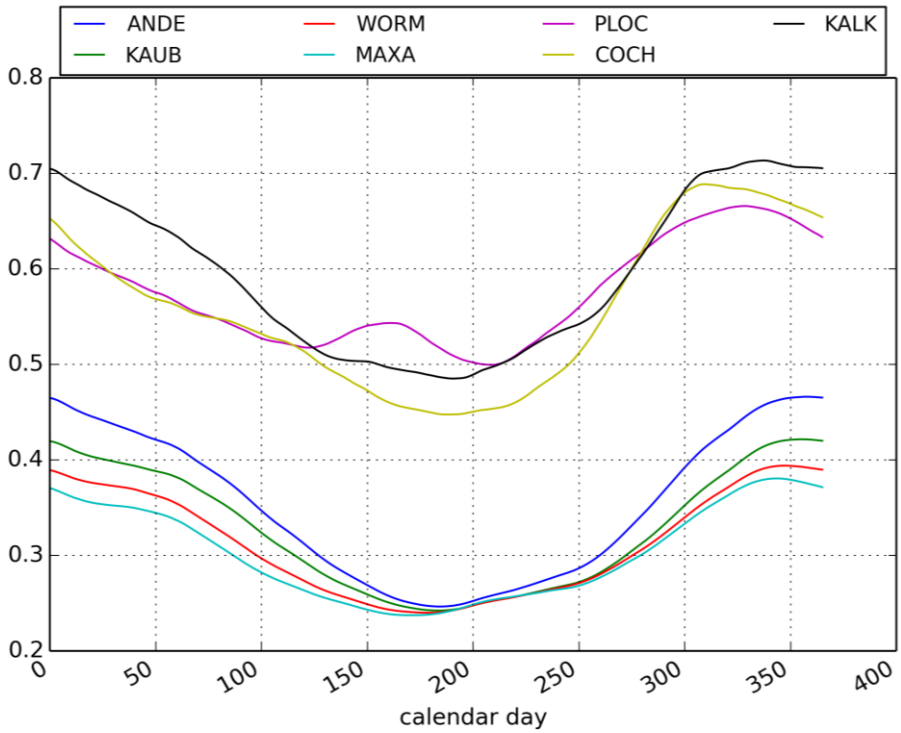

Figure 3-15 annual cycle of standard deviation divided by annual cycle of mean

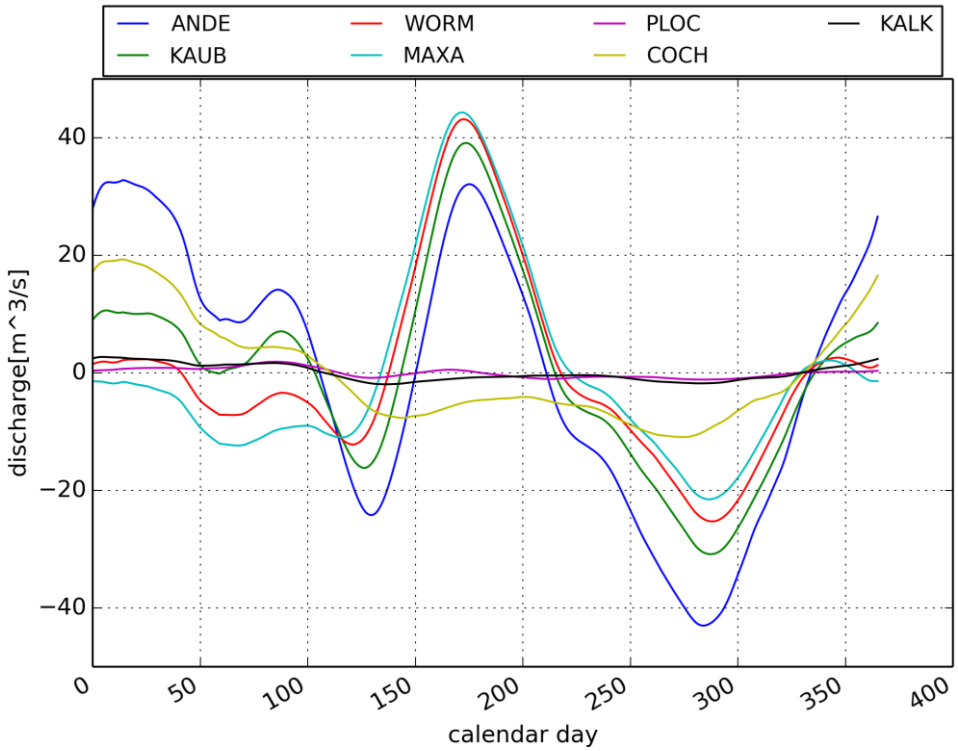

Figure 3-16 annual cycle of mean after subtraction of annual cycle of mean (standardization1)

3.3.2 Standardization2: Time Series divided by Annual Cycle of Standard Deviation after Subtraction of Annual Cycle of Mean

In the previous section, it was seen that seasonality of standard deviation still exists after the subtraction of annual cycle of mean from the original time series. Here, the original time series is divided by annual cycle of standard deviation after the subtraction of annual cycle of mean in order to check the property of standardized time series. This type of standardization is going to be called standardization2 in this study.

For example, the discharge data of January 1st are to be divided by the annual cycle of standard deviation of January 1st. Figure 3-17 shows the sample of discharge time series after this calculation.

After this standardization of time series, its annual cycle of mean (Figure 3-18 left) and annual cycle of standard deviation (Figure 3-18 right) is again calculated.

Due to the division, the time series is rescaled, therefore the range of discharge is between -0.5~12[m^3/s] in this sample of discharge time series (Figure 3-17). The scale of mean and standard deviation also become smaller (Figure 3-18).

Due to this scaling effect, it can be said, the seasonality in the time series is reduced. However, even if it is small, there still exists seasonality in terms of annual cycle of mean and standard deviation. Especially, if empirical autocopula is calculated from the time series, the scaling effects are supposed not to appear in copulas, because marginal is removed from original distribution in copulas.

Again, if time lag k gets bigger in autocopula, it will not represent direct relation between two random variables, but more seasonal behavior of the time series. Therefore, the asymmetries for large *k* (*k > 30*[days]) in section 3.2 are supposed to be capturing the asymmetry of these annual cycles.

This annual cycle of mean itself is not symmetric and this could dominate the behavior of asymmetry for lager time lag *k*. For example, the reason of smaller *asymmetry2* for gauging stations Maxau and Worms (Figure 3-8 and Figure 3-9) is that those annual cycles are symmetric in terms of *asymmetry2* (Figure 3-11).

In Appendix A, it is checked if these two different standardizations could bring different result. The results show there are certain difference especially for lager lag time *k* [days], but not big differences for smaller *k* [days].

Standardization2 is clearly better to reduce the impacts of seasonal standard deviation, although the analyses in this study were done based on standardization1. In Appendix A, the results of standardization2 are compared with the results of standardization1, which indicates the results with standardization1 in following chapters are still acceptable, because the investigations in this study are mainly for small lag time k due to the focus on the anthropogenic influence.

It seems there exist many different ways to standardize data. Proper processing of data should be needed depending on the purpose of the investigation and copula used for analyzing data.

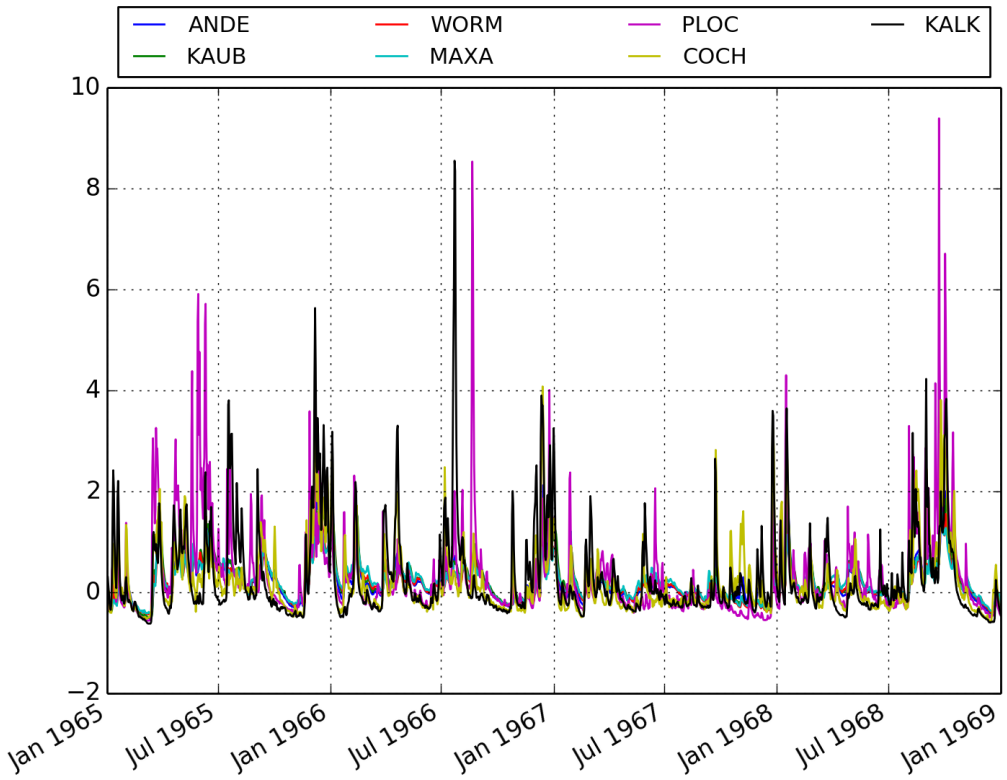

Figure 3-17 sample of discharge time series divided by annual cycle of standard deviation after subtraction of annual cycle of mean

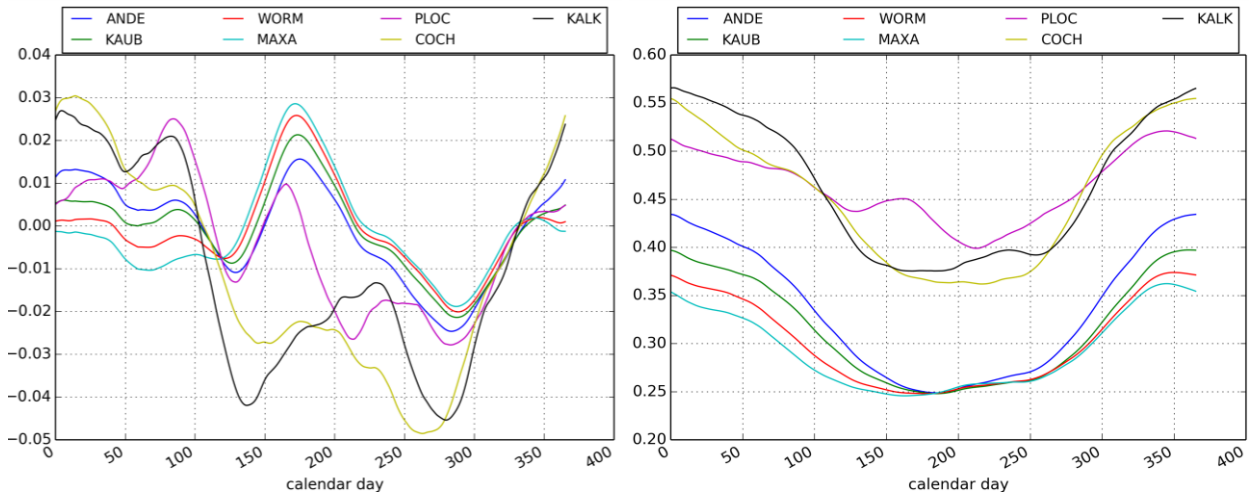

Figure 3-18 annual cycle of mean (left) and annual cycle of standard deviation (right) calculated for discharge time series which are divided by annual cycle of standard deviation after subtraction of annual cycle of mean from original time series (standardization2)

3.4 Asymmetry Changes without Seasonal Effect

In the previous section, annual cycles for the different statistics are investigated to clarify the effect of seasonality. In order to assess the periodic behavior of asymmetries without the seasonal effect, the method to subtract the annual cycle of mean from the original (standardization1) is investigated. Using this method, the average of calendar days get close to constant (Figure 3-16), but the dependence structure of time series remains.

3.4.1 Asymmetry1 after Subtraction of Annual Cycle

Variations of *asymmetry1* corresponding to time lag *k* [days] are calculated for 7 discharge time series data in which the annual cycle is subtracted.

Figure 3-6 shows the cyclic behavior of asymmetry1 from gauging stations Maxau, Worms, Kaub, which are supposed to be influenced by the annual cycle of mean as discussed in previous section. Figure 3-19 shows the *asymmetry1* after the subtraction of annual cycle of mean. The cyclic behavior of *asymmetry1* get weaker for Maxau, Worms, Kaub, instead Kalkofen, Cochem and Plochingen become stronger.

Due to the standardization1, cyclic behavior of *asymmetry1* from Kalkofen, Cochem and Plochingen should not be caused by annual cycle of mean, but is considered to be caused by the annual cycle of standard deviation.

The standard deviation is big for the gauging station with big discharge. But, it is not sure the impact of such deviation is still strong in copula. Division of original data by standard deviation could give some insight for this deviation as shown in Figure 3-16(right). In this figure, deviation is clearly bigger for Kalkofen, Cochem and Plochingen, thus the impact of deviation is big in those autocopulas. This could be the reason of behavior of asymmetry1 in Figure 3-19.

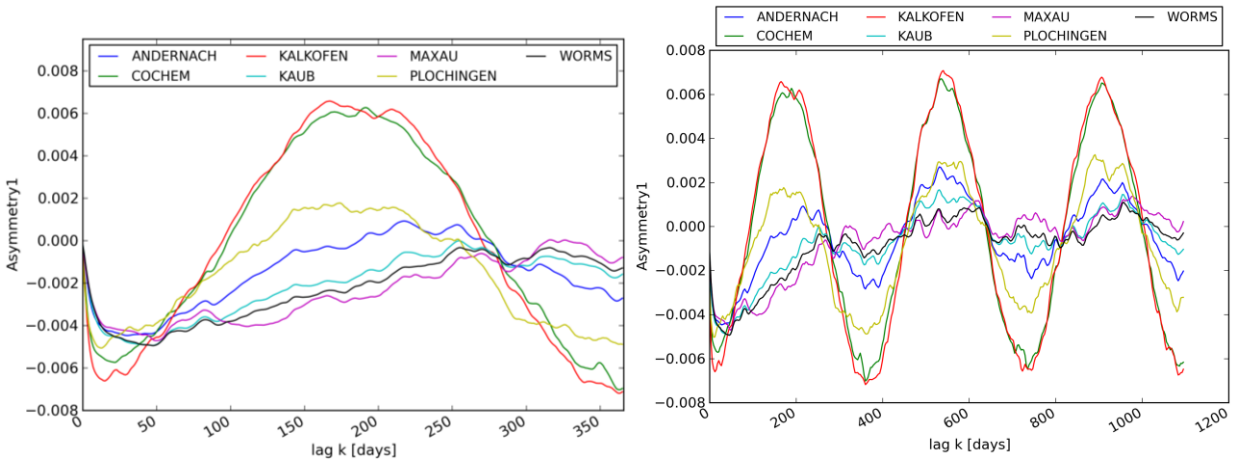

Figure 3-19 variation of *asymmetry1* after subtraction of annual average for *0 < k < 360*[days](left) and for *0 < k <1200*[days](right)

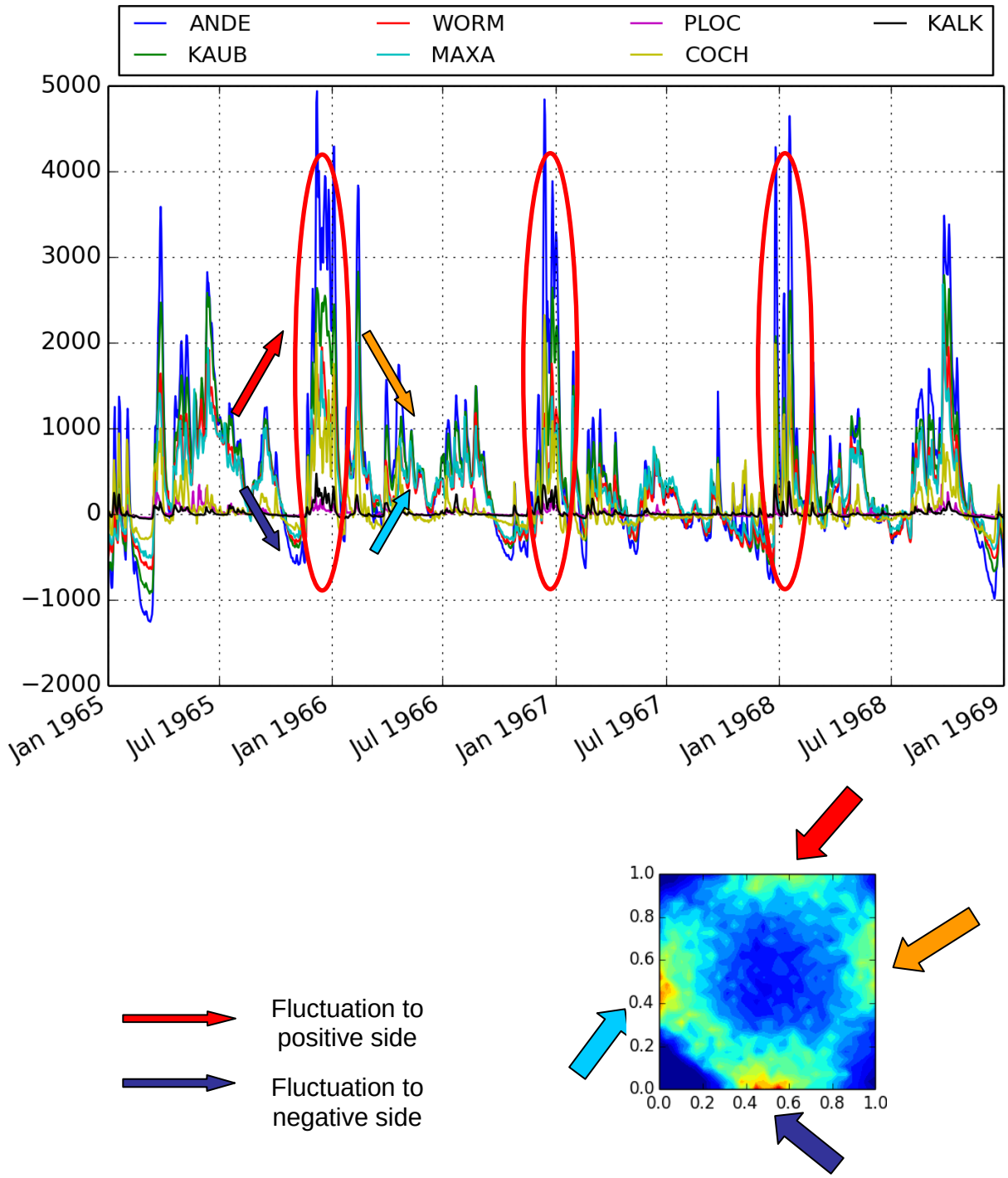

Figure 3-20 visualization of the causality of periodic changes of *asymmetry1* in empirical autocopula of Cochem after subtraction of annual cycle from original data (standardization1)

Figure 3-20 figure shows why the periodic behavior of *asymmetry1* is still present after the subtraction of annual cycle (mean). Also this shows why the empirical autocopula for k = 180 shows circular structure for gauging station Cochem and Kalkofen in Figure 3-4.

In this example, there are small oscillations in summer and big oscillations in winter due to the seasonal rainfall. The time lag *k = 180* [days] means comparing two values in different seasons; for example, if one is in rainy season and another in dry season. This means, if the quantile of one of

the value is in the middle (around $u = 0.5$) , which means dry season, the quantile of the other is either very high (close $u = 1.0$) or very low (close to $u = 0$)

The *asymmetry1* is very high for $k = 180$ [days] for Kalkofen und Plochingen in Figure 3-19. This can also be explained by the empirical autocopula from Cochem shown in Figure 3-20 (right bottom) in which there are more plots on upper right corner while there is almost no plots at the lower left corner. The reason can be the following: although the water level increases drastically in winter, but the period of extremely high flow is still short and usually water level stays less than average after subtraction of annual cycle in winter. Therefore the amount of fluctuation to positive side and negative side is not the same.

Also this empirical autocopula (Figure 3-20 right bottom), will not be very high or low value of *asymmetry2*, because same amount of plots exist on the upper-left corner and lower-right corner.

The intensity of periodic behavior of *asymmetry1* can be different from catchment to catchment reflecting the property of its seasonality, thus the discharge data from certain gauging stations doesn't show this behavior. However, this periodicity of *asymmetry1* would typically happen due to asymmetric behavior of discharge increase and decrease.

3.4.2 Asymmetry2 after Subtraction of Annual Cycle

In the previous section, the periodic behavior of *asymmetry1* with or without the standardization of time series was investigated. In fact, this standardization has certain impact for the large lag time *k*, but less impacts for the small lag time *k*, which is supposed to be more important to estimate the catchment characteristic.

In this section, the subtraction of annual cycle of mean is also tested to see the periodic behavior of *asymmetry2* as shown in Figure 3-21.

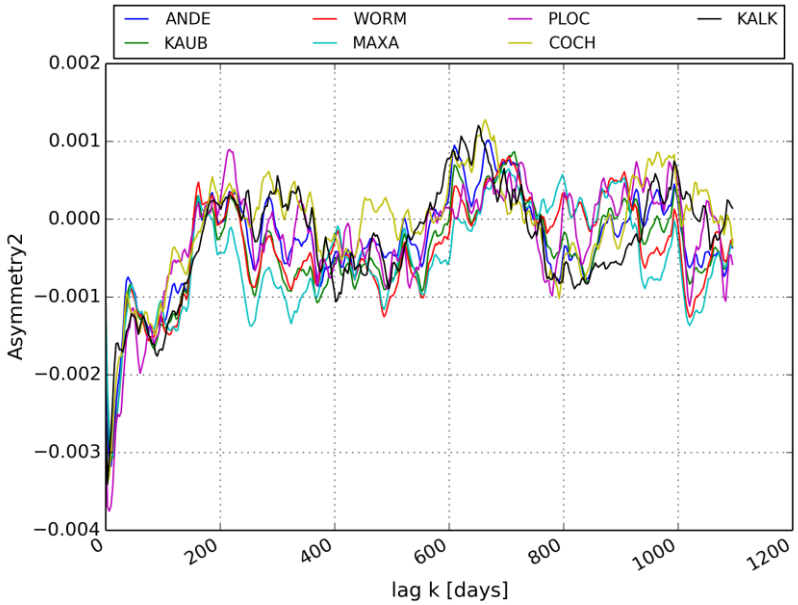

Figure 3-21 variation of *asymmetry2* after subtraction of annual average (standardization1) corresponding to time lag k [*days*]

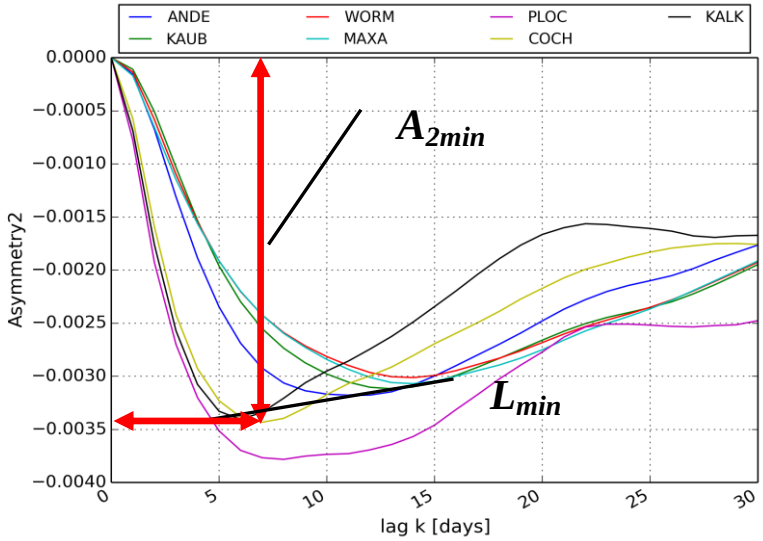

Figure 3-22 definition of Minimum *Asymmetry2* A_{2min} and its Lag L_{min} (for Cochem)

The apparent difference is that the behavior of *asymmetry2* after time lag $k > 50$ is reduced in comparison to the *asymmetry2* in Figure 3-9 . The important point in this figure is that the sharp

drop down of *asymmetry2* happen only for small time lag *k*, which should reflects the immediate increase of water level after rainfall or slower recession after cease of rain.

Now, the two lengths, which possibly represents the catchment characteristic, are suggested based on the *asymmetry2* corresponding to the time lag *k* as shown in Figure 3-22.

- A_{2min} ,**Minimum of *Asymmetry2***: Minimum value of the asymmetry2 for time lag $k < 25$ [days]. This measure is assumed to reflect the intensity of the difference between the water increase to peak flow and decrease to the based flow.

- L_{min}, **Lag Time at the Minimum of *Asymmetry2***: the lag time k, at which A_{2min} ,Minimum of *Asymmetry2*, is obtained. This measure is assumed to be related to the duration that the water level increases to peak flow

In the following sections, the analysis will be done based on these measures.

3.5 Asymmetries and Catchment Characteristics

As it was defined based on the *asymmetry2* in the previous section, A_{2min} represents minimum of *asymmetry2*, which represents the intensity in terms of discharge increase, and L_{min} represents lag at minimum, which can be more affected by the concentration time of the catchment. In this section, the relations between these criterions and catchment sizes are compared for 50 discharge gauging stations from Germany including the river Danube, Weser, Main and Neckar.

In Figure 3-23, the size of the catchments is plotted along the x-axis and A_{2min} (minimum of *asymmetry2*) in the y-axis. It can be seen that for the smaller catchments, A_{2min} shows more variance. This variance decreases as the catchment size increases in the case of the Rhine and its tributaries.

One of the possible reasons is that, in the case of the upstream of the Rhine or the Danube, the big runoff events are driven more by snow melting which could intensify the amount of discharge in some events. Therefore A_{2min} is bigger in comparison to the same size catchments.

Similarly the time to the peak discharge due to the snow melt is longer than discharge due to the rainfall. Therefore, L_{min} is bigger for smaller catchments of Rhine mainstream and Danube as shown Figure 3-24.

Figure 3-25 shows the relation between A_{2min} and L_{min}. In this result, there seems linear relation between A_{2min} and L_{min} independent from catchment size and river.

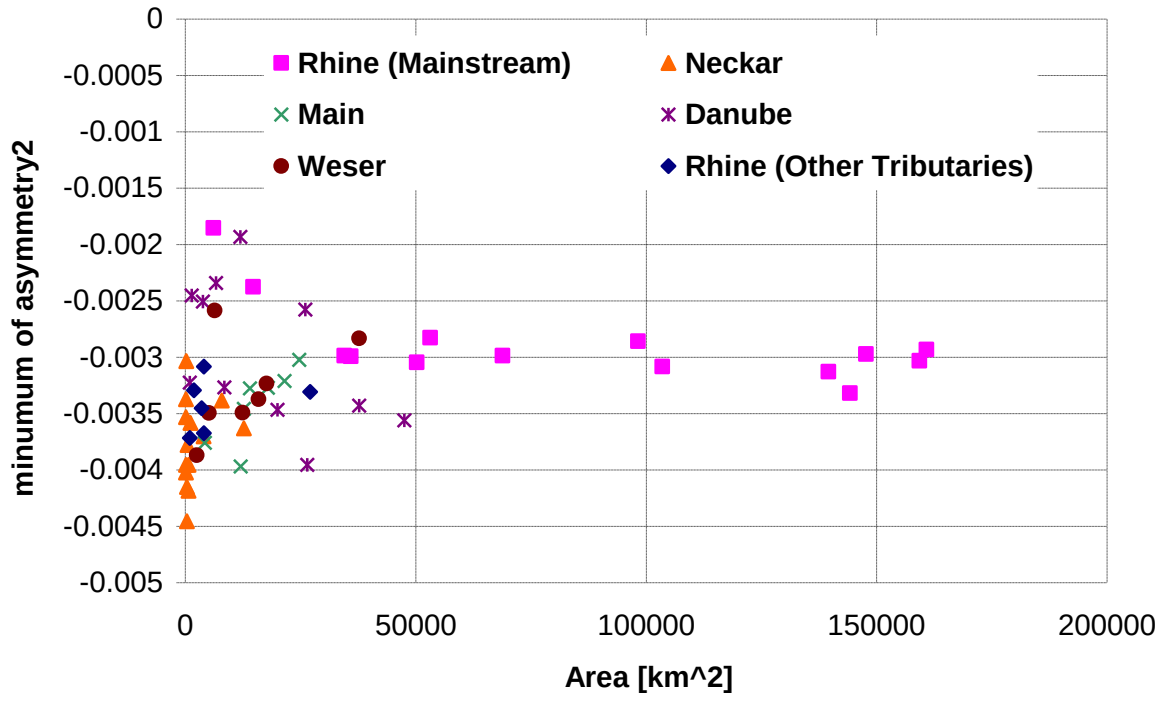

Figure 3-23 relation between the catchment areas and minimum of *asymmetry2*

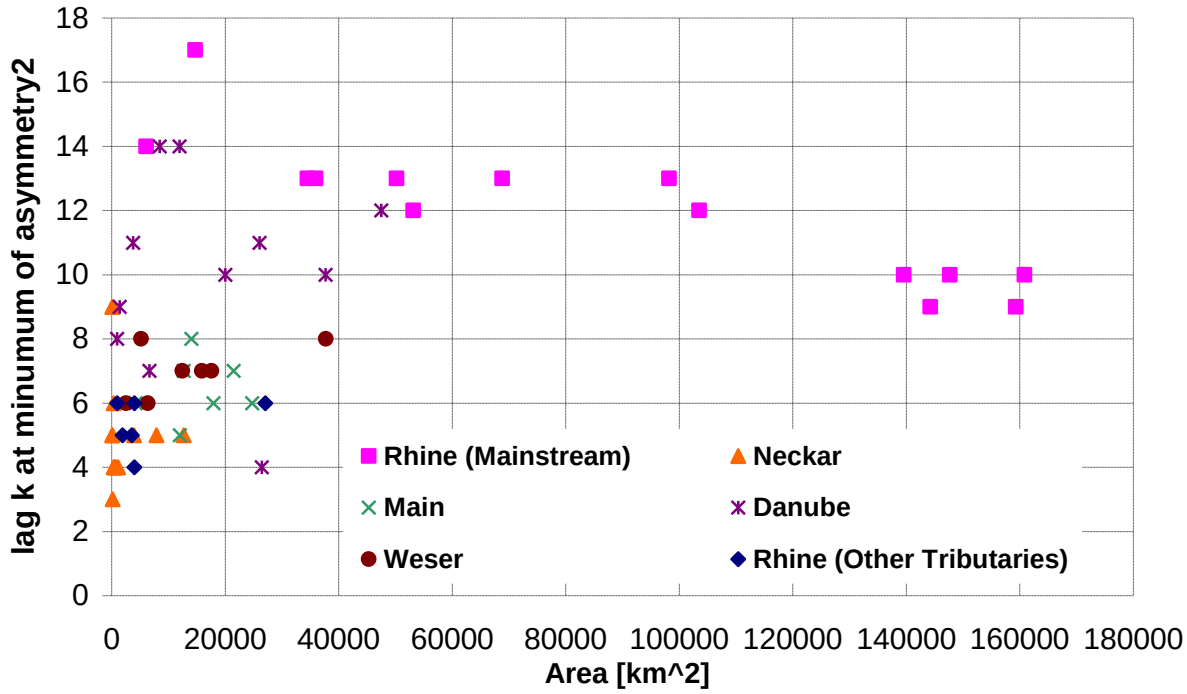

Figure 3-24 the relation between lags at minimum and the catchment areas

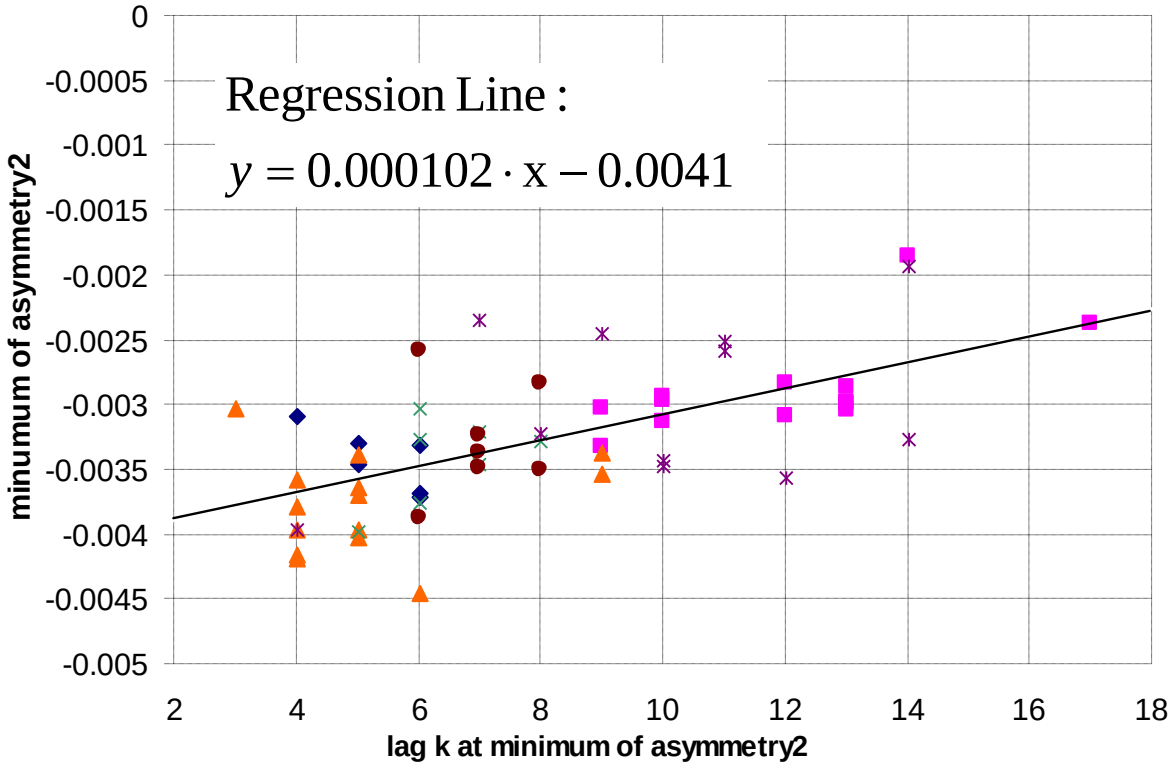

Figure 3-25 the relation between minimum of *asymmetry2* and lag *k* at minimum

3.6 Temporal Change of Asymmetries

The relation between the asymmetries and catchment characteristics are examined in the previous section. In this section, the temporal change of the catchment characteristics will be discussed, assuming the temporal change reflects the anthropogenic impact on the catchments for last 100 years. For this purpose, the moving time window is introduced to calculate the asymmetry from a certain time interval instead of calculating empirical copula from entire time series data.

Moving time window is nothing but the time interval to calculate the empirical copula or statistics. In this case, the interval of the window is set to 10 years and the copula for 10×365 daily discharge data is to be calculated. Then, the minimum of asymmetry and its lag can be calculated in the same way in section 3.4.2 for this moving time window.

One interesting finding is that the behavior of *asymmetry2* is different around the year 1945, which will be explained in the following section.

3.6.1 Changes of Asymmetry2 in Moving Time Window

Figure 3-26 shows the change of A_{2min} (Minimum of *Asymmetry2*) and Figure 3-27 shows the change of L_{min} (Lag at Minimum of *Asymmetry2*) in a moving time window respectively. Here, the asymmetries of empirical copulas are not calculated from the entire time series, but from the data in the moving time window with 10 years interval. For example the asymmetry on January, 1, 1910 is calculated from the data between 1st of January in 1905 to Dec 31st in 1914.

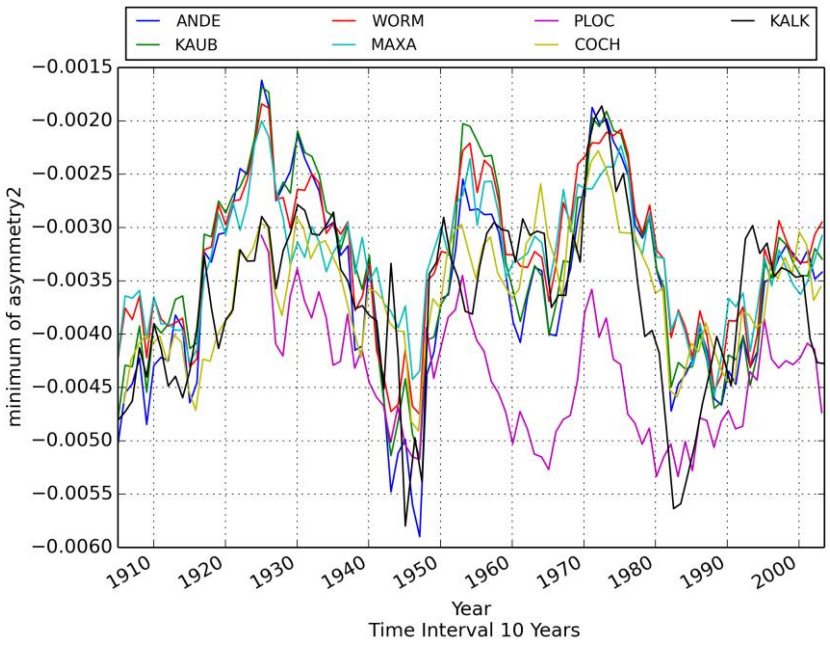

Figure 3-26 Temporal change of A_{2min} (Minimum of *asymmetry2*) in moving time window with 10 years interval

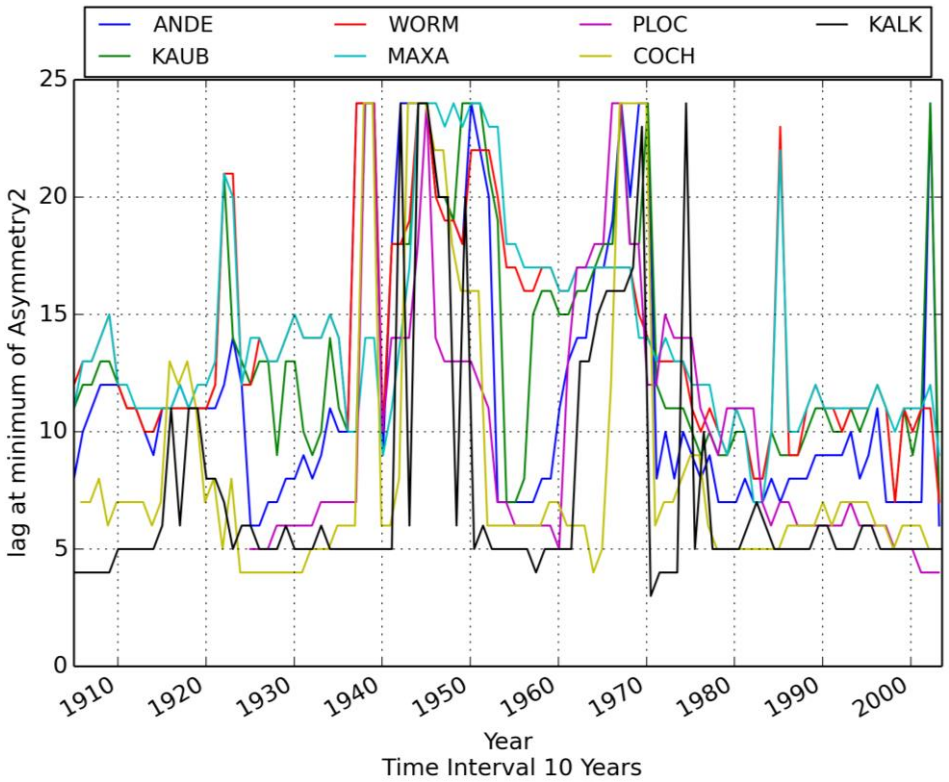

Figure 3-27 temporal change of L_{min} (lag time k at minimum of *asymmetry2*) with moving time window of 10 years interval

Around 1945, A_{2min} drops down and L_{min} goes up significantly for the data from all the measuring stations. Also around 1965 L_{min} increases and around 1915 and 1975 A_{2min} decreases in unusual way, which indicates possibly the structural change due to the anthropogenic impact.

Figure 3-28 shows the empirical copulas of the discharge data from Andernach from the 10-year-intervals around 1945 and 1975 for time lag $k = 5$[days] together with their densities. The reason that *asymmetry2* is smaller for the years around 1945 can be seen in the upper left corner of the plots (red circle in the figures): in the left panel (1945) there are more points than in the right panel (1975).

In Figure 3-28, not only the upper-left corner, but the entire distribution is stretched out for the empirical copula around 1945 (left) than around 1975 (right) as shown by blue arrows in the figures. As it will be discussed in Chapter 7, this can be the reason that the copula variance is high around this period.

If we look at the observed discharge record around 1945 and 1975 as shown in Figure 3-29, it can be hardly seen that there are differences with respect to the frequency or the peaks of the discharges.

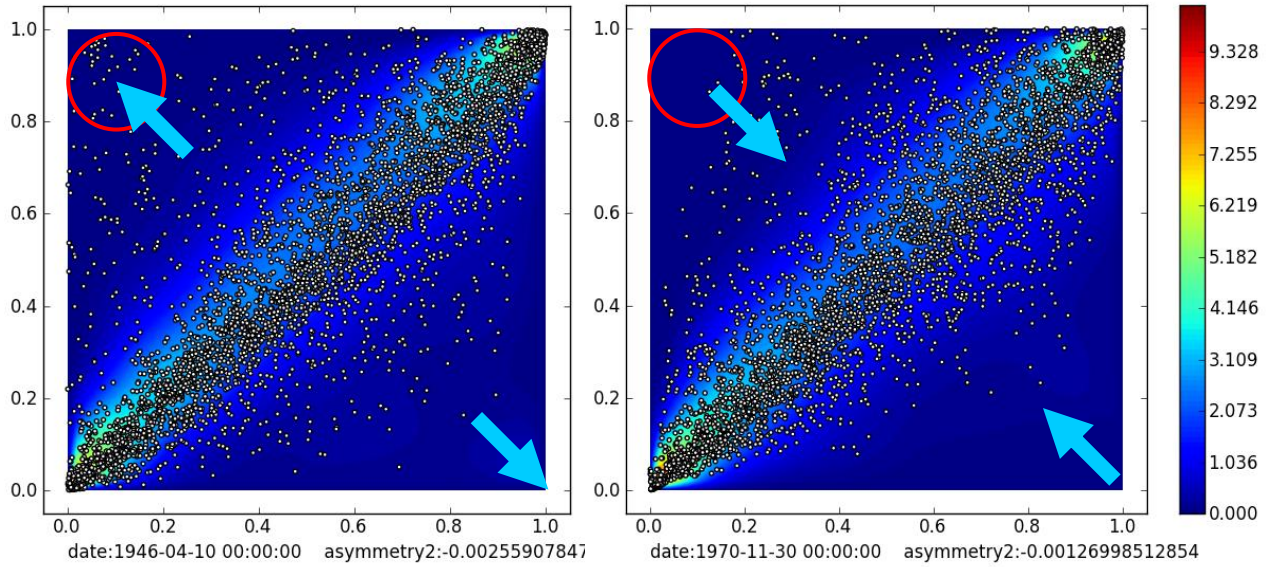

Figure 3-28 empirical autocopula frequency (white plots) and its density (colored contour) for the lag k = 5 around the year 1945 (left) and 1970 (right)

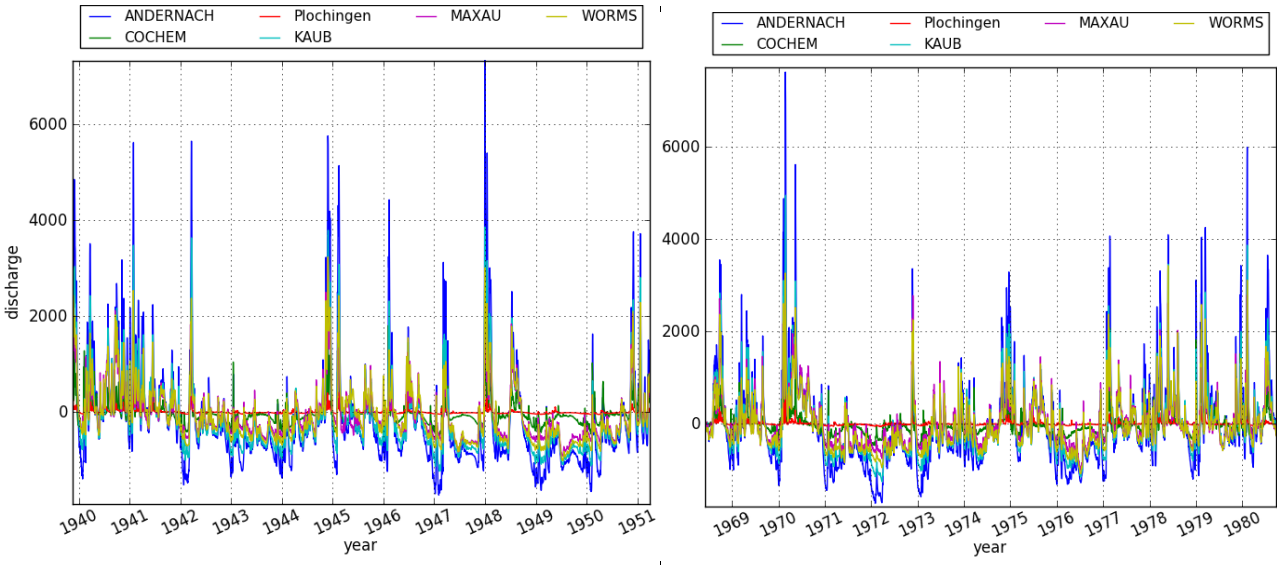

Figure 3-29 observed discharge time series (standardization1) around the year 1945 (left) and 1975 (right)

The question now is what is the difference between the years around 1945 and 1975, what is happening those years. In order to inquire the differences, the asymmetries corresponding to lag time *k* are calculated around 1930, 1945 and 1973.

For the case year around 1930, we can see the typical drop down for the time lag k < 15 down to $A_{2min} = -0.035$.

But for the case of years around 1945, no clear drop can be seen for the lag $k < 15$, but gradual decrease up to $A_{2min} = -0.004 \sim -0.0055$ for the lag time $k < 30$ can be seen.

The more interesting case is for the years around 1973. It can be seen a small drop down ($A_{2min} = -0.02 \sim -0.025$) for the lag time $k < 15$ exist, but for the lag time around $k = 30$, there is a second

drop down (A_{2min} =- *0.02 ~ - 0.040*) which can be same or bigger than the drop down for lag time $k < 15$. This seems to be the reason why L_{min} is so big around 1945 or 1973.

In fact, 1945 and 1973 are not completely different situations, but rather similar situations, in which the first drop down of *asymmetry2* is small and does not cause A_{2min} (minimum value of *asymmetry2*) there, but rather A_{2min} shifted to right and gave rise to A_{2min} around $k = 30 \sim 40$.

Because the drop down of *asymmetry2* for lag time k < 15 is a consequence of rapid increase of discharge during flood events, furthermore, it's accounting more for the big flood events like snow melting in the beginning of spring, therefore, this behavior of *asymmetry2* is saying, the discharge in the flood events around those periods could be not so intensive and not so speedy in comparison to the other period.

Actually, if we have a closer look at the discharge data around 1945 and 1973, then we can see, there are winters and springs in which no big flood events are observed for certain periods. As it is shown in the moving average (Figure 3-33) around 1945 and 1973 had less discharges on average, which implies there was less precipitation.

This could be explained simply because of the rainfall events around 1945 and 1975 which are not so many in terms of quantity and intensity, therefore the amount of peak discharge and the speed to the peak discharge become smaller and slower. Otherwise, the property of rainfall events are the same, but the catchment characteristics were different in those periods.

However, it is still not clear that the strange behavior of *asymmetry2* is caused due to the random behavior of yearly rainfalls or the anthropogenic impacts like destruction of infrastructures after the war around 1945 or due to intensive urbanization and industrialization around 1975.

The possibility of rainfall as the source of unusual behavior will be discussed in Chapter 5.

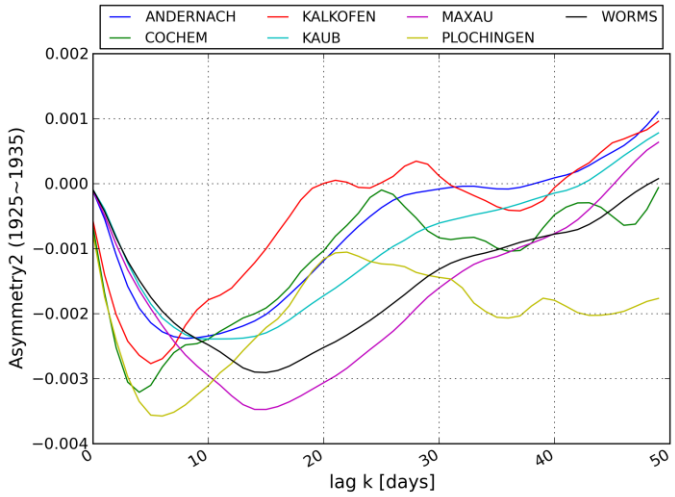

Figure 3-30 *Asymmetry2* corresponding to time lag *k* [days] from the data between 1925 and 1935

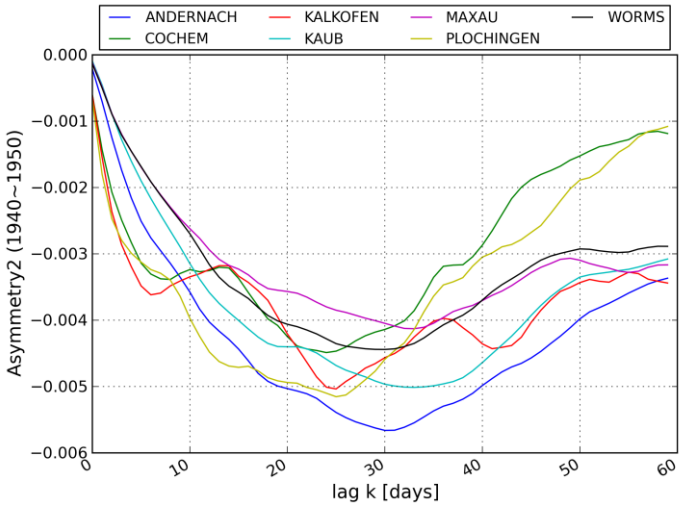

Figure 3-31 *Asymmetry2* corresponding to time lag *k* [days] from the data around 1945 (data between 1940 and 1950)

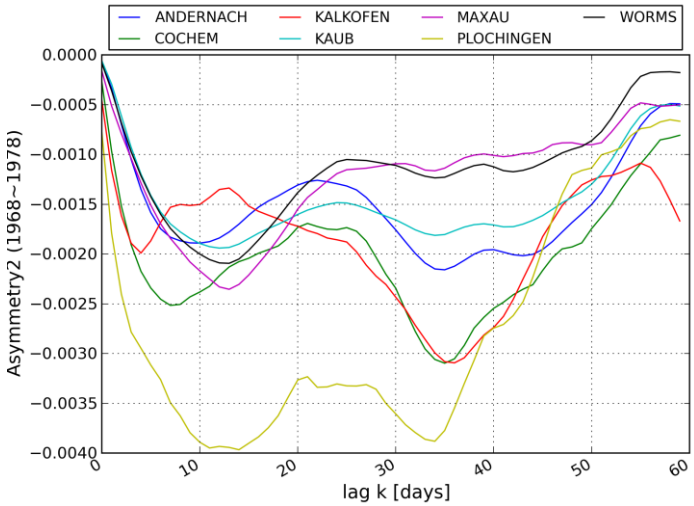

Figure 3-32 *Asymmetry2* corresponding to time lag *k* [days] from the data between 1968 and 1978

3.6.2 Temporal Change of statistics (mean, standard deviation)

Figure 3-33 and Figure 3-34 show mean and standard deviation in moving time window. There are some periods in which averages of discharge are smaller (1945, 1961, and 1975). It can be assumed, if there is less precipitation, and then there will be less discharge and smaller standard deviation. This is the case for the years 1960, 1975. But, what special for 1945 is that even the average of the discharge in this time interval is small, the deviation is still big. Sample of discharge time series around 1945 and 1975 can be seen in Figure 3-29.

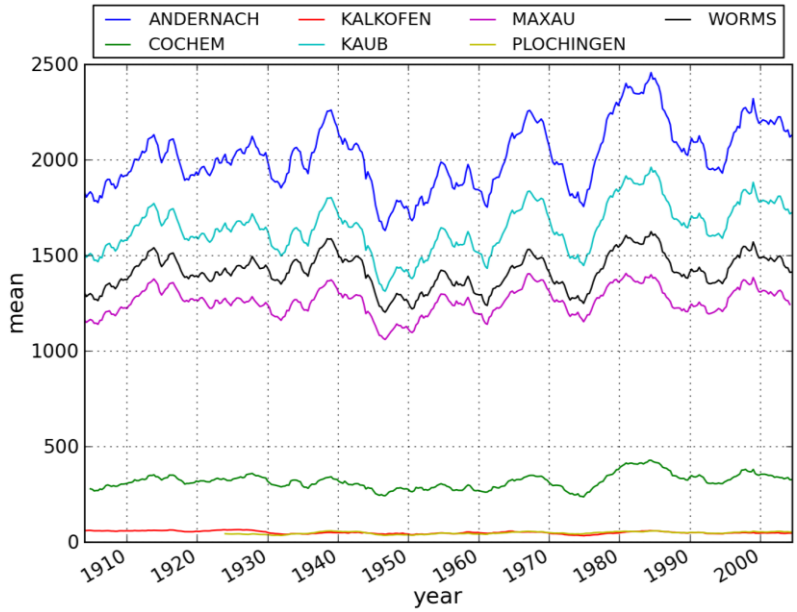

Figure 3-33 moving average of discharge [m^3/day] in 8 years moving time window

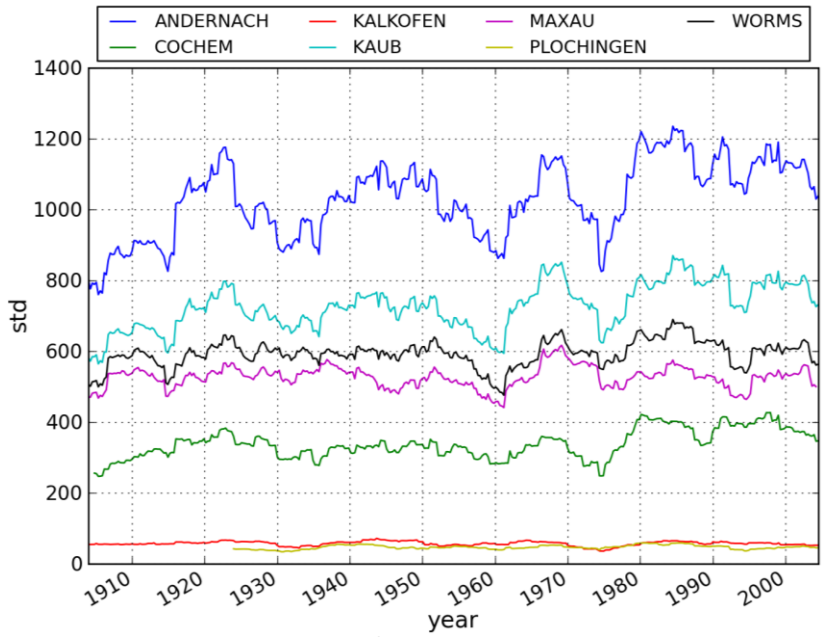

Figure 3-34 standard deviation of discharge [m^3/day] in 8 years moving time window

3.6.3 Temporal Change of Asymmetry2 in other Catchments

In the previous section, the behavior of *asymmetry2* around 1945 and 1975 could be unique for the investigated catchments (Andernach, Kaub, Worms Maxau, Plochingen, Kalkofen, Cochem). In this section, the same analysis was done for the further rivers in other regions (Weser, Main, Danube) and results are summarized in Appendix B.

The interesting point is that, A_{2min} and L_{min} of the other regions behave similarly around 1945 and 1980.The behavior of mean and standard deviation in moving time window is also similar except for 1945. In the investigated catchments, the mean is low and standard deviation is high around 1945. But in the other regions both tend to be high.

3.6.4 Temporal Change of Asymmetry1

Figure 3-35 and Figure 3-37 show the changes of *asymmetry1* in the moving time window. *Asymmetry1* is supposed to be more related with rainfall itself and less with catchment characteristic according to the analysis in 3.4.1.

In fact, these results are hard to interpret, because the lag at minimum of *asymmetry1* keeps fluctuating time to time. The meaning of Minimum of *asymmetry1* and Lag at minimum of *asymmetry1* is less clear. It looks there are some structure in the around year 1920 in Figure 3-35 or around 1930 Figure 3-37, but still difficult to conclude anything and this might have happened by chance.

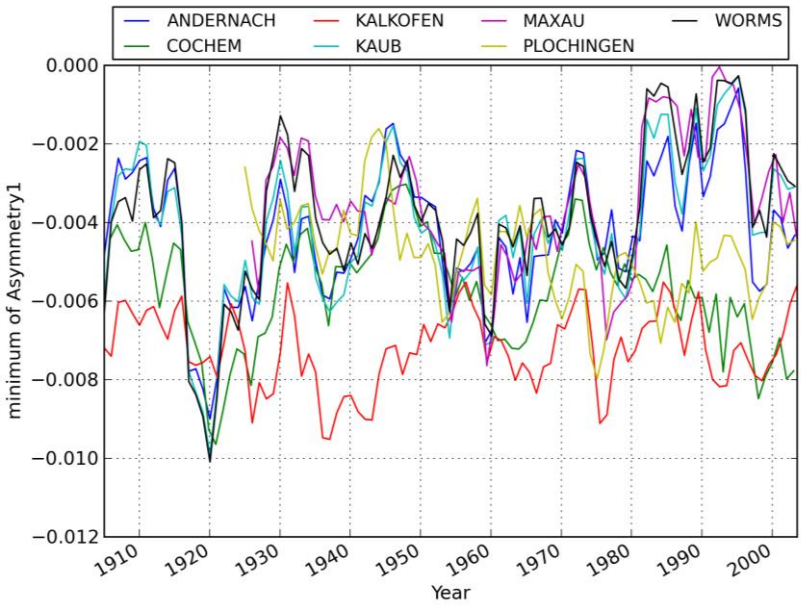

Figure 3-35 Changes of *asymmetry1* (Minimum) in moving time window

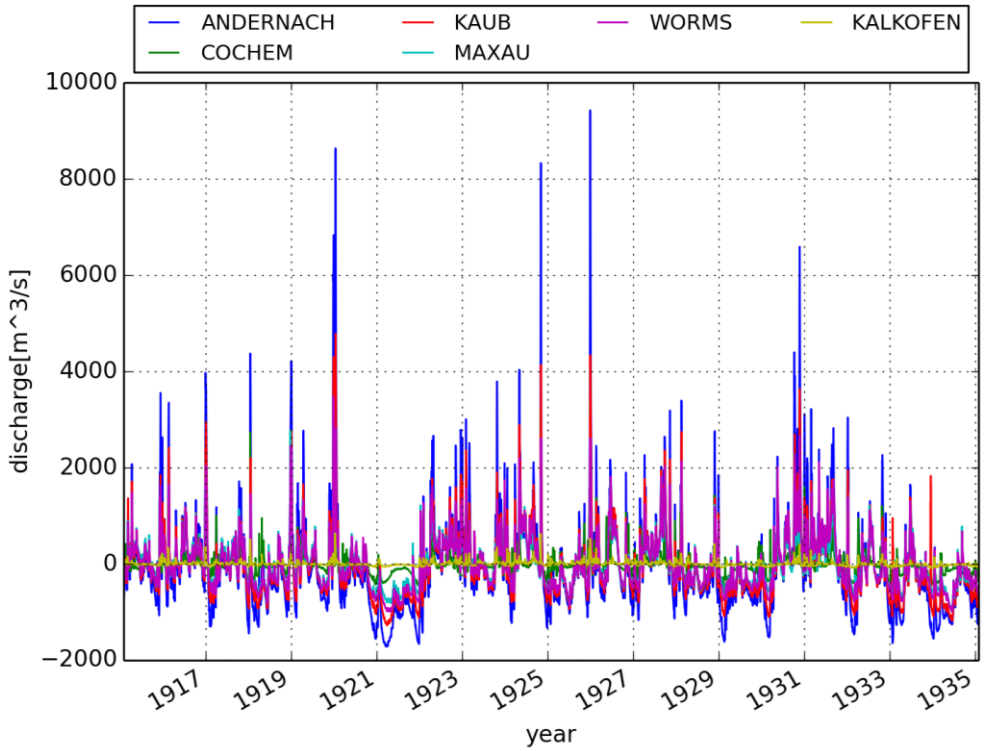

Figure 3-36 observed discharge time series (standrization1) around 1920 ~ 1930

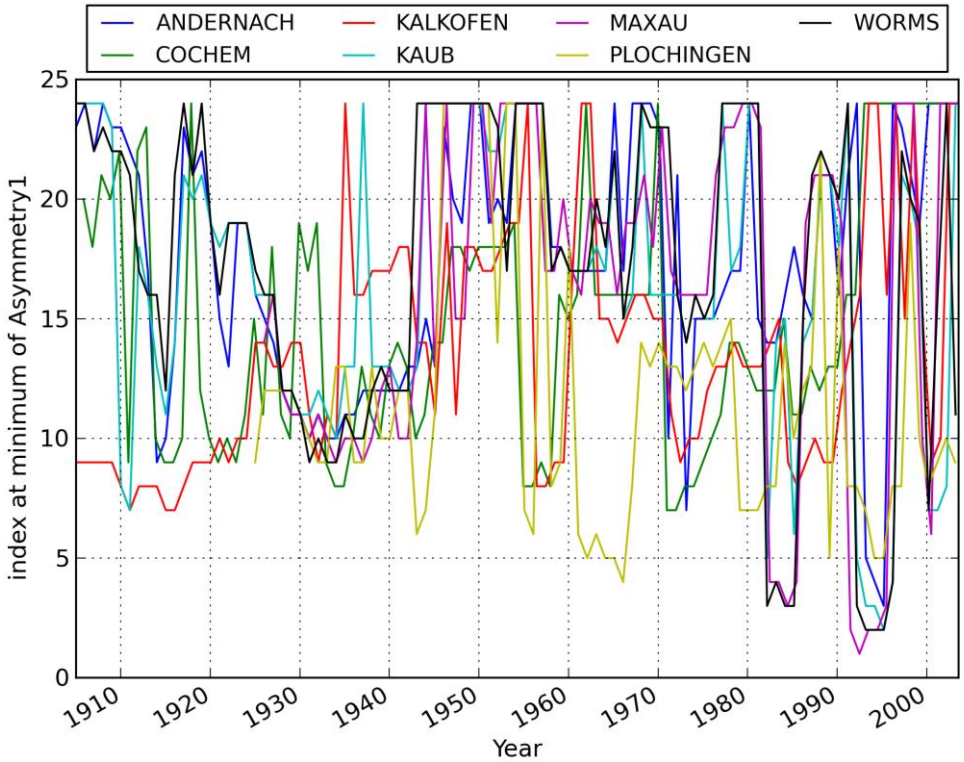

Figure 3-37 changes of a*symmetry1* (lag at minimum) in moving time window

In this chapter, cross copula was newly introduced as copula version of correlation matrix, showing visually the dependence structure of different random variables from 7 discharge gauging stations

(Figure 3-2). Autocopulas with time lags *k*, which are the growing research interest of today, were also calculated for same discharge data set (Figure 3-4).

The autocopulas of discharge data set are clearly different for different time lag *k*. Therefore, its characteristic is further investigated especially with asymmetry, a function defined on copulas (Figure 3-6, Figure 3-7, Figure 3-8, Figure 3-9).

The interesting point of the results was that asymmetries (*asymmetry1* and *asymmetry2*) show cyclic behavior with a period of 365 days, which is a clear sign of seasonality that the asymmetry is influenced by annual cycle. Therefore, the annual cycle of mean and standard deviation of discharge were secondary investigated (Section 3.3). Through this analysis, it was concluded that the variation of asymmetries corresponding to time lag *k* can be partially explained by annual cycle of mean and standard deviation especially for bigger time lag *k*.

In order to reduce the influence of seasonality in asymmetries, two methods are suggested in this study: one is standardization1 which subtracts the annual cycle of mean from the original data and another is standardization2 which divides the original data by annual cycle of standard deviation after subtraction of annual cycle of mean (Figure 3-19, Figure 3-21). These methods can reduce the impacts of annual cycle in asymmetry especially for autocopulas with larger time lags.

One of the objectives of this research is to detect the change of anthropogenic impacts, whose information is assumed to be in autocopulas for smaller time lag k. For this aim, the behavior of asymmetry for smaller time lag *k* is further investigated and two measures are defined: one is A_{2min}, which is minimum value of the *asymmetry2* for time lag $k < 25$ [days] and another is L_{min} which is lag time *k* at minimum of *asymmetry2* (Figure 3-22).

Because asymmetry2 is caused by unequal ratio of water increase and decrease, this measure is considered to be related to catchment characteristic for short lag time *k*. It was confirmed that different catchments have different values of *asymmetry2* (Figure 3-23, Figure 3-24).

Now the interest of the research is whether this characteristic changes for different time period due to anthropogenic influences or not. Therefore, temporal change of asymmetry2 is calculated from discharge time series in moving time window (Figure 3-26). The result shows asymmetry seems not fully constant or random, but showing certain common behavior for all the discharge data for example around 1945 and 1970. The reason was investigated and it was found that 2 dimensional autocopula is narrower for certain period (1970) and wider (1945), which should be the reason causing different values of *asymmetry2* in different periods (Figure 3-28).

The reason of different empirical autocopulas for different period is further investigated with moving average and moving standard deviation (Figure 3-33,Figure 3-34), but it could not be concluded that temporal change of asymmetry2 is caused only by anthropogenic impacts.

4 Seasonal Analysis of Empirical Autocopula

In the previous section, the impacts of seasonality are reduced from the time series by subtracting the annual cycle of mean. But, in this section, seasonality itself is investigated by separating the data into different seasons and calculating the empirical autocopulas and its asymmetry from them.

For this analysis, the seasonal time window is set to the time interval of 60 days. For example, in order to calculate the asymmetry of August, the center of the time window is set to 15th of August and takes the values of consecutive 60 days. In this way, 59 pairs of values for the empirical autocopula with time lag $k = 1$ for one year (59 pairs due to time lag $k = 1$. If time lag $k = 2$, then 58 pairs can be used for calculation) and 59 × 100 pairs of values for 100 years can be used for the calculation of an empirical autocopula.

Figure 4-1 shows the empirical autocopulas of the selected season (January, March, May, July, September, November) from the gauging station Andernach. The difference can be seen, especially, on the upper left corner of the figures (see red circles in the figure) of empirical autocopulas for lag $k > 10$, which could result in the different *asymmetry2* for given time lag k. The behavior of discharge or rainfall in January and March is assumed to be strongly influenced by seasonal rainfall and snow melting, thus more plots on the upper left corners of empirical autocopulas and subsequently result in smaller *asymmetry2*. The Results shows the behaviors of asymmetry are clearly different from season to season.

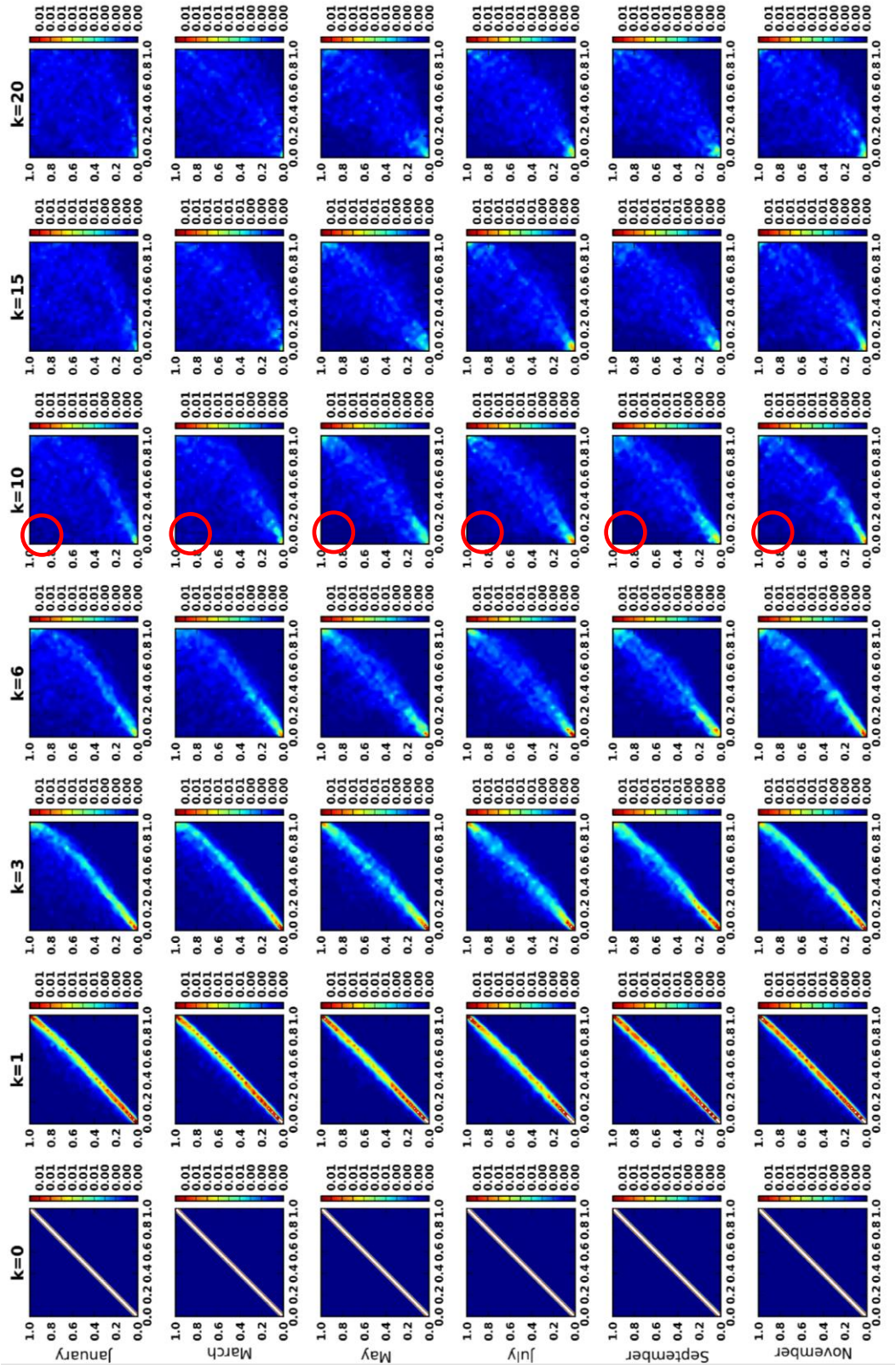

Figure 4-1 empirical autocopulas of time series data (discharge from measuring station Andernach) with different time lag k [days] in different season

4.1 Asymmetry in Different Seasons

Now, *asymmetry2* corresponding to different time lags *k* in different seasons is shown in Figure 4-2. The time window for the seasonal interval is again set to 60 days and the central day of the interval is set to the middle of the month (15^{th} in the case of January). Here, the seasonal behavior of asymmetry is apparently different from month to month principally due to the seasonal climatic behavior as summarized below:

Winter season (December, January, February):
- the structure of *asymmetry2* is clear
- A_{2min} is around *-0.004 ~ -0.005* and L_{min} is around $k = 7$
- *Asymmetry2* increases around time lag k = *10 ~ 15*, which could be related to the sharp and rapid water increase due to seasonal precipitation or snow melting.

Spring season (March, April, May):
- Drop down of *asymmetry2* is less clear
- A_{2min} is less intensive around - *0.002 ~ -0.003* and L_{min} gets bigger.

Summer season (June, July, August, September):
- Drop down of *asymmetry2* is not clear any more
- The value of A_{2min} is around - *0.001 ~ - 0.002* in Cochem, Plochingen, Kalkofen, which are located in the tributary of the Rhine.
- The results of Maxau, Worms, Kaub and Andernach are supposed to capture the rainfall-runoff events without snow melt in summer. This can be the reason that there is no drop down for small lag time *k*.

For the rest of the seasons (October, November), the drop down of *asymmetry2* gets more intensive again, but the structure of drop down and increase of *asymmetry2* is still not clear. Therefore L_{2min}, lag at minimum of *asymmetry2*, gets bigger (*> 20*).

In Figure 4-3 Annual Cycle of A_{2min} (Minimum of *Asymmetry2*) and L_{2min} (Lag at Minimum of *Asymmetry2*) are shown. For the calculation of A_{2min} and L_{2min} here, seasonal time window is again set to 60 days, A_{2min} and L_{2min} are calculated by shifting the seasonal time window within 1 ~ 366 of calendar days. The obtained annual cycle of asymmetries is smoothed in the same way in section 3.3.

The conclusion is that the structure of drop down is most clear in December, January and February, which is caused by the seasonal rainfall and partially snow melt. Therefore A_{2min} and L_{2min} could reflect the characteristics of this period. If no rains of usual event happen in this period, A_{2min} and L_{2min} can be strongly affected.

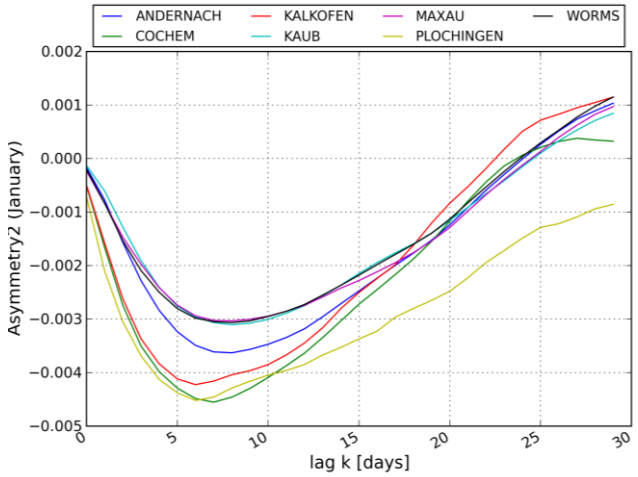
ANDERNACH
COCHEM
KALKOFEN
KAUB
MAXAU
PLOCHINGEN
WORMS
Asymmetry2 (January)
lag k [days]

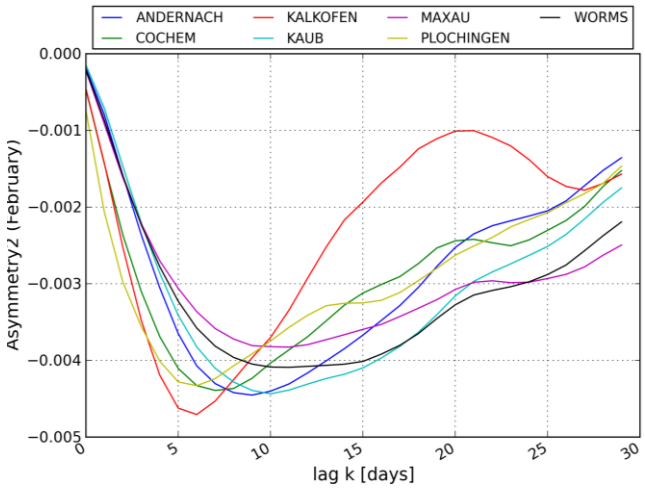
ANDERNACH
COCHEM
KALKOFEN
KAUB
MAXAU
PLOCHINGEN
WORMS
Asymmetry2 (February)
lag k [days]

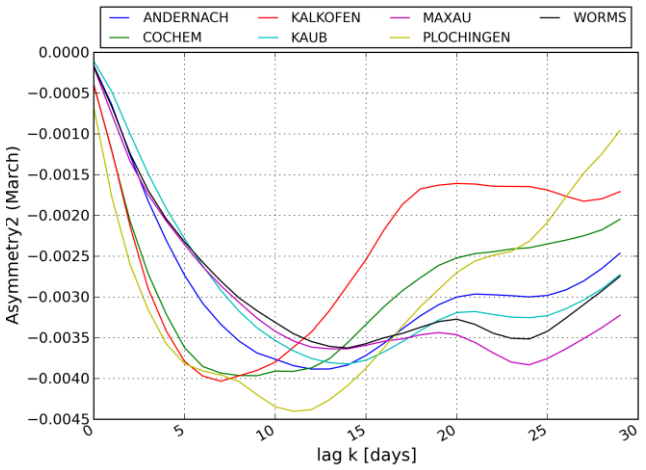
ANDERNACH
COCHEM
KALKOFEN
KAUB
MAXAU
PLOCHINGEN
WORMS
Asymmetry2 (March)
lag k [days]

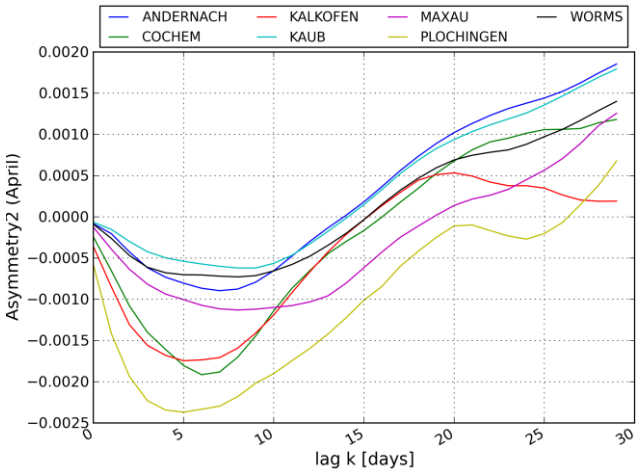
ANDERNACH
COCHEM
KALKOFEN
KAUB
MAXAU
PLOCHINGEN
WORMS
Asymmetry2 (April)
lag k [days]

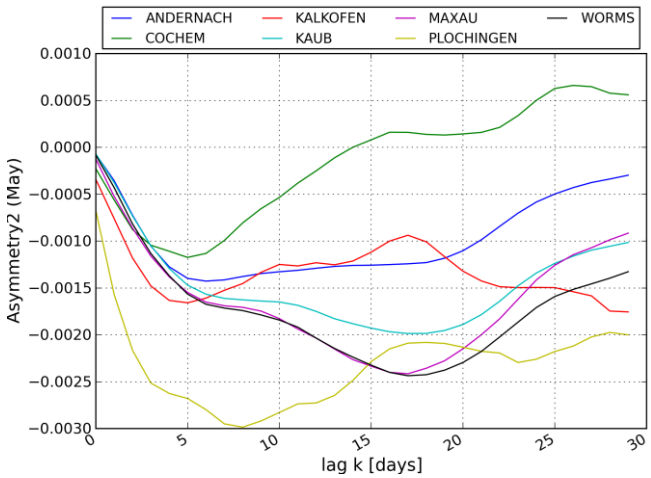
ANDERNACH
COCHEM
KALKOFEN
KAUB
MAXAU
PLOCHINGEN
WORMS
Asymmetry2 (May)
lag k [days]

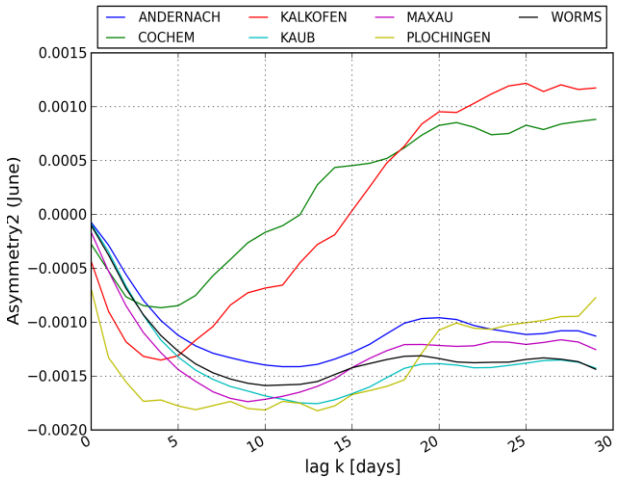
ANDERNACH
COCHEM
KALKOFEN
KAUB
MAXAU
PLOCHINGEN
WORMS
Asymmetry2 (June)
lag k [days]

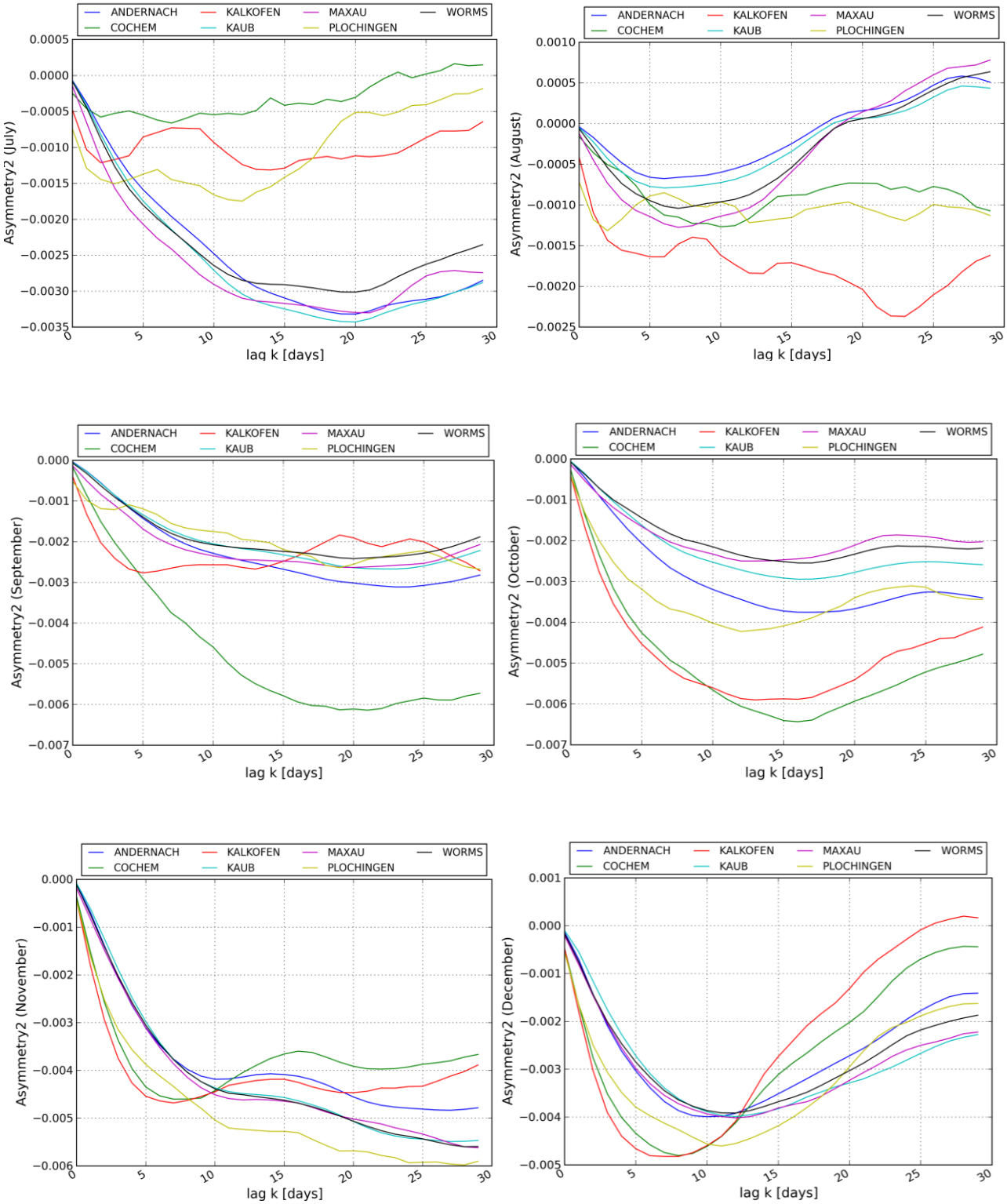

Figure 4-2 Asymmetry with different time lag *k* in different Seasons (January ~ December)

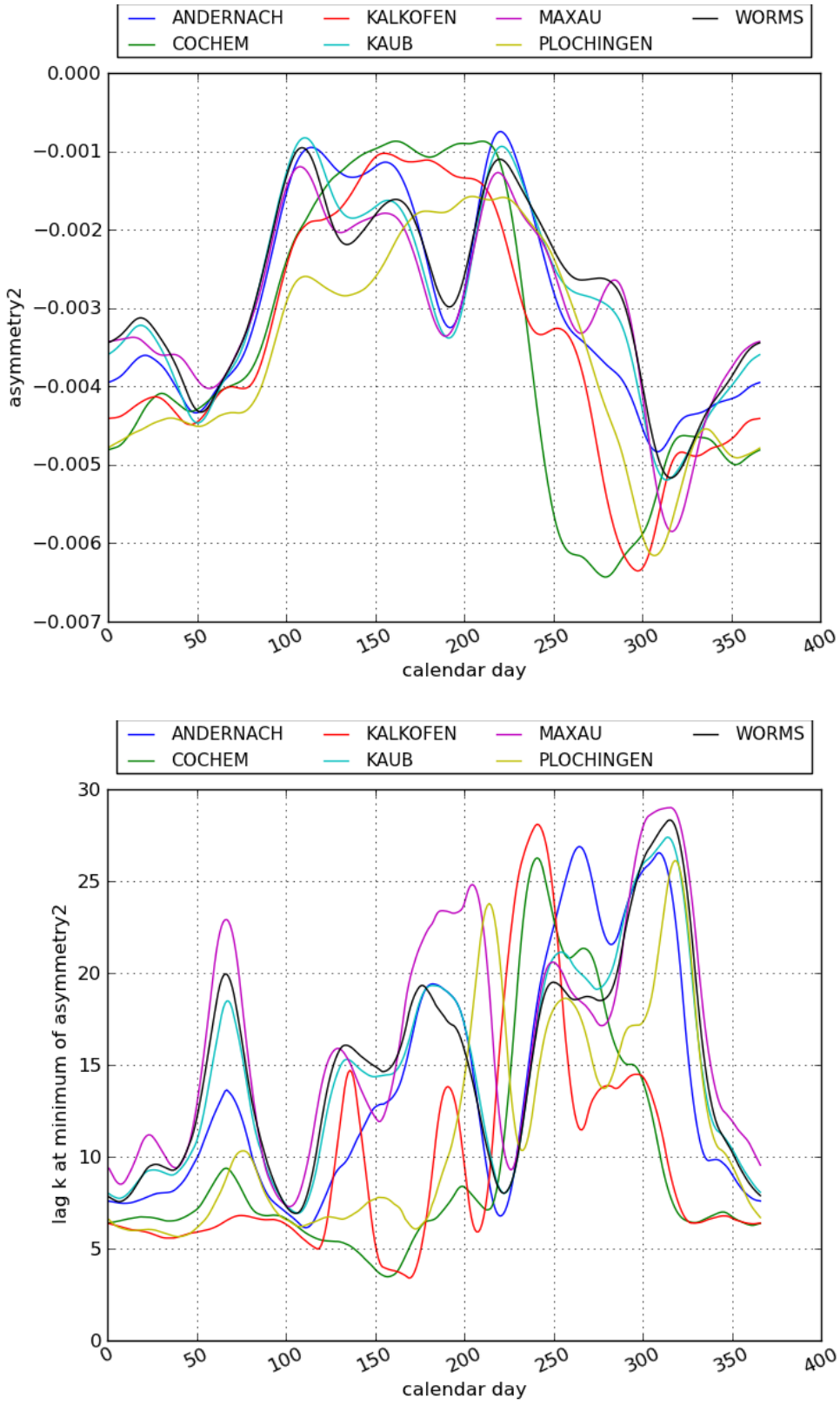

Figure 4-3 Annual Cycle of A_{2min} (Minimum of *Asymmetry2*) and L_{2min} (Lag at Minimum of *Asymmetry2*)

4.2 Temporal Change of Seasonal Behavior of Asymmetry

In the previous section, it is now clear that the behavior of *asymmetry2*, especially A_{2min} (minimum of *asymmetry2*) and L_{min} (lag k at the minimum of *asymmetry2*) is totally different from month to month.

This is caused mainly by the seasonal climatic behavior. For example, the precipitation in summer is more advective and intensive, but the duration of rainfall events could be shorter, while the duration of rainfall events tends to be longer with less deviation in winter.

Thus, the behavior of A_{2min} and L_{min}, which are investigated in the previous chapter (3.4, 3.5, 3.6), has the integrated information of these seasonal behaviors. Especially the A_{2min} and L_{min}, which are the parameters quantifying the structure of drop down in *asymmetry2* for the smaller lag time k, are significant only for the winter period because this structure of drop down rarely exists in summer (section 4.1 and Figure 4-2).

However, this seasonal behavior could still change in different time periods in last 100 years. In order to investigate the changes in the past, the time series data are now separated into two seasons, summer and winter. Then, the changes of asymmetries are calculated in moving time window again similar to the analysis in the previous sections.

For example, for the analysis of winter, the data from October, November, December, January, February and March are selected from the original entire time series and new time series are merged by combining them. In this case, the seasonal window is roughly 180 days, so 180 data can be used from the 1 year observation records, eventually 180 × 10 data can be used for the 10 years moving time window.

Due to the scarcity of data, the changes of asymmetry might be influenced by the specific events, but we can see how the progresses of asymmetry are different in the summer and winter period.

Figure 4-4 shows the change of *asymmetry2* for the winter period. The very interesting point is that the result is quite similar to the result of entire data shown in Figure 3-26 and Figure 3-27. But the Figure 4-5, which shows the same result of summer period, seems not much relevant to the behavior from the entire data. This means, in a word, winter is more dominant for behavior of *asymmetry2* for entire period than summer.

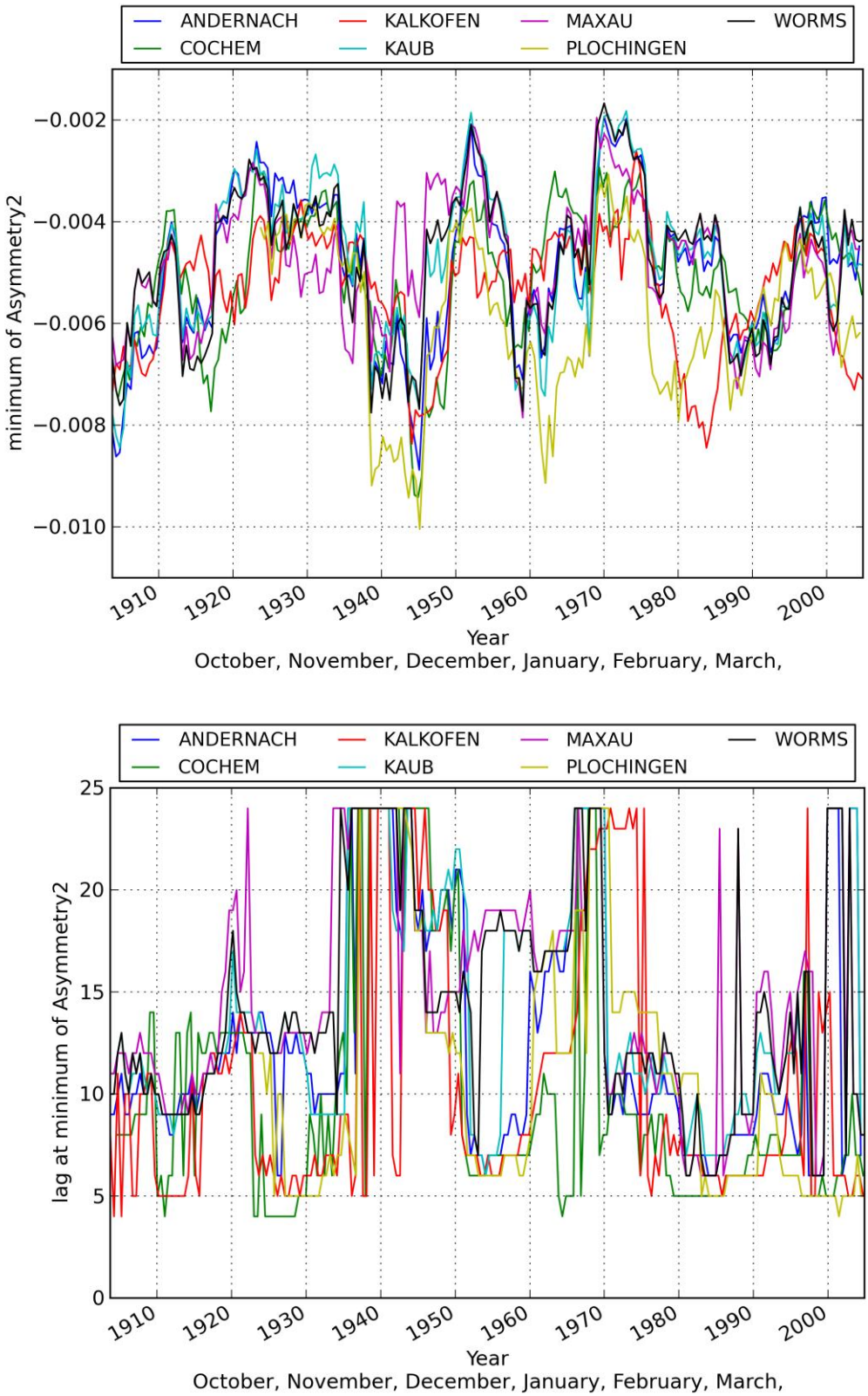

Figure 4-4 temporal change of *asymmetry2* in the winter period (top: A_{2min} minimum of *asymmetry2*, bottom: L_{2min} lag at the minimum of *asymmetry2*)

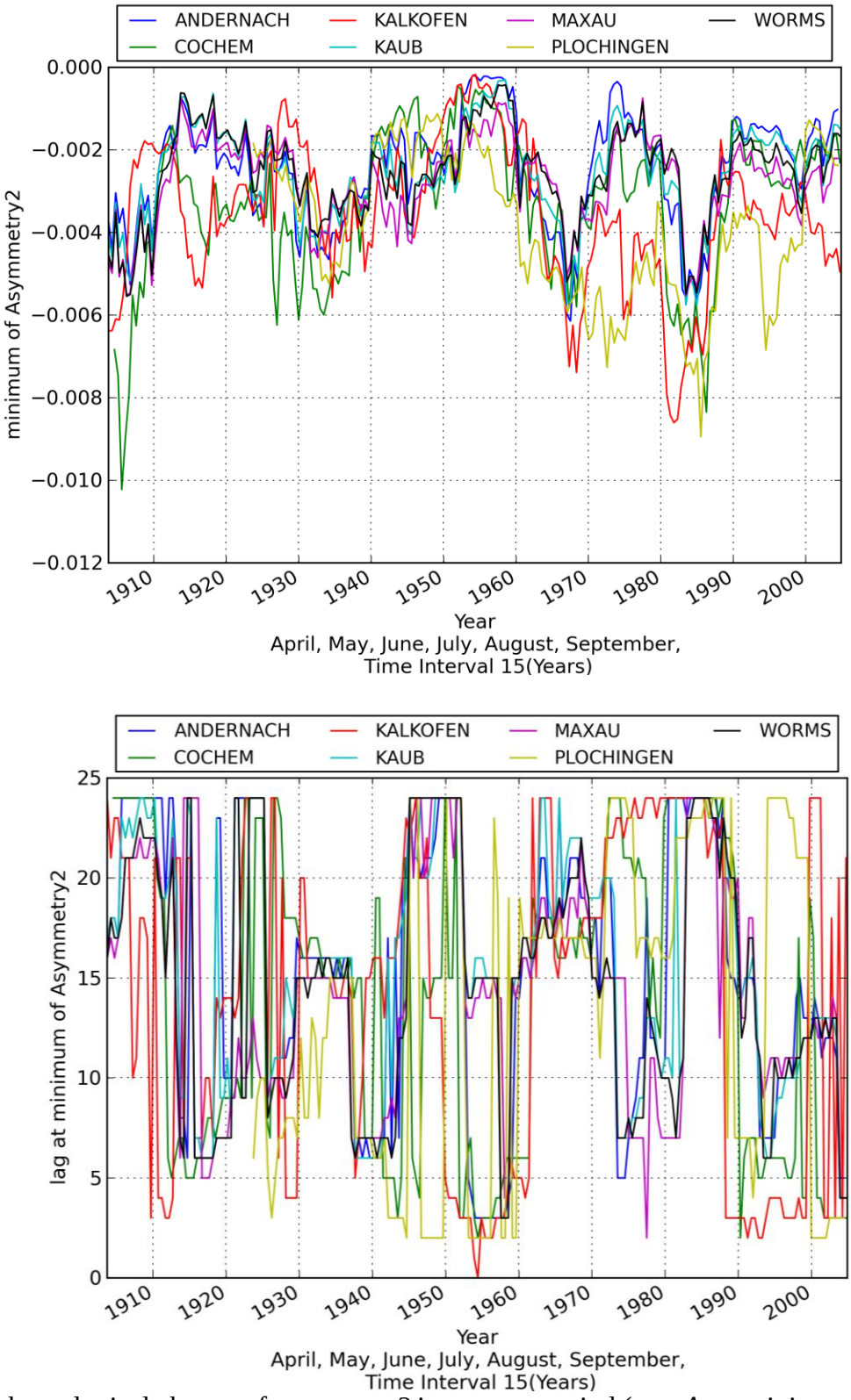

Figure 4-5 chronological change of *asymmetry2* in summer period (top: A_{2min} minimum of *asymmetry2*, bottom: L_{2min} lag at the minimum of *asymmetry2*)

This interpretation is understandable, because big and long runoff events come usually in winter for the river Rhine while rainfall-runoff events in summer can be locally intensive, but for a whole

catchment, its duration and intensity can be shorter and smaller. This gives less impact on drop down of *asymmetr-y2* shown in Figure 3-22.

If there are less rainfall-runoff events in winter, then the influence of the winter period on the behavior of *asymmetry2* gets weaker and characteristic of summer period can come up. In summer period the structure of drop down is not clear, as a consequence, L_{2min} gets longer and A_{2min} gets closer to 0 according to the analysis in Chapter 4.1 as shown in Figure 4-2.

Figure 4-6 shows mean and standard deviation in moving time window for winter and summer season. The figure indicates, 1945 and 1975 are both relatively dry both in winter and summer, but the standard deviation around 1945 in winter is usually high.

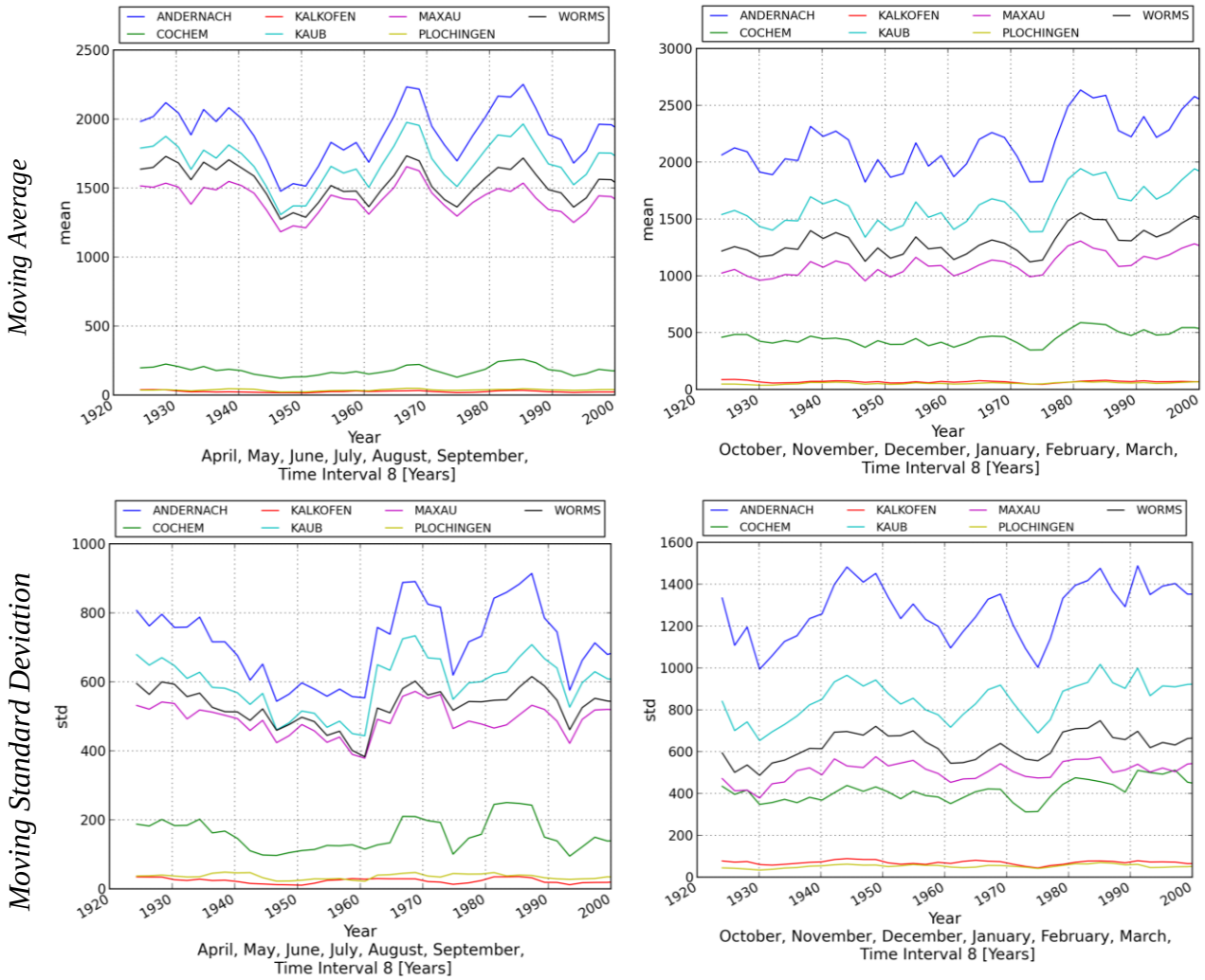

Figure 4-6 Moving Average and Standard Deviation in summer and winter

Although it is suspected that discharges in winter have more impacts on the behavior of *asymmetry2* in moving time window, it is still difficult to mean discharge or its standard deviation in winter period cause the unusual behavior.

The problem of this analysis is that, even if the data of certain season was chosen, the structure of asymmetry, namely drop down of *asymmetry2*, is not clear for certain period. Although it is

possible to separate into smaller seasons, it will be too much detail for less data, then it gets harder to conclude something.

In the next section, as the last part of asymmetry analysis, asymmetries for quite small lags (k = *1*, *2*, *3*[days]) will be investigated, where we don't look at the minimum (A_{2min} and L_{2min}) any more, but just look at the value of *asymmetry2*.

4.3 Behavior of Asymmetry for the Small Lag Times (*k = 1,2,3* [days])

In the previous section, the behavior of *asymmetry2* seems dominated rather by the discharges in winter period. In this section, the focus is not on minimum of asymmetry (A_{2min} or L_{2min}), but just look at the asymmetries for quite small lags (*k = 1, 2, 3* [days]). This can be regarded as relatively instantaneous reaction of catchment, thus it might represent the catchment characteristics more.

The results of *asymmetry1* for summer and winter period are shown in Figure 4-7. The results of *asymmtery2* for summer and winter period are shown in Figure 4-8. The remarks are summarized:

Asymmetry1 **(**Figure 4-7***)***:

In summer:

- The results from the gauging stations with small catchments like Kalkofen, Plochingen, and Cochem are different from the rest.
- The values from those stations (Kalkofen, Plochingen, and Cochem) vary a lot.

In winter

- There are drop downs of *asymmetry1* around 1920 and 1965.
- Not only the results from Kalkofen, Plochingen, and Cochem, but also the results from other stations are also varying.

Asymmetry2 (Figure 4-8):
The values of *asymmetry2* for Kalkofen, Plochingen, and Cochem are smaller for both winter and summer season.

In summer

- There is a clear drop down in summer around 1938

In winter

- for the winter period, there is a drop down between 1980~ 1985

Since *asymmetry1* is supposed to represent the configuration of rainfalls as discussed in section 2.5, the catchment size and location has the great impact on *asymetry1*. Therefore, the results of asymmetry1 for smaller catchments like Kalkofen, Plochingen, and Cochem are different from others.

In smaller catchments, water level in the river rises quickly and down to the normal state in short time. There are less impacts of snow melt or the variations of climatic inside a catchment. This can lead the smaller values of *asymetry1 and assymetry2* in these catchments.

Figure 4-9 shows the behavior of *asymmetry1* and *asymmetry2* for time lag k = 1, 2, 3 of entire season. The results seem to be the integration of the behavior in summer and winter period.

4.3.1 Asymmetry1 for k = 1, 2, 3 [days]

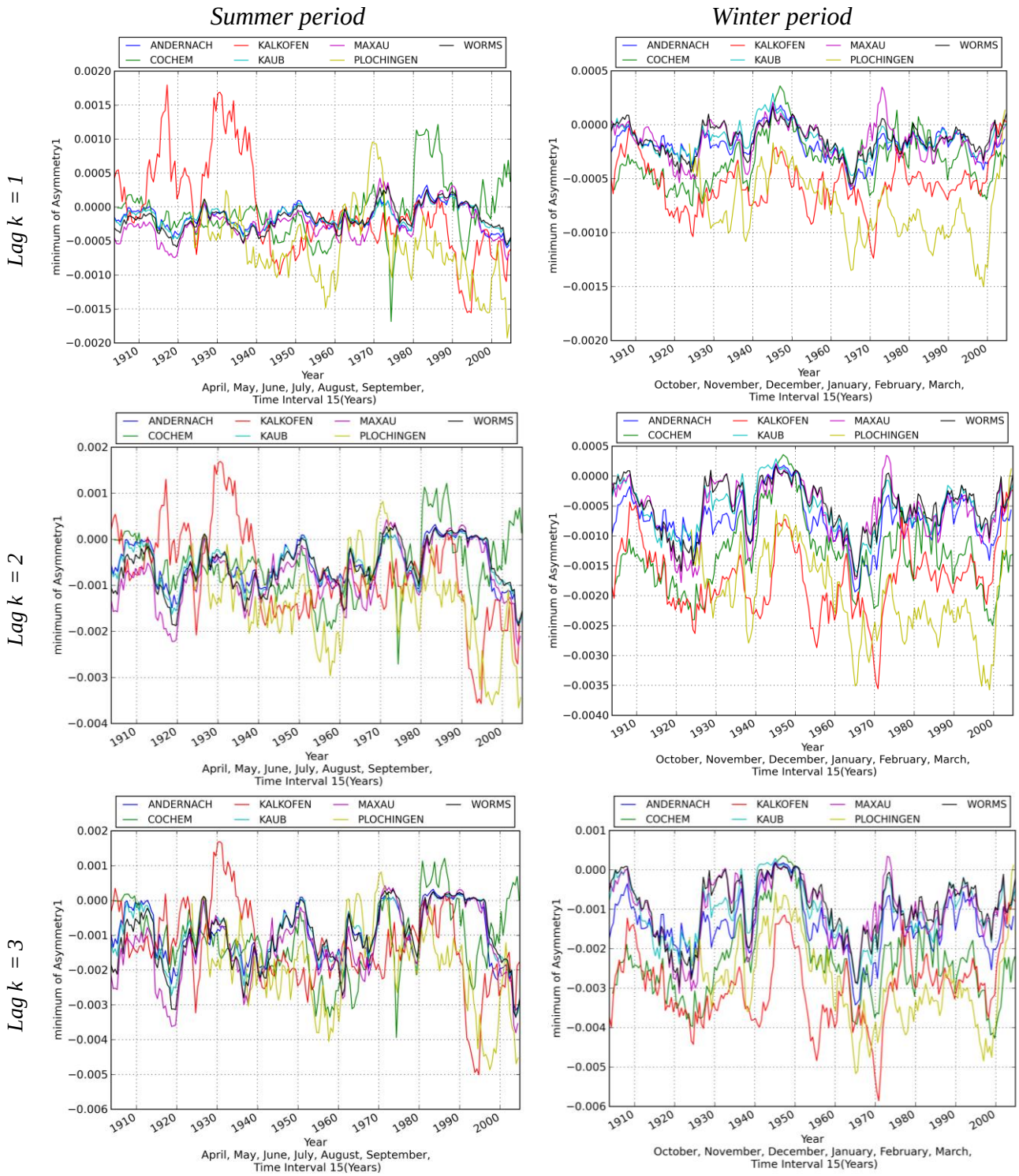

Figure 4-7 *Asymmetry1* in summer period and winter period for time lag k = 1, 2, 3 [days]

4.3.2 Asymmetry2 for k = 1, 2, 3 [days]

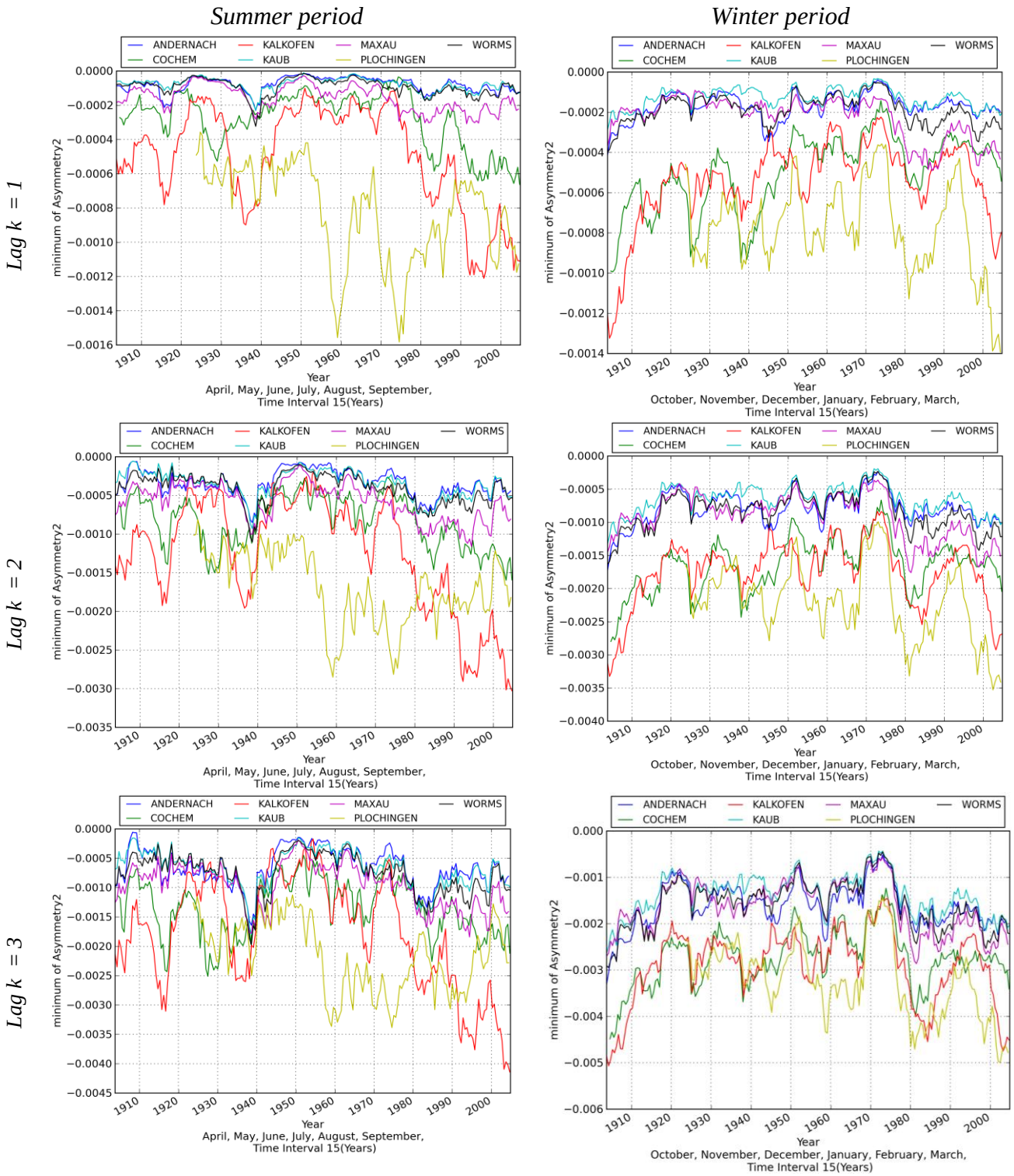

Figure 4-8 *Asymmetry2* in summer period and winter period for time lag k = 1, 2, 3 [days]

4.3.3 Asymmetry for the Entire Year

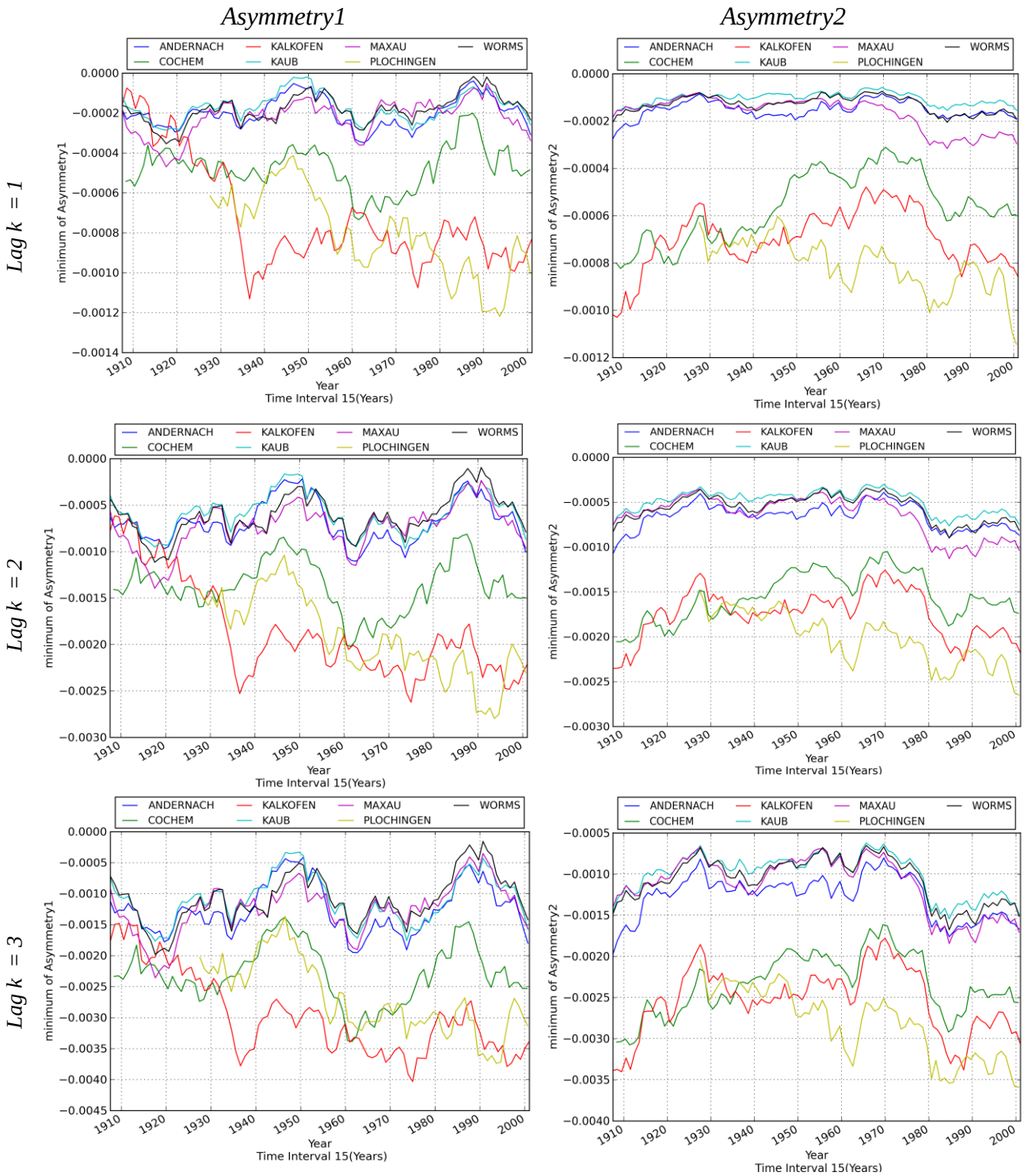

Figure 4-9 *Asymmetry1* and *Asymmetry2* for time lag k = 1, 2, 3 [days] for the whole season (no seasonal separation of original data)

In this chapter, seasonal behavior of autocopulas is investigated due to the important fact that the autocopulas and its asymmetries are different for different seasons, although the analyses in other chapters are done without separating the data into different seasons.

It was concluded the drop down structure of *asymmetry2*, A_{2min} and L_{min}, was clear in the data of winter, but not in summer (Figure 4-2). It could be also said that temporal change of *asymmetry2* in moving time window is more dominated by behavior of winter (Figure 4-4).

There is a fact that A_{2min} and L_{min} might represent only the characteristics of winter, which could lead the assumption that *asymmetry2* is influenced by seasonal rainfall in winter period

For the last part the temporal behavior of asymmetry for small time lag k = 1, 2, 3 for winter and summer are investigated. It seems difficult to extract further meaningful information, but will be investigated with another method in chapter 7.

The interest of this study is whether these behaviors are caused by the change of catchment characteristic or caused by the behavior of rainfall. However, the conclusion of these investigations is that, it is still very difficult to detect the significant change of the catchments. The results imply the runoff events in winter dominate the change of *asymmetry2*.

5 Analysis of Rainfall with Copula

In the previous chapter, it was not clear whether the unusual behavior of asymmetries is caused by the unusual behavior of rainfall or catchments characteristics. The goal of this chapter is to investigate stochastic properties of rainfall data.

For this purpose, daily precipitation data of 525 stations in Baden-Württemberg are investigated, which is offered from the German weather service. The stations are located in the entire region of Baden-Württemberg in Germany, but each station has different observation periods. The problem in rainfall data is temporal and spatial inhomogeneity.

The approach in this study is to average all the existing daily precipitation data in entire Baden-Württemberg or certain regions for each day so that one representative averaged daily precipitation can be obtained. Figure 5-1 shows the number of existing data and the daily precipitation averaged for entire Baden-Württemberg. It can be seen that less amount of rainfall data exists before 1930, around 1945 and after 2004. The data might not be really reliable before 1950 and after 2000, but it is still worth to show in order to know what is happening around 1945 or after 2000, because daily discharge data exists since 1900 and averaged daily precipitation has precious information to understand them.

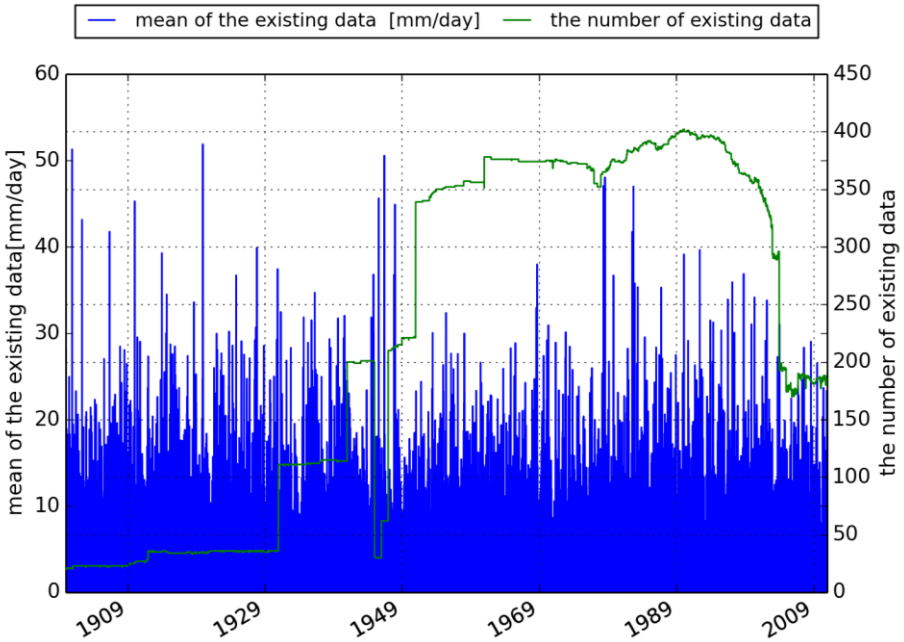

Figure 5-1 the number of existing data and the daily precipitations as average of existing data in Baden-Württemberg

5.1 Statistical and Copula Based Analysis of API

The number of existing data and locations of measuring stations changed over time. Therefore it is not apparent how representative this averaged daily precipitation over Baden-Württemberg is. This averaged precipitation can integrate information about Baden-Württemberg. A number of statistical and copula based analysis was done in this section for the comparison between observed discharge and rainfall data so that it can be specified whether the behavior of asymmetry is caused by rainfall or anthropogenic impacts.

However, the characteristics of the time series of precipitation is completely different from discharge, thus a different method for analysis is needed. Here, antecedent precipitation index (API) is used, which makes it possible to investigate precipitation data in a similar way to discharge data:

$$API(t+1) = \alpha API(t) + P(t+1) \tag{5.1}$$

where α is a constant and should be between 0 and 1. $\alpha = 0.85$ was chosen for this analysis. API can be considered as an index for soil moisture and thus also influences the amount of water released to river. It is noted that in the definition of API there is no consideration of physically based processes such as evapotranspiration, ground water flow or routing.

For example, Figure 5-2 shows a part of an API time series. It can be immediately seen that there exists *asymmetry1*, which means there are more often low values in two consecutive days than high values, and a*symmetry2*, which characterizes the water increase and decrease.

In the Figure 5-3, Figure 5-4, Figure 5-5, Figure 5-6, the typical statistics such as annual cycle or moving average of API are shown similar to the analysis done in chapter 3.

The point is that the statistical behavior of API in moving window is actually similar to the one from discharge data. For example, around 1945, there is less amount of precipitation in terms of moving average, but its standard deviation is big similar to the case of discharge data (Figure 3-33 Figure 3-34).

Now Figure 5-8, Figure 5-7 show the temporal changes of *asymmetry1* and *asymmetry2*. These results of *asymmetry1* and *asymmetry2* are comparable to the results from discharge data (Figure 3-26, Figure 3-27, Figure 3-35). In Figure 5-10, temporal change of *asymmetry2* of API and discharges are plotted in one graph. It can be clearly seen that the behaviors of $\boldsymbol{A_{2min}}$ (Asymmetry2 at minimum) before 1920, around 1945 and after 1980 are similar. This means, the drop down of *asymmetry2* around 1945 and 1985 is more likely to be caused by the specific realization of random behavior of rainfall.

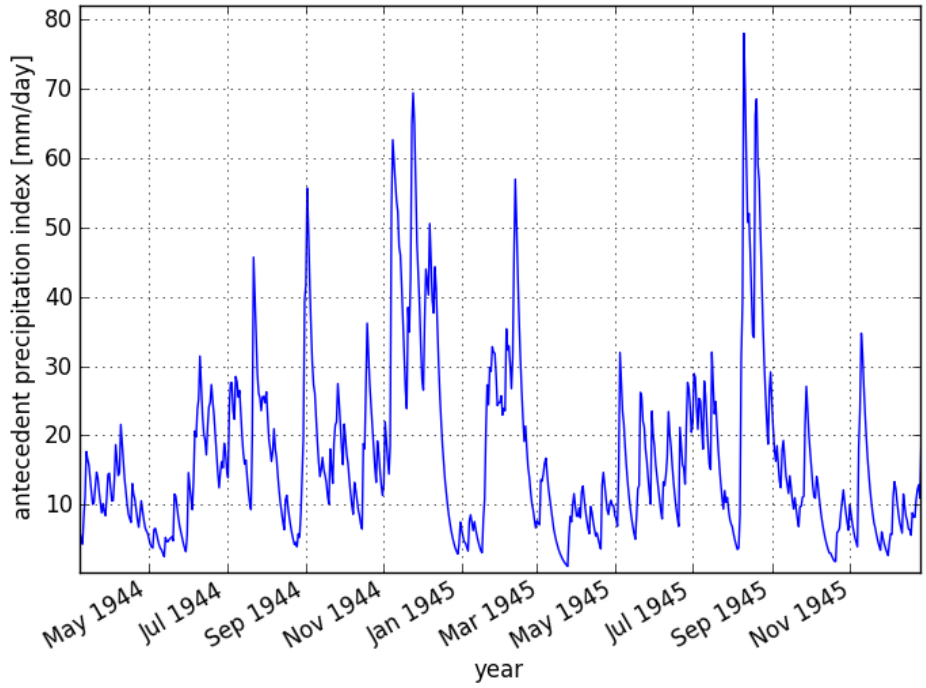

Figure 5-2 Sample of Antecedent Precipitation Index time series

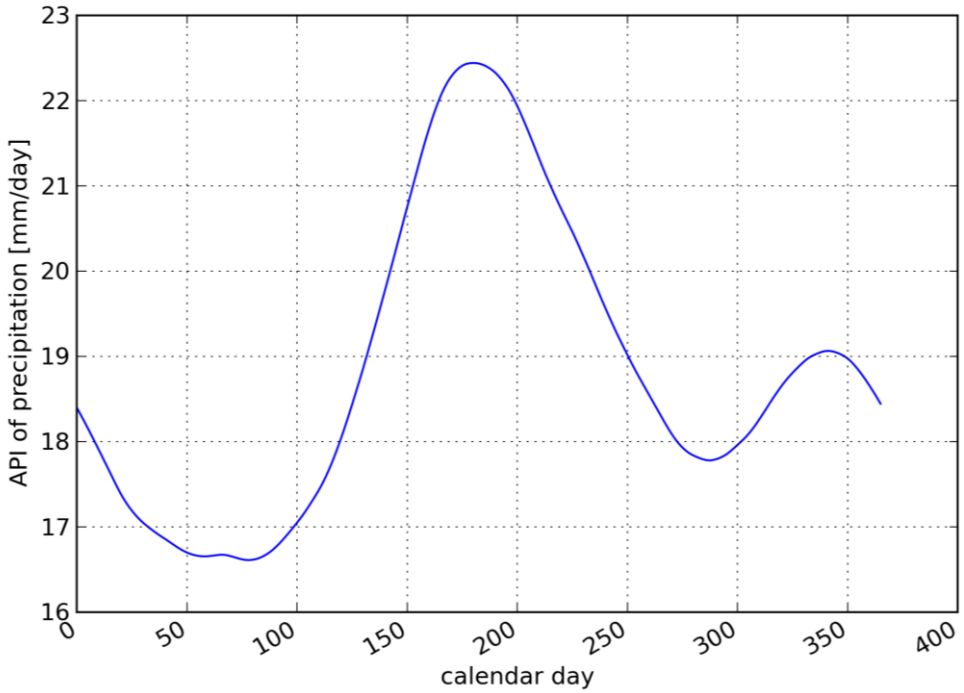

Figure 5-3 annual cycle of mean of the API of regionally averaged daily precipitation from Baden-Württemberg

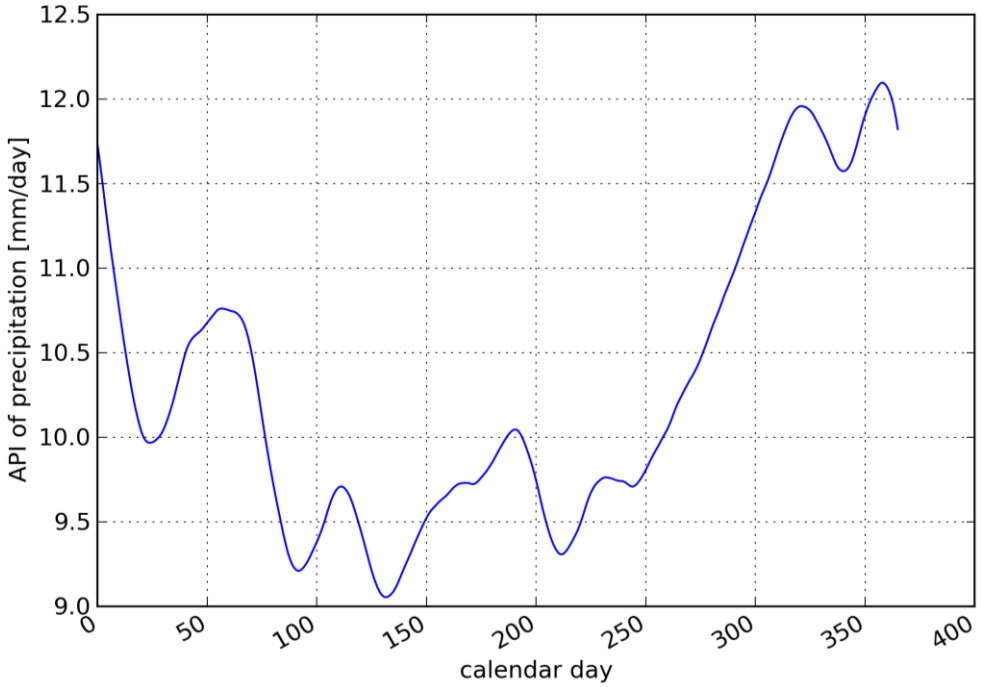

Figure 5-4 annual cycle of standard deviation of the API of regional average daily precipitation from Baden-Württemberg

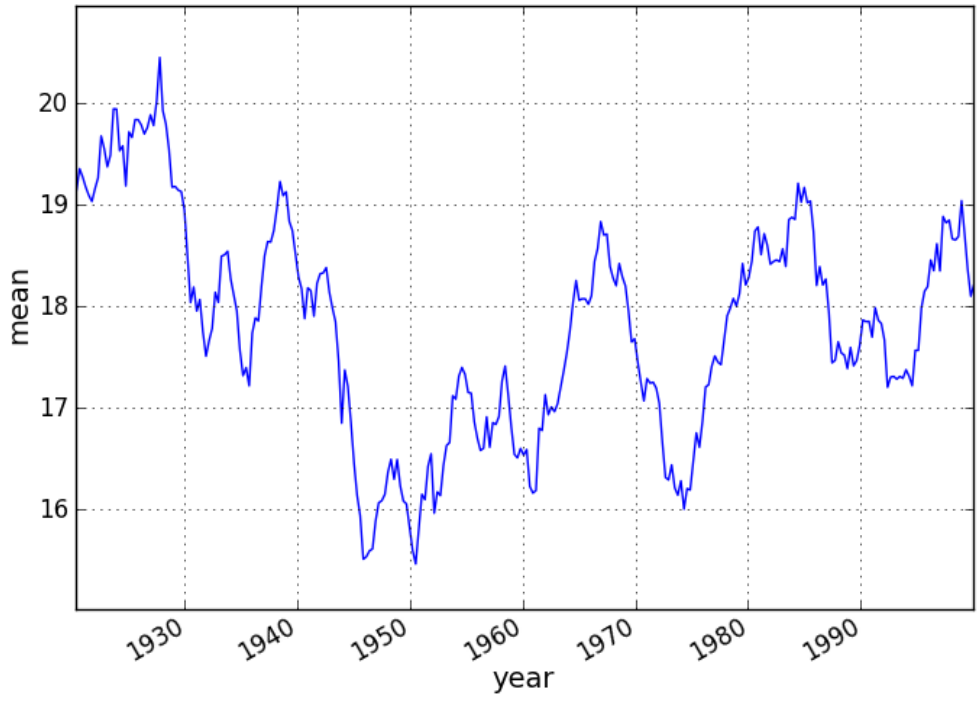

Figure 5-5 Moving Average of API time series calculated for averaged daily precipitations of entire Baden-Württemberg region

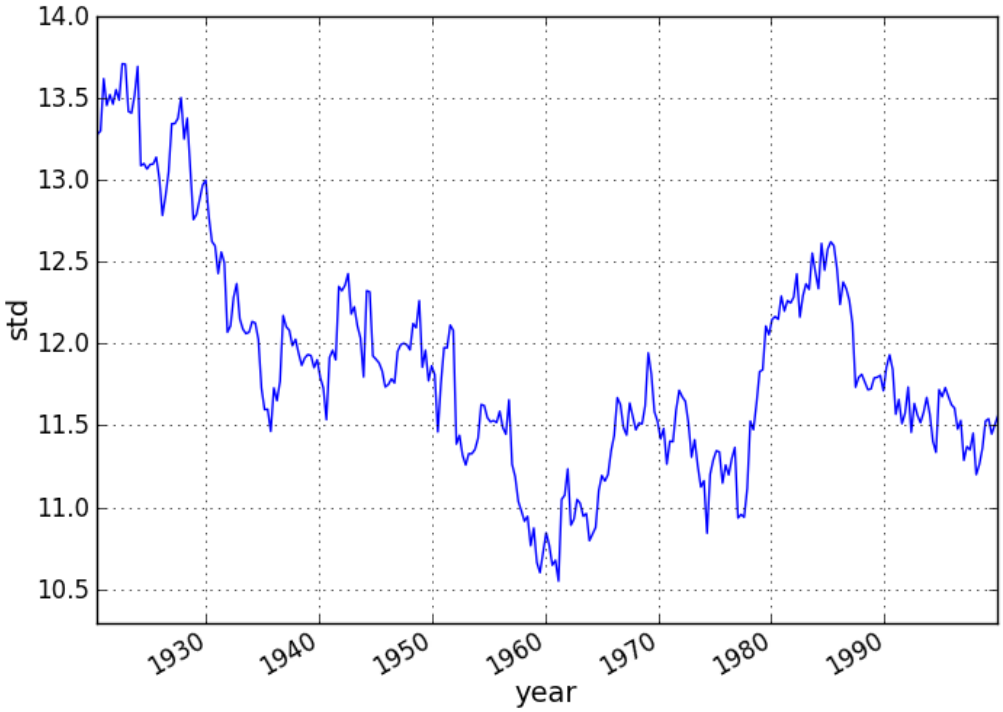

Figure 5-6 Moving standard deviation of API time series calculated for averaged daily precipitations of entire Baden-Württemberg region

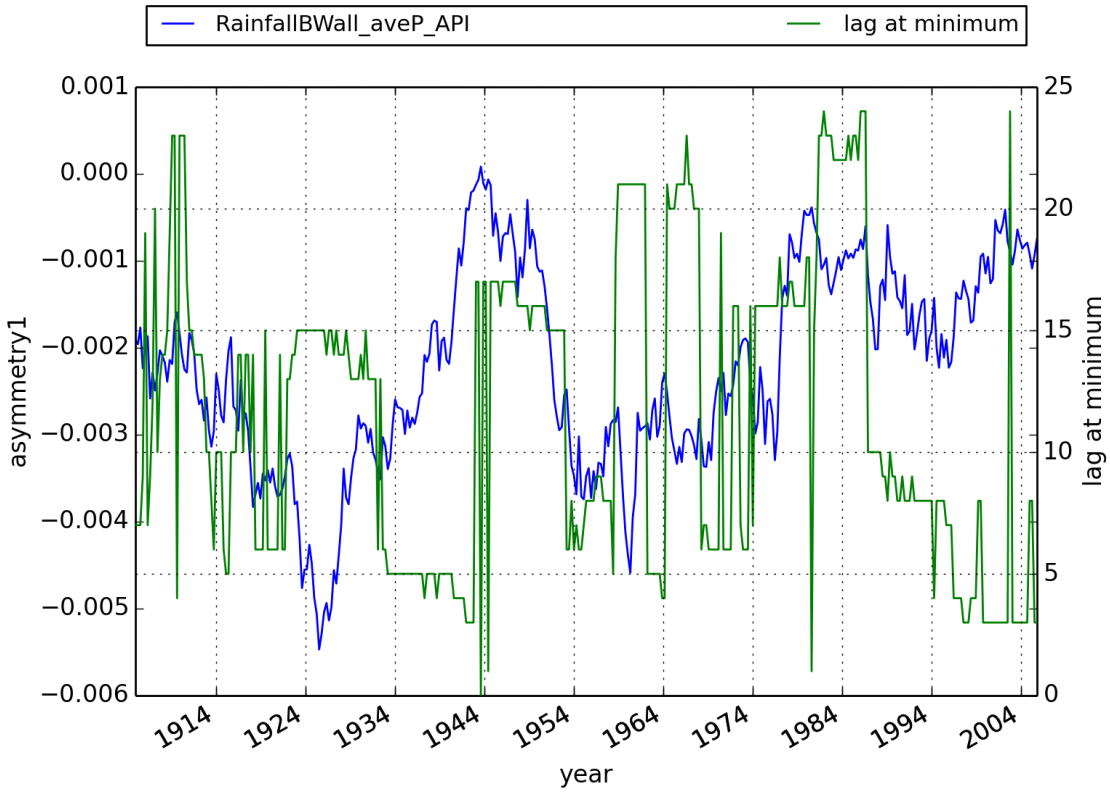

Figure 5-7 temporal change of *asymmetry1* (minimum and lag at minimum) of API in moving time window of 10 years interval

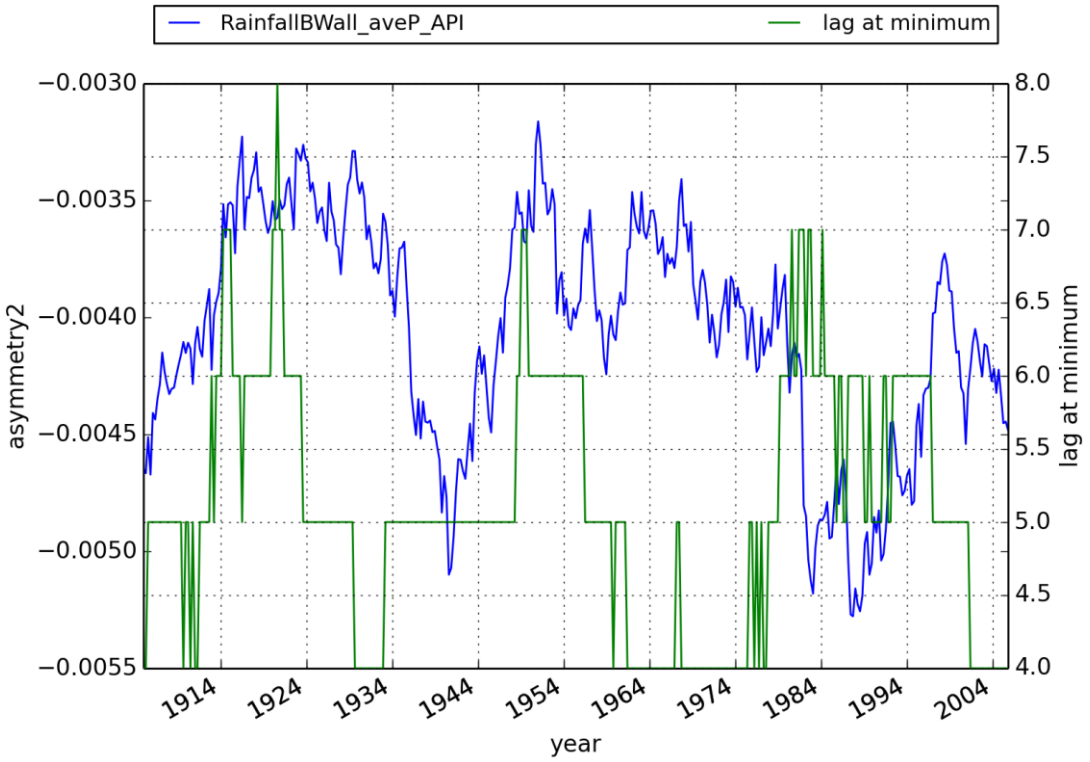

Figure 5-8 temporal change of *asymmetry2* (minimum A_{2min} and lag at minimum L_{min}) of API in moving time window of 10 years interval

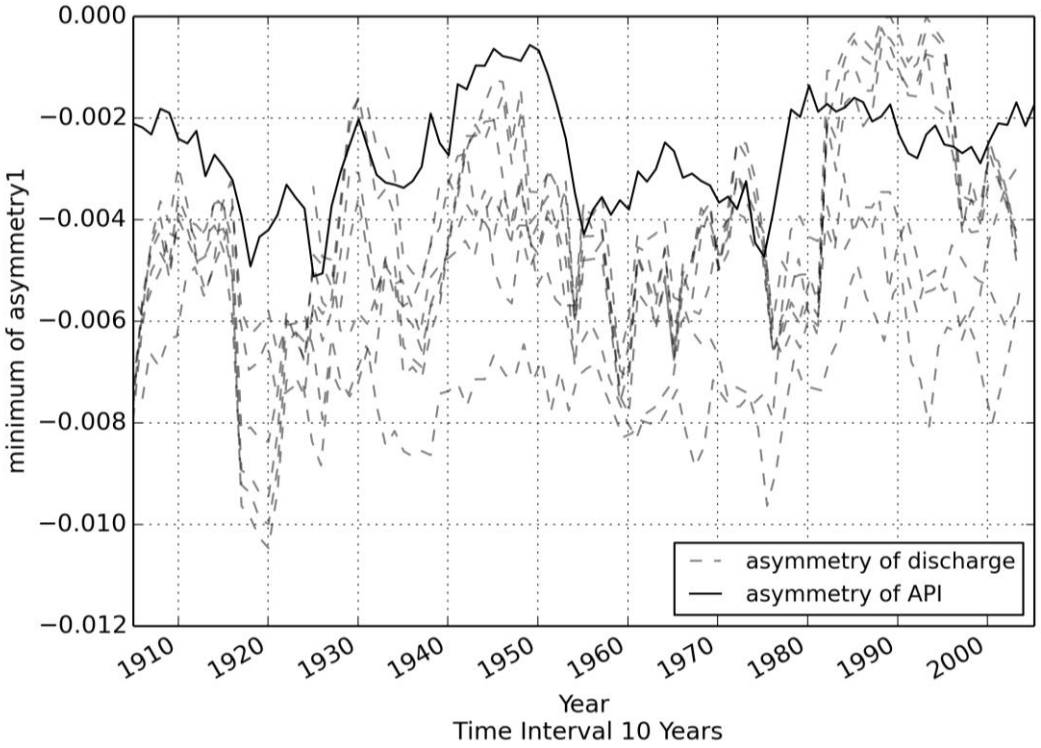

Figure 5-9 Temporal change of minimum of *asymmetry1* for API and discharges (Andernach, Kaub, Worms Maxau, Cochem, Plochingen, Kalkofen)

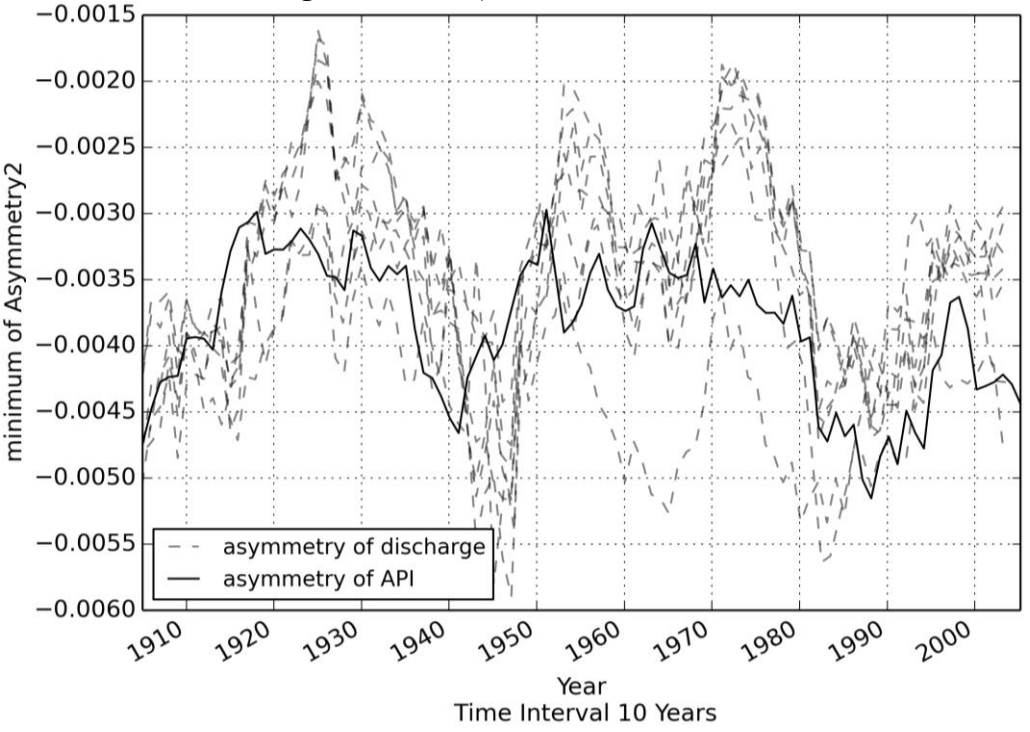

Figure 5-10 Temporal change of minimum of *asymmetry2* for API and discharges (Andernach, Kaub, Worms Maxau, Cochem, Plochingen, Kalkofen)

5.2 Analysis of Rainfall in the Small Regions

The existence of daily precipitation data without discontinuity for such a long time period is rare, especially before 1950. Even if a little amount of data is available, it is not ascertained that the data represents entire catchment due to the spatial and temporal variability of precipitation.

However, as a test case, a detailed investigation for a few continuous daily precipitations time series is done in the regions in which the continuous data exists since 1945 so that any signal of changes or unusual behavior can be detected.

It is found that certain regions of Baden-Württemberg have longer records without missing value: (1) northwestern BW, (2) northeastern BW, (3) southern BW and (4) Center of BW. The analysis based on asymmetry was done for these data same to the previous sections.

Figure 5-11 shows the number of existing data and the average of those daily precipitations. There exist at least one and at most 9 data in these regions for investigated period, although it is not assured how representable these data for the rainfall characteristic of each region is. But, there is possibility it could give some insight about the behavior of rainfall inside Baden-Württemberg region and the source that temporal behavior of asymmetry comes from.

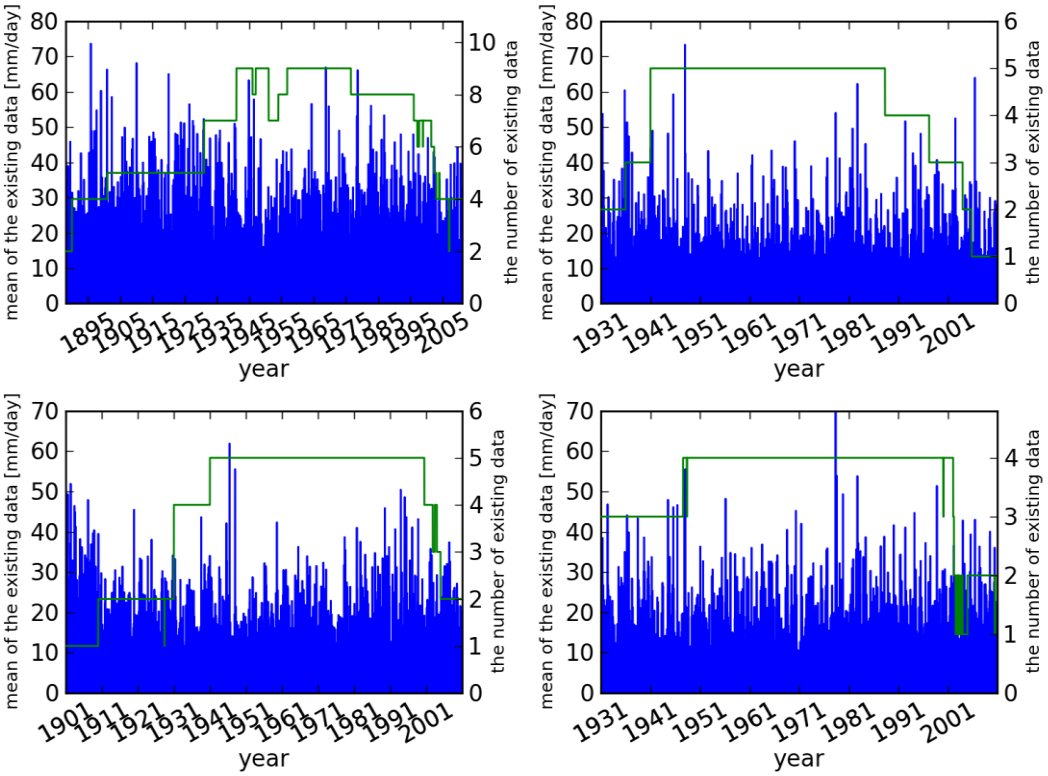

Figure 5-11 the number of existing data and averaged precipitation in each region of Baden-Württemberg and its regional average. (1) South of BW (upper left), (2) Northwest of BW (upper right), (3) Northeast of BW (bottom left), (4) Center of BW (bottom right)

Figure 5-12 and Figure 5-13 show the annual cycle of mean and standard deviation respectively. The figures show rainfall comes mainly in summer for all the regions and partially in winter. But the standard deviation is apt to be high in winter in the region where annual cycle of mean is relatively high in winter.

Figure 5-14 and Figure 5-15 shows the statistics (mean and standard deviation) in moving time window. Mean is small around 1945 and 1970 for all the regions and big around 1980. Standard deviation is a bit high around 1980 for South of BW and North East of BW, but all the regions behave similar for other period.

Figure 5-16 and Figure 5-17 shows the temporal change of minimum of asymmtery2 A_{min2} and lag at minimum L_{min}. A_{min2} is small around 1945 and after 1980 for all the regions.

These results confirm that similar behavior of asymmetry2 can be seen in smaller regional scale.

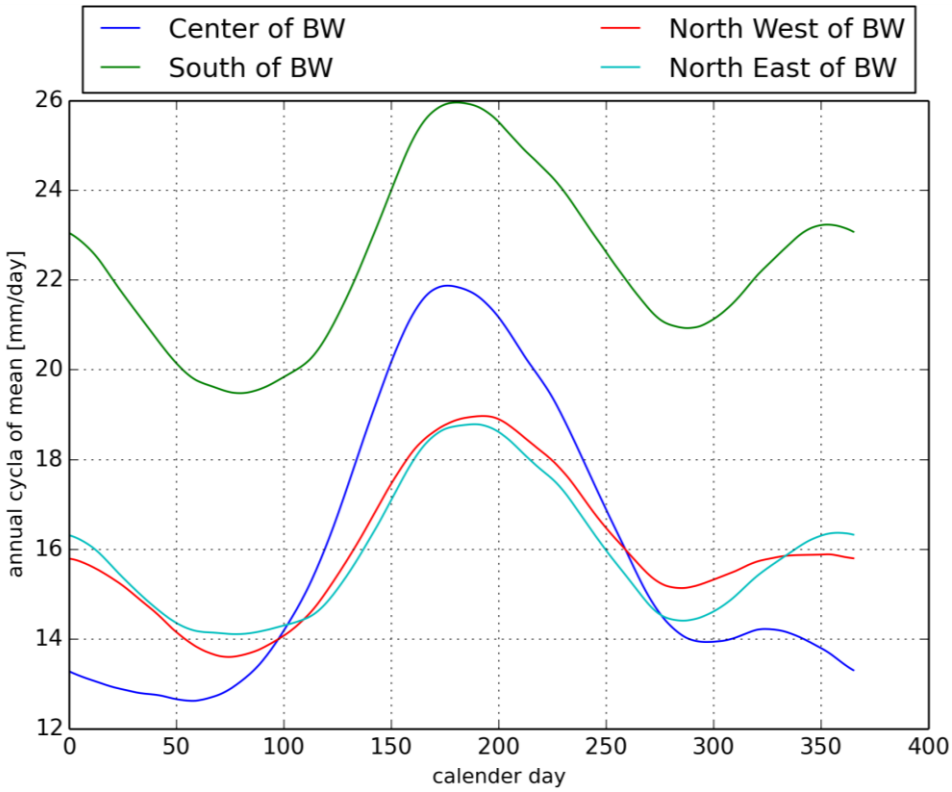

Figure 5-12 Annual Cycle of Mean of API from 4 different regions in Baden-Württemberg

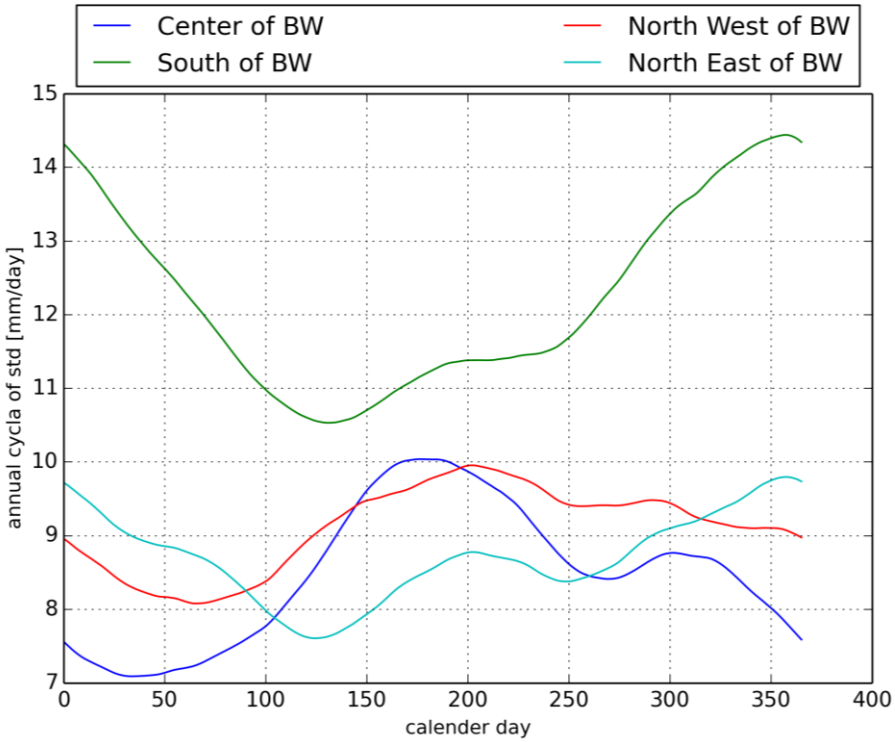

Figure 5-13 Annual Cycle of Standard Deviation of API from 4 different regions in Baden-Württemberg

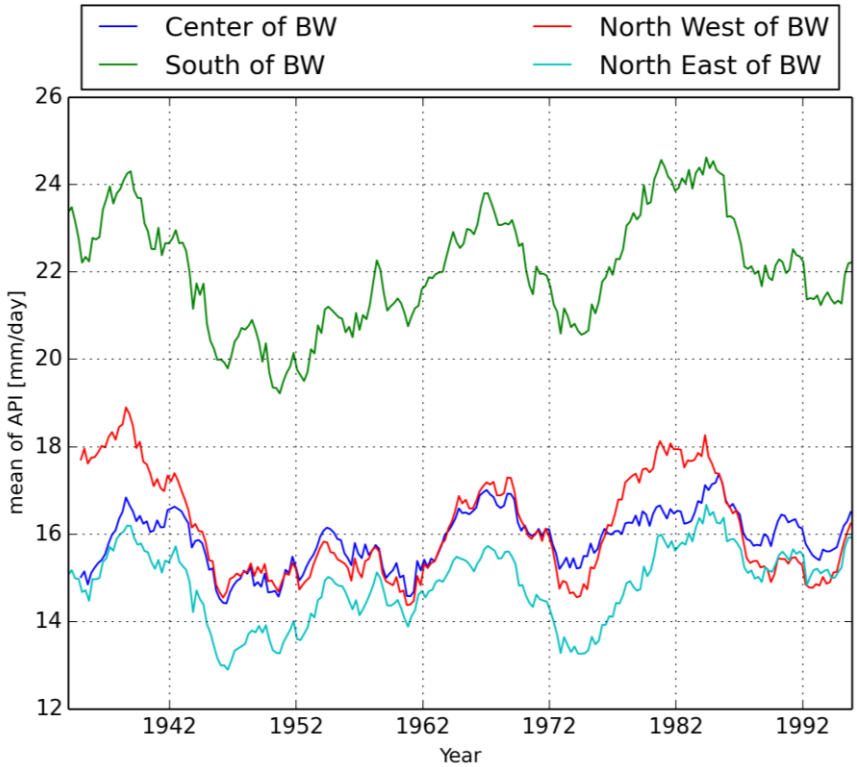

Figure 5-14 Temporal change of mean of API in the moving time window from 4 different regions in Baden-Württemberg

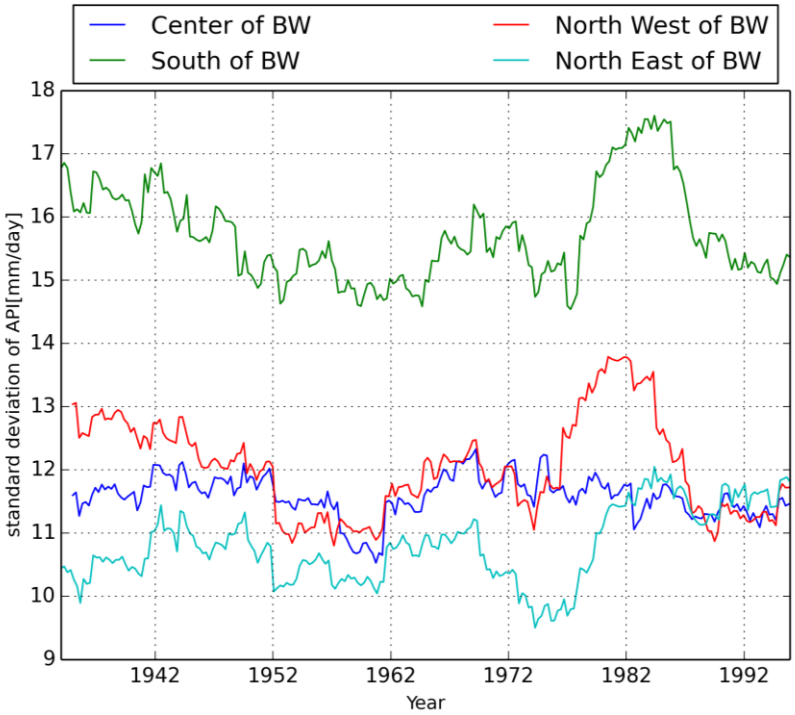

Figure 5-15 Temporal change of the standard deviation of API in the moving time window from 4 different regions in Baden-Württemberg

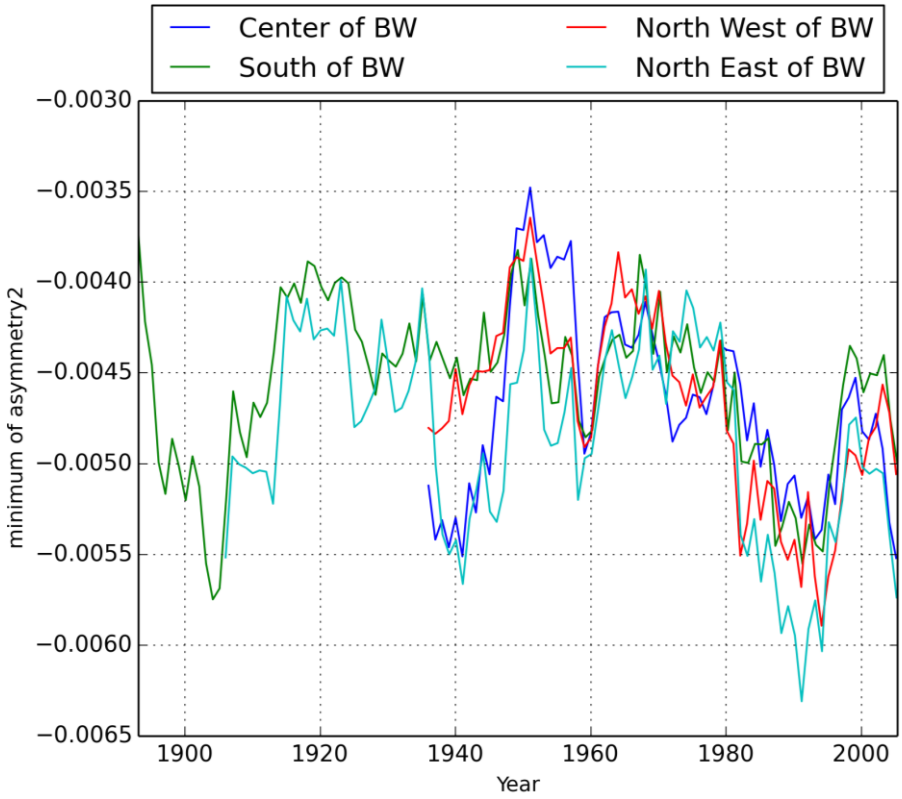

Figure 5-16 Temporal change of the minimum of *asymmetry2* (A_{2min}) calculated from API time series for 4 different regions in Baden-Württemberg

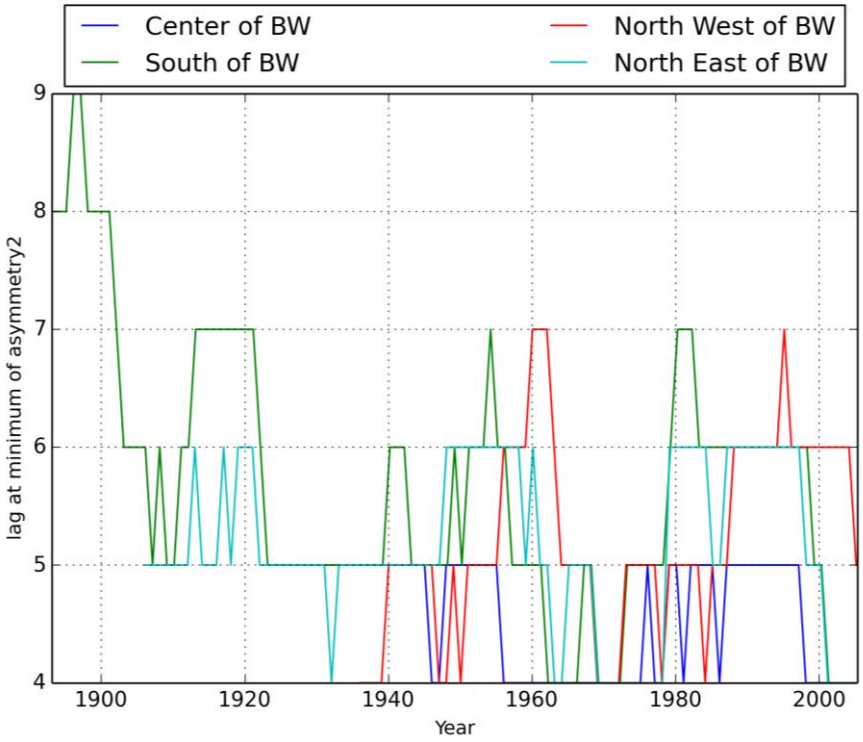

Figure 5-17 Temporal change of lag k at minimum (L_{min}) of *asymmetry2* calculate from API time series for 4 different regions in Baden-Württemberg

In this chapter, asymmetries of precipitation time series were investigated using API after averaging the 525 daily precipitation data of the region. The interesting point of this result was that there was temporal change of *asymmetry2* in moving time window which is similar to the result of discharge data, which support more the assumption that behavior of *asymmetry2* is mainly dominated by the rainfall.

In the second part of this chapter, the API time series of smaller regions in which only a few daily precipitation data exist are investigated as a test case. It was seen that the structure of drop down of *asymmetry2*, namely A_{2min} and L_{min}, are somehow similar to the case with 525 daily precipitation data.

6 Hydrological Model and Copula

The results in the previous section indicate the temporal behavior of asymmetry is likely to arise not from the catchment characteristics, but from precipitation. The approach in this chapter is that, if a more accurate hydrological model can be set up with a constant parameter set calibrated for the entire simulation period, the simulated discharge should not reflect any influence of anthropogenic impact, because the HBV model is supposed not to change. At the same time, stochastic properties of observed discharge are supposed to keep changing, because the catchment in nature can change due to the anthropogenic impacts, climate change or any other possible reasons during the simulation period. Then, the time series of observed and simulated discharge can be stochastically analyzed with the help of copula to detect any difference.

Based on this idea, a conceptual hydrological model, HBV (Bergström 1976 ; Bergström, Singh, and others 1995), is set up and calibrated using data for last 30 years from Neckar Catchment. For stochastic analysis, 50 parameter sets are independently calibrated using the simulated annealing algorithm (Kirkpatrick, Jr., and Vecchi 1983) and 50 different time series of simulated discharges are generated to be compared with observed discharge.

The main problem for this task is that more data is required to set up and run the hydrological model to simulate a discharge time series of a catchment. However, in comparison to the discharge data it is in general hard to find long term continuous data without missing values for precipitations and temperature. In this study, one of the catchment in upper Neckar Region, Suessen, was chosen and simulation period was set between 1970 and 2000 in terms of data continuity.

This is a kind of pioneering work, but it is recommendable to construct more precise physically based model combined with complete climate data for better representation of the catchment and rainfall-runoff process in order to achieve the goal of this analysis.

The HBV model was selected for this study because it does not require too extensive input data. There are several versions of HBV, but in this study, the model considering topographic conditions is chosen in which a catchment is composed of several sub-catchments representing different elevation zones and different parameters are introduced for each sub-catchment.

The study is based on the previous work of (Kamkaew 2013). A brief description of this HBV model is given in section 6.1, calibration process and generated parameter sets are presented in section 6.2 and the result of stochastic analysis with Copula is shown in section 0.

6.1 HBV Model

The HBV model consists of three main routines for "snow accumulation and melt", "evapotranspiration estimating and soil moisture accounting" and "runoff response and routing processes" (Figure 6-1). The HBV model in this study set a catchment as primary hydrologic unit. One catchment can be further divided into homogeneous zones based on elevations. Input data are observed precipitation and air temperature and estimates of potential evapotranspiration. The time step is usually one day, but shorter time steps are possible. The following sections provide detailed descriptions of each routine.

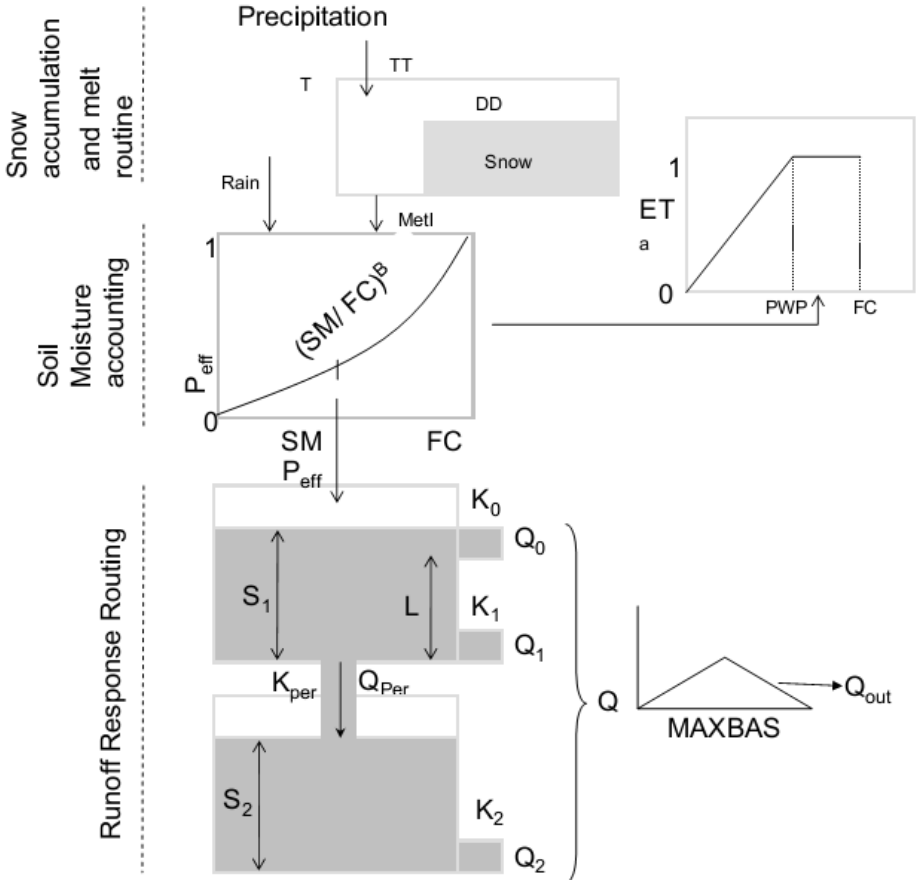

Figure 6-1 Schematic of modified HBV Model (Singh, 2010)

The description about the model structure and meaning of the symbols are shown below (Table 6-1).

Table 6-1 List of the symbols used for description of HBV model

$MELT$	$[LT^{-1}]$	=	snowmelt rate as water equivalent
DD	$[L\theta^{-1}T^{-1}]$	=	degree-day factor
T	$[\theta]$	=	mean daily air temperature
TT	$[\theta]$	=	threshold temperature for snowmelt initiation
PE_a	[L]	=	adjusted potential evapotranspiration
C	$[\theta^{-1}]$	=	a model parameter accounting for snow melting
T	$[\theta]$	=	mean daily air temperature
T_m	$[\theta]$	=	long-term mean monthly air temperature
PE_m	[L]	=	long-term mean monthly potential evapotranspiration
E_a	[L]	=	actual evapotranspiration
PWP	[L]	=	soil moisture limit where evapotranspiration decreases
SM	[L]	=	actual soil-moisture (water) content
P_{eff}	[L]	=	effective precipitation
FC	[L]	=	field capacity, maximum soil-moisture storage capacity
β	[L]	=	a model parameter, shape coefficient
P	[L]	=	daily sum precipitation
Q_0	$[LT^{-1}]$	=	near-surface flow
Q_1	$[LT^{-1}]$	=	interflow
Q_{perc}	$[LT^{-1}]$	=	percolation
Q_2	$[LT^{-1}]$	=	baseflow
K_0	$[T^{-1}]$	=	near-surface flow storage coefficient
K_1	$[T^{-1}]$	=	interflow storage coefficient
K_{perc}	$[T^{-1}]$	=	percolation coefficient
K_2	$[T^{-1}]$	=	baseflow storage coefficient
S_i	[L]	=	upper zone reservoir water storage level
S_b	[L]	=	lower zone reservoir water storage level
L	[L]	=	threshold water level for near-surface flow
A_{sc}	[L]	=	catchment or subcatchment area

6.1.1 Snow Accumulation and Melt Routine

Snow accumulation and snow melt rate are calculated based on a degree-day method. In this method, the snowmelt starts at the temperature above the threshold value (TT) and the rate is proportional to the increase in daily temperature above TT :

$$MELT = DD \cdot (T - TT) \tag{6.1}$$

Both the temperature and precipitation differences due to elevation are considered in this routine. TT (normally $0^{\circ}C$) determines if the precipitation falls as snow or rain. Thus, precipitation input is modeled as snow or rain according to prevailing temperature. Parameters to be estimated for the snow routine during the calibration are DD and TT.

6.1.2 Evapotranspiration and Soil Moisture

The soil moisture routine is the main part of runoff formation. The routine is based on two functions: evapotranspiration and the actual soil-moisture. The evapotranspiration is estimated based on monthly values of potential evapotranspiration. In order to improve model performance when either spring or summer is much colder than normal and when daily changes of the weather inputs need to be taken into account, a correction factor based on mean daily temperatures, long-term averages of monthly temperature and potential evapotranspiration are included according to the following equation:

$$PE_a = (1 + C \cdot (T - T_m)) \cdot PE_m \tag{6.2}$$

The actual soil-moisture contributes to the magnitude of the actual evapotranspiration (E_a). E_a increases as the soil becomes wetter (high water content) and until the soil-moisture limit (PWP) is reached. E_a remains almost constant at the PWP limit until the maximum soil-moisture storage, field capacity (FC), is reached (Figure 6-2 A). E_a value is non-negative and always in the range of 0 and PE_a:

$$\begin{aligned} E_a &= PE_a \frac{SM}{PWP} \quad \text{for } SM < PWP \\ E_a &= PE_a \quad \text{for } SM \geq PWP \end{aligned} \tag{6.3}$$

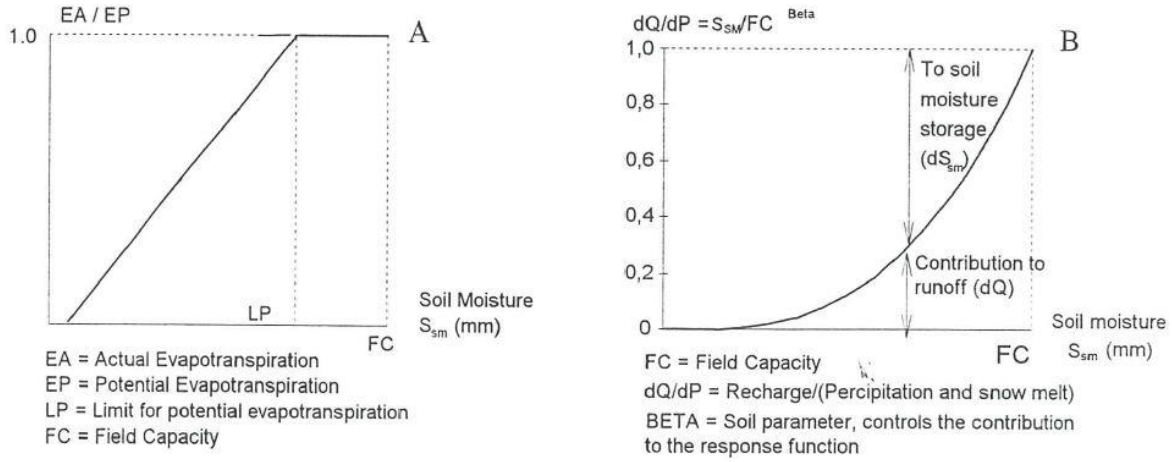

Figure 6-2 A) Actual evapotranspiration as a function of the actual soil-moisture content, B) Relative distribution to runoff from precipitation and snowmelt as a function of soil-moisture deficit.

The contribution of precipitation to runoff occurs when the FC is reached (Figure 6-2 B). The soil-moisture accounting routine computes an index of the wetness of the entire catchment and

integrates interception and soil moisture storage. The routine is controlled by two free parameters, FC and β. β controls the contribution to the response function or the increase in soil moisture storage from each millimeter of rainfall or snow melt. This is calculated using the following relation.

$$P_{eff} = \left(\frac{SM}{FC}\right)^{\beta} \cdot \left(P + MELT\right) \tag{6.4}$$

6.1.3 Runoff Response Routine

Excessing water from the soil moisture routine is modeled by the response routine in which two conceptual reservoirs arranged one over another simulates the discharge at the outlet of the catchment. The upper zone reservoir represents the drainage from the near-surface flow and interflow, while the lower zone reservoir represents the drainage from the base flow. Both reservoirs are connected in series by a constant percolation rate and are considered linear with a constant recession coefficient. In addition to the regular outlet, the upper reservoir also features a threshold-dependent runoff component: only if the reservoir level exceeds a certain threshold, will fast runoff from the upper outlet (Q_0) occur.

$$\begin{aligned}
Q_0 &= \begin{cases} \frac{1}{K_0} \cdot (S_i - L) \cdot A_{sc} & \text{for } S > L \\ 0 & \text{for } S \le L \end{cases} \\
Q_1 &= \frac{1}{K_1} \cdot (S_i) \cdot A_{sc} \\
Q_{perc} &= \frac{1}{K_{perc}} \cdot (S_i) \cdot A_{sc} \\
Q_2 &= \frac{1}{K_2} \cdot (S_b) \cdot A_{sc}
\end{aligned} \tag{6.5}$$

Total runoff from the reservoirs (the sum of Q_0,Q_1,*and* Q_2) is then smoothened through the transformation function (a filter), which evaluates the effects of water storage in reservoirs (i.e. lakes and aquifers) and stream channels, and also the effect of travel time from the origins of the flow to the outlets. The transformation function consists of a triangular weighting function (Unit Hydrograph) with one free parameter, *MAXBAS*.

$$Q = g(t, MAXBAS)\cdot)(Q_0 + Q_1 + Q_2) \tag{6.6}$$

where Q is the current overall discharge and *MAXBAS* is the duration of the triangular weighting function (Unit Hydrograph). However, the *MAXBAS* is set to 1 in this study.

In summary, there are 15 parameters to describe the HBV model, out of which 11 parameters were used for calibration in this study.

6.1.4 Data Descriptions

The required input data for this study are climatic data (precipitation, temperature and evapotranspiration) and discharge data. The precipitation and temperature data is measured at daily time steps and were obtained from the DWD (Deutscher Wetterdienst - German Meteorological Service).

a) Precipitation

Precipitation is the main input for the HBV model. Daily amounts of precipitation within the 20 km radius of the study catchment were acquired from the DWD for the period from 1971 to 2000 (Figure 6-3). The point measured data from the precipitation stations were interpolated and extrapolated in order to calculate areal surface values for each elevation class of the catchments. Thiessen polygon method was used for the interpolation. Missing data at some of the precipitation stations were interpolated from the twelve nearest neighboring stations using the inverse distance weighting method.

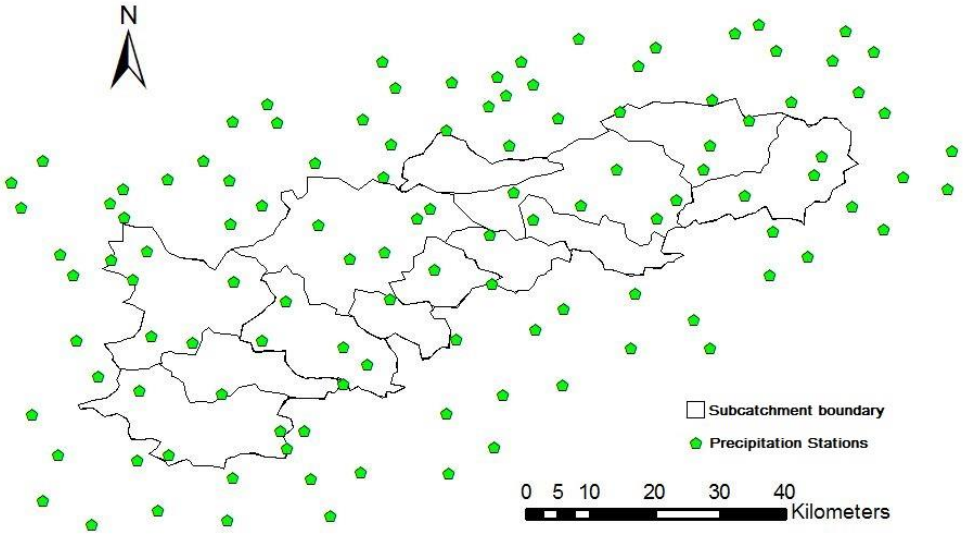

Figure 6-3 Precipitation stations network in and around the study catchment

The highly variable topography causes highly varying precipitation in the study catchment (Das 2006). The precipitation data, averaged over the observed time period, exhibit a weak annual cycle, with maximum precipitation in summer for the catchments, located in the high altitude of the Black Forest (the north-west of the catchment, subcatchment Horb). Figure 6-4 represents the annual sum and annual average precipitation of the study catchment.

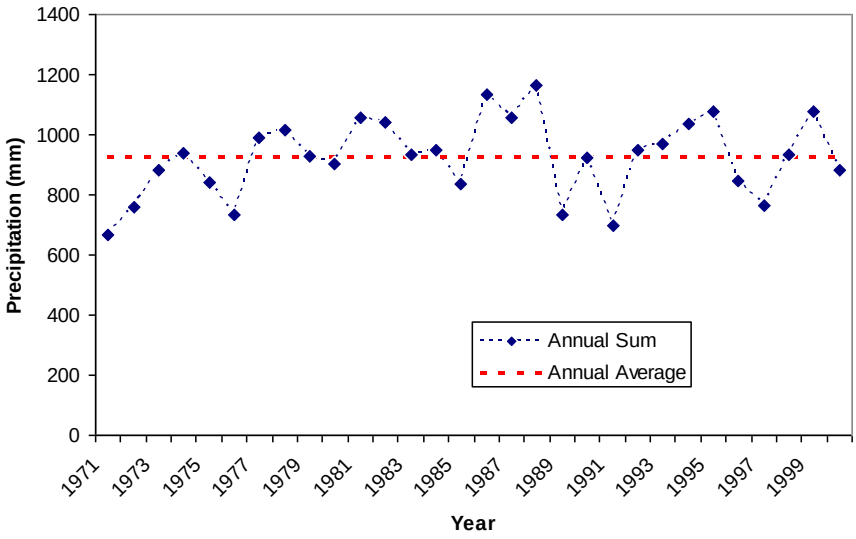

Figure 6-4 Annual sum and annual average precipitations of Neckar catchment

b) Temperature and Evapotranspiration

Temperature is another input of the HBV model that influences the snow accumulation and melting processes and evapotranspiration. Daily mean temperature values distributed in and within 20 km radius of the study catchment were also acquired from the DWD for the period from 1971 to 2000 (Figure 6-5). The raw daily temperature was corrected with the dry adiabatic lapse rate and then extrapolated to each elevation zone.

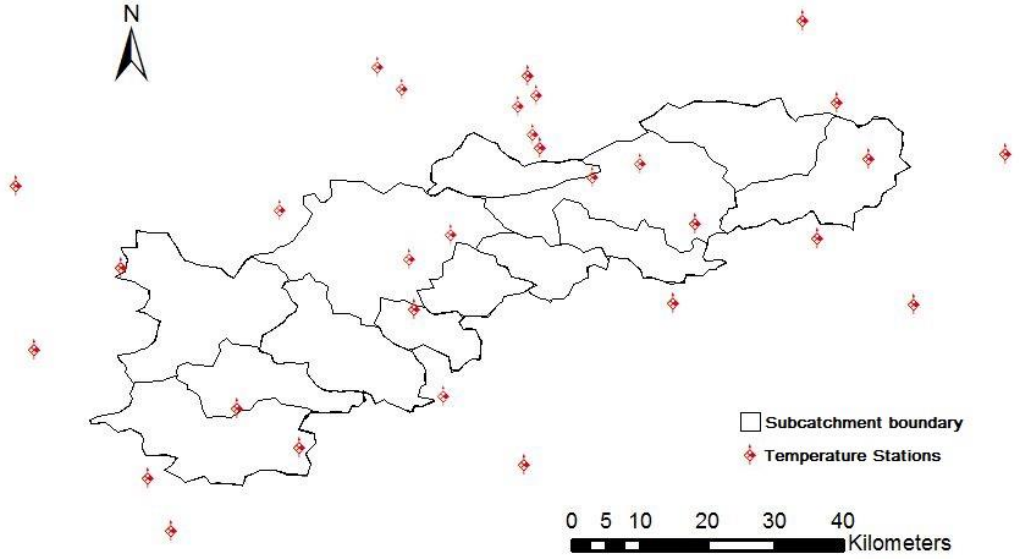

Figure 6-5 Temperature stations network in and around the study catchment.

The monthly long term average temperature values and the monthly long term average potential evapotranspiration values were taken from the 5th KLIWA report (Klämt, A. and Arbeitskreis KLIWA, 2005) and the 12th KLIWA report (Klämt and Günther, 2008), respectively. These values were used in both the semi-distributed and the lumped models.

6.2 Calibrated Parameter Sets

The HBV model has the 11 parameters to calibrate for each subcatchment. The HBV model used in this study has 6 elevation zones, which means, there are 6 different snow melting, soil moisture and runoff response routines corresponding to each elevation zones, then it has 41 parameters in total. Now, 50 sets of parameters are generated for the catchment Suessen by simulated annealing algorithm using Nash-Sutcliffe for optimization criteria.

Optimization algorithm, simulated annealing, mimics the physical process of annealing, which is the process of growing a crystal in a fluid by melting the fluid at higher temperature and cooling slowly to a lower temperature in a way that minimizes the energy of the system. The parameters of hydrological model can be optimized with this optimization algorithm by improving Nash-Sutcliffe coefficient as objective function, which is calculated based on the difference between simulated and observed discharge:

$$NS = 1 - \frac{\sum_{i=1}^{N}(Q_o(t_i) - Q_s(t_i))^2}{\sum_{i=1}^{N}(Q_o(t_i) - \overline{Q_o})^2} \tag{6.7}$$

where

$Q_o(t_i)$	[L^3T^{-1}]	=	observed daily discharge
$Q_s(t_i)$	[L^3T^{-1}]	=	simulated daily discharge
$\overline{Q_o}$	[L^3T^{-1}]	=	mean of observed daily discharge
N	[-]	=	number of time steps

There are also other criterions to describe the performance of the models

RAD (relative accumulated volume difference):

$$RAD = \sum_{i=1}^{N}(Q_s(t_i) - Q_o(t_i)) \Big/ \sum_{i=1}^{N} Q_o(t_i) \tag{6.8}$$

AI (agreement index):

$$AI = 1 - \sum_{i=1}^{N}\left(Q_o(t_i) - Q_s(t_i)\right)^2 \Big/ \sum_{i=1}^{N}\left(\left|Q_s(t_{i)} - \overline{Q_o}\right| + \left|Q_o(t_i) - \overline{Q_o}\right|\right)^2 \tag{6.9}$$

RMSE(root mean square error):

$$RMSE = \left(\frac{1}{N}\left(\sum_{i=1}^{N}\left(Q_s(t_i) - Q_o(t_i)\right)^2\right)\right)^{0.5} \tag{6.10}$$

AD (accumulated volume difference):

$$RAD = \sum_{i=1}^{N} (Q_s(t_i) - Q_o(t_i) \tag{6.11}$$

The descriptive statistics about the performances of the discharges generated by 50 parameter sets are summarized in Table 6-2. This shows the calibration of 50 parameters sets for HBV are acceptable.

	NS	***RAD***	***AI***	***RMSE***	***AD***	***BIAS***
Min	0.80	-0.15	0.94	2.43	-9275.23	-0.85
Max	0.83	0.07	0.95	2.70	4471.16	0.41
Mean	0.80	-0.06	0.94	2.63	-3684.21	-0.34
Std	0.01	0.06	0.00	0.06	3427.79	0.31

Table 6-2 the performance of calibrated parameter sets

6.3 Result of Stochastic Analysis with Copula

Figure 6-6 shows *asymmetry2* of 50 simulated and one observed discharges corresponding to time lag *k* similar to the analysis in section 3.2. Figure 6-7 shows temporal change of A_{2min} (minimum of *asymmetry2)* and L_{min} (Lag at minimum) calculated from simulated and observed discharges in moving time window with the size of 3000 days. Figure 6-8 shows sample of observed and simulated discharge time series for certain period.

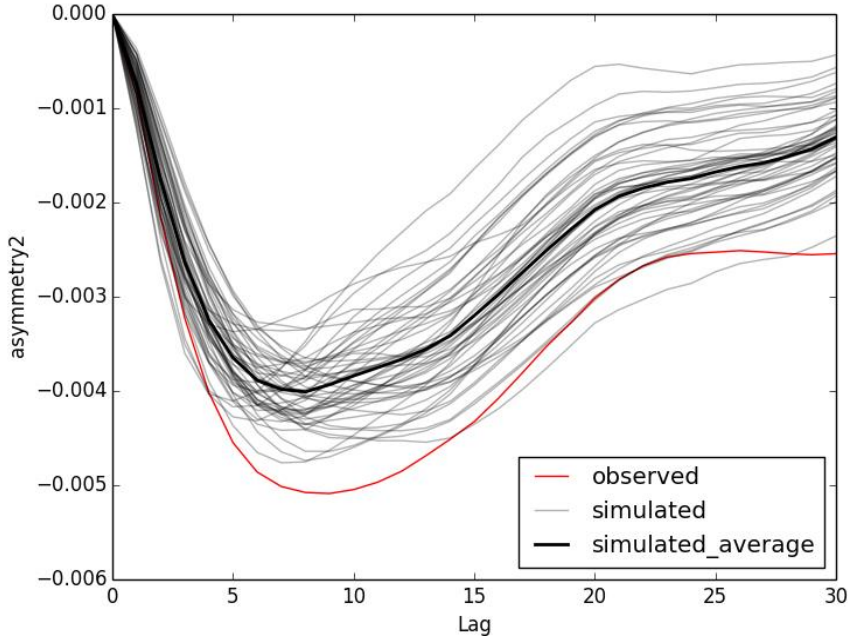

Figure 6-6 variation of *asymmetry2* corresponding to lag *k* [days] calculated from observed (red) and simulated (black) discharge time series

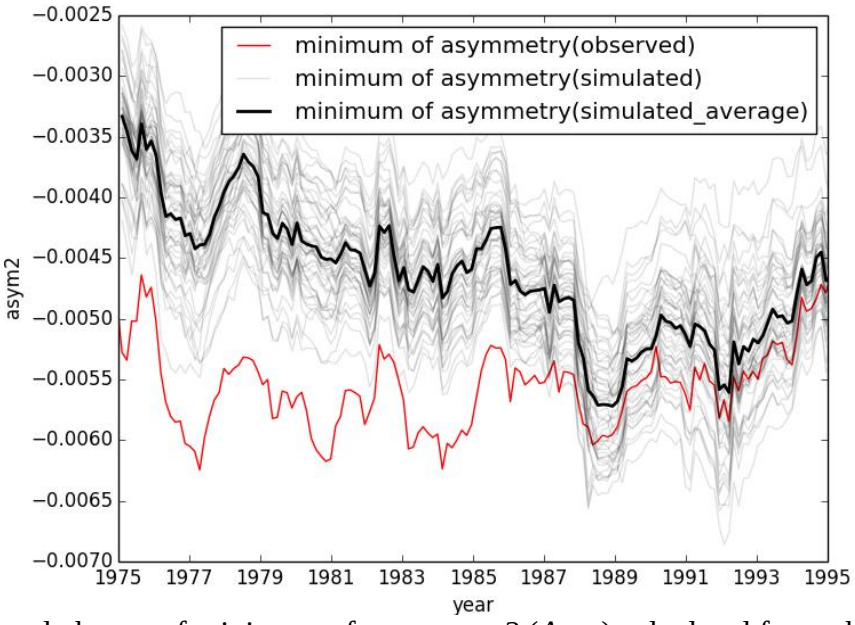

Figure 6-7 temporal change of minimum of *asymmetry2* (A_{2min}) calculated from observed (red) and simulated (black) discharge

This result also shows the *asymmetry2* from observed data is almost always smaller than the mean of *asymmetry2* from observed one. This could indicate, the hydrological model calibrated by the Nash-Sutcliff coefficients does not represent the catchment well in terms of *asymmetry2* and possibly there exists some systematical errors in this hydrological modeling.

There are 2 findings in this figure: 1) the local structure of asymmetry2 is quite similar. 2) *Asymmetry2* of observed discharge undershoots the simulated one.

1) This means, even though the scale of asymmetry2 is different between observed and simulated one, its behavior is similar. It can be said, these behaviors are affected by the realization of rainfall events. As shown in the sample of observed and simulated discharges (Figure 6-8), the simulation is successful in certain sense and realizations of rainfall-runoff event are well represented. Therefore, these local structures are similar.

2) This means, the reproduction of discharge time series is not perfect in terms of *asymmetry2*. This can also be seen in the sample discharges (Figure 6-8). In this result, simulated discharges apt to overshoot the observed one at the peak and undershoot for the base flow. The model generates the runoff, where no runoff events are observed. This is supposed to come from the imperfection of model and data, causing the smaller value of *asymmetry2* for observed discharge.

Also, there seems to exist trend that minimum of asymmery2 of simulated discharge is globally minimum around 1989. This result is rather contradicting to the expected result, because the discharge data simulated by HBV model with fixed parameters should not have any anthropogenic influence, therefore its stochastic property should not change. This implies, at least, the temporal characteristics of rainfall are keep changing for the time window 3000 days independent from the catchment itself. Also one of the possible explanations for not changing *asymmetry2* of observed discharge is that observed discharge reflects not only on the stochastic property of precipitation but also the anthropogenic impacts or possible other the natural processes, which attenuates the change of stochastic property.

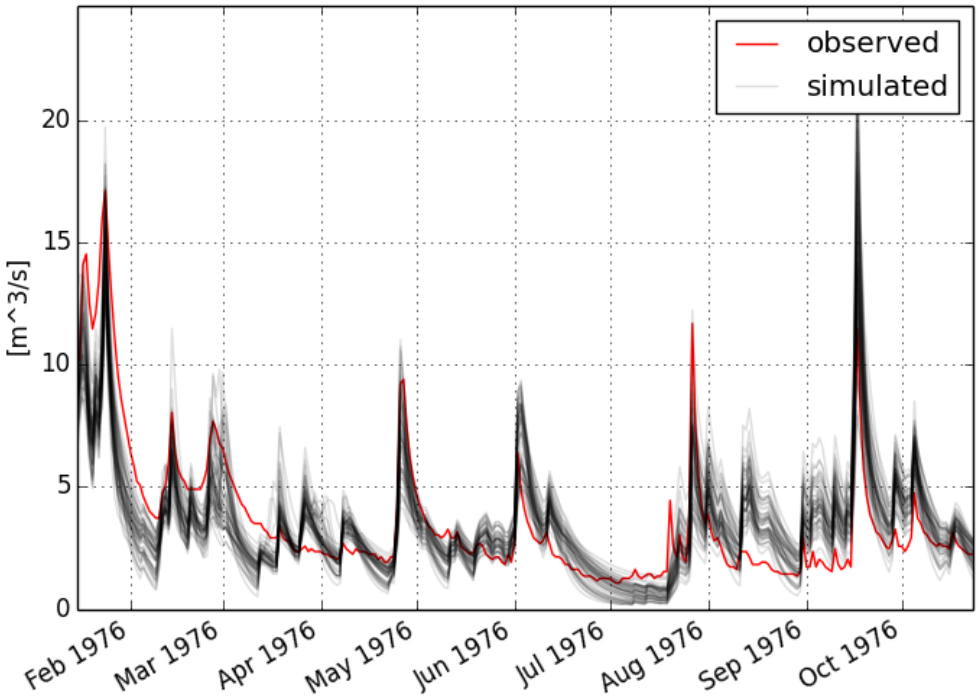

Figure 6-8 sample of observed (red) and simulated (black) discharge time series

In this chapter, HBV model was set up with the assumption that the discharge data simulated by the hydrological model with fixed parameter should not contains the impact of changing catchment. With this model, 50 different parameter sets are independently calibrated and 50 discharge time series are generated. First, the performance of these parameter sets is checked and secondary stochastic characteristic of these simulated time series are tested with copulas.

The interesting point of the result was that *asymmetry2* of observed discharge time series undershoots the simulated one, which indicates systematic error of this hydrological modeling. Also, it was shown that the stochastic property of simulated discharge time series keeps changing although the parameters of HBV model were fixed for simulation period. This also indicates temporal behavior of *asymmetry2* is more influenced by rainfall similar to the result in previous chapter.

7 Time Series Analysis with Copula Distance

In the previous chaoter, it was shown that asymmetry could also be influenced by the rainfall-runoff events as realizations of random behavior of rainfall. In this chapter, the influence of precipitation will be tested in the other approach.

The function of asymmetry (Figure 2-2) emphasizes the values on the corner of the copula domain, which corresponds to large increase of discharge after the rainfall or snow melting. However, anthropogenic change of the catchment influences other flow situations which cannot be quantified well by the function of asymmetry. In this section, copula distance is suggested instead, which can measure possible unusual behavior in the entire domain of copulas:

$$\text{Copula Distance}: D = \int_0^1 \int_0^1 \left(C^*(u_1, u_2) - C(u_1, u_2) \right)^2 du_1 du_2 \tag{7.1}$$

This is said to be Cramer von Mises type distance, which is a measure between two probability distributions, applied for copulas. The equation is defined above, but it is still of interest how and which empirical copulas should be taken for the analysis of time series data.

7.1 Copula Distance in Moving Time Window

One idea is that an empirical copula can be obtained from an entire time series which contains the averaged information of all the time points (*global copula*). Also an empirical copula can be calculated from a certain interval of the time series (*local copula*). To be precise, these *global copula* and *local copula* are formulated with the help of definition of empirical copula in section 2.2 :

$c^*_{global}(\mathbf{u})$: n-dimensional empirical autocopula calculated from entire time series

$c^*_{local}(\mathbf{u}, t, w)$: n-dimensional empirical autocopula calculated from time series in the time window *w* at time *t,* which is set to the center of the time interval

Where $c^*_{global}(\mathbf{u})$ and $c^*_{local}(\mathbf{u}, t, w)$ are density functions of empirical copula as defined in section 2.2. For this analysis, *w* = 3000 [days] is taken for the time window size for *local copula*.

What needs to be known is the change of dependence structure in a certain time period. This can be achieved by calculating the copula distance between global copula and local copula in moving time window. Based on this idea, a new measure, *copula distance type1*, is introduced:

$$D_1(t) = \int_0^1 \ldots \int_0^1 \left(c^*_{global}(\mathbf{u}) - c^*_{local}(\mathbf{u}, t) \right)^2 du_1 \ldots du_n \tag{7.2}$$

In this analysis, empirical autocopulas are calculated by taking consecutive 3 values, which means

$$\mathbf{u} = (u_0, u_1, u_2) \tag{7.3}$$

where $u_0 = F_z(Z(t)), u_1 = F_z(Z(t+1)), u_2 = F_z(Z(t+2))$ in case of the discrete time series.

Distance type 1 is showing the local differences of the dependence structure in comparison to the entire time series. If the dependence structure of local copula at time *t* is different from the ordinary state, $D_1(t)$ gives higher values.

Also *copula distance type 2* is suggested as follows:

$$D_2(t) = \int_0^1 \ldots \int_0^1 \left(c^*_{local}(\mathbf{u}, t - w/2) - c^*_{local}(\mathbf{u}, t + w/2) \right)^2 du_1 \ldots du_n \tag{7.4}$$

Where *w* is the window size and is 3000 days in this analysis.

For the *distance type 2*, the copulas to compare are both local copulas. This means, the two empirical copulas are calculated from the 2 time intervals, which are consecutive two time windows without overlapping part and moving together. This shows the point at which the structure of copulas started to change.

Figure 7-1 shows results of discharge time series data from measuring station Andernach. The changes of the *copula distance type1*, *copula distance type2*, *asymmetry1* and *asymmetry2* for small time lags (*k = 5, 10*) and the observed discharge data in the moving time window are shown.

The interesting thing is that $D_1(t)$ result is in unusual high around 1945 and 1982, which is not clearly seen in asymmetry. $D_2(t)$ is maximum around 1973 and also high around 1945, which indicates the structure of copula started to change at this time point.

Through the careful inspection of the result, comparing with the results in the previous section 3.6 and section 5.1, it can be said that the *copula distance type1* is related to the unusual behavior of *asymmetries* especially for the time around 1945 and 1982. *Copula distance type2* indicates the structure started to change around 1973.

The same analyzes from other gauging stations (Cochem, Kalkofen, Kaub, Maxau, Plochingen, Worms) are shown in Appendix B. Similar tendency can be seen for the year around 1945 and 1982 from the results of tributaries of Rhine such as Plochingen and Cochem, but not from the result of Kalkofen. This tendency (high value of $D_1(t)$ around 1945 and 1982) is common for discharge data of river Rhine and Main, but not really the case for the discharge data from river Elbe and Danube.

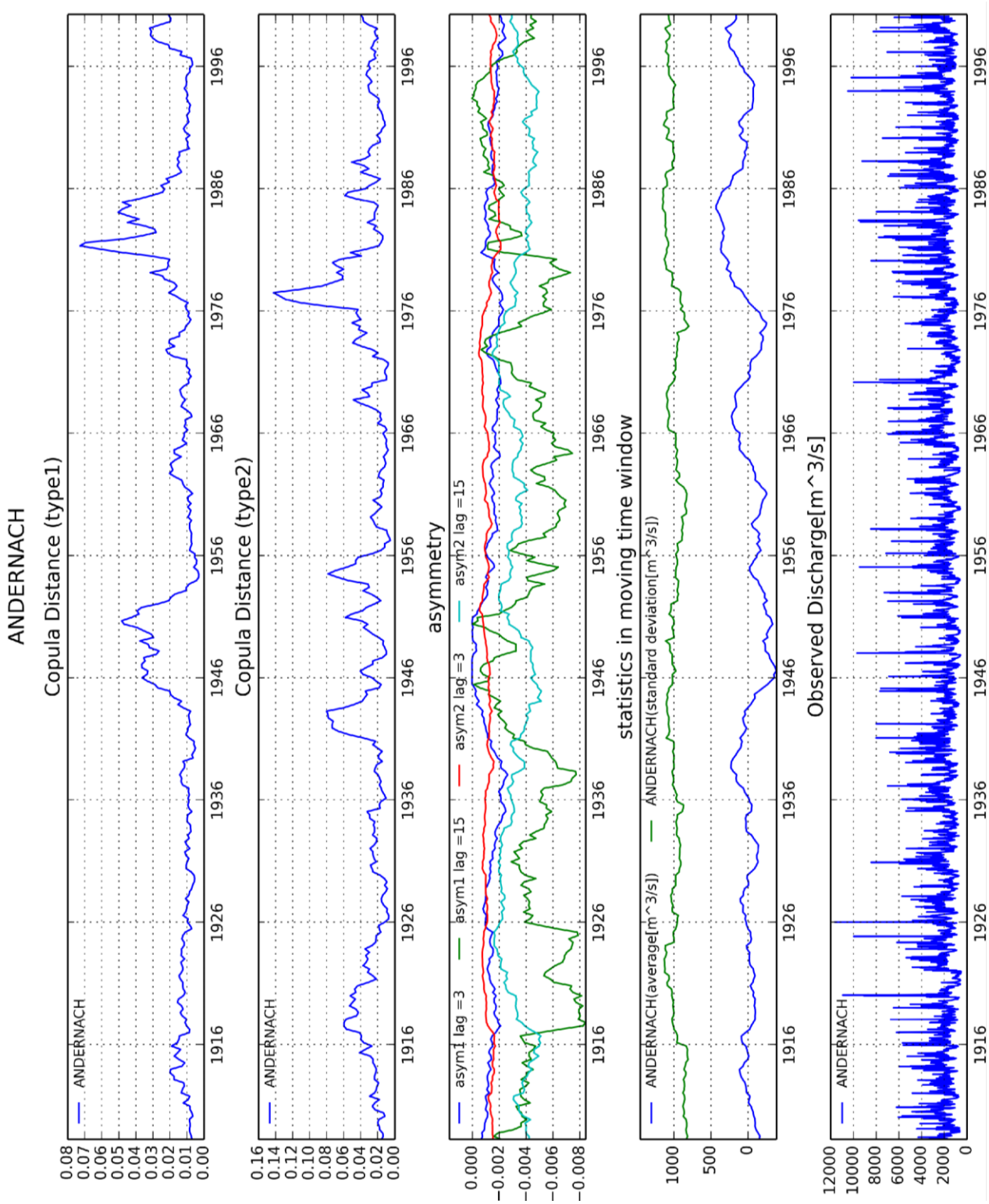

Figure 7-1 Analysis of Copula Distance for Andernach: Temporal change of copula distance type1 (top), copula distance type2 (second), asymmetry (third), mean and standard deviation (forth) and observed discharge (bottom)

7.2 Copula Variance

The interesting point of copula distance in moving time window is that, density function of copula itself can be regarded as random variable, then local copula can be regarded as a realization of copula and global copula can be regarded as mean of copula. Furthermore, copula variance can be defined as a measure to describe how variable autocopula of a time series is.

The distance between two copula density functions for n-dimensional case is defined:

$$Dis(c_1, c_2) = \int_0^1 \cdots \int_0^1 \left(c_1(\mathbf{u}) - c_2(\mathbf{u}) \right)^2 du_1 \ldots du_n \tag{7.5}$$

Then the copula distance can be defined as integration of *copula distance type1* between the time t_1 and t_2:

$$Var_{cop}(c) = \frac{1}{t_2 - t_1} \int_{t_1}^{t_2} Dis\left(c_{local}(\mathbf{u}, t), c_{global}(\mathbf{u}) \right) dt \tag{7.6}$$

The copula variance of discrete time series for 3 dimensional copula can be calculated as follow:

$$Var^*_{cop}(c) = \frac{1}{n} \sum_{n=1}^{N} \int_0^1 \int_0^1 \int_0^1 \left(c^*_{local}(u_0, u_1, u_2, t_n) - c^*_{global}(u_0, u_1, u_2) \right) du_0 du_1 du_2 \tag{7.7}$$

where t_n is the time in discrete time series with $n = 1,\ldots, N$.

7.2.1 Observed and Simulated Discharge with Copula Variance

Here, the analysis of copula distance is applied to the simulated and observed data generated in section 0. First, *copula distance type1* is calculated for one observed and 50 simulated discharges, which are calculated from 50 different parameter sets (Figure 7-2).

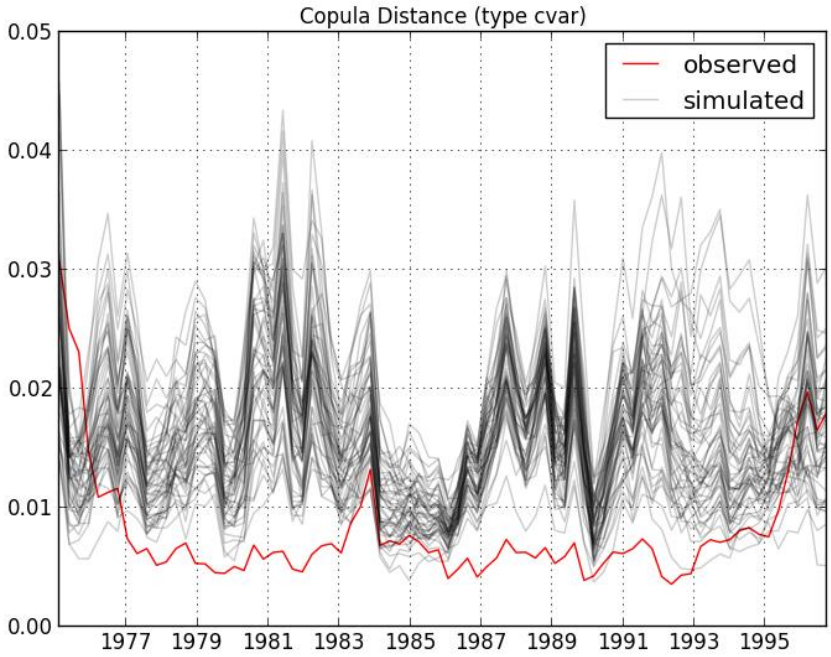

Figure 7-2 *copula distance type1* of 1 observed and 50 simulated discharges at gauging station Suessen

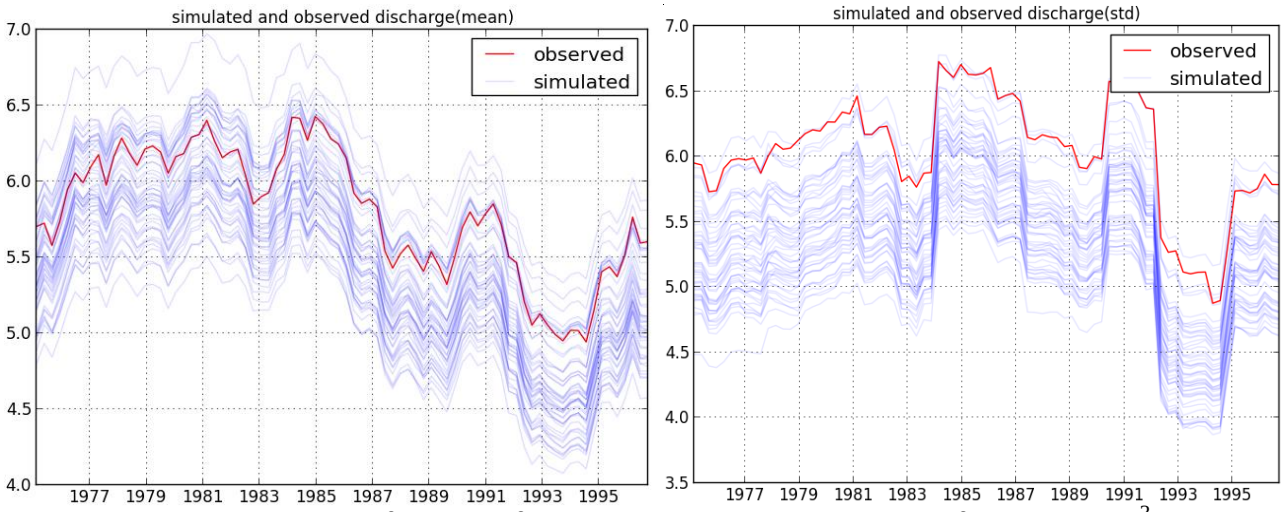

Figure 7-3 temporal change of mean (left) and standard deviation (right) of discharge [m^3/s] at gauging station Suessen in moving time window

The interesting point of this graph is that *copula distance type1* of simulated discharge (black line) is bigger than observed one (red line). The result is actually similar to the analysis of observed and

simulated discharge with *asymmetry2* in the previous chapter (section 6.3) in the sense that the temporal stochastic characteristic is keeps changing.

Figure 7-3 shows the change of standard deviation (left) and average (right) of simulated discharge (blue line) and observed discharge (red line) in moving time window. The standard deviation of observed data is actually higher than the simulated one, while copula variance is smaller.

Similar to the case in the previous chapter, the possible reason for this is that the natural system is more complicated than the hydrological model used. Therefore, the change of dependence structure is attenuated for the observed data.

In Figure 7-4, *copula variance* is calculated by integrating *copula distance type1* in Figure 7-2 for 50 simulated and 1 observed discharge data. As it can be seen in Figure 7-2 , *copula variance* is clearly smaller for observed data.

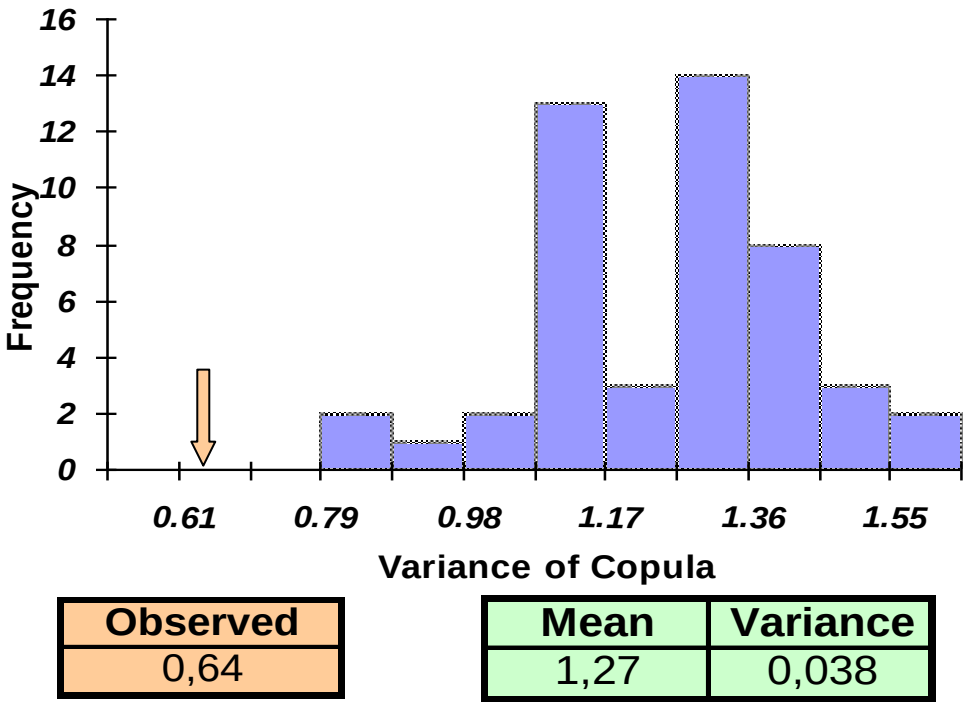

Figure 7-4 Histogram of copula variances calculated from 50 simulated discharges (mean and variance of copula variance of simulated discharges are shown in green box and copula variance of observed discharge is shown in orange box) and observed discharge

7.3 Copula Correlation

In the previous section, copula variance was defined as a variability characteristic of copula itself. Here, it is investigated whether covariance and correlation can be defined for two copula densities c_1 and c_2:

$$Cov_{cop}(c_1, c_2) = \frac{1}{t_2 - t_1} \int_{t_2}^{t_1} \int_0^1 \dots \int_0^1 \left(c_{1,local}(\mathbf{u}, t) - c_{1,global}(\mathbf{u})\right)\left(c_{2,local}(\mathbf{u}, t) - c_{2,global}(\mathbf{u})\right) du_1 \dots du_n dt \tag{7.8}$$

where $Cov_{cop}(c_1, c_2)$ is copula covariance of copula density c_1 and c_2. Here, $c_{global}(\mathbf{u})$ can be regarded as mean of copula, $c_{local}(\mathbf{u}, t)$ as a realization of copula at time t. Then copula correlation can be defined:

$$Cor_{cop}(c_1, c_2) = \frac{Cov_{cop}(c_1, c_2)}{\sqrt{Var_{cop}(c_1)} \cdot \sqrt{Var_{cop}(c_2)}} \tag{7.9}$$

Also *copula distance type3* is defined as temporally *not integrated version* of the copula correlation similar to *copula distance type1*:

$$D_3(t) = \frac{\int_0^1 \dots \int_0^1 \left(c^*_{1,local}(\mathbf{u}, t) - c^*_{1,global}(\mathbf{u})\right)\left(c^*_{2,local}(\mathbf{u}, t) - c^*_{2,global}(\mathbf{u})\right) du_1 \dots du_n}{\sqrt{Var_{cop}(c_1)} \cdot \sqrt{Var_{cop}(c_2)}} \tag{7.10}$$

Figure 7-5 shows *copula distance type3* between the discharge time series at gauging station Worms and Maxau. It also shows *copula distance type1* of both time series and correlation in moving time window. The gauging station Worms and Maxau are closely located in the same river reach, thus they should and actually behave similarly with strong correlation. The correlation between both discharge data in moving time window is over 0.92 especially before 1974 and decreases after 1974 down to 0.9.

On the contrary, *copula distance type3* is relatively small before 1974, but starts to increase at 1974. This means, the change of dependence structure which happened to the both discharge time series after 1974 is similar. It can be seen that copula distance type 1 is high for the time period in which the copula correlation is high. The value of copula correlation is 0.858 for these two discharge time series.

Figure 7-6 also shows *copula distance type3* between the discharge time series at gauging station Plochingen and Cochem. They are located in different tributaries of the river Rhine and approximately 200 km away. This can be the reason that the correlation between both discharge time series in moving time window is smaller (0.6 ~ 0.75) than the correlation between Worms and Maxau (0.9~0.95). But, the result still shows that there is certain period where *copula distance type3* is high, although the correlation in moving time window at this period is not really high. The copula correlation for these two discharges is 0.599.

It should be noted that, the period where *copula distance type3* is high and the period where correlation is high does not always coincide. This phenomenon might be explained by the characteristic that an autocopula has more detailed information about temporal dependence structure than autocorrelation. Copula correlation or *copula distance type3* is comparing this detailed information. This would be the reason that autocorrelation is different from *copula distance type3* in same time window.

In the next section, correlation in moving time window and copula correlation are going to be investigated for a set of discharge data (Andernach, Maxau, Cochem, Plochingen, Kalkofen)

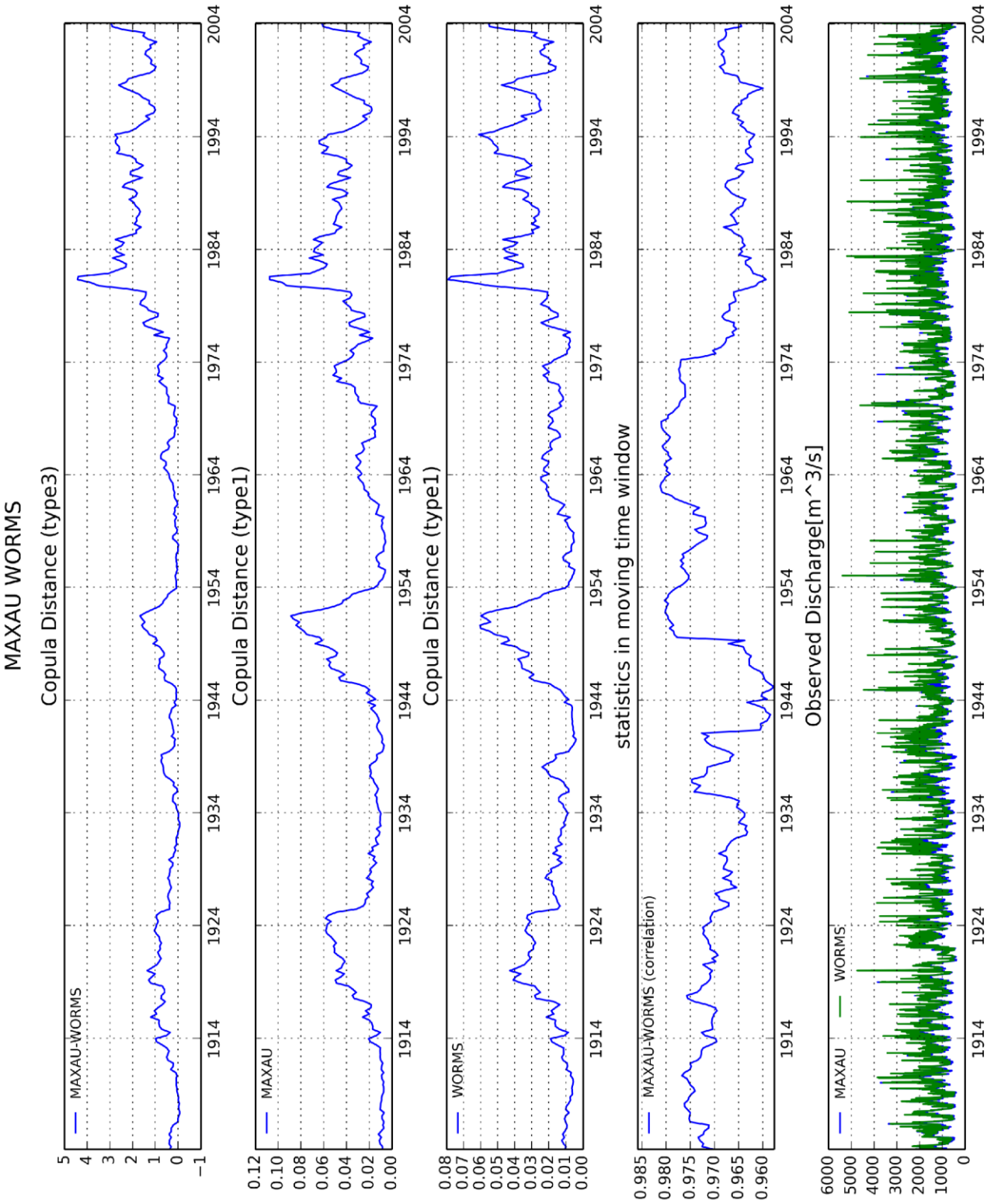

Figure 7-5 Analysis of Copula Distance between discharge time series of gauging stations Worms and Maxau : *Copula Distance Type3* between Worms and Maxau(top), *copula distance type1* for Worms (second), *copula distance type1* for Worms (third) and correlation in moving time window (fourth) and observed discharges (bottom)

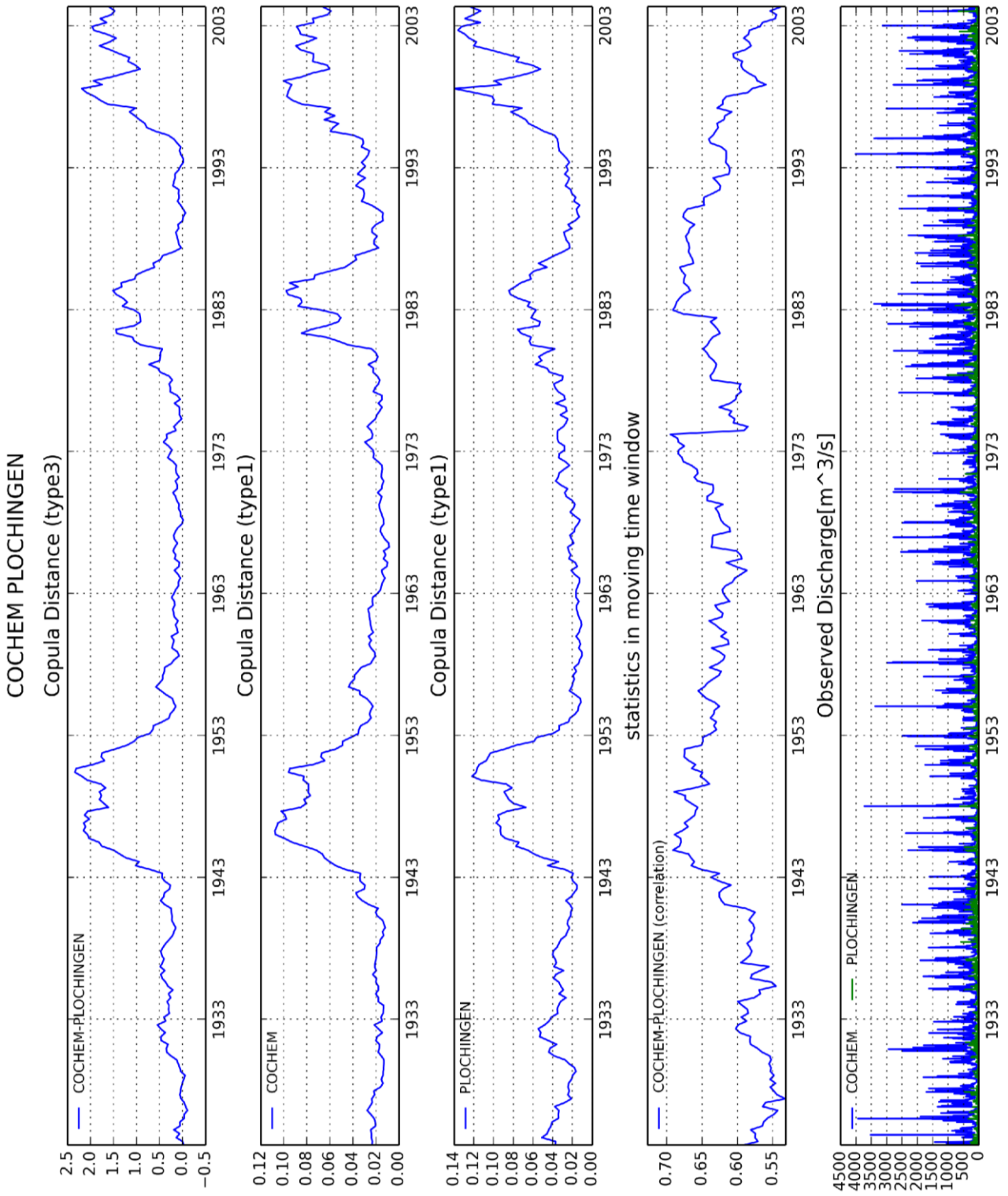

Figure 7-6 Analysis of Copula Distance between discharge time series of gauging stations Plochingen and Cochem : *Copula Distance Type3* between Plochingen and Cochem(top), *copula distance type1* for Plochingen (second), *copula distance type1* for Cochem (third) and correlation in moving time window (fourth) and observed discharges (bottom)

7.3.1 Copula Distance Analysis for a Set of Discharge Data

In this section, the copula correlations in moving time window with 3000 [days] interval are investigated for a set of data (Andernach, Maxau, Cochem, Plochingen, Kalkofen). For the comparison, *copula distance type1* (Figure 7-7), *copula distance type3* (Figure 7-8) and correlation in moving time window (Figure 7-9) are calculated and visualized.

It can be seen in Figure 7-7 that *copula distance type1* is high between 1943 and 1953. This result indicates the dependence structure of this time period is different from the other part. Figure 7-8 shows that *copula distance type3* between 1943 and 1953 is high, which indicates this unusual behaviour of dependence structure are closely related each other. The same behaviour can be seen also around 1980 and 2000.

The correlations of all the possible pairs of discharge time series in moving time window are also shown in Figure 7-9. In general, the correlations in moving time window are changing for all the period, but it is not easy to conclude there is remarkable behaviour between 1943 and 1953 in terms of correlation in comparison with the analysis by *copula distance type1* and *copula distance type3*

The gauging stations of these discharges are located in the same region (Southwest Germany). There might have been same change in all the sub-catchments or the weather condition was special for these regions. This can be the reason that the behaviour of copulas is similar for certain time period.

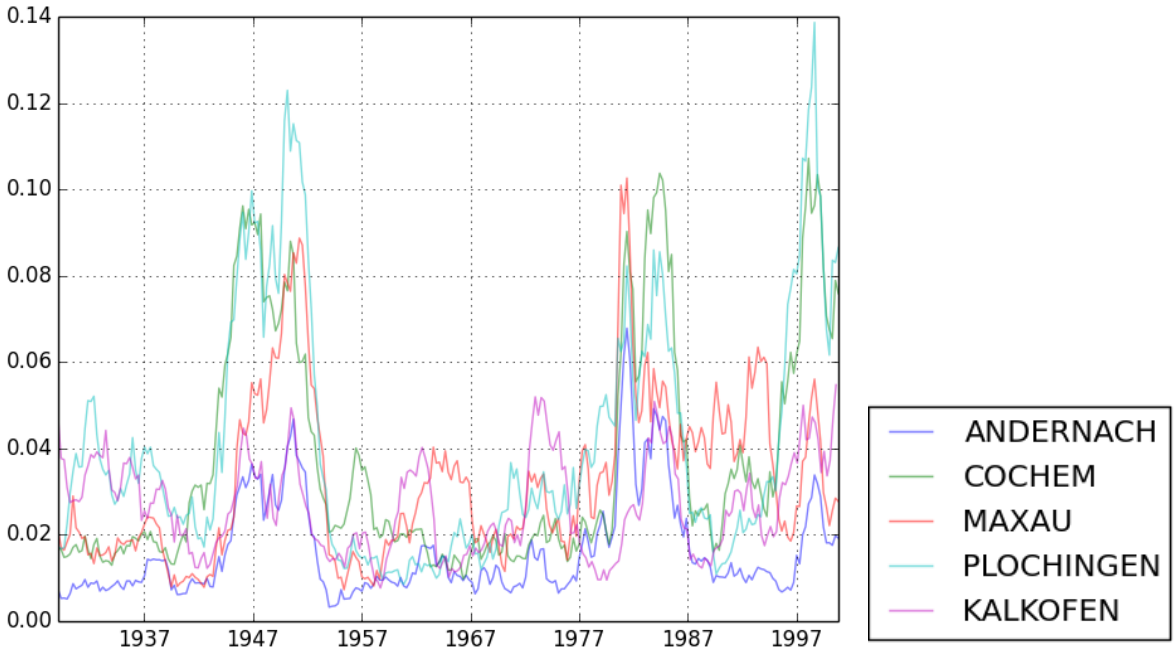

Figure 7-7 *Copula Distance type1* of discharge data from gauging stations Andernach, Cochem, Maxau, Plochingen and Kalkofen

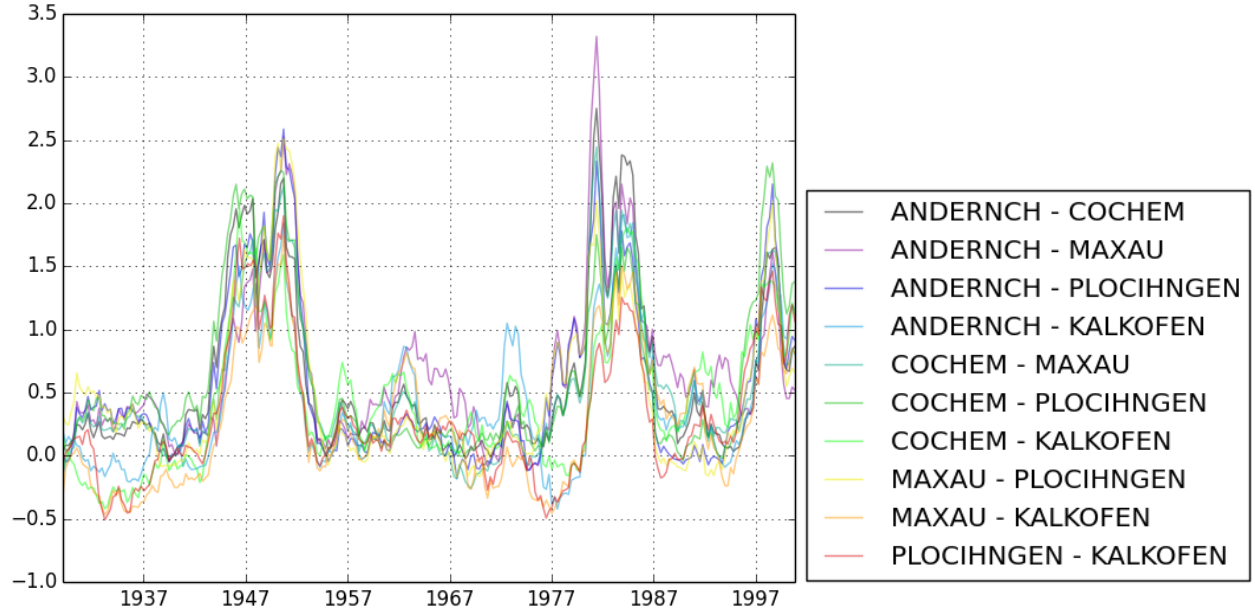

Figure 7-8 *Copula Distance type3* between discharge time series (Andernach, Cochem, Kalkofen, Maxau, Plochingen)

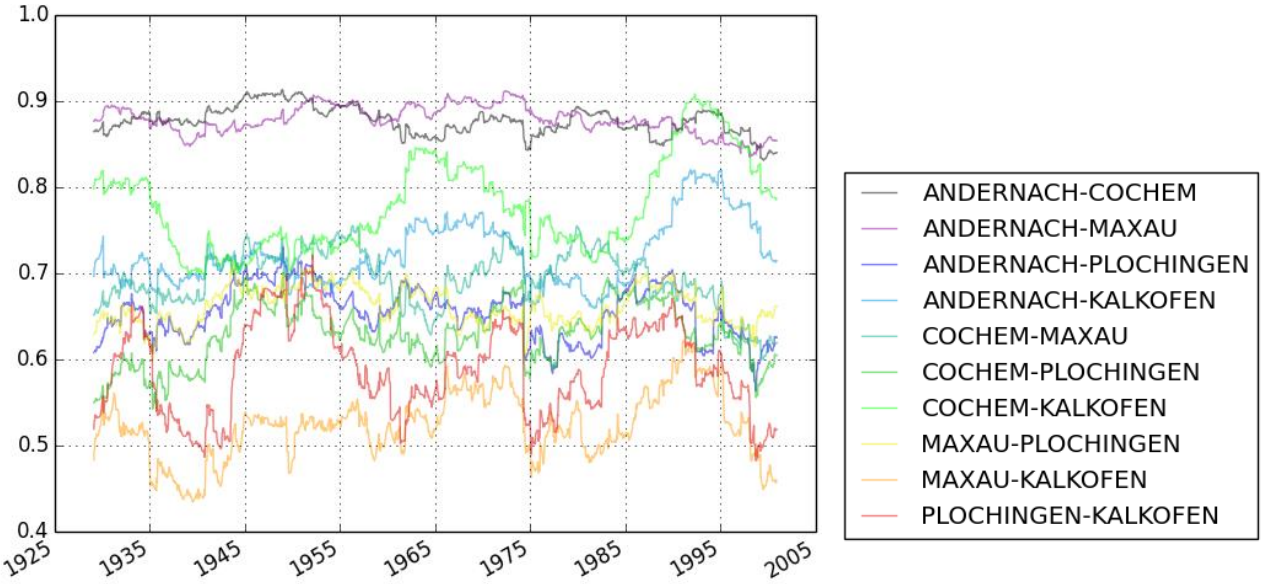

Figure 7-9 Correlation between discharge time series (Andernach, Cochem, Kalkofen, Maxau, Plochingen) in moving time window

7.3.2 Copula Distance Analysis of APIs

Similar to the analysis in the previous section, copula correlations are investigated for the daily precipitation data of Baden-Württemberg in the moving time window with 3000 [days] interval.

Same to the analysis in Chapter 5, API (Antecedent Precipitation Index) is used instead of precipitation time series. There are 525 daily precipitation stations in Baden-Württemberg in total, but observation period is different depending on the stations, therefore the number of existing data is not homogeneous as mentioned in Chapter 5.

Figure 7-10 shows *copula distance type1* of the APIs of average precipitation in each region:(1) entire BW,(2) center of BW (3) southwest of BW (4) northwest of BW (5) northeast of BW. The reason that c*opula distance type1* shows unusual behavior after 1997 and before 1907 might be explained by the smaller number of existing data of daily precipitation. Thus, same copula distance is plotted for 1930~2000 in, Figure 7-11 and Figure 7-12.

In the previous section, the remarkable behavior was found around 1947 in discharge data (also around 1980 and 2000). This can be also seen in the API time series, but not that much clear in comparison with discharge data. For example, *copula distance type1* is between 0.02~0.05 around 1947 for API, while *copula distance type1* for discharge is between 0.04~0.1. The signal of *copula distance type1* of API around 1980 is also not that much clear in comparison with discharge.

The behavior of *copula distance type3* from APIs are shown in Figure 7-11.This shows there are peaks around 1947 ,1980 and 2000 similar to the results from discharge time series, but it looks more noisy.

Figure 7-12 shows the correlations between these API time series in moving time window. This result is also fluctuating and difficult to recognize unusual behavior around 1947 and 1980.

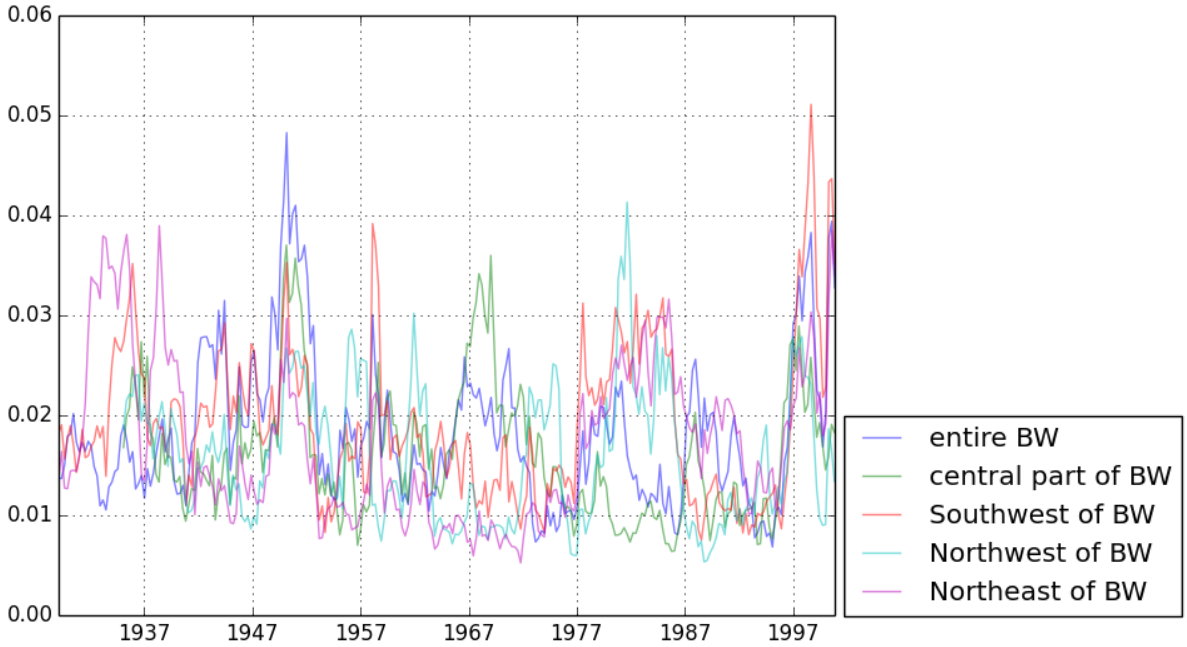

Figure 7-10 *Copula Distance Type1* of the APIs (Antecedent Precipitation Index) of average precipitation in each region of Baden-Württemberg

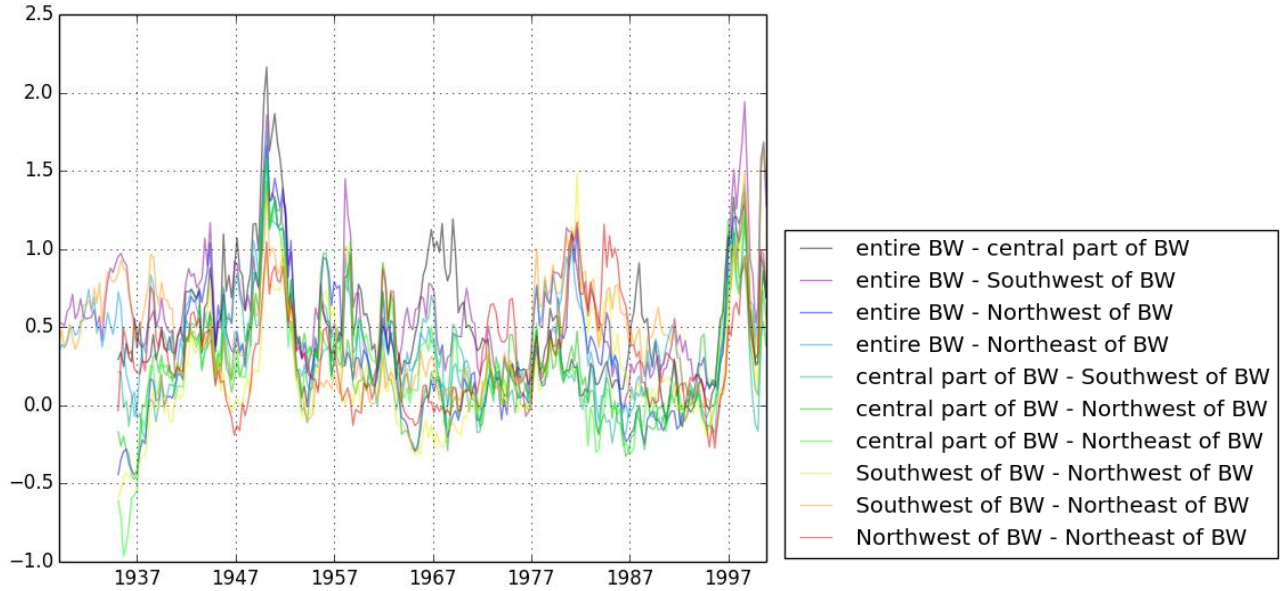

Figure 7-11 *Copula Distance Type3* between the APIs (Antecedent Precipitation Index) of average precipitation in each region of Baden-Württemberg state in Germany

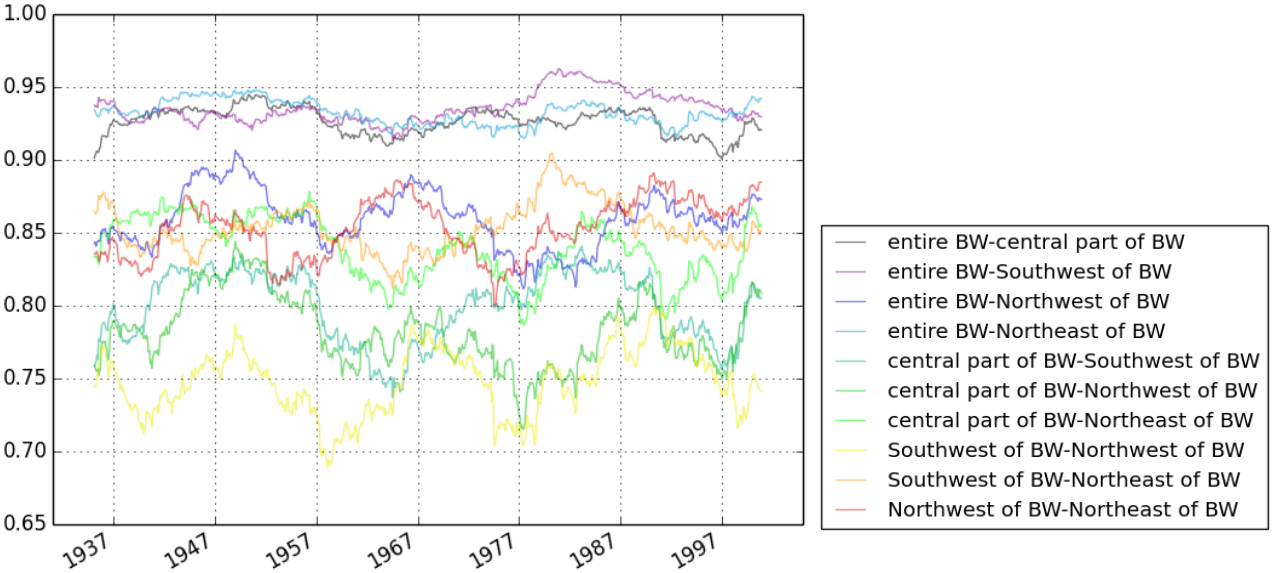

Figure 7-12 Correlations in the moving time window between the APIs (Antecedent Precipitation Index) of average precipitation in each region

7.3.3 Copula Distance Analysis between API and discharge time series

In the previous sections, it was seen that there are signals that temporal dependence structure have been changed around 1947, 1980 and 2000 in both discharge and API time series (Figure 7-8, Figure 7-11). The question here is whether there is any relation between time series of discharge and API in terms of autocopula.

Figure 7-13 shows *Copula Distance Type3* between one API time series (averaged for entire Baden-Württemberg region) to 7 discharge time series (Andernach, Kaub, Worms, Cochem, Maxau, Plochingen, Kalkofen). *Copula Distance Type3* should give high value, if the change happened to autocopula in the time window is same for two time series as discussed in section 7.3.

The figure could indicate the change of temporal structure happened to discharge and API is quite similar around 1947 and around 2000. There is small peak around 1980, but not that much around 1947. This result implies, the unusual behavior of discharge time series around 1947 and around 2000 are caused by time series of API, but the relation can be small around 1980.

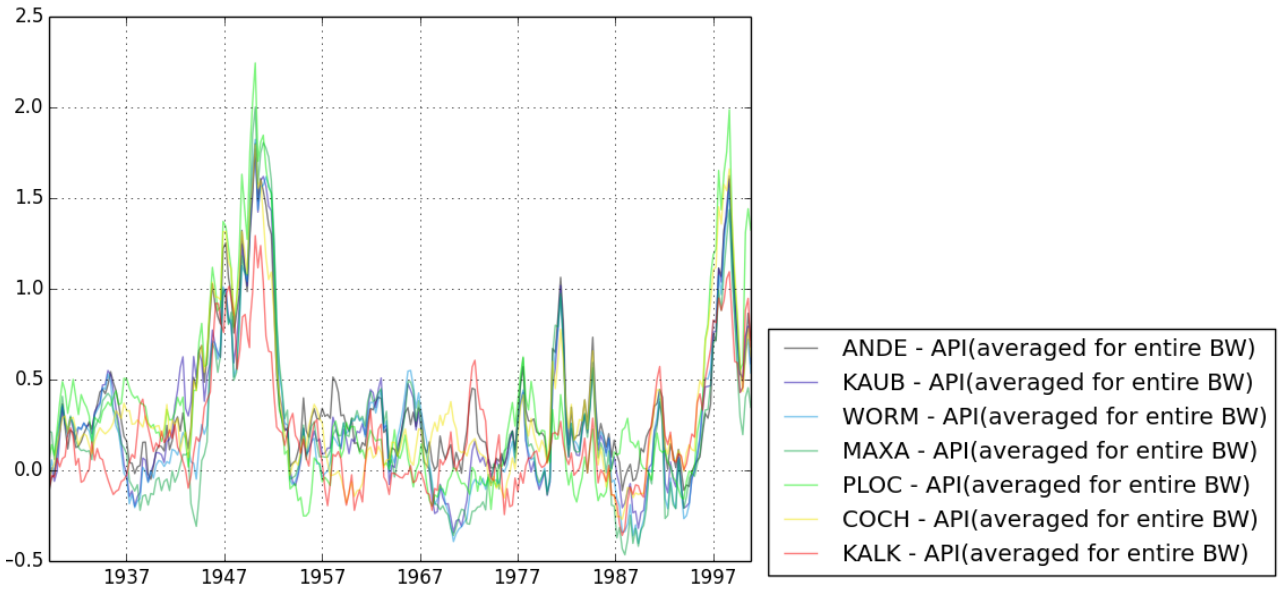

Figure 7-13 *Copula Distance Type3* between the API (average of entire Baden-Württemberg region) and discharge data (Andenach, Kaum, Worms, Maxau, Plochingen, Cochem, Kalkofen

7.3.4 Copula Correlation between Simulated and Observed Discharges

In this section, the analysis of copula correlation is applied for one observed and 50 simulated discharge data sets generated in chapter 6. Copula correlations are calculated for 50 pairs of time series data for one observed and 50 simulated discharge time series (Figure 7-14). Also 50 × 50 pairs of time series data between 50 simulated discharges (Figure 7-15). The results show the change of dependence structure is related each other in terms of copula correlation more between simulated discharges, but not that much for the case between simulated and observed discharges.

Figure 7-16 shows *copula distance type3*, which is not integrated version of copula correlation as shown in Eq. (7.10). The figure indicates the correlation between observed and simulated is in general smaller than the one between simulated discharges.

The first point is that the time series of *copula distance type3* between simulated discharges are quite similar to the time series of *copula distance type1* shown in Figure 7-2. The reason is that, they are generated by same HBV model although the parameters of HBV model used for simulation are different and independently calibrated. Therefore, those time series are quite similar. If c_1 and c_2 are same in Eq. (7.8), then it is same to the definition of copula distance type1 in Eq. (7.2). This can be the reason that the result of *copula distance type3* in Figure 7-16 is similar to the result of *copula distance type1* in Figure 7-2.

The second point is that, on contrary to the results between simulated discharges, the time series of *copula distance type3* between observed and simulated discharges are not so close. They are even negatively correlated around 1977 and 1993, while *copula distance type3* between simulated discharges are positive. The reason is not clear and careful investigation is needed.

Figure 7-17 shows correlations between observed and simulated discharges are similar to Figure 7-16. Correlations between simulated discharges are higher than the ones between observed and simulated discharges as expected. Correlations between observed and simulated discharges are lower around 1993 in comparison to the other period. Same correlations around 1977 are also slightly lower, but not that much in comparison with copula correlation around 1977.

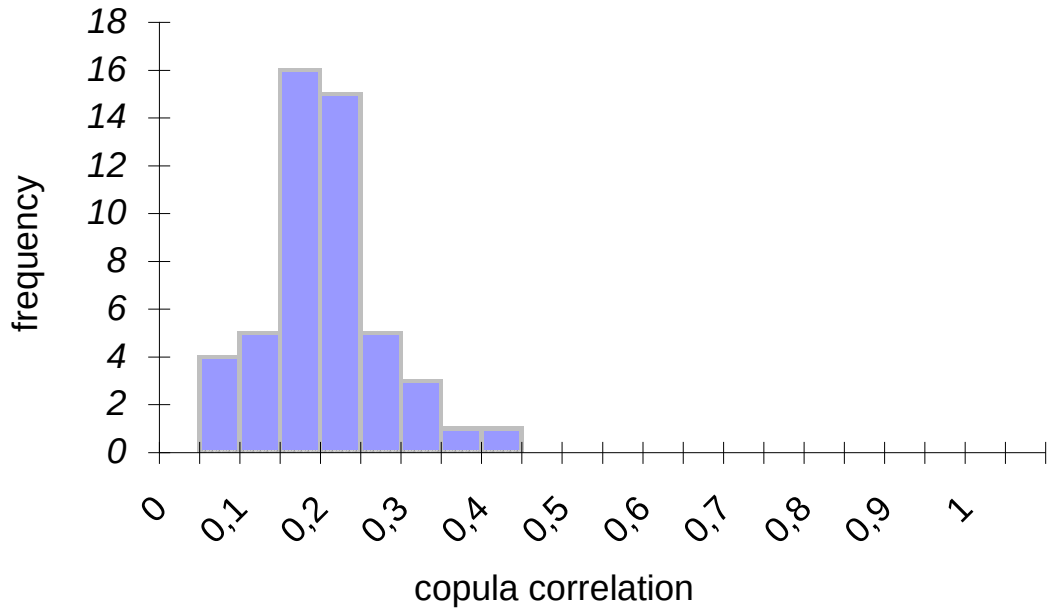

Figure 7-14 Histogram of copula correlation from observed and simulated discharge time series

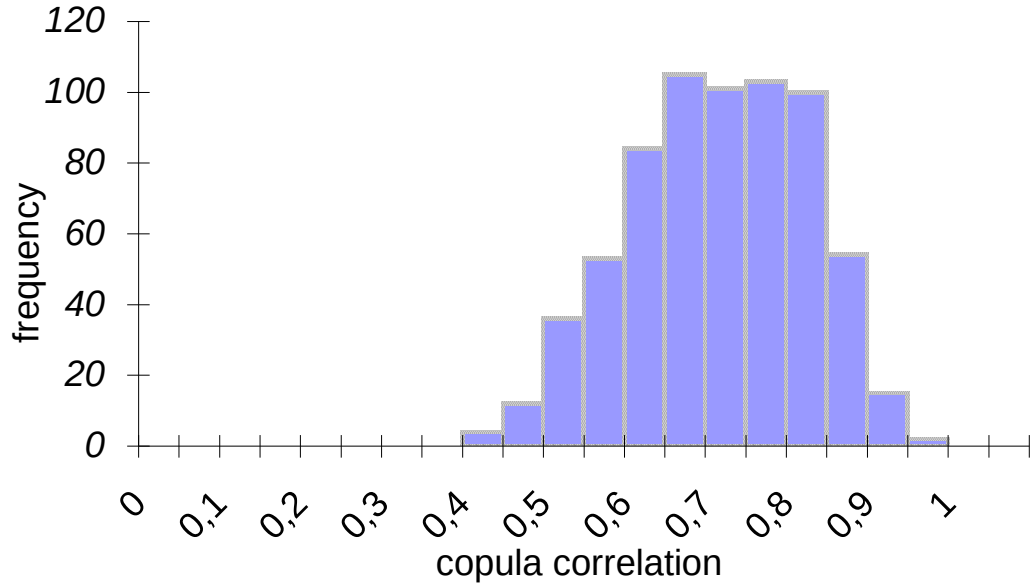

Figure 7-15 Histogram of copula correlation between simulated discharge time series

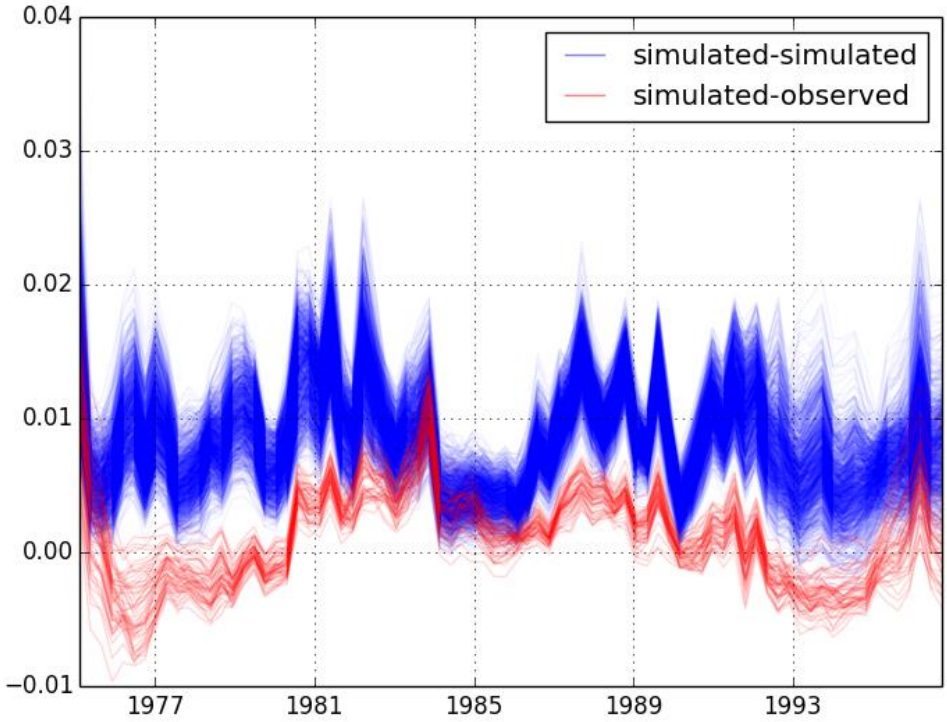

Figure 7-16 *Copula Distance Type3* between simulated discharge (blue) and between observed and simulated discharge (red)

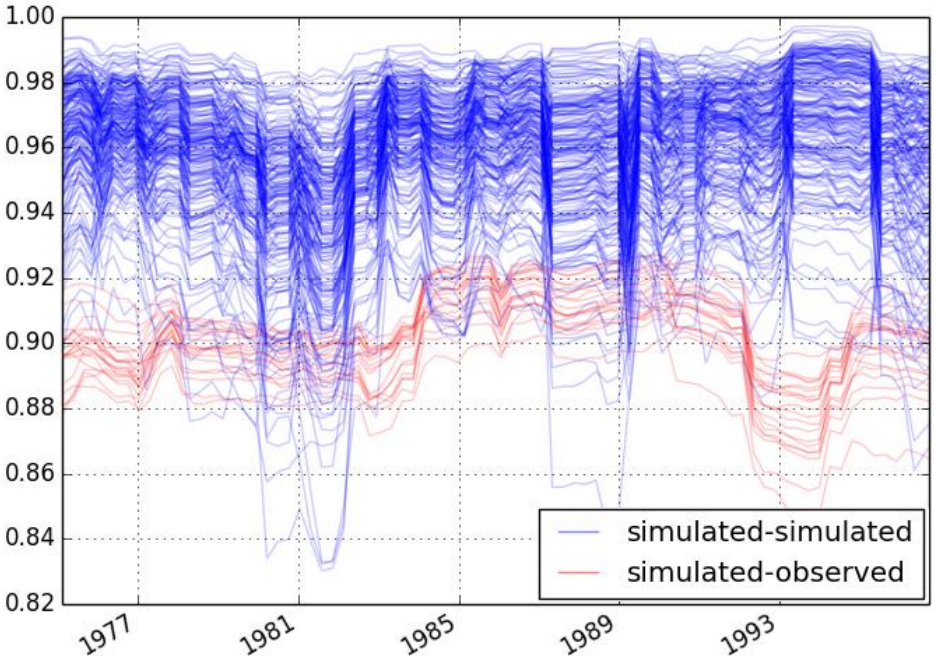

Figure 7-17 temporal change of correlation between simulated discharge (blue) and between observed and simulated discharge (red)

In this chapter, time series analysis with copula distance is newly introduced.

Copula can describe the dependence structure of multiple random variables, but copula itself is regarded as random function in this chapter. Then, global copula can be defined as mean of changing copula and local copula as a realization of copula at certain time step.

Based on this idea, copula variance, copula covariance and copula correlation are newly introduced. *Copula distance type1*, *copula distance type2* and *copula distance type3* are defined as temporally not integrated version of copula distances for detection of anthropogenic impacts from discharge time series comparing it with precipitation (API) time series data.

The interesting point of the result of *copula distance type1* was that there were clear unusual behaviors around 1945, 1980 and 2000 in the discharge data of target region. It was found that there was interdependency of this usual state of copula between discharge data using *copula distance type3*.

In the previous chapters, API and discharge time series of this region had shown already similar behavior in terms of asymmetry2. Therefore, it was checked if there was any interdependency between API and discharge time series in terms of *copula distance type3*. The conclusion is that there is clear relation especially between these unusual state of copula around 1945 and 2000 of API and discharge time series, but relation is weaker around 1980.

Simulated discharge time series generated in chapter 6 was also investigated with copula distances. The interesting finding was that copula variance in moving time widow of observed discharge was smaller than simulated one, while variance in moving time window of observed discharge time is bigger than the simulated one. It was also seen that there were period that dependence structures of simulated and observed discharge are similar and opposite.

8 Non-parametric Simulation of Discharge Time Series based on Copulas

In the previous sections, the analysis of discharge data was done based on empirical copulas and its asymmetry. In this section, non-parametric statistical simulation of discharge data is suggested with non-parametric copulas. The idea is based on the geostatistical interpolation using copulas (Bárdossy and Li 2008). This is an extended version of this method to the time series with kernel density estimation.

The generated time series data has better statistical properties such as *asymmetry*, which exists in the observed data, as shown in Figure 8-2 while the synthetic data generated by ARIMA don't have it. This method could be used for example for the assessment of proper operation of dams or irrigation systems, because generated time series can properly represent the curves of increment and decrement of discharge.

8.1 Sequential Conditional Simulation for Time Series

Once multidimensional copulas are estimated by kernel density estimation with beta kernel, realizations of a variable in the copula can be simulated based on the sequential conditional distribution. When a *m*-dimensional copula is estimated and the realizations of *m-1* random variables of *previous time steps* are given as $Z_1 = z_1, Z_2 = z_2, ..., Z_{n-1} = z_{m-1}$, then the distribution function of random variable Z at a current time step is given as follow:

$$\begin{aligned} & C\left(u \mid U_1 = u_1, U_2 = u_2, ..., U_{m-1}\right) = P\left(U < u \mid U_1 = u_1, u_2, ..., U_{m-1} = u_{m-1}\right) \\ & = \int_0^u c\left(u \mid u_1, u_2, ..., u_{m-1}\right) du = \frac{\int_0^u c\left(u, u_1, u_2, ..., u_{m-1}\right) du}{c\left(u_1, u_2, ..., u_{m-1}\right)} \end{aligned} \tag{8.1}$$

m-dimensional copula in above equation can be estimated, using beta kernel density estimation with bandwidth *h* introduced in section 1.1.

Although the empirical distribution of given multivariate data is not really independent, but its kernel can be expressed simply by its multiplication:

$$f\left(x, y\right) = \frac{1}{n} \sum_{i=1}^{n} K_h\left(x - x_i\right) K_g\left(y - y_i\right) \tag{8.2}$$

Since the multidimensional copula density is estimated as follows:

$$\hat{c}_h\left(u_1,u_2,...,u_m\right)=\frac{1}{N}\sum_{i=1}^{N}\prod_{j=1}^{m}K\left(u_j,U_{ij},h\right) \tag{8.3}$$

Then, its cumulative function $C\left(U<u\,|\,U_1<u_1,U_2<u_2,...,u_{m-1}\right)$ can be estimated by:

$$\begin{aligned}\hat{C}_h\left(u\,|\,U_1<u_1,U_2<u_2,...,u_{m-1}\right)&=\frac{\int_0^u\hat{c}\left(u,u_1,u_2,...,u_{m-1}\right)du}{\hat{c}\left(u_1,u_2,...,u_{m-1}\right)}\\&=\frac{\sum_i^N\left[\left(\int_0^x K\left(x,X_i,h\right)dx\right)\prod_{j=1}^{m-1}K\left(x_j,X_{ij},h\right)\right]}{\frac{1}{N}\sum_{i=1}^{N}\prod_{j=1}^{m-1}K\left(x_j,X_{ij}\right)}\end{aligned} \tag{8.4}$$

Here, *N* is the number of observations and *m* is the dimension of the copula.

This equation leads to the sequential conditional simulation of time series in autoregressive way similar to a Markov Chain, assuming $Z_1,Z_2,...,Z_i$ are the random variables at *i* time steps before. Using the equation (8.4), the new value of conditional simulation *Z* at current time step *t* can be calculated by applying the inverse function of the cumulative conditional distribution function to an uniformly distributed random number between [0,1]. Then, the empirical marginal distribution of the discharge time series is attached to the simulated values of *u* using the inverse cumulative empirical distribution function.

.

8.2 Copula Auto Regressive Simulation

Unlike the classic time series model, ARIMA, there is no assumption for copula based autoregressive simulation that Gaussian dependence should exist between temporal random variables. Using beta kernel density estimation, different temporal classes can be flexibly fit in non-parametric way. Therefore the asymmetric property will be preserved in the time series which is generated by copula based statistical simulation.

As it was discussed in previous sections, multidimensional copulas can be constructed from observations with arbitrary time lags. If the value of the current time step is conditioned by the values at one and two time steps before, then 3 dimensional conditional copula can be defined as follow:

$$C\left(u \mid U_1 = u_1, U_2 = u_2\right) = \int_0^u c\left(u \mid u_1, u_2\right) du = \frac{\int_0^u c\left(u, u_1, u_2\right) du}{c\left(u_1, u_2\right)} \tag{8.5}$$

where $u = F_z\left(Z\left(t\right)\right), u_1 = F_z\left(Z\left(t+1\right)\right), u_2 = F_z\left(Z\left(t+2\right)\right)$. In this case the corresponding copula based auto regressive model is noted as **Copula AR** (0,1,2).

Copula AR (0,1,2) refers to sequential conditional simulation based on 3 dimensional copulas, in which (0,1,2) corresponds to the consecutive 3 random variables u, u_1, u_2, as defined in Eq. (8.5).

The application of ARIMA needs careful treatment for parameter estimation and stability conditions. This could be true to copula based autoregressive simulation. As a test case, the performance and behavior of the copula based on auto regressive simulation will be evaluated in this section. Also, Copula AR with higher dimensional copula is tested in Appendix D.

In this section, discharge time series at gauging station Andernach was generated for 3000 days with the copula based auto regressive model.

First sequential conditional simulation is carried out in the copula domain based on Eq. (8.5). Then, the empirical marginal distribution of the discharge time series (Figure 8-1) is attached to the simulated values of *u* using the inverse cumulative empirical distribution function.

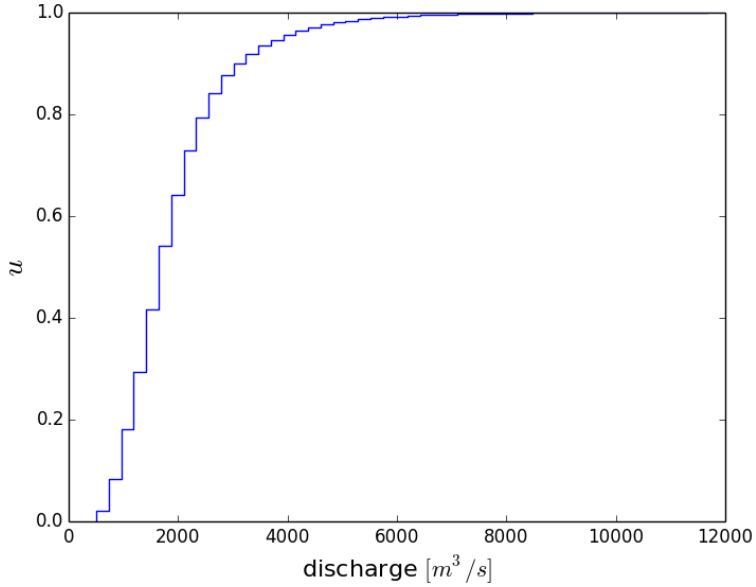

Figure 8-1 Empirical cumulative distribution function of discharge data from Andernach

The result of Copula AR(0,1,2) is shown in Figure 8-2. The sample of time series from simulated and observed discharge is shown on the top of this figure. *Asymmetry1* and *asymmetry2* corresponding to time lag *k*, power spectral in log scale are shown in the middle of this figure. Also 2 dimensional empirical autocopulas for both simulated and observed discharges are shown in the bottom of this figure.

The Copula AR (0,1), Copula AR (0,1,2,3), Copula AR (0,1,2,3,4), Copula AR (0,1,2,3,4,5,6,7,8,9) are also tested and shown in Appendix D, but Copula AR (0,1,2) will be discussed first as a descent version of simulation.

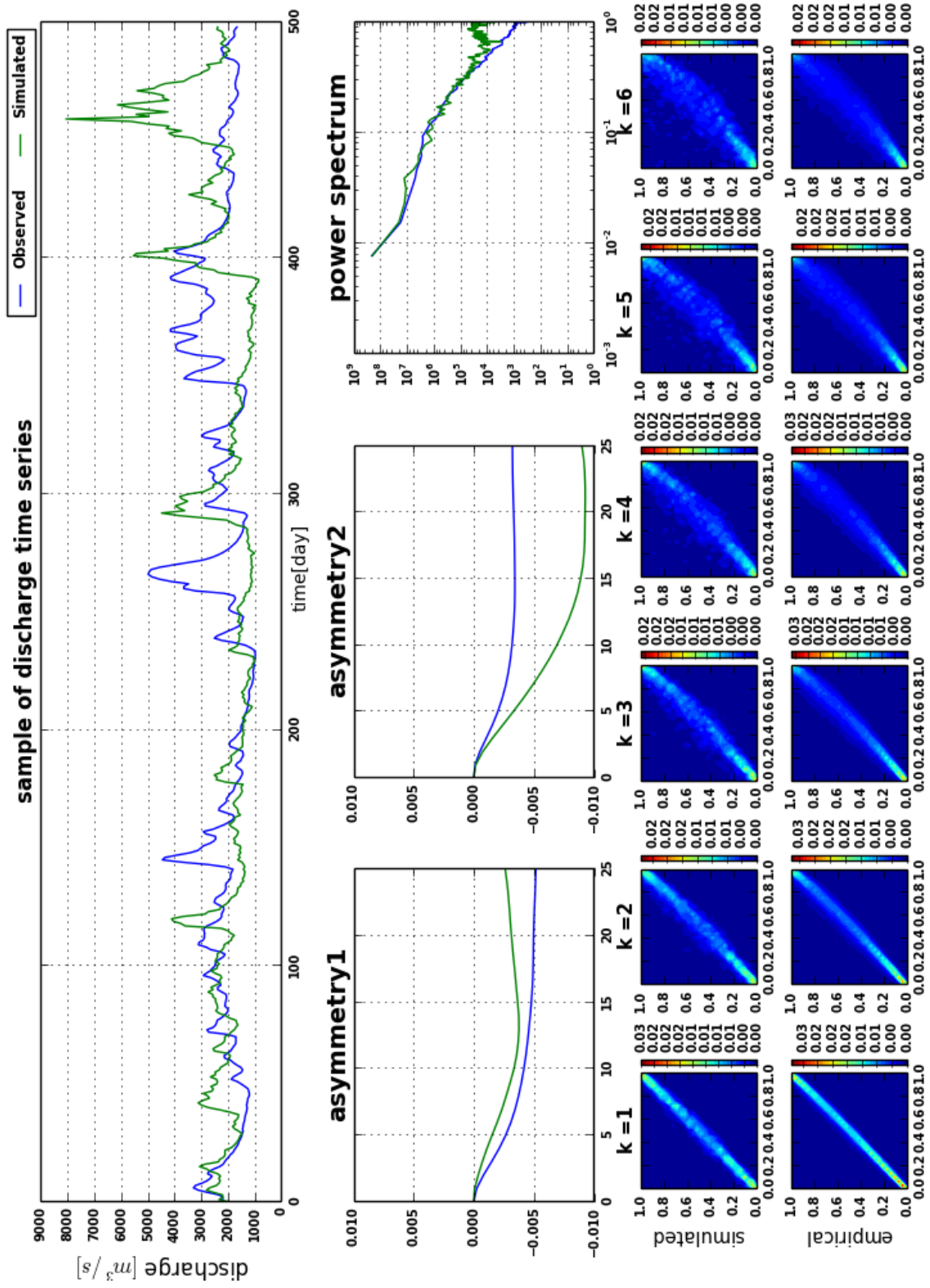

Figure 8-2 test case of non-Gaussian simulation of discharge time series data based on the 3 dimensional copula estimated by beta kernel smoothing (lag *k = 0, 1, 2*)

In the Figure 8-2 (top), part of a sequentially simulated time series is shown with its original observed time series for the comparison. The simulated result shows the typical structure of asymmetry in discharge data, namely the sharp rise of discharge to the peak and longer recession time.

Figure 8-2 (middle) shows the asymmetries (*asymmetry1* and *asymmetry2*) of simulated and observed discharge corresponding to time lags *k* [days]. The existence of asymmetry is clear also in these figures, but asymmetry of simulated and observed discharges do not fit each other especially for bigger time lag *k*[days]. The reason can be that the dimension of copula used for simulation is 3, therefore it can reproduce the asymmetric structure well for smaller time lag *k*, but it is not so precise for bigger *k*. There is a figure showing the power spectrum of time series. However, not big difference can be identified in frequency domain.

The last one, Figure 8-2 (bottom), shows the 2 dimensional empirical autocopulas calculated from the simulated and observed time series. Observed data has approximately 30000 days daily discharge record, while simulated one has 3000 days due to the constraints of calculation time. Therefore, the visualized empirical copula of simulated data looks not smooth.

In these figures, density of empirical copula is bigger in lower left corner for simulated discharges than observed discharge. This means, the dependence structure is not well reproduced for the smaller values. This can be caused by the bias of beta kernel, although the kernel has advantages to reduce the bias on the corner.

Further examples of a copula based autoregressive model and its simulation can be found in Appendix D. Copula based autoregressive simulation with higher dimensional copula or with different combinations of lags are presented in the appendix.

The results in Appendix D show that simulation with higher dimensional copula does not improve the performance of simulations in terms of asymmetry, although its optimization of band width and statistical simulation is numerically demanding. It is concluded simulation with 3 or 4 dimensional copula gives reasonably good results for the discharge time series. This can be interpreted, 3 or 4 dimensional copula has characteristic information for short term events of discharge, although it cannot reproduce the long term event such as temporal change of mean, variance or asymmetry.

In this chapter, Copula AR, sequential conditional simulation of time series using autocopulas estimated by kernel density estimation, was tested. It could reproduce the asymmetric structure to a certain extent, but main problems are 1) asymmetries are not exactly same to the observed discharge 2) asymmetry and dependence structures cannot be reproduced especially for lager time lag k. 3) it is numerically expensive to use higher order of copula estimated by kernel density estimation.

9 Conclusion and Outlook

The application of copulas for time series data is new. Asymmetries of Copula in discharge time series are focused for the first part of this study. However, it was not easy to detect the anthropogenic impacts on the catchments in asymmetry of discharge data. Therefore, further analyses were attempted especially with copula distance in the second part of this study.

In chapter 1, the motivation and background of this study were presented. Short summary of hydrological study was given in the context of time series analysis

In chapter 2, the mathematical background of copula was explained with the emphasis on asymmetry in copulas and application of copulas in time series.

In chapter 3, the relation between asymmetry and catchment characteristics was investigated. It was seen each catchment has a different characteristic in terms of *asymmetry2*. The *asymmetry2* is more variable for smaller catchments and converges to certain value for large catchment areas. The temporal changes of asymmetries were also investigated, but relation between anthropogenic impacts and discharge was not successfully proven.

In chapter 4, the seasonal change of asymmetry was investigated. It was seen the dependence structure is clearly different depending on the seasons. The empirical copula calculated from the entire time series or part of the time series is already the mixture of the copulas in different seasons. It was concluded this diversity makes the analysis of discharge with copula difficult.

In chapter 5, the asymmetry and temporal structure of empirical autocopula calculated from precipitation in Baden-Württemberg region was analyzed using API. The result shows some similarity can be found in terms of temporal change of asymmetry. This implies the asymmetric characteristic of copula in discharge might be originated from rainfall.

In chapter 6, HBV model was set up based on the assumption that discharge time series simulated by hydrological model with fixed parameters should not have the anthropogenic influence or change of catchment characteristic. The result shows temporal change of *asymmetry2* exists in the discharge time series simulated by HBV model. This means, the impacts of precipitation time series must be considered for the analysis of temporal change of copula calculated from discharge time series.

In chapter 7, the analysis with copula distance is newly introduced in this study. *Copula distance type1* is to compare the empirical copula of entire time series and the empirical copula of certain time periods. The clear signal was detected that, the dependence structure of certain time period is different from the rest around 1945, 1980 and 2000. The interdependency of this unusual state of copula is compared by *copula distance type3.* This signal seemed caused by the precipitation around 1945 and 2000, but the signal around 1980 was less related to the rainfall. Integrated version of *copula distance type1* and *copula distance type3* is newly defined as copula variance and copula correlation, which illuminate the new characteristics of time series.

In chapter 8, non-parametric simulation of discharge based on Copulas was introduced based on geostatistical interpolation using copulas (Bárdossy and Li 2008) as a new method to predict or generate the time series. It was shown that the simulated discharge shows asymmetric properties similar to those of the observed discharge. The dependence structure for low dimensional copula is well reproduced with lower dimensional copula. But, the reproduction of dependence structure in higher dimension with higher dimensional copula with kernel density based method was not really successful.

The application of copula for time series analysis seems promising. Empirical autocopula is a more data driven method, which retains more information than the copulas estimated with parametric methods, but it is also numerically more demanding. The effective way to analyze time series and build up time series model based on copula should be further explored.

Appendix A Result of the Standardization2

In Section 3.3, it was discussed how the annual cycle of discharge time series looks like and the possibility to normalize the data. In order to reduce the impacts of seasonality, annual cycle of mean is subtracted from the original time series (standardization1) in this study.

However, as it was discussed, there is another way to standardize the data by means of dividing original data by annual cycle of deviation after subtraction of annual cycle of mean (standardization2). In this Appendix, the results of standardization2 are shortly presented.

Figure 3-14 shows annual cycle of standard deviation of each discharge time series. The standard deviation is usually high in winter and low in summer. Therefore, possible effect of standardization2 is that the impacts of runoff events in winter can be reduced and the impacts in summer increase on copulas.

Figure A-2 shows variation of *asymmetry2* corresponding to lag time *k* [days] after standardization2 while Figure 3-21 shows the same result with sandardization1. The influence of seasonal effect is reduced similar to Figure 3-21. Definition and Analysis for A2min, Minimum of asymmetry, and $\boldsymbol{L_{min}}$, Lag time a minimum is valid for standardization2.

Figure A-3 shows temporal change of A_{2min} (top) and L_{min} (bottom) while Figure 3-26 and Figure 3-27 show same result for standardization1. These results are also quite similar to case of standardization1, showing the drop down of A_{2min} around 1945 and 1983.

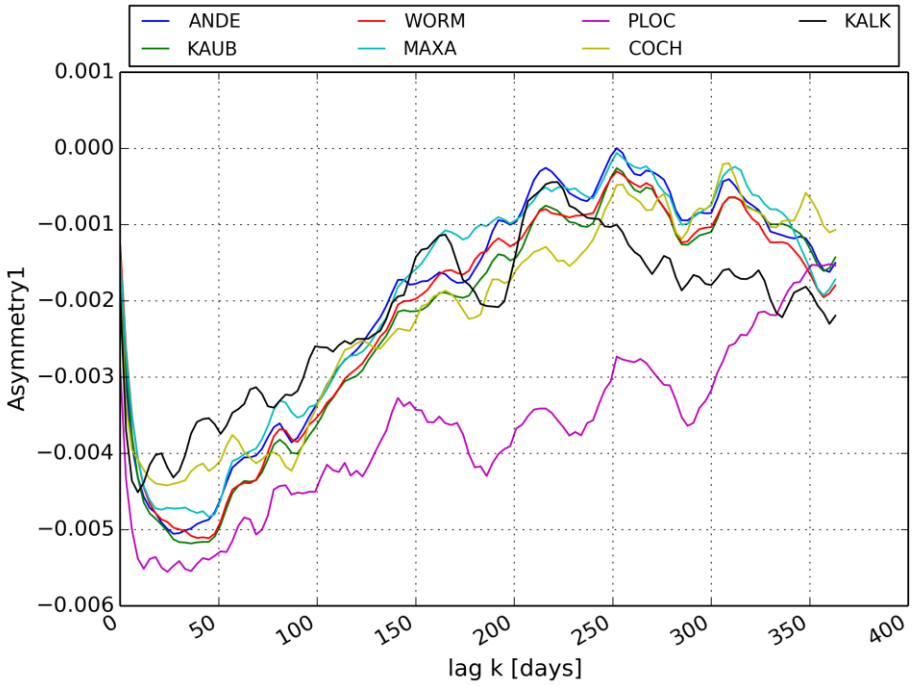

Figure A-1 change of *asymmetry1* divided by annual cycle of standard deviation after subtraction of annual average (standardization2)

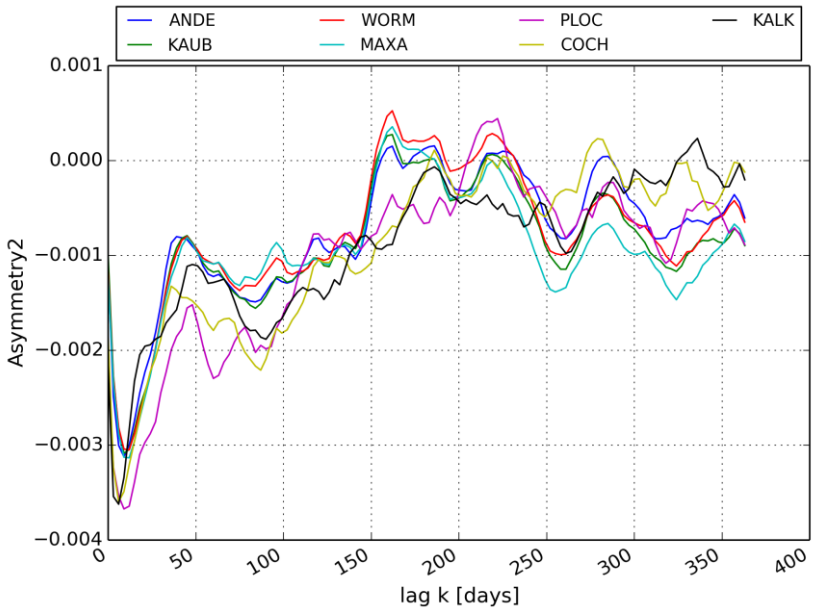

Figure A-2 change of *asymmetry2* divided by annual cycle of standard deviation after subtraction of annual average (standardization2)

Figure A-4 shows variation of *Asymmetry2* corresponding to time lag *k* in different time periods for standardization2 while Figure 3-30, Figure 3-31 and Figure 3-32 shows the same result for standardization1. These results are also similar, showing clear structure of drop down between 1930 and 1940, no clear structure of drop down between 1940 and 1950 and less clear structure between 1968 and 1978.

Figure A-5 shows analysis of copula distance for standardized discharge time series (standardization2) of Andernach same to the Figure 7-1 in chapter 7. Please note that the discharge time series of simulated and observed discharge in the bottom of figure has now mean = 0 and standard deviation = 0. The result of copula distance tpye1 and type2 are not much different form the result of standardization1

It can be concluded that the standardization1 and standardization2 do not bring much difference in the results of copula based stochastic analysis with smaller lag time k [*days*]. In general, it is assumed to affect more the results as lag time k [*days*] increases, because the influence of direct relation between two random variables are much stronger for small time lag *k* [*days*] and impacts of annual cycle is negligible for small *k*.

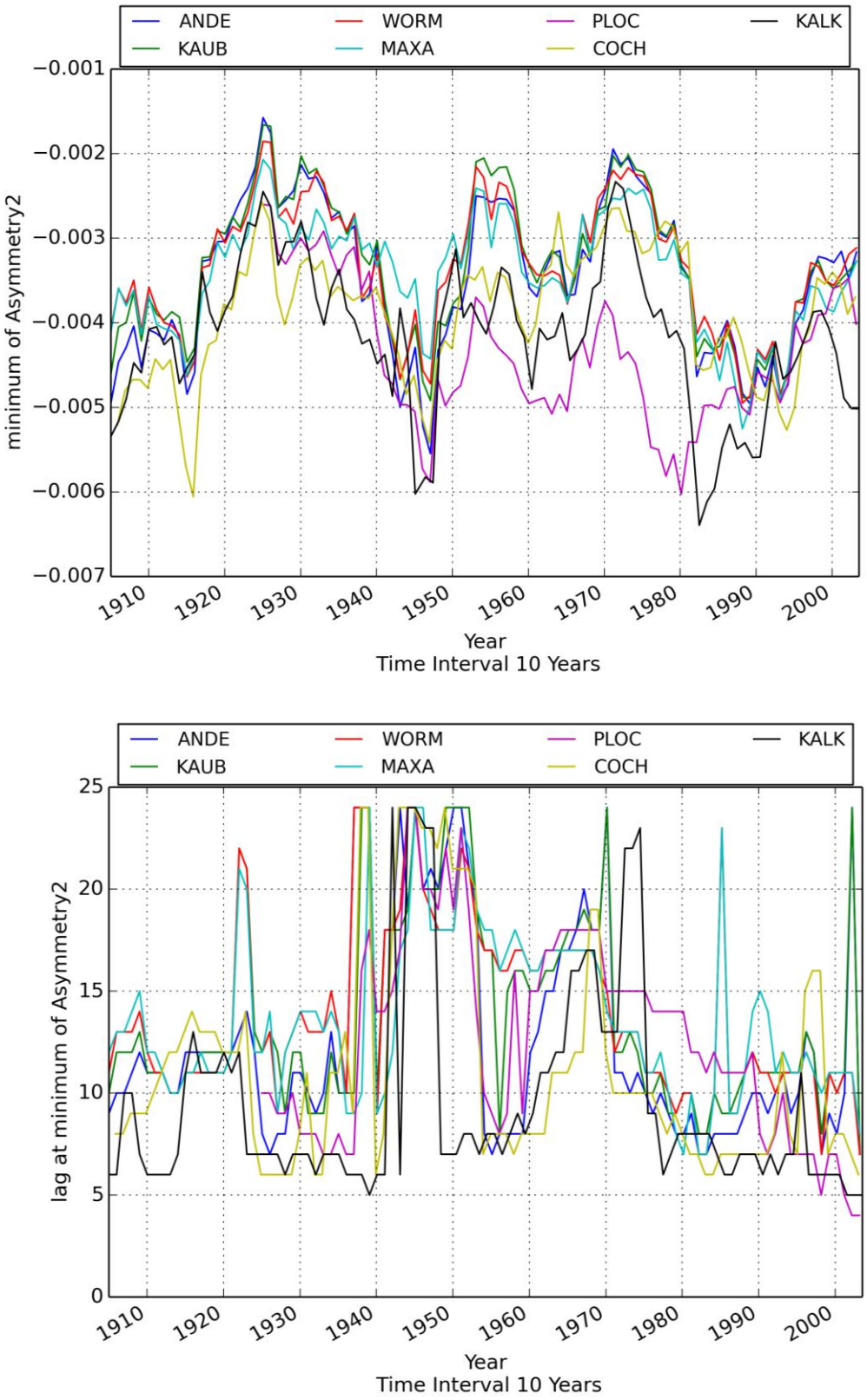

Figure A-3 Temporal change of A_{2min} (Minimum of *asymmetry2*) and L_{min} (Lag at minimum of *asymmetry2*) in moving time window with 10 years interval for standardization2

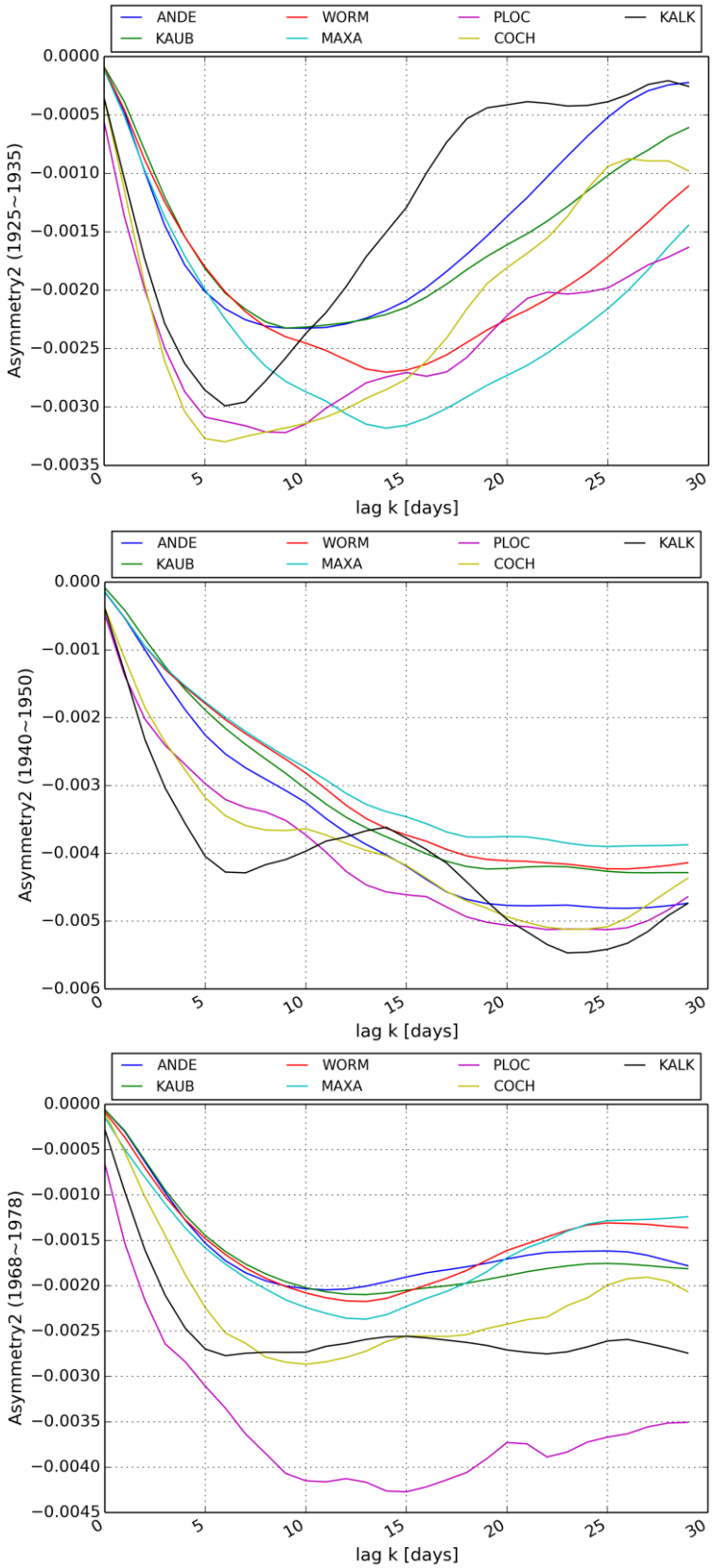

Figure A-4 Variation of *Asymmetry2* corresponding to time lag k for discharge time series data between 1925 and 1935(top), between 1940 and 1950 (middle) and between 1968 and 1978(bottom)

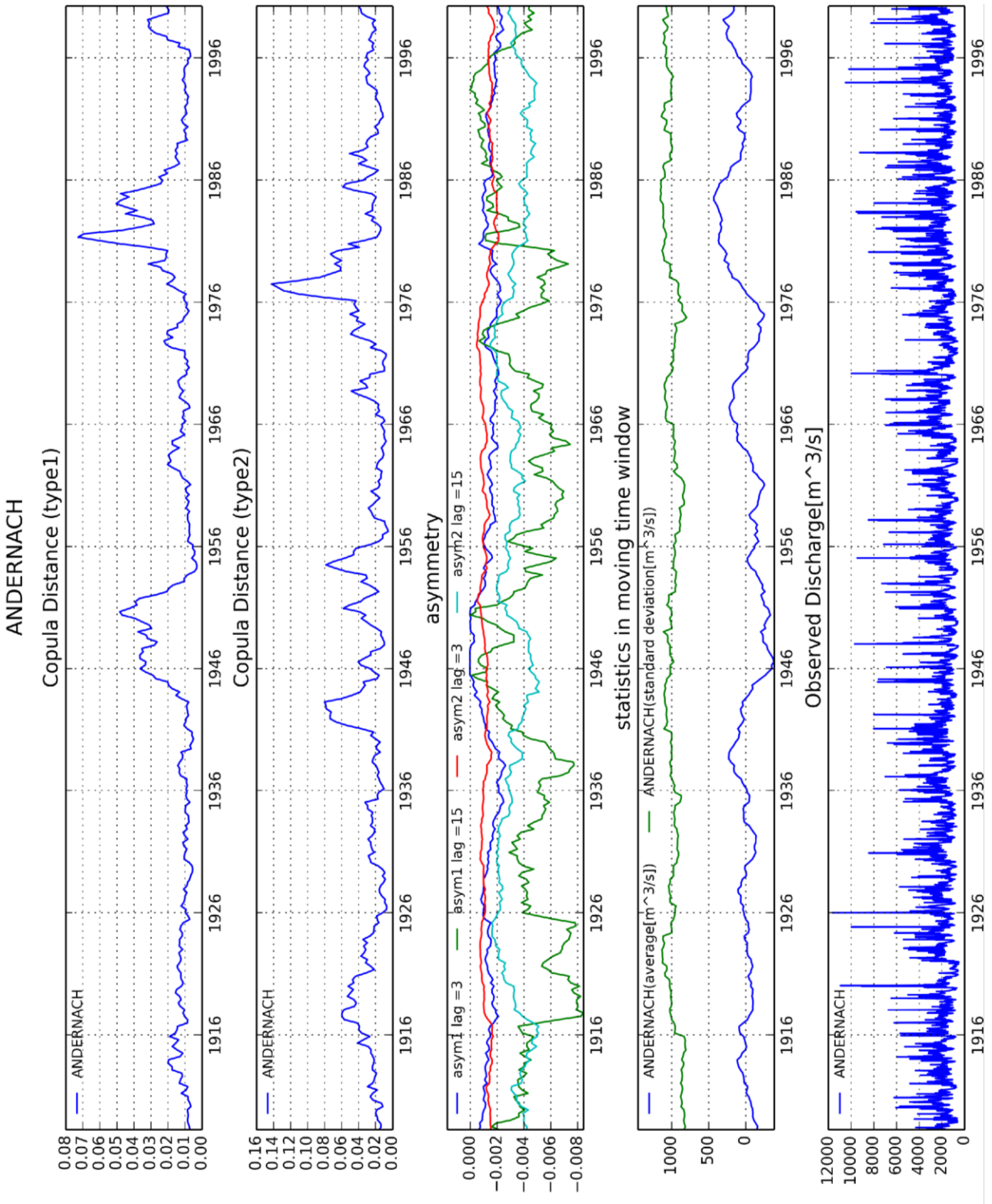

Figure A-5 Analysis of Copula Distance for the discharge data from Andernach with standardization2

Appendix B Temporal Change of Asymmetry2 in Other Regions

In section 3.6 the temporal change of asymmetry was investigated for the discharge time series in the target region (Andernach, Kaub, Worms, Maxau, Cochem, Plochingen, Kalkofen).

Here, the same analysis was done in the other regions:

1) The Main river as right tributary of Rhine (Figure B-1)
2) Upper part of Danube located in southeast of Germany (Figure B-2)
3) The Weser river located in the north of Germany (Figure B-3)
4) Downstream of Elbe located in Northeast of Germany (Figure B-4)

The interesting point is that the similar behavior of *asymmetry2* can also be seen in the river of other regions. Drop down around 1945 and 1983 happened to all the regions. It also coincides that the value of *asymmetry2* goes up around 1970 for all the regions including Rhine in Figure 3-26.

It is less likely to happen that the realization of precipitation or weather for certain period is exactly same in other regions. Therefore, the possibility that same kind of change might have happened to all the German rivers or catchments around 1945, 1970 and 1983 cannot be denied. But, this also does not explain that the temporal behavior of asymmetry in API time series is similar to the discharge as shown in Figure 5-10.

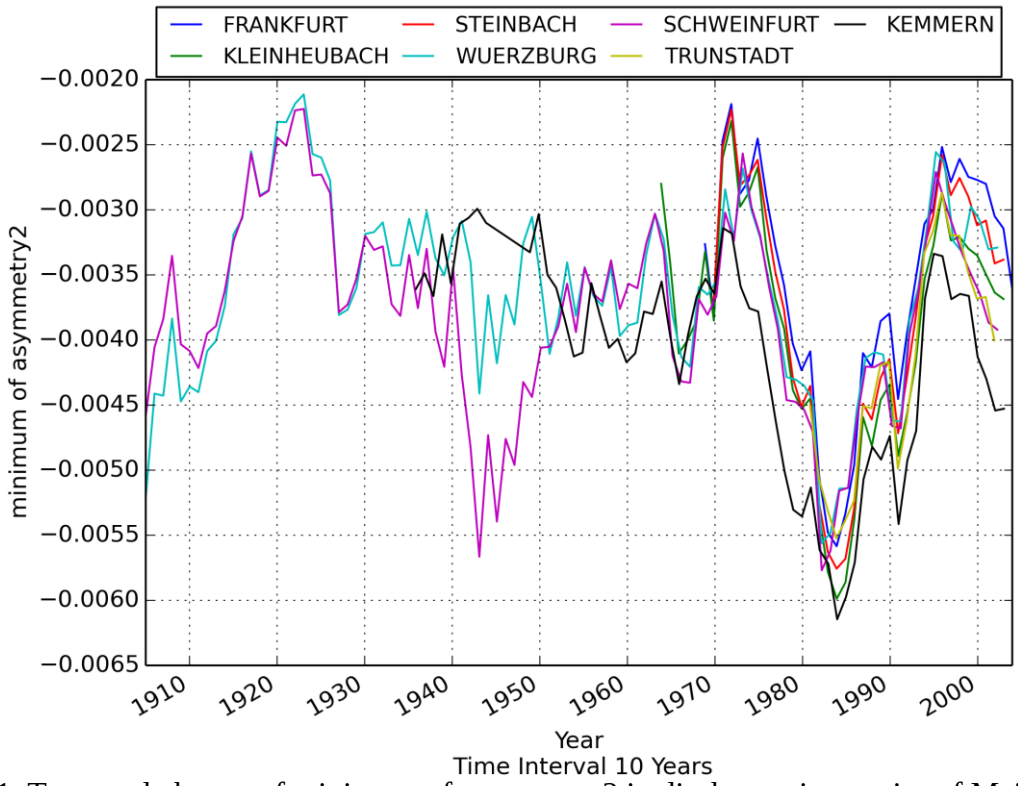

Figure B-1 Temporal change of minimum of asymmetry2 in discharge time series of Main

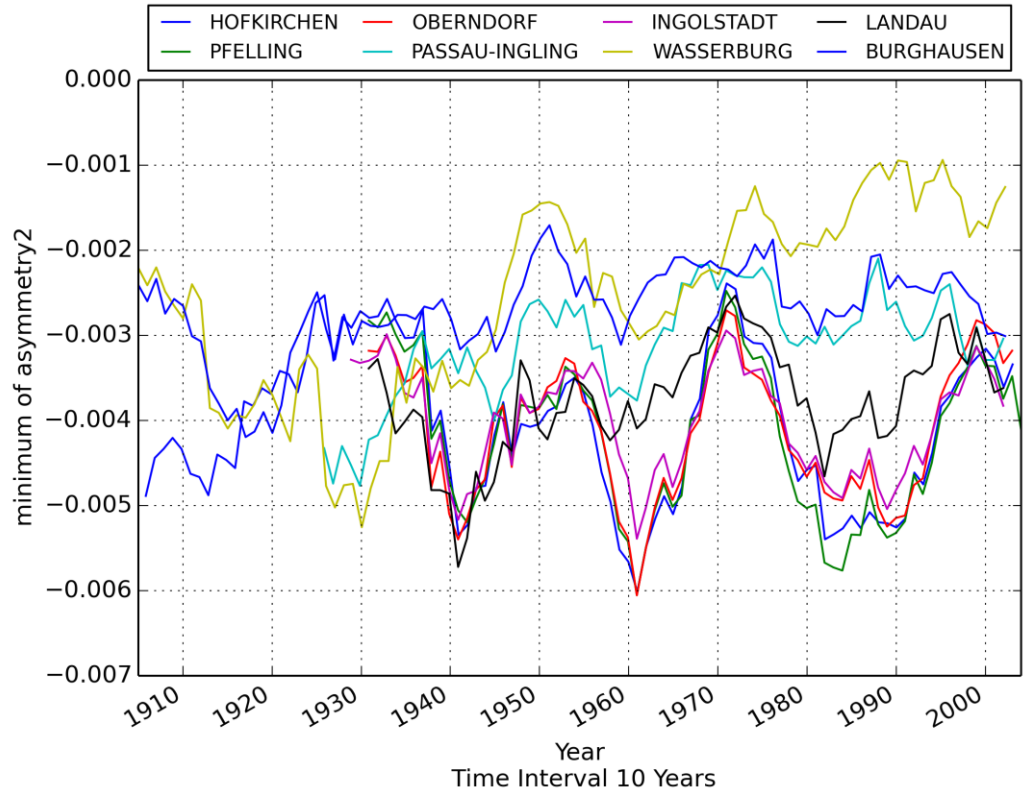

Figure B-2 Temporal change of minimum of asymmetry2 in discharge time series of upper part of Elbe

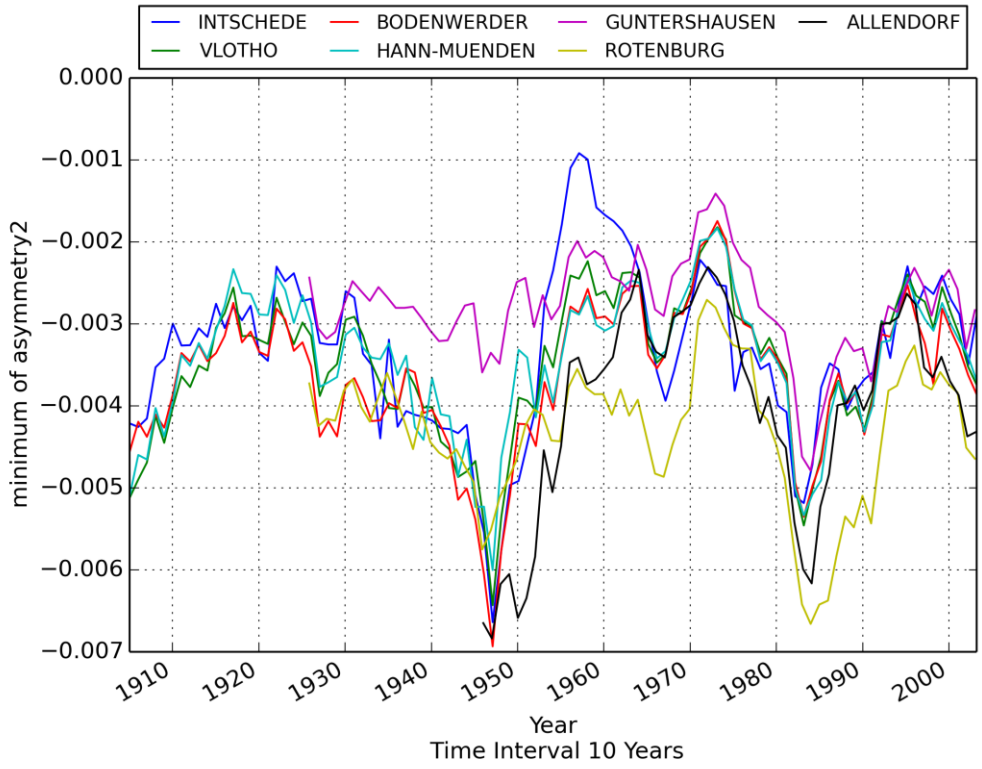

Figure B-3 Temporal change of minimum of asymmetry2 in discharge time series of Weser

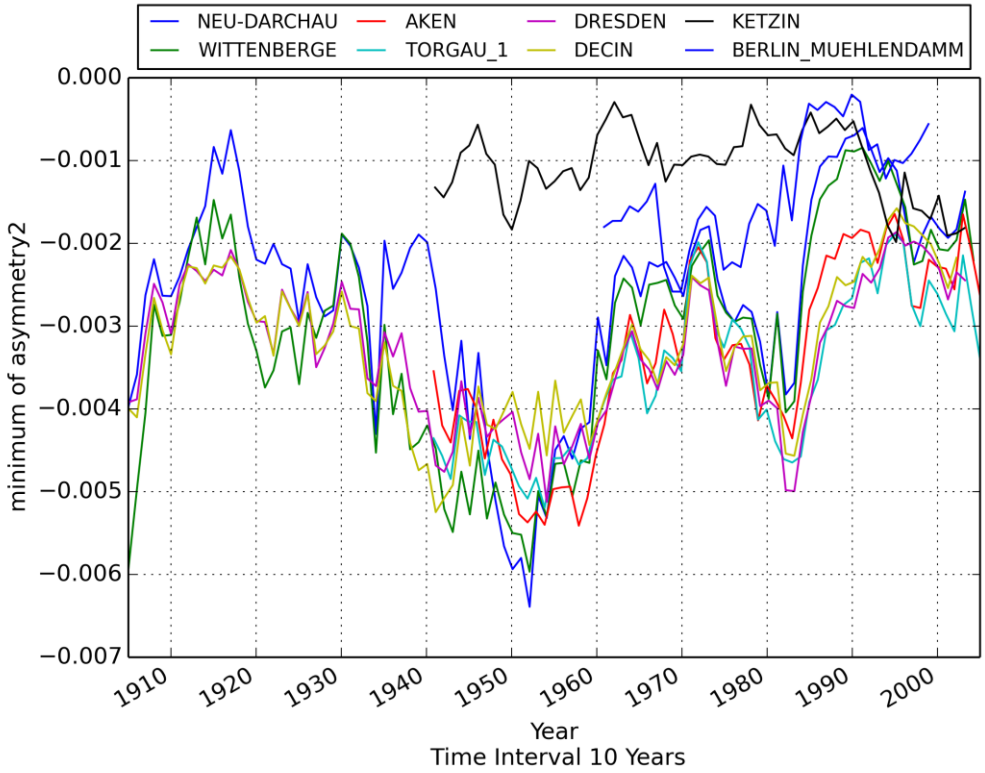

Figure B-4 Temporal change of minimum of asymmetry2 in discharge time series of Danube

Appendix C Copula Distance Type1 of Other Stations

(KAUB, WORMS, MAXAU, COCHEM,PLOCHINGEN,KALKOFEN)

In Figure 7-1 at section7.1, detailed analysis of copula distance (*copula distance type1*, *type2*, *asymmetry1*, *asymmetry2*, statistics in moving time window) was done for discharge time series data from Andernach. In this Section, the same analysis is carried out for the rest of the data (Kaub, Maxau, Worms, Cochem, Plochingen, Kalkofen).

The interesting point is that, *copula distance of type1* is always high around 1945 for all the stations and in 1980 all the stations except for Kalkofen. This cannot be clearly captured by asymmetry or statistics in moving time windows.

Copula distance type2 also indicates change of structure started a few years before and after 1980.

The observed discharge is also plotted in the same figures, but unusual behavior cannot be easily recognized.

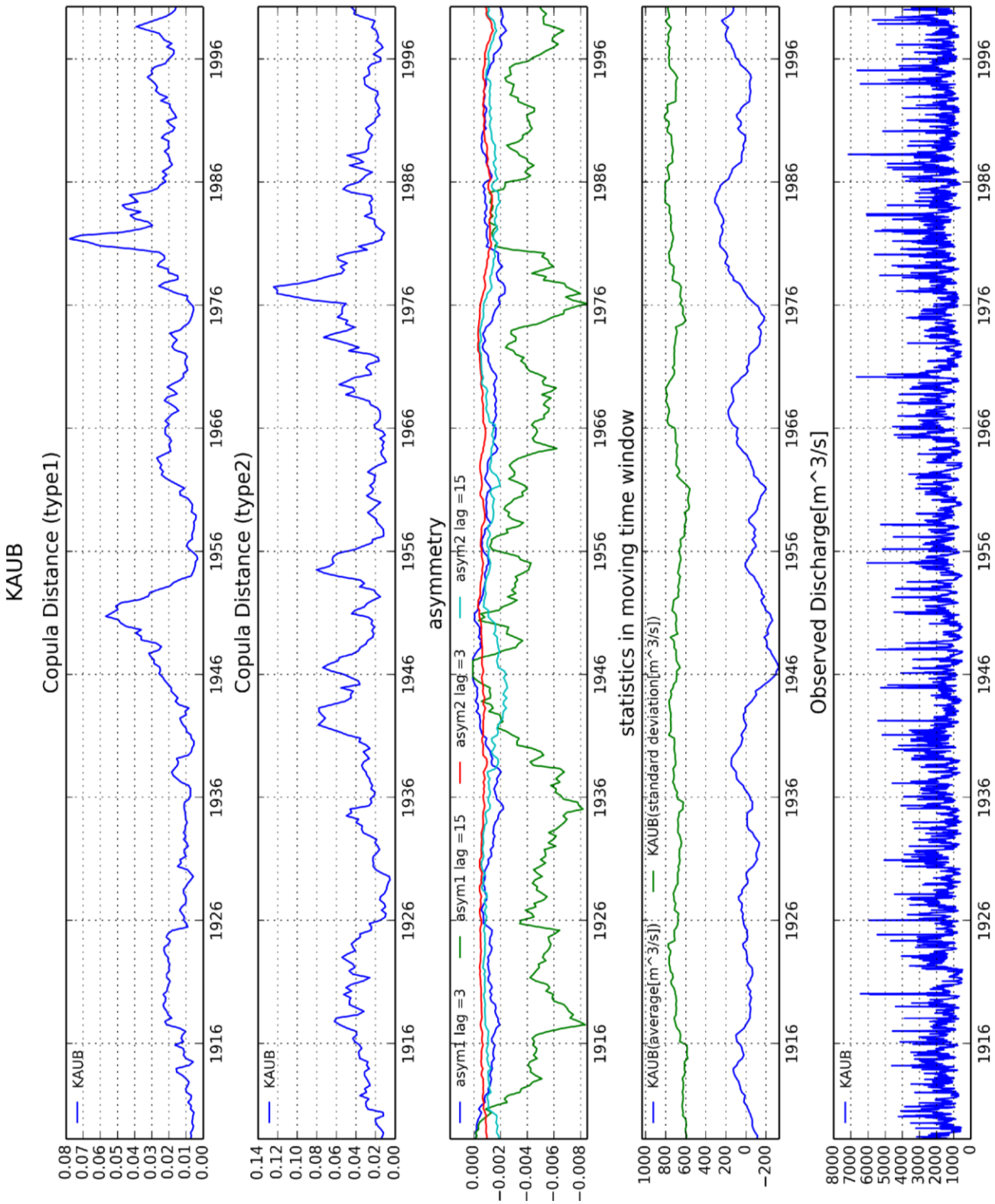

Figure C-1 Analysis of copula distance for discharge time series from Kaub

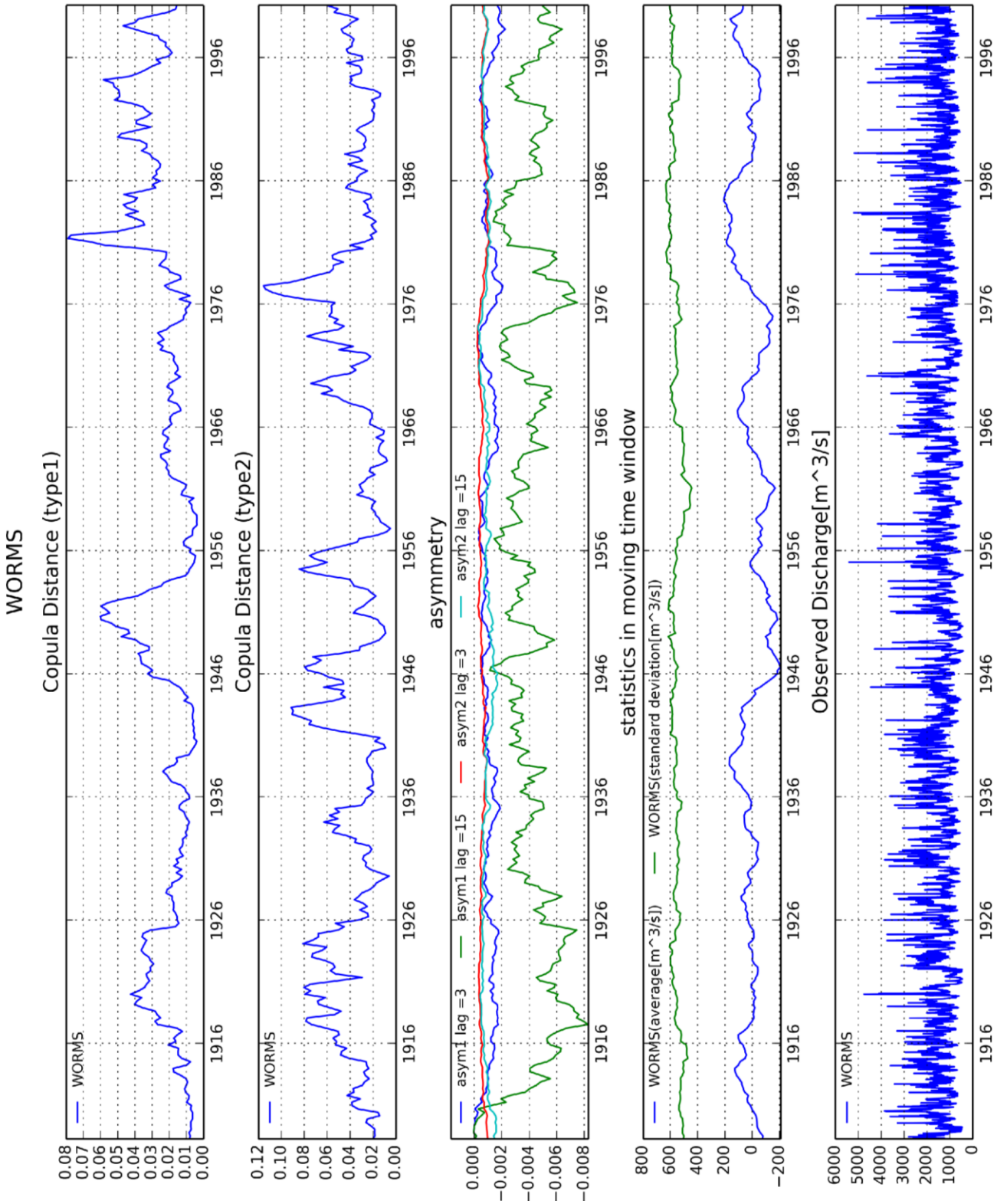

Figure C-2 Analysis of copula distance for discharge time series from Worms

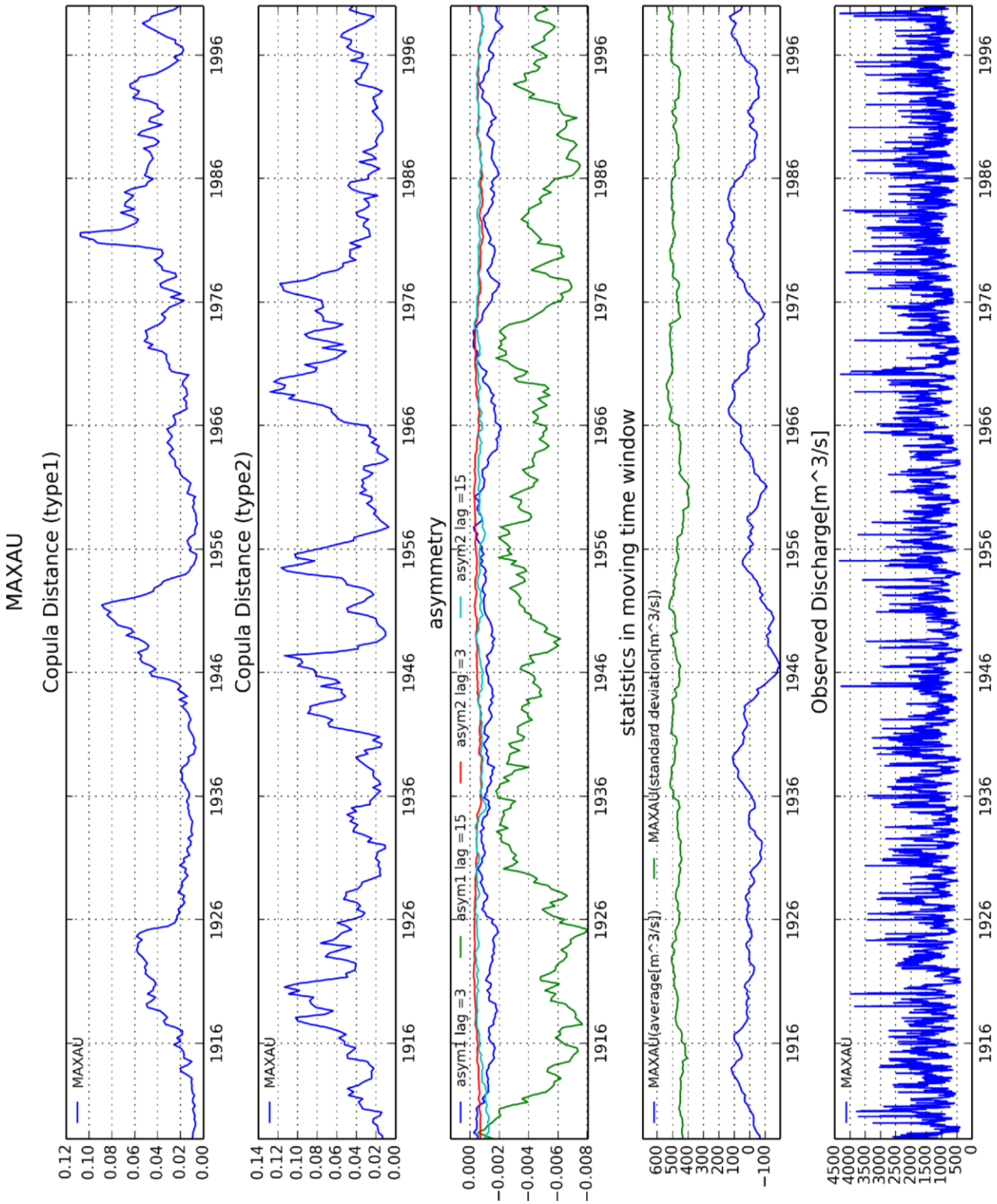

Figure C-3 Analysis of copula distance for discharge time series from Maxau

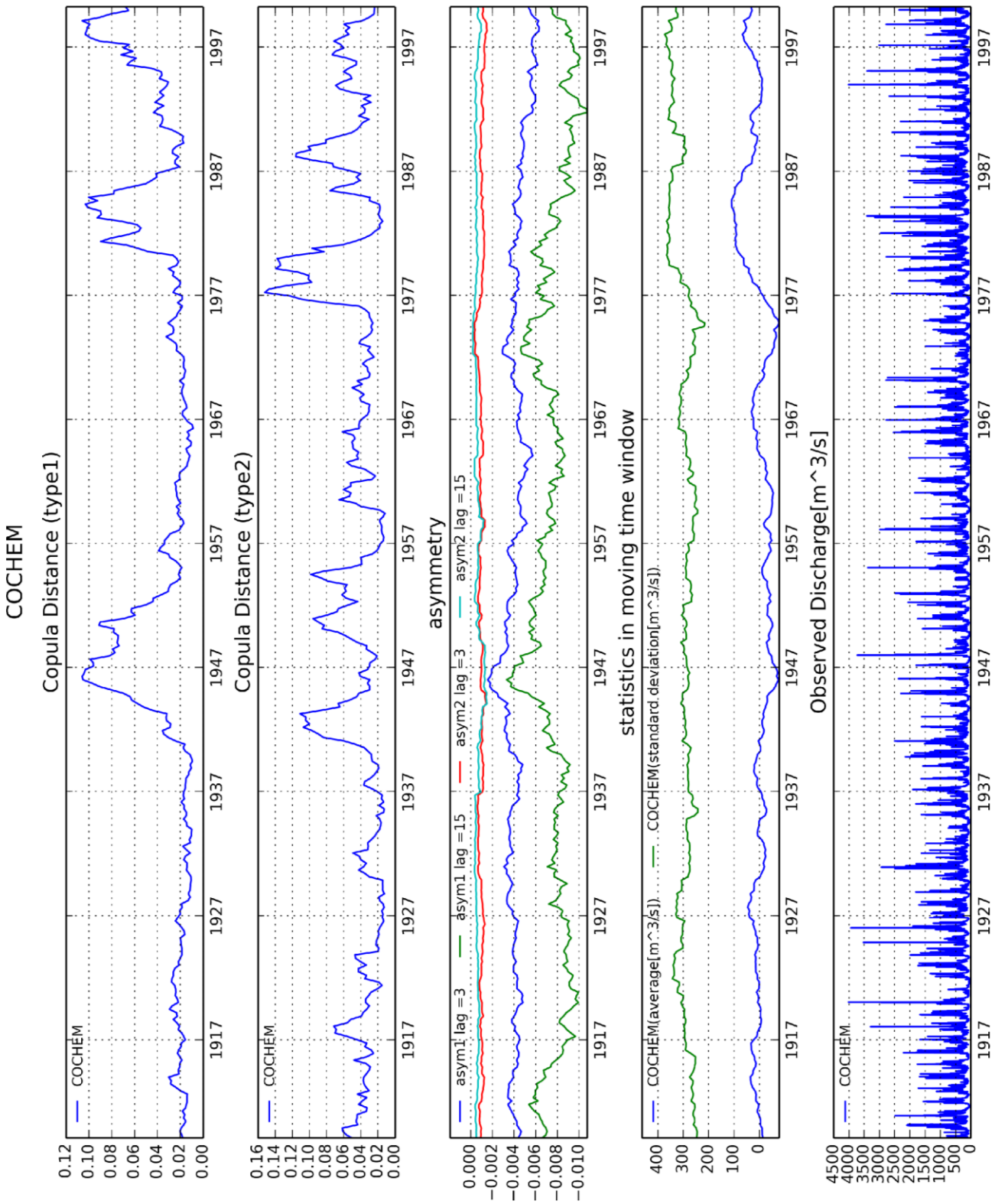

Figure C-4 Analysis of copula distance for discharge time series from Cochem

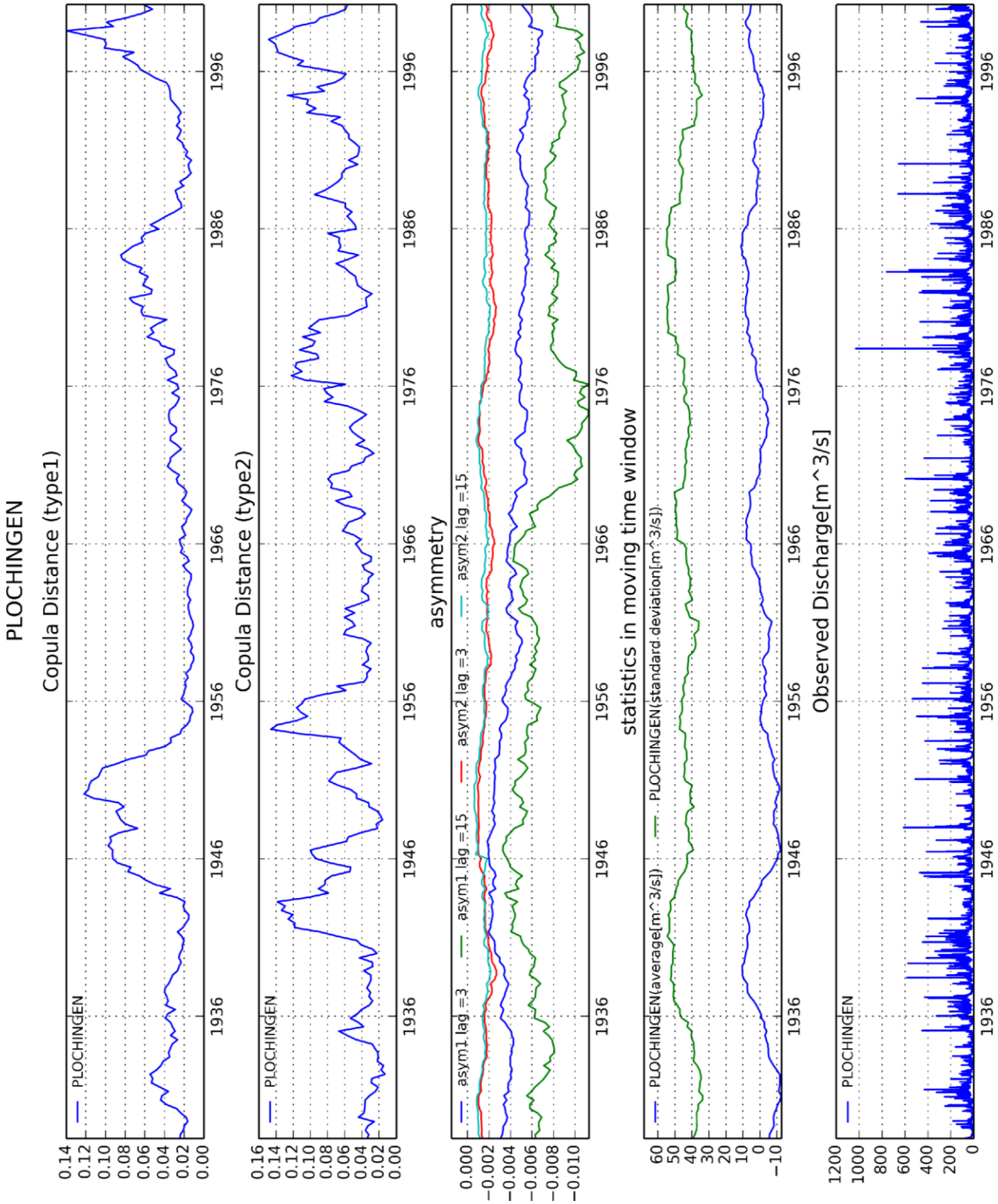

Figure C-5 Analysis of copula distance for discharge time series from Plochingen

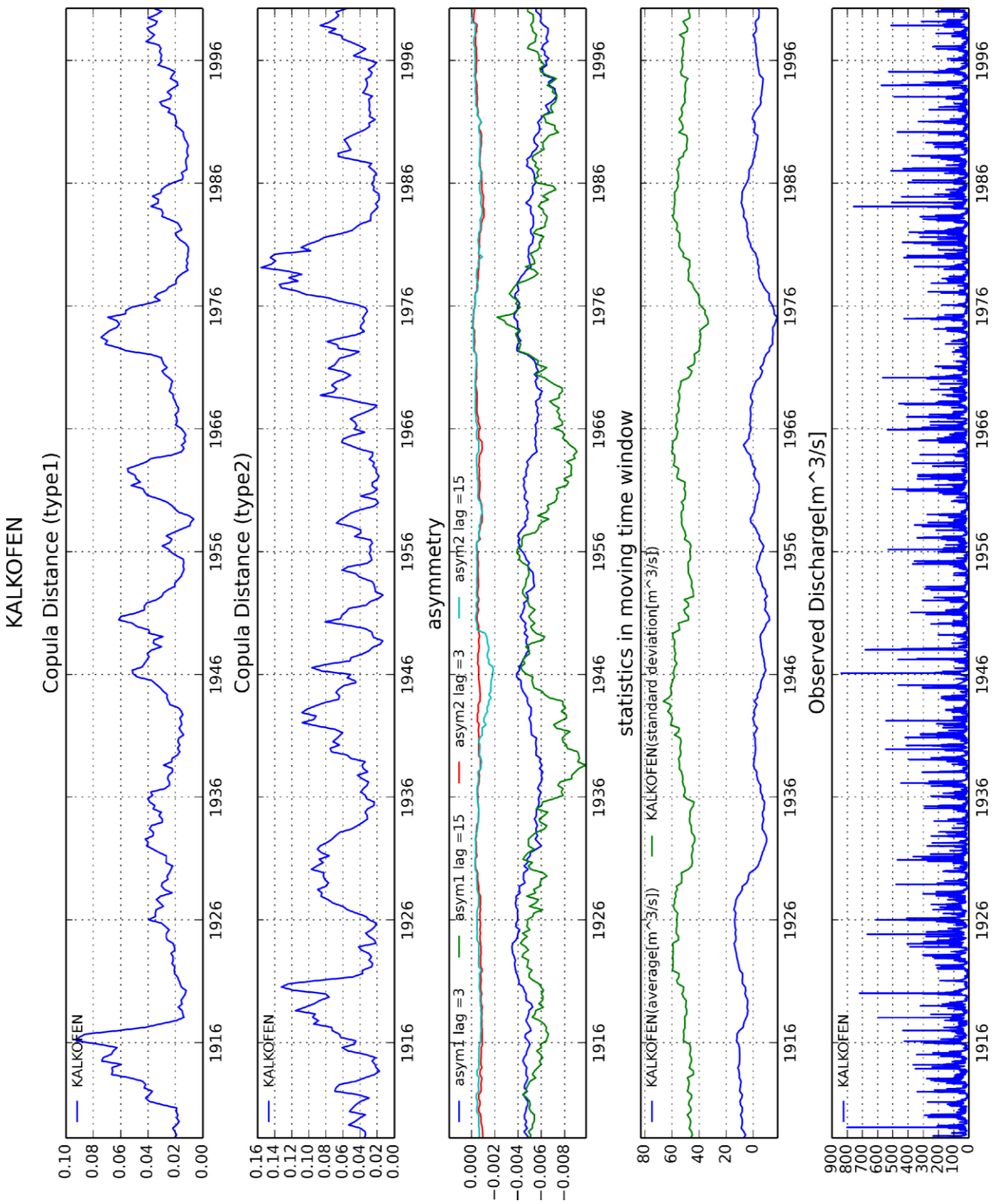

Figure C-6 Analysis of copula distance for discharge time series from Kalkofen

Appendix D Copula based Autoregressive Simulation

In Chapter 8, Non-parametric Simulation of Discharge Time Series based on Copulas, was suggested and time series was simulated based on 3 dimensional copulas.

In this section, the benchmarks of this statistical simulation are performed especially for copulas with higher dimensions.

As it was mentioned in Chapter 8, statistical simulation with higher dimensional copula does not really improve the result, although it needs more calculation time.

Figure D-1 shows the statistical simulation with 2 dimensional copula. The discharge time series in this figure already shows the characteristics of *asymmetry1* and *asymmetry2*.

The statistical simulation was done with higher dimensional copulas, but it should be noted that there is bias also in kernel density estimation with Beta Kernel and this bias increases for higher dimensional copula.

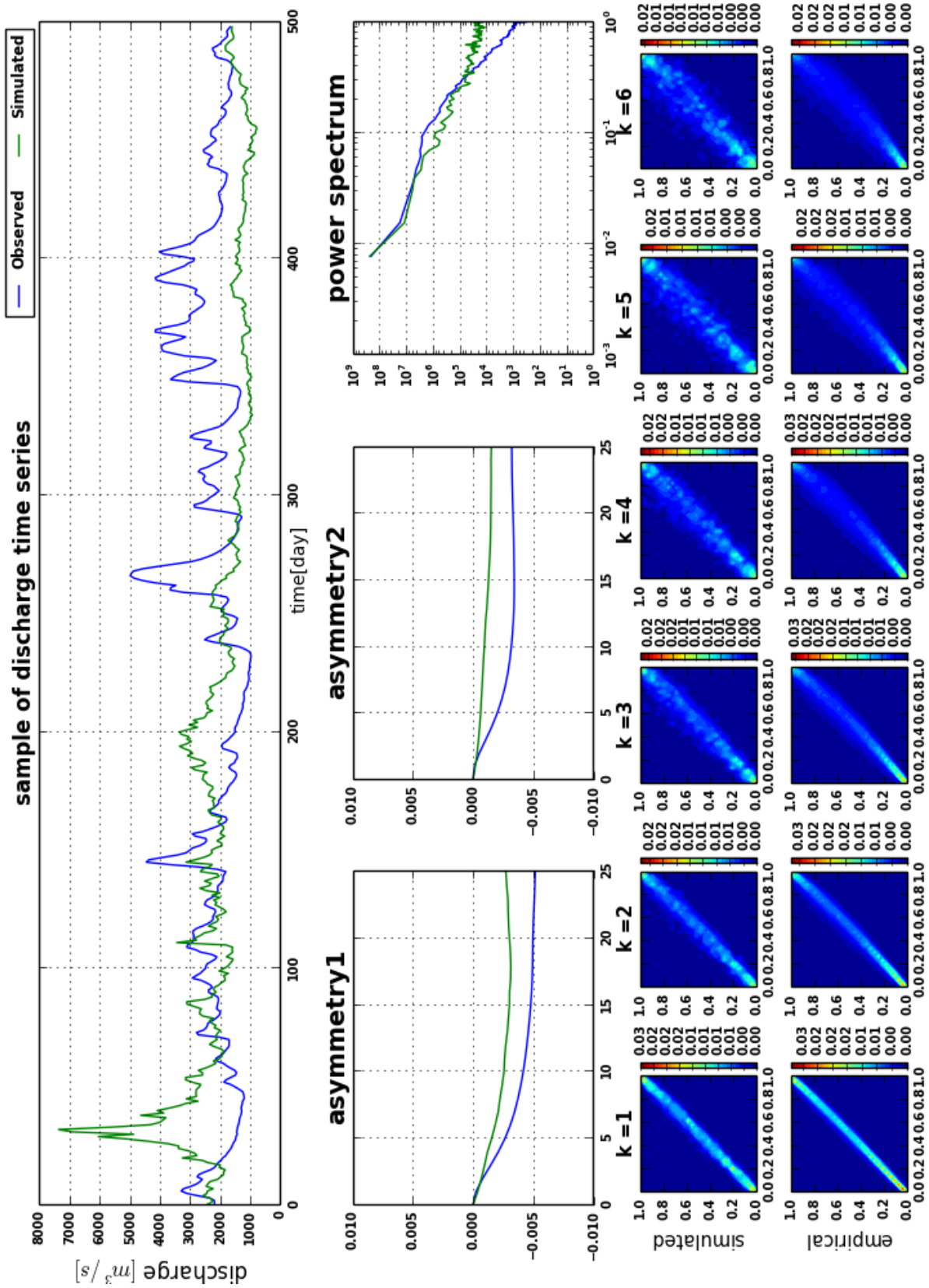

Figure D-1 Result of Copula AR (0,1)

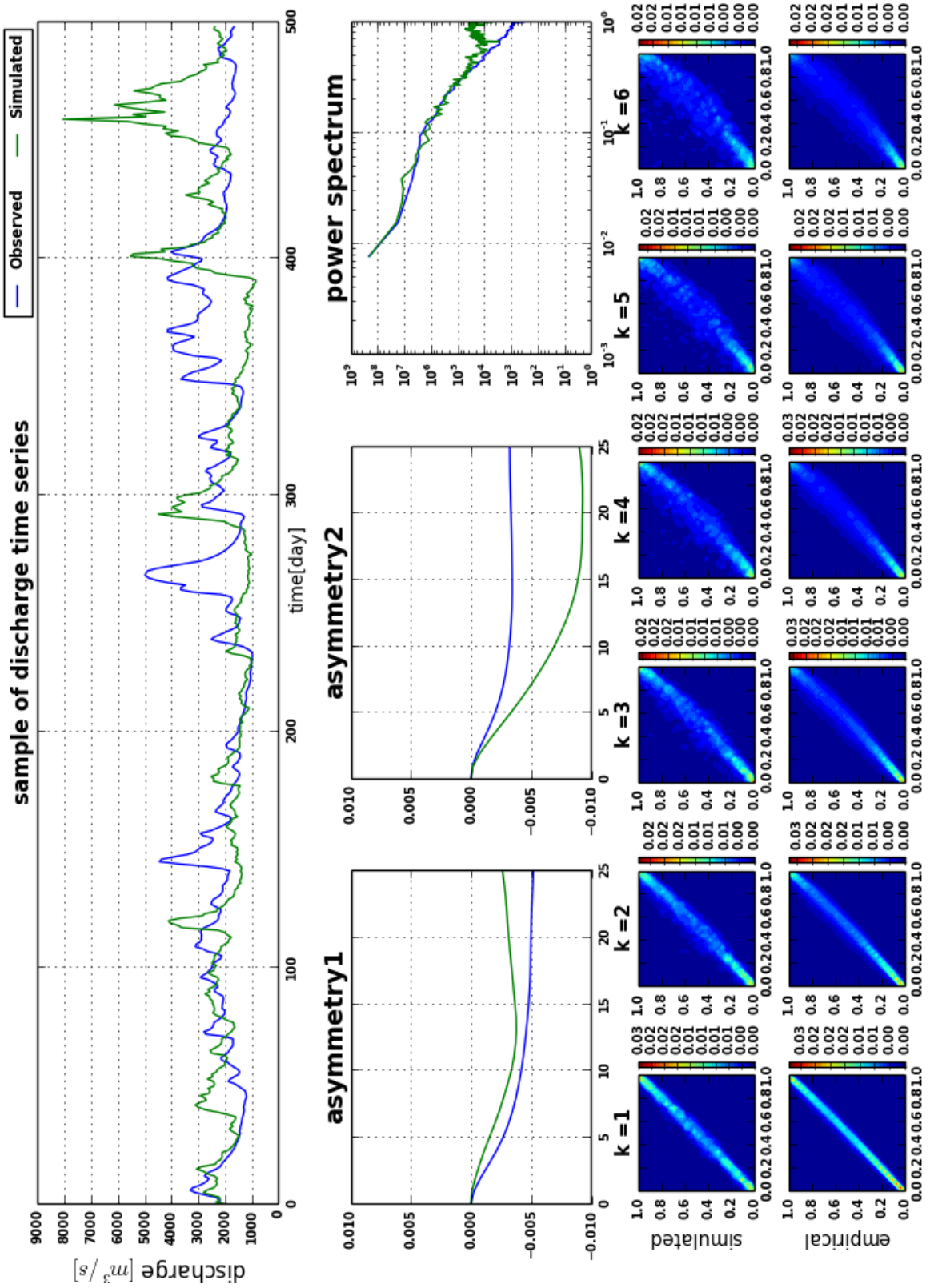

Figure D-2 Result of CopulaAR(0,1,2,3)

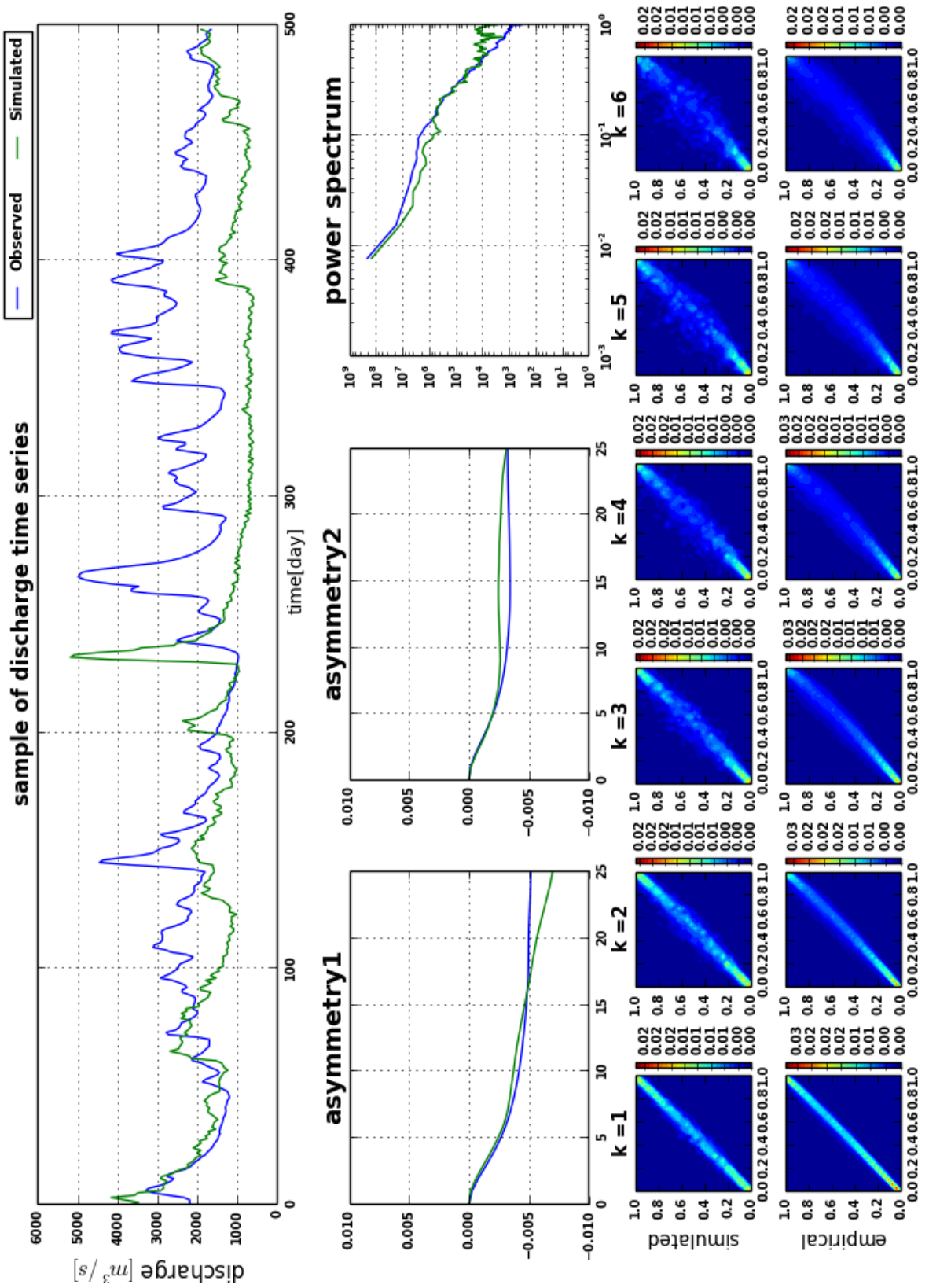

Figure D-3 Result of Copula AR(0,1,2,3,4,5,6,7,8,9)

Bibliography

Bárdossy, A., and G. G. S. Pegram. 2009. “Copula Based Multisite Model for Daily Precipitation Simulation.” *Hydrology & Earth System Sciences* 13(12).

Bárdossy, András. 2006. “Copula-Based Geostatistical Models for Groundwater Quality Parameters.” *Water Resources Research* 42(11):n/a–n/a. Retrieved February 10, 2014 (http://doi.wiley.com/10.1029/2005WR004754).

Bárdossy, András, and Jing Li. 2008. “Geostatistical Interpolation Using Copulas.” *Water Resources Research* 44(7).

Bergström, S. 1976. *Development and Application of a Conceptual Runoff Model for Scandinavian Catchments*. Department of Water Resources Engineering, Lund Institute of Technology, University of Lund.

Bergström, Sten, V. P. Singh, and others. 1995. “The HBV Model.” *Computer models of watershed hydrology*. 443–76.

Box, George E. P., and Gwilym M. Jenkins. 1976. “Time Series Analysis, Control, and Forecasting.”

Chen, Song Xi. 2000. “Beta Kernel Smoothers for Regression Curves.” *Statistica Sinica* 10(1):73–92.

Das, Tapash. 2006. “The Impact of Spatial Variability of Precipitation on the Predictive Uncertainty of Hydrological Models.” Stuttgart: Inst. f. Wasserbau.

Fleming, Sean W., A. Marsh Lavenue, Alaa H. Aly, and Alison Adams. 2002. “Practical Applications of Spectral Analysis to Hydrologic Time Series.” *Hydrological processes* 16(2):565–74.

Huang, Norden E. et al. 1998. “The Empirical Mode Decomposition and the Hilbert Spectrum for Nonlinear and Non-Stationary Time Series Analysis.” *Proceedings of the Royal Society of London. Series A: Mathematical, Physical and Engineering Sciences* 454(1971):903–95.

Joe, Harry. 1997. *Multivariate Models and Multivariate Dependence Concepts*. CRC Press.

Kamkaew, Kitti. 2013. “Statistical Analysis of Discharge and Development of Time Series Model Using Copulas.” Universität Stuttgart.

Kim, Tae-Woong, Juan B. Valdés, and Chulsang Yoo. 2003. “Nonparametric Approach for Estimating Return Periods of Droughts in Arid Regions.” *Journal of Hydrologic Engineering* 8(5):237–46.

Kirkpatrick, Scott, D. Gelatt Jr., and Mario P. Vecchi. 1983. “Optimization by Simmulated Annealing.” *science* 220:671–80.

Li, Jing. 2010. *Application of Copulas as a New Geostatistical Tool*. Online-Aus. Stuttgart: Inst. f. Wasserbau. Retrieved (http://elib.uni-stuttgart.de/opus/volltexte/2010/5133).

Mead, Daniel Webster. 1919. *Hydrology: The Fundamental Basis of Hydraulic Engineering*. McGraw-Hill Book Company.

De Michele, C., and G1 Salvadori. 2003. “A Generalized Pareto Intensity-Duration Model of Storm Rainfall Exploiting 2-Copulas.” *Journal of Geophysical Research: Atmospheres (1984--2012)* 108(D2).

Moradkhani, Hamid, Kuo-Lin Hsu, Hoshin Gupta, and Soroosh Sorooshian. 2005. “Uncertainty Assessment of Hydrologic Model States and Parameters: Sequential Data Assimilation Using the Particle Filter.” *Water Resources Research* 41(5). Retrieved (http://dx.doi.org/10.1029/2004WR003604).

Nelsen, Roger B. 1999. *An Introduction to Copulas*. Springer.

Salvadori, G., and C. De Michele. 2007. “On the Use of Copulas in Hydrology: Theory and Practice.” *Journal of Hydrologic Engineering* Volume 12(August):369–80. Retrieved February 19, 2014 (http://ascelibrary.org/doi/abs/10.1061/(ASCE)1084-0699(2007)12:4(369)).

Sang, Yan-Fang, Zhonggen Wang, and Changming Liu. 2012. “Period Identification in Hydrologic Time Series Using Empirical Mode Decomposition and Maximum Entropy Spectral Analysis.” *Journal of Hydrology* 424-425:154–64.

Shannon, C. E. 1948. “A Mathematical Theory of Communication.” *Bell System Technical Journal* 27:379–423. Retrieved (http://dl.acm.org/citation.cfm?id=584093).

Sharifdoost, M., S. Mahmoodi, and E. Pasha. 2009. “A Statistical Test for Time Reversibility of Stationary Finite State Markov Chains.” *Applied Mathematical Sciences* 52:2563–74.

Singh, VP. 1997. “The Use of Entropy in Hydrology and Water Resources.” *Hydrological processes* 11:587–626. Retrieved (http://cleveland2.ce.ttu.edu/documents/copyright/S-AUTHORS/HYDPROC_1997_V11/hydproc_1997_v11.pdf).

Sklar, A. 1959. *Fonctions de Répartition À N Dimensions et Leurs Marges*. Publications de l’Institut de Statistique de L’Université de Paris 8. Retrieved (http://books.google.de/books?id=nreSmAEACAAJ).

Von Storch, Hans, Eduardo Zorita, and Ulrich Cubasch. 1993. “Downscaling of Global Climate Change Estimates to Regional Scales: An Application to Iberian Rainfall in Wintertime.” *Journal of Climate* 6(6):1161–71.

Ullrich, Daniel. 2005. “Rhein-Karte.png.” *CC-BY-SA*. Retrieved (http://en.wikipedia.org/wiki/File:Rhein-Karte.png).

Wu, Zhaohua et al. 2008. "The Modulated Annual Cycle: An Alternative Reference Frame for Climate Anomalies." *Climate dynamics* 31(7-8):823–41.

Institut für Wasser- und Umweltsystemmodellierung
Universität Stuttgart

Pfaffenwaldring 61
70569 Stuttgart (Vaihingen)
Telefon (0711) 685 - 64717/64749/64752/64679
Telefax (0711) 685 - 67020 o. 64746 o. 64681
E-Mail: iws@iws.uni-stuttgart.de
http://www.iws.uni-stuttgart.de

Verzeichnis der Mitteilungshefte

1 Röhnisch, Arthur: *Die Bemühungen um eine Wasserbauliche Versuchsanstalt an der Technischen Hochschule Stuttgart*, und
Fattah Abouleid, Abdel: *Beitrag zur Berechnung einer in lockeren Sand gerammten, zweifach verankerten Spundwand*, 1963

2 Marotz, Günter: *Beitrag zur Frage der Standfestigkeit von dichten Asphaltbelägen im Großwasserbau*, 1964

3 Gurr, Siegfried: *Beitrag zur Berechnung zusammengesetzter ebener Flächentragwerke unter besonderer Berücksichtigung ebener Stauwände, mit Hilfe von Randwert- und Lastwertmatrizen*, 1965

4 Plica, Peter: *Ein Beitrag zur Anwendung von Schalenkonstruktionen im Stahlwasserbau*, und Petrikat, Kurt: *Möglichkeiten und Grenzen des wasserbaulichen Versuchswesens*, 1966

5 Plate, Erich: *Beitrag zur Bestimmung der Windgeschwindigkeitsverteilung in der durch eine Wand gestörten bodennahen Luftschicht*,
und
Röhnisch, Arthur; Marotz, Günter: *Neue Baustoffe und Bauausführungen für den Schutz der Böschungen und der Sohle von Kanälen, Flüssen und Häfen; Gestehungskosten und jeweilige Vorteile*, sowie Unny, T.E.: *Schwingungsuntersuchungen am Kegelstrahlschieber*, 1967

6 Seiler, Erich: *Die Ermittlung des Anlagenwertes der bundeseigenen Binnenschiffahrtsstraßen und Talsperren und des Anteils der Binnenschiffahrt an diesem Wert*, 1967

7 *Sonderheft anläßlich des 65. Geburtstages von Prof. Arthur Röhnisch mit Beiträgen von* Benk, Dieter; Breitling, J.; Gurr, Siegfried; Haberhauer, Robert; Honekamp, Hermann; Kuz, Klaus Dieter; Marotz, Günter; Mayer-Vorfelder, Hans-Jörg; Miller, Rudolf; Plate, Erich J.; Radomski, Helge; Schwarz, Helmut; Vollmer, Ernst; Wildenhahn, Eberhard; 1967

8 Jumikis, Alfred: *Beitrag zur experimentellen Untersuchung des Wassernachschubs in einem gefrierenden Boden und die Beurteilung der Ergebnisse*, 1968

9 Marotz, Günter: *Technische Grundlagen einer Wasserspeicherung im natürlichen Untergrund*, 1968

10 Radomski, Helge: *Untersuchungen über den Einfluß der Querschnittsform wellenförmiger Spundwände auf die statischen und rammtechnischen Eigenschaften*, 1968

11 Schwarz, Helmut: *Die Grenztragfähigkeit des Baugrundes bei Einwirkung vertikal gezogener Ankerplatten als zweidimensionales Bruchproblem*, 1969

12 Erbel, Klaus: *Ein Beitrag zur Untersuchung der Metamorphose von Mittelgebirgsschneedecken unter besonderer Berücksichtigung eines Verfahrens zur Bestimmung der thermischen Schneequalität*, 1969

13 Westhaus, Karl-Heinz: *Der Strukturwandel in der Binnenschiffahrt und sein Einfluß auf den Ausbau der Binnenschiffskanäle*, 1969

14 Mayer-Vorfelder, Hans-Jörg: *Ein Beitrag zur Berechnung des Erdwiderstandes unter Ansatz der logarithmischen Spirale als Gleitflächenfunktion*, 1970

15 Schulz, Manfred: *Berechnung des räumlichen Erddruckes auf die Wandung kreiszylindrischer Körper*, 1970

16 Mobasseri, Manoutschehr: *Die Rippenstützmauer. Konstruktion und Grenzen ihrer Standsicherheit*, 1970

17 Benk, Dieter: *Ein Beitrag zum Betrieb und zur Bemessung von Hochwasserrückhaltebecken*, 1970

18 Gàl, Attila: *Bestimmung der mitschwingenden Wassermasse bei überströmten Fischbauchklappen mit kreiszylindrischem Staublech*, 1971, vergriffen

19 Kuz, Klaus Dieter: *Ein Beitrag zur Frage des Einsetzens von Kavitationserscheinungen in einer Düsenströmung bei Berücksichtigung der im Wasser gelösten Gase*, 1971, vergriffen

20 Schaak, Hartmut: *Verteilleitungen von Wasserkraftanlagen*, 1971

21 *Sonderheft zur Eröffnung der neuen Versuchsanstalt des Instituts für Wasserbau der Universität Stuttgart mit Beiträgen von* Brombach, Hansjörg; Dirksen, Wolfram; Gàl, Attila; Gerlach, Reinhard; Giesecke, Jürgen; Holthoff, Franz-Josef; Kuz, Klaus Dieter; Marotz, Günter; Minor, Hans-Erwin; Petrikat, Kurt; Röhnisch, Arthur; Rueff, Helge; Schwarz, Helmut; Vollmer, Ernst; Wildenhahn, Eberhard; 1972

22 Wang, Chung-su: *Ein Beitrag zur Berechnung der Schwingungen an Kegelstrahlschiebern*, 1972

23 Mayer-Vorfelder, Hans-Jörg: *Erdwiderstandsbeiwerte nach dem Ohde-Variationsverfahren*, 1972

24 Minor, Hans-Erwin: *Beitrag zur Bestimmung der Schwingungsanfachungsfunktionen überströmter Stauklappen*, 1972, vergriffen

25 Brombach, Hansjörg: *Untersuchung strömungsmechanischer Elemente (Fluidik) und die Möglichkeit der Anwendung von Wirbelkammerelementen im Wasserbau*, 1972, vergriffen

26 Wildenhahn, Eberhard: *Beitrag zur Berechnung von Horizontalfilterbrunnen*, 1972

27 Steinlein, Helmut: *Die Eliminierung der Schwebstoffe aus Flußwasser zum Zweck der unterirdischen Wasserspeicherung, gezeigt am Beispiel der Iller*, 1972

28 Holthoff, Franz Josef: *Die Überwindung großer Hubhöhen in der Binnenschiffahrt durch Schwimmerhebewerke*, 1973

29 Röder, Karl: *Einwirkungen aus Baugrundbewegungen auf trog- und kastenförmige Konstruktionen des Wasser- und Tunnelbaues*, 1973

30 Kretschmer, Heinz: *Die Bemessung von Bogenstaumauern in Abhängigkeit von der Talform*, 1973

31 Honekamp, Hermann: *Beitrag zur Berechnung der Montage von Unterwasserpipelines*, 1973

32 Giesecke, Jürgen: *Die Wirbelkammertriode als neuartiges Steuerorgan im Wasserbau*, und Brombach, Hansjörg: *Entwicklung, Bauformen, Wirkungsweise und Steuereigenschaften von Wirbelkammerverstärkern*, 1974

33 Rueff, Helge: *Untersuchung der schwingungserregenden Kräfte an zwei hintereinander angeordneten Tiefschützen unter besonderer Berücksichtigung von Kavitation*, 1974

34 Röhnisch, Arthur: *Einpreßversuche mit Zementmörtel für Spannbeton - Vergleich der Ergebnisse von Modellversuchen mit Ausführungen in Hüllwellrohren*, 1975

35 *Sonderheft anläßlich des 65. Geburtstages von Prof. Dr.-Ing. Kurt Petrikat mit Beiträgen von*: Brombach, Hansjörg; Erbel, Klaus; Flinspach, Dieter; Fischer jr., Richard; Gàl, Attila; Gerlach, Reinhard; Giesecke, Jürgen; Haberhauer, Robert; Hafner Edzard; Hausenblas, Bernhard; Horlacher, Hans-Burkhard; Hutarew, Andreas; Knoll, Manfred; Krummet, Ralph; Marotz, Günter; Merkle, Theodor; Miller, Christoph; Minor, Hans-Erwin; Neumayer, Hans; Rao, Syamala; Rath, Paul; Rueff, Helge; Ruppert, Jürgen; Schwarz, Wolfgang; Topal-Gökceli, Mehmet; Vollmer, Ernst; Wang, Chung-su; Weber, Hans-Georg; 1975

36 Berger, Jochum: *Beitrag zur Berechnung des Spannungszustandes in rotationssymmetrisch belasteten Kugelschalen veränderlicher Wandstärke unter Gas- und Flüssigkeitsdruck durch Integration schwach singulärer Differentialgleichungen*, 1975

37 Dirksen, Wolfram: *Berechnung instationärer Abflußvorgänge in gestauten Gerinnen mittels Differenzenverfahren und die Anwendung auf Hochwasserrückhaltebecken*, 1976

38 Horlacher, Hans-Burkhard: *Berechnung instationärer Temperatur- und Wärmespannungsfelder in langen mehrschichtigen Hohlzylindern*, 1976

39 Hafner, Edzard: *Untersuchung der hydrodynamischen Kräfte auf Baukörper im Tiefwasserbereich des Meeres*, 1977, ISBN 3-921694-39-6

40 Ruppert, Jürgen: *Über den Axialwirbelkammerverstärker für den Einsatz im Wasserbau*, 1977, ISBN 3-921694-40-X

41 Hutarew, Andreas: *Beitrag zur Beeinflußbarkeit des Sauerstoffgehalts in Fließgewässern an Abstürzen und Wehren*, 1977, ISBN 3-921694-41-8, vergriffen

42 Miller, Christoph: *Ein Beitrag zur Bestimmung der schwingungserregenden Kräfte an unterströmten Wehren*, 1977, ISBN 3-921694-42-6

43 Schwarz, Wolfgang: *Druckstoßberechnung unter Berücksichtigung der Radial- und Längsverschiebungen der Rohrwandung*, 1978, ISBN 3-921694-43-4

44 Kinzelbach, Wolfgang: *Numerische Untersuchungen über den optimalen Einsatz variabler Kühlsysteme einer Kraftwerkskette am Beispiel Oberrhein*, 1978, ISBN 3-921694-44-2

45 Barczewski, Baldur: *Neue Meßmethoden für Wasser-Luftgemische und deren Anwendung auf zweiphasige Auftriebsstrahlen*, 1979, ISBN 3-921694-45-0

46 Neumayer, Hans: *Untersuchung der Strömungsvorgänge in radialen Wirbelkammerverstärkern*, 1979, ISBN 3-921694-46-9

47 Elalfy, Youssef-Elhassan: *Untersuchung der Strömungsvorgänge in Wirbelkammerdioden und -drosseln*, 1979, ISBN 3-921694-47-7

48 Brombach, Hansjörg: *Automatisierung der Bewirtschaftung von Wasserspeichern*, 1981, ISBN 3-921694-48-5

49 Geldner, Peter: *Deterministische und stochastische Methoden zur Bestimmung der Selbstdichtung von Gewässern*, 1981, ISBN 3-921694-49-3, vergriffen

50 Mehlhorn, Hans: *Temperaturveränderungen im Grundwasser durch Brauchwassereinleitungen*, 1982, ISBN 3-921694-50-7, vergriffen

51 Hafner, Edzard: *Rohrleitungen und Behälter im Meer*, 1983, ISBN 3-921694-51-5

52 Rinnert, Bernd: *Hydrodynamische Dispersion in porösen Medien: Einfluß von Dichteunterschieden auf die Vertikalvermischung in horizontaler Strömung*, 1983, ISBN 3-921694-52-3, vergriffen

53 Lindner, Wulf: *Steuerung von Grundwasserentnahmen unter Einhaltung ökologischer Kriterien*, 1983, ISBN 3-921694-53-1, vergriffen

54 Herr, Michael; Herzer, Jörg; Kinzelbach, Wolfgang; Kobus, Helmut; Rinnert, Bernd: *Methoden zur rechnerischen Erfassung und hydraulischen Sanierung von Grundwasserkontaminationen*, 1983, ISBN 3-921694-54-X

55 Schmitt, Paul: *Wege zur Automatisierung der Niederschlagsermittlung*, 1984, ISBN 3-921694-55-8, vergriffen

56 Müller, Peter: *Transport und selektive Sedimentation von Schwebstoffen bei gestautem Abfluß*, 1985, ISBN 3-921694-56-6

57 El-Qawasmeh, Fuad: *Möglichkeiten und Grenzen der Tropfbewässerung unter besonderer Berücksichtigung der Verstopfungsanfälligkeit der Tropfelemente*, 1985, ISBN 3-921694-57-4, vergriffen

58 Kirchenbaur, Klaus: *Mikroprozessorgesteuerte Erfassung instationärer Druckfelder am Beispiel seegangsbelasteter Baukörper*, 1985, ISBN 3-921694-58-2

59 Kobus, Helmut (Hrsg.): *Modellierung des großräumigen Wärme- und Schadstofftransports im Grundwasser*, Tätigkeitsbericht 1984/85 (DFG-Forschergruppe an den Universitäten Hohenheim, Karlsruhe und Stuttgart), 1985, ISBN 3-921694-59-0, vergriffen

60 Spitz, Karlheinz: *Dispersion in porösen Medien: Einfluß von Inhomogenitäten und Dichteunterschieden*, 1985, ISBN 3-921694-60-4, vergriffen

61 Kobus, Helmut: *An Introduction to Air-Water Flows in Hydraulics*, 1985, ISBN 3-921694-61-2

62 Kaleris, Vassilios: *Erfassung des Austausches von Oberflächen- und Grundwasser in horizontalebenen Grundwassermodellen*, 1986, ISBN 3-921694-62-0

63 Herr, Michael: *Grundlagen der hydraulischen Sanierung verunreinigter Porengrundwasserleiter*, 1987, ISBN 3-921694-63-9

64 Marx, Walter: *Berechnung von Temperatur und Spannung in Massenbeton infolge Hydratation*, 1987, ISBN 3-921694-64-7

65 Koschitzky, Hans-Peter: *Dimensionierungskonzept für Sohlbelüfter in Schußrinnen zur Vermeidung von Kavitationsschäden*, 1987, ISBN 3-921694-65-5

66 Kobus, Helmut (Hrsg.): *Modellierung des großräumigen Wärme- und Schadstofftransports im Grundwasser*, Tätigkeitsbericht 1986/87 (DFG-Forschergruppe an den Universitäten Hohenheim, Karlsruhe und Stuttgart) 1987, ISBN 3-921694-66-3

67 Söll, Thomas: *Berechnungsverfahren zur Abschätzung anthropogener Temperaturanomalien im Grundwasser*, 1988, ISBN 3-921694-67-1

68 Dittrich, Andreas; Westrich, Bernd: *Bodenseeufererosion, Bestandsaufnahme und Bewertung*, 1988, ISBN 3-921694-68-X, vergriffen

69 Huwe, Bernd; van der Ploeg, Rienk R.: *Modelle zur Simulation des Stickstoffhaushaltes von Standorten mit unterschiedlicher landwirtschaftlicher Nutzung*, 1988, ISBN 3-921694-69-8, vergriffen

70 Stephan, Karl: *Integration elliptischer Funktionen*, 1988, ISBN 3-921694-70-1

71 Kobus, Helmut; Zilliox, Lothaire (Hrsg.): *Nitratbelastung des Grundwassers, Auswirkungen der Landwirtschaft auf die Grundwasser- und Rohwasserbeschaffenheit und Maßnahmen zum Schutz des Grundwassers*. Vorträge des deutsch-französischen Kolloquiums am 6. Oktober 1988, Universitäten Stuttgart und Louis Pasteur Strasbourg (Vorträge in deutsch oder französisch, Kurzfassungen zweisprachig), 1988, ISBN 3-921694-71-X

72 Soyeaux, Renald: *Unterströmung von Stauanlagen auf klüftigem Untergrund unter Berücksichtigung laminarer und turbulenter Fließzustände*,1991, ISBN 3-921694-72-8

73 Kohane, Roberto: *Berechnungsmethoden für Hochwasserabfluß in Fließgewässern mit überströmten Vorländern*, 1991, ISBN 3-921694-73-6

74 Hassinger, Reinhard: *Beitrag zur Hydraulik und Bemessung von Blocksteinrampen in flexibler Bauweise*, 1991, ISBN 3-921694-74-4, vergriffen

75 Schäfer, Gerhard: *Einfluß von Schichtenstrukturen und lokalen Einlagerungen auf die Längsdispersion in Porengrundwasserleitern*, 1991, ISBN 3-921694-75-2

76 Giesecke, Jürgen: *Vorträge, Wasserwirtschaft in stark besiedelten Regionen; Umweltforschung mit Schwerpunkt Wasserwirtschaft*, 1991, ISBN 3-921694-76-0

77 Huwe, Bernd: *Deterministische und stochastische Ansätze zur Modellierung des Stickstoffhaushalts landwirtschaftlich genutzter Flächen auf unterschiedlichem Skalenniveau*, 1992, ISBN 3-921694-77-9, vergriffen

78 Rommel, Michael: *Verwendung von Kluftdaten zur realitätsnahen Generierung von Kluftnetzen mit anschließender laminar-turbulenter Strömungsberechnung*, 1993, ISBN 3-92 1694-78-7

79 Marschall, Paul: *Die Ermittlung lokaler Stofffrachten im Grundwasser mit Hilfe von Einbohrloch-Meßverfahren*, 1993, ISBN 3-921694-79-5, vergriffen

80 Ptak, Thomas: *Stofftransport in heterogenen Porenaquiferen: Felduntersuchungen und stochastische Modellierung*, 1993, ISBN 3-921694-80-9, vergriffen

81 Haakh, Frieder: *Transientes Strömungsverhalten in Wirbelkammern,* 1993, ISBN 3-921694-81-7

82 Kobus, Helmut; Cirpka, Olaf; Barczewski, Baldur; Koschitzky, Hans-Peter: *Versucheinrichtung zur Grundwasser und Altlastensanierung VEGAS, Konzeption und Programmrahmen*, 1993, ISBN 3-921694-82-5

83 Zang, Weidong: *Optimaler Echtzeit-Betrieb eines Speichers mit aktueller Abflußregenerierung*, 1994, ISBN 3-921694-83-3, vergriffen

84 Franke, Hans-Jörg: *Stochastische Modellierung eines flächenhaften Stoffeintrages und Transports in Grundwasser am Beispiel der Pflanzenschutzmittelproblematik*, 1995, ISBN 3-921694-84-1

85 Lang, Ulrich: *Simulation regionaler Strömungs- und Transportvorgänge in Karstaquiferen mit Hilfe des Doppelkontinuum-Ansatzes: Methodenentwicklung und Parameteridentifikation*, 1995, ISBN 3-921694-85-X, vergriffen

86 Helmig, Rainer: *Einführung in die Numerischen Methoden der Hydromechanik*, 1996, ISBN 3-921694-86-8, vergriffen

87 Cirpka, Olaf: *CONTRACT: A Numerical Tool for Contaminant Transport and Chemical Transformations - Theory and Program Documentation* -, 1996, ISBN 3-921694-87-6

88 Haberlandt, Uwe: *Stochastische Synthese und Regionalisierung des Niederschlages für Schmutzfrachtberechnungen*, 1996, ISBN 3-921694-88-4

89 Croisé, Jean: *Extraktion von flüchtigen Chemikalien aus natürlichen Lockergesteinen mittels erzwungener Luftströmung*, 1996, ISBN 3-921694-89-2, vergriffen

90 Jorde, Klaus: *Ökologisch begründete, dynamische Mindestwasserregelungen bei Ausleitungskraftwerken*, 1997, ISBN 3-921694-90-6, vergriffen

91 Helmig, Rainer: *Gekoppelte Strömungs- und Transportprozesse im Untergrund - Ein Beitrag zur Hydrosystemmodellierung*-, 1998, ISBN 3-921694-91-4, vergriffen

92 Emmert, Martin: *Numerische Modellierung nichtisothermer Gas-Wasser Systeme in porösen Medien,* 1997, ISBN 3-921694-92-2

93 Kern, Ulrich: *Transport von Schweb- und Schadstoffen in staugeregelten Fließgewässern am Beispiel des Neckars*, 1997, ISBN 3-921694-93-0, vergriffen

94 Förster, Georg: *Druckstoßdämpfung durch große Luftblasen in Hochpunkten von Rohrleitungen 1997*, ISBN 3-921694-94-9

95 Cirpka, Olaf: *Numerische Methoden zur Simulation des reaktiven Mehrkomponententransports im Grundwasser*, 1997, ISBN 3-921694-95-7, vergriffen

96 Färber, Arne: *Wärmetransport in der ungesättigten Bodenzone: Entwicklung einer thermischen In-situ-Sanierungstechnologie*, 1997, ISBN 3-921694-96-5

97 Betz, Christoph: *Wasserdampfdestillation von Schadstoffen im porösen Medium: Entwicklung einer thermischen In-situ-Sanierungstechnologie*, 1998, ISBN 3-921694-97-3

98 Xu, Yichun: *Numerical Modeling of Suspended Sediment Transport in Rivers*, 1998, ISBN 3-921694-98-1, vergriffen

99 Wüst, Wolfgang: *Geochemische Untersuchungen zur Sanierung CKW-kontaminierter Aquifere mit Fe(0)-Reaktionswänden,* 2000, ISBN 3-933761-02-2

100 Sheta, Hussam: *Simulation von Mehrphasenvorgängen in porösen Medien unter Einbeziehung von Hysterese-Effekten*, 2000, ISBN 3-933761-03-4

101 Ayros, Edwin: *Regionalisierung extremer Abflüsse auf der Grundlage statistischer Verfahren*, 2000, ISBN 3-933761-04-2, vergriffen

102 Huber, Ralf: *Compositional Multiphase Flow and Transport in Heterogeneous Porous Media*, 2000, ISBN 3-933761-05-0

103 Braun, Christopherus: *Ein Upscaling-Verfahren für Mehrphasenströmungen in porösen Medien*, 2000, ISBN 3-933761-06-9

104 Hofmann, Bernd: *Entwicklung eines rechnergestützten Managementsystems zur Beurteilung von Grundwasserschadensfällen*, 2000, ISBN 3-933761-07-7

105 Class, Holger: *Theorie und numerische Modellierung nichtisothermer Mehrphasenprozesse in NAPL-kontaminierten porösen Medien,* 2001, ISBN 3-933761-08-5

106 Schmidt, Reinhard: *Wasserdampf- und Heißluftinjektion zur thermischen Sanierung kontaminierter Standorte*, 2001, ISBN 3-933761-09-3

107 Josef, Reinhold:, *Schadstoffextraktion mit hydraulischen Sanierungsverfahren unter Anwendung von grenzflächenaktiven Stoffen*, 2001, ISBN 3-933761-10-7

108 Schneider, Matthias: *Habitat- und Abflussmodellierung für Fließgewässer mit unscharfen Berechnungsansätzen*, 2001, ISBN 3-933761-11-5

109 Rathgeb, Andreas: *Hydrodynamische Bemessungsgrundlagen für Lockerdeckwerke an überströmbaren Erddämmen*, 2001, ISBN 3-933761-12-3

110 Lang, Stefan: *Parallele numerische Simulation instätionärer Probleme mit adaptiven Methoden auf unstrukturierten Gittern*, 2001, ISBN 3-933761-13-1

111 Appt, Jochen; Stumpp Simone: *Die Bodensee-Messkampagne 2001, IWS/CWR Lake Constance Measurement Program 2001*, 2002, ISBN 3-933761-14-X

112 Heimerl, Stephan: *Systematische Beurteilung von Wasserkraftprojekten,* 2002, ISBN 3-933761-15-8, vergriffen

113 Iqbal, Amin: *On the Management and Salinity Control of Drip Irrigation,* 2002, ISBN 3-933761-16-6

114 Silberhorn-Hemminger, Annette: *Modellierung von Kluftaquifersystemen: Geostatistische Analyse und deterministisch-stochastische Kluftgenerierung,* 2002, ISBN 3-933761-17-4

115 Winkler, Angela: *Prozesse des Wärme- und Stofftransports bei der In-situ-Sanierung mit festen Wärmequellen,* 2003, ISBN 3-933761-18-2

116 Marx, Walter: *Wasserkraft, Bewässerung, Umwelt - Planungs- und Bewertungsschwerpunkte der Wasserbewirtschaftung,* 2003, ISBN 3-933761-19-0

117 Hinkelmann, Reinhard: *Efficient Numerical Methods and Information-Processing Techniques in Environment Water,* 2003, ISBN 3-933761-20-4

118 Samaniego-Eguiguren, Luis Eduardo: *Hydrological Consequences of Land Use / Land Cover and Climatic Changes in Mesoscale Catchments*, 2003, ISBN 3-933761-21-2

119 Neunhäuserer, Lina: *Diskretisierungsansätze zur Modellierung von Strömungs- und Transportprozessen in geklüftet-porösen Medien*, 2003, ISBN 3-933761-22-0

120 Paul, Maren: *Simulation of Two-Phase Flow in Heterogeneous Poros Media with Adaptive Methods*, 2003, ISBN 3-933761-23-9

121 Ehret, Uwe: *Rainfall and Flood Nowcasting in Small Catchments using Weather Radar*, 2003, ISBN 3-933761-24-7

122 Haag, Ingo: *Der Sauerstoffhaushalt staugeregelter Flüsse am Beispiel des Neckars - Analysen, Experimente, Simulationen -,* 2003, ISBN 3-933761-25-5

123 Appt, Jochen: *Analysis of Basin-Scale Internal Waves in Upper Lake Constance,* 2003, ISBN 3-933761-26-3

124 Hrsg.: Schrenk, Volker; Batereau, Katrin; Barczewski, Baldur; Weber, Karolin und Koschitzky, Hans-Peter: *Symposium Ressource Fläche und VEGAS - Statuskolloquium 2003, 30. September und 1. Oktober 2003,* 2003, ISBN 3-933761-27-1

125 Omar Khalil Ouda: *Optimisation of Agricultural Water Use: A Decision Support System for the Gaza Strip,* 2003, ISBN 3-933761-28-0

126 Batereau, Katrin: *Sensorbasierte Bodenluftmessung zur Vor-Ort-Erkundung von Schadensherden im Untergrund*, 2004, ISBN 3-933761-29-8

127 Witt, Oliver: *Erosionsstabilität von Gewässersedimenten mit Auswirkung auf den Stofftransport bei Hochwasser am Beispiel ausgewählter Stauhaltungen des Oberrheins*, 2004, ISBN 3-933761-30-1

128 Jakobs, Hartmut: *Simulation nicht-isothermer Gas-Wasser-Prozesse in komplexen Kluft-Matrix-Systemen*, 2004, ISBN 3-933761-31-X

129 Li, Chen-Chien: *Deterministisch-stochastisches Berechnungskonzept zur Beurteilung der Auswirkungen erosiver Hochwasserereignisse in Flussstauhaltungen,* 2004, ISBN 3-933761-32-8

130 Reichenberger, Volker; Helmig, Rainer; Jakobs, Hartmut; Bastian, Peter; Niessner, Jennifer: *Complex Gas-Water Processes in Discrete Fracture-Matrix Systems: Upscaling, Mass-Conservative Discretization and Efficient Multilevel Solution,* 2004, ISBN 3-933761-33-6

131 Hrsg.: Barczewski, Baldur; Koschitzky, Hans-Peter; Weber, Karolin; Wege, Ralf: *VEGAS - Statuskolloquium 2004,* Tagungsband zur Veranstaltung am 05. Oktober 2004 an der Universität Stuttgart, Campus Stuttgart-Vaihingen, 2004, ISBN 3-933761-34-4

132 Asie, Kemal Jabir: *Finite Volume Models for Multiphase Multicomponent Flow through Porous Media*. 2005, ISBN 3-933761-35-2

133 Jacoub, George: *Development of a 2-D Numerical Module for Particulate Contaminant Transport in Flood Retention Reservoirs and Impounded Rivers,* 2004, ISBN 3-933761-36-0

134 Nowak, Wolfgang: *Geostatistical Methods for the Identification of Flow and Transport Parameters in the Subsurface,* 2005, ISBN 3-933761-37-9

135 Süß, Mia: *Analysis of the influence of structures and boundaries on flow and transport processes in fractured porous media*, 2005, ISBN 3-933761-38-7

136 Jose, Surabhin Chackiath: *Experimental Investigations on Longitudinal Dispersive Mixing in Heterogeneous Aquifers,* 2005, ISBN: 3-933761-39-5

137 Filiz, Fulya: *Linking Large-Scale Meteorological Conditions to Floods in Mesoscale Catchments,* 2005, ISBN 3-933761-40-9

138 Qin, Minghao: *Wirklichkeitsnahe und recheneffiziente Ermittlung von Temperatur und Spannungen bei großen RCC-Staumauern*, 2005, ISBN 3-933761-41-7

139 Kobayashi, Kenichiro: *Optimization Methods for Multiphase Systems in the Subsurface - Application to Methane Migration in Coal Mining Areas*, 2005, ISBN 3-933761-42-5

140 Rahman, Md. Arifur: *Experimental Investigations on Transverse Dispersive Mixing in Heterogeneous Porous Media,* 2005, ISBN 3-933761-43-3

141 Schrenk, Volker: *Ökobilanzen zur Bewertung von Altlastensanierungsmaßnahmen,* 2005, ISBN 3-933761-44-1

142 Hundecha, Hirpa Yeshewatesfa: *Regionalization of Parameters of a Conceptual Rainfall-Runoff Model*, 2005, ISBN: 3-933761-45-X

143 Wege, Ralf: *Untersuchungs- und Überwachungsmethoden für die Beurteilung natürlicher Selbstreinigungsprozesse im Grundwasser,* 2005, ISBN 3-933761-46-8

144 Breiting, Thomas: *Techniken und Methoden der Hydroinformatik - Modellierung von komplexen Hydrosystemen im Untergrund*, 2006, 3-933761-47-6

145 Hrsg.: Braun, Jürgen; Koschitzky, Hans-Peter; Müller, Martin: *Ressource Untergrund: 10 Jahre VEGAS: Forschung und Technologieentwicklung zum Schutz von Grundwasser und Boden,* Tagungsband zur Veranstaltung am 28. und 29. September 2005 an der Universität Stuttgart, Campus Stuttgart-Vaihingen, 2005, ISBN 3-933761-48-4

146 Rojanschi, Vlad: *Abflusskonzentration in mesoskaligen Einzugsgebieten unter Berücksichtigung des Sickerraumes,* 2006, ISBN 3-933761-49-2

147 Winkler, Nina Simone: *Optimierung der Steuerung von Hochwasserrückhaltebecken-systemen,* 2006, ISBN 3-933761-50-6

148 Wolf, Jens: *Räumlich differenzierte Modellierung der Grundwasserströmung alluvialer Aquifere für mesoskalige Einzugsgebiete*, 2006, ISBN: 3-933761-51-4

149 Kohler, Beate: *Externe Effekte der Laufwasserkraftnutzung*, 2006, ISBN 3-933761-52-2

150 Hrsg.: Braun, Jürgen; Koschitzky, Hans-Peter; Stuhrmann, Matthias: *VEGAS-Statuskolloquium 2006,* Tagungsband zur Veranstaltung am 28. September 2006 an der Universität Stuttgart, Campus Stuttgart-Vaihingen, 2006, ISBN 3-933761-53-0

151 Niessner, Jennifer: *Multi-Scale Modeling of Multi-Phase - Multi-Component Processes in Heterogeneous Porous Media*, 2006, ISBN 3-933761-54-9

152 Fischer, Markus: *Beanspruchung eingeerdeter Rohrleitungen infolge Austrocknung bindiger Böden,* 2006, ISBN 3-933761-55-7

153 Schneck, Alexander: *Optimierung der Grundwasserbewirtschaftung unter Berücksichtigung der Belange der Wasserversorgung, der Landwirtschaft und des Naturschutzes*, 2006, ISBN 3-933761-56-5

154 Das, Tapash: *The Impact of Spatial Variability of Precipitation on the Predictive Uncertainty of Hydrological Models,* 2006, ISBN 3-933761-57-3

155 Bielinski, Andreas: *Numerical Simulation of CO_2 sequestration in geological formations*, 2007, ISBN 3-933761-58-1

156 Mödinger, Jens: *Entwicklung eines Bewertungs- und Entscheidungsunterstützungssystems für eine nachhaltige regionale Grundwasserbewirtschaftung*, 2006, ISBN 3-933761-60-3

157 Manthey, Sabine: *Two-phase flow processes with dynamic effects in porous media - parameter estimation and simulation,* 2007, ISBN 3-933761-61-1

158 Pozos Estrada, Oscar: *Investigation on the Effects of Entrained Air in Pipelines,* 2007, ISBN 3-933761-62-X

159 Ochs, Steffen Oliver: *Steam injection into saturated porous media – process analysis including experimental and numerical investigations*, 2007, ISBN 3-933761-63-8

160 Marx, Andreas: *Einsatz gekoppelter Modelle und Wetterradar zur Abschätzung von Niederschlagsintensitäten und zur Abflussvorhersage, 2007,* ISBN 3-933761-64-6

161 Hartmann, Gabriele Maria: *Investigation of Evapotranspiration Concepts in Hydrological Modelling for Climate Change Impact Assessment*, 2007, ISBN 3-933761-65-4

162 Kebede Gurmessa, Tesfaye: *Numerical Investigation on Flow and Transport Characteristics to Improve Long-Term Simulation of Reservoir Sedimentation*, 2007, ISBN 3-933761-66-2

163 Trifković, Aleksandar: *Multi-objective and Risk-based Modelling Methodology for Planning, Design and Operation of Water Supply Systems*, 2007, ISBN 3-933761-67-0

164 Götzinger, Jens: *Distributed Conceptual Hydrological Modelling - Simulation of Climate, Land Use Change Impact and Uncertainty Analysis*, 2007, ISBN 3-933761-68-9

165 Hrsg.: Braun, Jürgen; Koschitzky, Hans-Peter; Stuhrmann, Matthias: *VEGAS – Kolloquium 2007,* Tagungsband zur Veranstaltung am 26. September 2007 an der Universität Stuttgart, Campus Stuttgart-Vaihingen, 2007, ISBN 3-933761-69-7

166 Freeman, Beau: *Modernization Criteria Assessment for Water Resources Planning; Klamath Irrigation Project, U.S.*, 2008, ISBN 3-933761-70-0

167 Dreher, Thomas: *Selektive Sedimentation von Feinstschwebstoffen in Wechselwirkung mit wandnahen turbulenten Strömungsbedingungen*, 2008, ISBN 3-933761-71-9

168 Yang, Wei: *Discrete-Continuous Downscaling Model for Generating Daily Precipitation Time Series*, 2008, ISBN 3-933761-72-7

169 Kopecki, Ianina: *Calculational Approach to FST-Hemispheres for Multiparametrical Benthos Habitat Modelling,* 2008*,* ISBN 3-933761-73-5

170 Brommundt, Jürgen: *Stochastische Generierung räumlich zusammenhängender Niederschlagszeitreihen*, 2008, ISBN 3-933761-74-3

171 Papafotiou, *Alexandros: Numerical Investigations of the Role of Hysteresis in Heterogeneous Two-Phase Flow Systems*, 2008, ISBN 3-933761-75-1

172 He, Yi: *Application of a Non-Parametric Classification Scheme to Catchment Hydrology*, 2008, ISBN 978-3-933761-76-7

173 Wagner, Sven: *Water Balance in a Poorly Gauged Basin in West Africa Using Atmospheric Modelling and Remote Sensing Information*, 2008, ISBN 978-3-933761-77-4

174 Hrsg.: Braun, Jürgen; Koschitzky, Hans-Peter; Stuhrmann, Matthias; Schrenk, Volker: *VEGAS-Kolloquium 2008 Ressource Fläche III*, Tagungsband zur Veranstaltung am 01. Oktober 2008 an der Universität Stuttgart, Campus Stuttgart-Vaihingen, 2008, ISBN 978-3-933761-78-1

175 Patil, Sachin: *Regionalization of an Event Based Nash Cascade Model for Flood Predictions in Ungauged Basins*, 2008, ISBN 978-3-933761-79-8

176 Assteerawatt, Anongnart: *Flow and Transport Modelling of Fractured Aquifers based on a Geostatistical Approach,* 2008, ISBN 978-3-933761-80-4

177 Karnahl, Joachim Alexander: *2D numerische Modellierung von multifraktionalem Schwebstoff- und Schadstofftransport in Flüssen*, 2008, ISBN 978-3-933761-81-1

178 Hiester, Uwe: *Technologieentwicklung zur In-situ-Sanierung der ungesättigten Bodenzone mit festen Wärmequellen,* 2009, ISBN 978-3-933761-82-8

179 Laux, Patrick: *Statistical Modeling of Precipitation for Agricultural Planning in the Volta Basin of West Africa,* 2009, ISBN 978-3-933761-83-5

180 Ehsan, Saqib: *Evaluation of Life Safety Risks Related to Severe Flooding,* 2009, ISBN 978-3-933761-84-2

181 Prohaska, Sandra: *Development and Application of a 1D Multi-Strip Fine Sediment Transport Model for Regulated Rivers,* 2009, ISBN 978-3-933761-85-9

182 Kopp, Andreas: *Evaluation of CO_2 Injection Processes in Geological Formations for Site Screening,* 2009, ISBN 978-3-933761-86-6

183 Ebigbo, Anozie: *Modelling of biofilm growth and its influence on CO_2 and water (two-phase) flow in porous media,* 2009, ISBN 978-3-933761-87-3

184 Freiboth, Sandra: *A phenomenological model for the numerical simulation of multiphase multicomponent processes considering structural alterations of porous media*, 2009, ISBN 978-3-933761-88-0

185 Zöllner, Frank: *Implementierung und Anwendung netzfreier Methoden im Konstruktiven Wasserbau und in der Hydromechanik*, 2009, ISBN 978-3-933761-89-7

186 Vasin, Milos: *Influence of the soil structure and property contrast on flow and transport in the unsaturated zone*, 2010, ISBN 978-3-933761-90-3

187 Li, Jing: *Application of Copulas as a New Geostatistical Tool*, 2010, ISBN 978-3-933761-91-0

188 AghaKouchak, Amir: *Simulation of Remotely Sensed Rainfall Fields Using Copulas*, 2010, ISBN 978-3-933761-92-7

189 Thapa, Pawan Kumar: *Physically-based spatially distributed rainfall runoff modelling for soil erosion estimation*, 2010, ISBN 978-3-933761-93-4

190 Wurms, Sven: *Numerische Modellierung der Sedimentationsprozesse in Retentionsanlagen zur Steuerung von Stoffströmen bei extremen Hochwasserabflussereignissen*, 2011, ISBN 978-3-933761-94-1

191 Merkel, Uwe: *Unsicherheitsanalyse hydraulischer Einwirkungen auf Hochwasserschutzdeiche und Steigerung der Leistungsfähigkeit durch adaptive Strömungsmodellierung*, 2011, ISBN 978-3-933761-95-8

192 Fritz, Jochen: *A Decoupled Model for Compositional Non-Isothermal Multiphase Flow in Porous Media and Multiphysics Approaches for Two-Phase Flow*, 2010, ISBN 978-3-933761-96-5

193 Weber, Karolin (Hrsg.): *12. Treffen junger WissenschaftlerInnen an Wasserbauinstituten*, 2010, ISBN 978-3-933761-97-2

194 Bliefernicht, Jan-Geert: *Probability Forecasts of Daily Areal Precipitation for Small River Basins,* 2011, ISBN 978-3-933761-98-9

195 Hrsg.: Koschitzky, Hans-Peter; Braun, Jürgen: *VEGAS-Kolloquium 2010 In-situ-Sanierung - Stand und Entwicklung Nano und ISCO -,* Tagungsband zur Veranstaltung am 07. Oktober 2010 an der Universität Stuttgart, Campus Stuttgart-Vaihingen*,* 2010*,* ISBN 978-3-933761-99-6

196 Gafurov, Abror: *Water Balance Modeling Using Remote Sensing Information - Focus on Central Asia,* 2010, ISBN 978-3-942036-00-9

197 Mackenberg, Sylvia: *Die Quellstärke in der Sickerwasserprognose: Möglichkeiten und Grenzen von Labor- und Freilanduntersuchungen,* 2010, ISBN 978-3-942036-01-6

198 Singh, Shailesh Kumar: *Robust Parameter Estimation in Gauged and Ungauged Basins,* 2010, ISBN 978-3-942036-02-3

199 Doğan, Mehmet Onur: *Coupling of porous media flow with pipe flow,* 2011, ISBN 978-3-942036-03-0

200 Liu, Min: *Study of Topographic Effects on Hydrological Patterns and the Implication on Hydrological Modeling and Data Interpolation,* 2011, ISBN 978-3-942036-04-7

201 Geleta, Habtamu Itefa: *Watershed Sediment Yield Modeling for Data Scarce Areas,* 2011, ISBN 978-3-942036-05-4

202 Franke, Jörg: *Einfluss der Überwachung auf die Versagenswahrscheinlichkeit von Staustufen,* 2011, ISBN 978-3-942036-06-1

203 Bakimchandra, Oinam: *Integrated Fuzzy-GIS approach for assessing regional soil erosion risks,* 2011, ISBN 978-3-942036-07-8

204 Alam, Muhammad Mahboob: *Statistical Downscaling of Extremes of Precipitation in Mesoscale Catchments from Different RCMs and Their Effects on Local Hydrology,* 2011, ISBN 978-3-942036-08-5

205 Hrsg.: Koschitzky, Hans-Peter; Braun, Jürgen: *VEGAS-Kolloquium 2011 Flache Geothermie - Perspektiven und Risiken,* Tagungsband zur Veranstaltung am 06. Oktober 2011 an der Universität Stuttgart, Campus Stuttgart-Vaihingen, 2011, ISBN 978-3-933761-09-2

206 Haslauer, Claus: *Analysis of Real-World Spatial Dependence of Subsurface Hydraulic Properties Using Copulas with a Focus on Solute Transport Behaviour,* 2011, ISBN 978-3-942036-10-8

207 Dung, Nguyen Viet: *Multi-objective automatic calibration of hydrodynamic models – development of the concept and an application in the Mekong Delta,* 2011, ISBN 978-3-942036-11-5

208 Hung, Nguyen Nghia: *Sediment dynamics in the floodplain of the Mekong Delta, Vietnam,* 2011, ISBN 978-3-942036-12-2

209 Kuhlmann, Anna: *Influence of soil structure and root water uptake on flow in the unsaturated zone,* 2012, ISBN 978-3-942036-13-9

210 Tuhtan, Jeffrey Andrew: *Including the Second Law Inequality in Aquatic Ecodynamics: A Modeling Approach for Alpine Rivers Impacted by Hydropeaking,* 2012, ISBN 978-3-942036-14-6

211 Tolossa, Habtamu: *Sediment Transport Computation Using a Data-Driven Adaptive Neuro-Fuzzy Modelling Approach,* 2012, ISBN 978-3-942036-15-3

212 Tatomir, Alexandru-Bodgan: *From Discrete to Continuum Concepts of Flow in Fractured Porous Media,* 2012, ISBN 978-3-942036-16-0

213 Erbertseder, Karin: *A Multi-Scale Model for Describing Cancer-Therapeutic Transport in the Human Lung,* 2012, ISBN 978-3-942036-17-7

214 Noack, Markus: *Modelling Approach for Interstitial Sediment Dynamics and Reproduction of Gravel Spawning Fish,* 2012, ISBN 978-3-942036-18-4

215 De Boer, Cjestmir Volkert: *Transport of Nano Sized Zero Valent Iron Colloids during Injection into the Subsurface*, 2012, ISBN 978-3-942036-19-1

216 Pfaff, Thomas: *Processing and Analysis of Weather Radar Data for Use in Hydrology*, 2013, ISBN 978-3-942036-20-7

217 Lebrenz, Hans-Henning: *Addressing the Input Uncertainty for Hydrological Modeling by a New Geostatistical Method*, 2013, ISBN 978-3-942036-21-4

218 Darcis, Melanie Yvonne: *Coupling Models of Different Complexity for the Simulation of CO_2 Storage in Deep Saline Aquifers*, 2013, ISBN 978-3-942036-22-1

219 Beck, Ferdinand: *Generation of Spatially Correlated Synthetic Rainfall Time Series in High Temporal Resolution - A Data Driven Approach*, 2013, ISBN 978-3-942036-23-8

220 Guthke, Philipp: *Non-multi-Gaussian spatial structures: Process-driven natural genesis, manifestation, modeling approaches, and influences on dependent processes*, 2013, ISBN 978-3-942036-24-5

221 Walter, Lena: *Uncertainty studies and risk assessment for CO_2 storage in geological formations*, 2013, ISBN 978-3-942036-25-2

222 Wolff, Markus: *Multi-scale modeling of two-phase flow in porous media including capillary pressure effects,* 2013, ISBN 978-3-942036-26-9

223 Mosthaf, Klaus Roland: *Modeling and analysis of coupled porous-medium and free flow with application to evaporation processes,* 2014, ISBN 978-3-942036-27-6

224 Leube, Philipp Christoph: *Methods for Physically-Based Model Reduction in Time: Analysis, Comparison of Methods and Application*, 2013, ISBN 978-3-942036-28-3

225 Rodríguez Fernández, Jhan Ignacio: *High Order Interactions among environmental variables: Diagnostics and initial steps towards modeling*, 2013, ISBN 978-3-942036-29-0

226 Eder, Maria Magdalena: *Climate Sensitivity of a Large Lake*, 2013, ISBN 978-3-942036-30-6

227 Greiner, Philipp: *Alkoholinjektion zur In-situ-Sanierung von CKW Schadensherden in Grundwasserleitern: Charakterisierung der relevanten Prozesse auf unterschiedlichen Skalen*, 2014, ISBN 978-3-942036-31-3

228 Lauser, Andreas: *Theory and Numerical Applications of Compositional Multi-Phase Flow in Porous Media*, 2014, ISBN 978-3-942036-32-0

229 Enzenhöfer, Rainer: *Risk Quantification and Management in Water Production and Supply Systems*, 2014, ISBN 978-3-942036-33-7

230 Faigle, Benjamin: *Adaptive modelling of compositional multi-phase flow with capillary pressure*, 2014, ISBN 978-3-942036-34-4

231 Oladyshkin, Sergey: *Efficient modeling of environmental systems in the face of complexity and uncertainty*, 2014, ISBN 978-3-942036-35-1

232 Sugimoto, Takayuki: Copula based Stochastic Analysis of Discharge Time Series, 2014, ISBN 978-3-942036-36-8

Die Mitteilungshefte ab der Nr. 134 (Jg. 2005) stehen als pdf-Datei über die Homepage des Instituts: www.iws.uni-stuttgart.de zur Verfügung.